UNIVERSITAT DE
BARCELONA

Synthesis of 2-Vinyl sphingolipids as S1PL inhibitors

Raquel Calderón i Almendro

ADVERTIMENT. La consulta d’aquesta tesi queda condicionada a l’acceptació de les següents condicions d'ús: La difusió d’aquesta tesi per mitjà del servei TDX (**www.tdx.cat**) i a través del Dipòsit Digital de la UB (**diposit.ub.edu**) ha estat autoritzada pels titulars dels drets de propietat intel·lectual únicament per a usos privats emmarcats en activitats d’investigació i docència. No s’autoritza la seva reproducció amb finalitats de lucre ni la seva difusió i posada a disposició des d’un lloc aliè al servei TDX ni al Dipòsit Digital de la UB. No s’autoritza la presentació del seu contingut en una finestra o marc aliè a TDX o al Dipòsit Digital de la UB (framing). Aquesta reserva de drets afecta tant al resum de presentació de la tesi com als seus continguts. En la utilització o cita de parts de la tesi és obligat indicar el nom de la persona autora.

ADVERTENCIA. La consulta de esta tesis queda condicionada a la aceptación de las siguientes condiciones de uso: La difusión de esta tesis por medio del servicio TDR (**www.tdx.cat**) y a través del Repositorio Digital de la UB (**diposit.ub.edu**) ha sido autorizada por los titulares de los derechos de propiedad intelectual únicamente para usos privados enmarcados en actividades de investigación y docencia. No se autoriza su reproducción con finalidades de lucro ni su difusión y puesta a disposición desde un sitio ajeno al servicio TDR o al Repositorio Digital de la UB. No se autoriza la presentación de su contenido en una ventana o marco ajeno a TDR o al Repositorio Digital de la UB (framing). Esta reserva de derechos afecta tanto al resumen de presentación de la tesis como a sus contenidos. En la utilización o cita de partes de la tesis es obligado indicar el nombre de la persona autora.

WARNING. On having consulted this thesis you’re accepting the following use conditions: Spreading this thesis by the TDX (**www.tdx.cat**) service and by the UB Digital Repository (**diposit.ub.edu**) has been authorized by the titular of the intellectual property rights only for private uses placed in investigation and teaching activities. Reproduction with lucrative aims is not authorized nor its spreading and availability from a site foreign to the TDX service or to the UB Digital Repository. Introducing its content in a window or frame foreign to the TDX service or to the UB Digital Repository is not authorized (framing). Those rights affect to the presentation summary of the thesis as well as to its contents. In the using or citation of parts of the thesis it’s obliged to indicate the name of the author.

UNIVERSITAT DE BARCELONA

FACULTAT DE FARMÀCIA I CIÈNCIES DE L'ALIMENTACIÓ

DEPARTAMENT DE FARMACOLOGIA, TOXICOLOGIA I QUÍMICA TERAPÈUTICA

PROGRAMA DE DOCTORAT DE QUÍMICA ORGÀNICA EXPERIMENTAL I INDUSTRIAL

SYNTHESIS OF 2-VINYL SPHINGOLIPIDS AS S1PL INHIBITORS

Memòria presentada per Raquel Calderón i Almendro per optar al títol de Doctora per la Universitat de Barcelona

Tesi realitzada al Departament de Química Biomèdica de l'Institut de Química Avançada de Catalunya (IQAC-CSIC)

Directors:	Tutor:
Dr. Antonio Delgado Cirilo Dr. José Luís Abad Saiz	Dr. Antonio Delgado Cirilo

Doctorand:

Raquel Calderón Almendro

BARCELONA, 2017

The present doctoral thesis has been carried out at the Institute of Advanced Chemistry of Catalonia (IQAC), which belongs to the Spanish National Research Council (CSIC).

This work was supported by grants from the Spanish Ministry of Economy and Competitiveness (Project CTQ2014-54743-R) and 'Fundació la Marató de TV3' (20112130 and 20112132).

"*Hay demasiado énfasis en el éxito y en el fracaso, y muy poco en cómo la persona progresa a través del esfuerzo. Disfruta del viaje, disfruta de cada momento y deja de preocuparte por la victoria y la derrota*" –

Matt Biondi

AGRADECIMIENTOS

Des de ben petita m’han interessat les ciències i, tot i que no tenia clar què volia ser de gran, sabia que hi estaria relacionat. Després de la selectivitat vaig triar la carrera de Farmàcia i per casualitats del destí, unes pràctiques de l’últim any em van dur a treballar al grup d’investigació del RUBAM. Han estat més de quatre anys de feina, amb molts dies de frustració però també amb moltes alegries, que no haguessin estat possibles ni haguessin sigut tant satisfactoris sense l’ajuda, la motivació i els esforços de tota la gent que m’ha acompanyat durant aquesta etapa.

Así pues, me gustaría empezar dando las gracias a mis directores de Tesis, el Dr. Antonio Delgado y el Dr. José Luís Abad, ya que esta tesis es fruto de la confianza que depositaron en mí. Me han otorgado la oportunidad de poder trabajar en el mundo de la investigación y han sido capaces de guiarme para que no parase de aprender ni un solo día.

No em puc oblidar del suport, tant tècnic com emocional, de les Dres. Gemma Fabriàs i Josefina Casas que em van obrir les portes de la Bioquímica, sense la qual aquesta tesi restaria incomplerta y de la que una farmacèutica com jo n’ha gaudit àmpliament.

Tampoco me olvido de los Dres. Jordi Bujons, Jordi García, Manuel Montejo y Juan Jesús López que colaboraron en este proyecto y cuyos consejos y experiencia nos han sido tan útiles.

Vull agrair també a tots els companys que ens hem anat trobant al CSIC durant aquests anys, tant per tot el que m’heu ensenyat com pels bons moments compartits, en especial a l’Ana Bilbao, l’Ana Pou i la Mireia Quintana que han fet amens molts moments d’estrès i m’han ajudat a convertir les penes en alegries. A la Ingrid Nieves per “adoptar-me” quan vaig arribar al laboratori i ensenyar-me, no només les eines bàsiques per treballar, sinó també a tenir criteri propi i a en Pol Sanllehí per tota l’ajuda amb els experiments de la liasa i els caps de setmana de treball al laboratori, que compartits es feien menys feixucs.

Als amics de la universitat pel vostre suport i comprensió en els moments més difícils i per les bones vivències compartides; en especial a en Victor Carrer i a la Sandra Vidal, que tot i que estàs lluny sempre t’he tingut ben a prop quan ho necessitava.

A en Roger per les hores de feina al Hidden, que feien d’escriure la tesi una tasca molt més divertida entre cafès, pastissos de pastanaga i somriures.

A la petita família que hem format amb la Zoí i l’Àngela, que fan que em senti com a casa. M’han animat cada un dels dies de la tesi i no m’imagino vivint amb unes altres companyes de pis millors.

A Jack por su apoyo y paciencia en todos los momentos de estrés, fines de semana en el laboratorio y trabajo hasta horas intempestivas.

Y por último a mis padres, mi hermana y a Marisol, por su apoyo incondicional, por ayudarme a hacer frente a los tiempos difíciles y porque sin ellos no habría llegado hasta aquí.

Muchas gracias por todo.

ABBREVIATIONS

2VS1P	2-vinylsphinganine-1-phosphate
ABC	ATP-binding cassette
ACN	Acetonitrile
AMA	9-anthrylmethoxyacetic acid
Boc	*tert*-Butoxycarbonyl
C1P	Ceramide-1-phosphate
cat.	Catalytic
CDase	Ceramidase
Cer	Ceramide
CERT	Ceramide transfer protein
CerS	Ceramide synthase
CH_2Cl_2	Dichloromethane
CK	Ceramide kinase
CPPase	Ceramide phosphate phosphatase
Cy	Cyclohexyl
DCA	Dichloroacetic acid
DhCer	Dihydroceramide
DIPEA	*N,N*-Diisopropylethylamine
DMAP	*N,N*-Dimethylpyridin-4-amine
DMF	*N,N*-Dimethylformamide
DMP	2,2-Dimethoxypropane
DMSO	Dimethyl sulfoxide
DOP	4-deoxypyridoxine
DOP-P	4-deoxypyridoxine 5’-phosphate
Dpl1p	*Saccharomyces cerevisiae* S1PL
EDC	*N*-(3-Dimethylaminopropyl)-*N*′-ethylcarbodiimide hydrochloride
ee	Enantiomeric excess
ER	Endoplasmic reticulum
ESI-MS	Electrospray Ionisation Mass Spectrometry
Et_3N	Triethylamine
Et_2O	Diethyl ether
EtOAc	Ethyl acetate
FBS	Fetal bovine serum

GABA-AT	GABA amino transferase
GalCase	Galactosyl ceramidase
GalCS	Galactosylceramide synthase
GCase	Glucosyl ceramidase
GCS	Glucosylceramide synthase
GC-MS	Gas chromatography- mass spectrometry
GlcCer	Glucosylceramide
KDSR	3-ketosphinganine reductase
HATU	(1-[Bis(dimethylamino)methylene]-1H-1,2,3-triazolo[4,5-b]pyridinium 3-oxid hexafluorophosphate)
HOBt	1-Hydroxybenzotriazole
HPLC	High pressure liquid chromatography Abbreviations
hS1PL	Human Sphingosine 1-phosphate lyase
IBX	2-Iodoxybenzoic acid
IC_{50}	Half maximal inhibitory concentration
IPA	isopropanol
KHMDS	Potassium bis(trimethylsilyl)amide
MALDI	Matrix-assisted laser desorption/ionization
MeOH	Methanol
$MgSO_4$	Magnesium sulfate
MPA	α-methoxyphenylacetic acid
MTBE	Methyl *tert*-butyl ether
MTPA	Mosher’s acid
NH_4Cl	Ammonium chloride
NMI	N-methylimidazole
NMR	Nuclear magnetic resonance
PE	Phosphoetanolamine
PLE	Porcine Liver Esterase
rt	Room temperature
S1P	Sphingosine-1-phosphate
S1PL	Sphingosine 1-phosphate lyase
S1PR	Sphingosine-1-phosphate receptor
Sa	Sphinganine (Dihydrosphingosine)
Sa1P	Sphinganine-1-phosphate
SK	Sphingosine kinase

SLs	Sphingolipids
SM	Sphingomyelin
SMase	Sphingomyelinase
SMS	Sphingomyelin synthase
So	Sphingosine
SPNS2	Spinster homologue 2
SPPase	Sphingosine phosphate phosphatase
SPT	Serine palmitoyl transferase
StS1PL	*Symbiobacterium thermophilum* S1PL
TBAF	Tetra-*n*-butylammonium fluoride
TBDPS	*tert*-Butyldiphenylsilyl
TBDPSCl	*tert*-Butyldiphenylsilyl chloride
TEA	Triethylamine
THF	Tetrahydrofuran
THI	2-acetyl-4-tetrahydroxybutylimidazole
TLC	Thin-layer chromatography
TMSBr	Bromotrimethylsilane
TNF	Tumour necrosis factor
Tris	2-amino-2-(hydroxymethyl)propane-1,3-diol
UV	Ultraviolet

TABLE OF CONTENTS

1. INTRODUCTION AND GENERAL OBJECTIVES 1

1.1 General Introduction .... - 3 -

1.2 Structure of the sphingolipids .... - 3 -

1.3 Metabolism of sphingolipids .... - 4 -

1.4 Sphingolipid signalling .... - 6 -

1.4.1 Ceramide (Cer) .... - 6 -

1.4.2 Ceramide-1-phosphate (C1P) .... - 7 -

1.4.4 Sphingosine-1-phosphate (S1P) .... - 9 -

1.5 Sphingosine 1-phosphate lyase (S1PL) .... - 11 -

1.5.1 Sphingolipid analogues as S1PL inhibitors .... - 13 -

1.5.2 Functional S1PL inhibitors .... - 13 -

1.5.3 Non lipidic SPL inhibitors .... - 14 -

1.6 Mechanism-based inhibitors .... - 16 -

1.7 General objectives .... - 17 -

2. RESULTS AND DISCUSSION 21

2.1 Approaches to enantiopure 2-vinyl sphingolipids from non-chiral or racemic precursors 23

2.1.1 Diastereoselective synthesis of (±)-*syn* and (±)-*anti*-2-vinyl aminophosphates **24**- 25 -

2.1.2 Use of lipases for the desymmetrization of diol **15** .... - 30 -

2.1.3 Chemical resolution of synthetic intermediates .... - 31 -

2.1.4 Simultaneous separation and resolution of (±)-*syn* and (±)-*anti*-21 by derivatization as MPA esters .... - 32 -

2.1.5. Configurational assignments .... - 35 -

2.1.5.1 Configuration at C_3 from phosphates **23** .... - 35 -

2.1.5.2 Configuration at C2 from carbamate *syn*-**33** .... - 38 -

2.1.6 Attempts to remove the MPA ester in phosphates **32** .... - 41 -

2.1.7 Vinyl Garner's aldehyde **42**, a new building block for an alternative approach to enantiomerically pure 2-vinyl sphingolipids .... - 43 -

2.1.8 Enantioselective approaches to **45** by chemical resolution of synthetic precursors.... - 46 -

2.1.9 Chemical resolution of (±)-*syn*-**45** and (±)-*anti*-**45** by derivatization as (*R*)-MPA esters .... - 48 -

2.1.9.1 Alternatives to the Steglich esterification .... - 50 -

2.1.10 Configurational assignments - 52 -

2.1.10.1 Configuration at C_3 from MPA esters **46** - 52 -

2.1.10.2 Configuration at C_2 from bicyclic carbamates **51** - 55 -

2.1.11 X-ray diffraction trials - 56 -

2.1.12 Synthesis of 2-vinyl dihydrosphingolipids - 57 -

2.1.13 Synthesis of 2-vinyl sphingolipids - 58 -

2.1.14 Conclusions - 63 -

2.2 Vibrational circular dichroism (VCD) studies to confirm the absolute configuration of 51 65

2.2.1 Introduction - 67 -

2.2.2 Conformational search - 68 -

2.2.3 Vibrational IR and VCD spectra - 73 -

2.2.4 Conclusions - 76 -

2.3 Biological assays 77

2.3.1 Introduction - 79 -

2.3.2 Inhibition of StS1PL using **RBM13** as substrate - 81 -

2.3.3 Inhibition of hS1PL using **RBM7-148** as substrate - 82 -

2.3.3.1 S1PL inhibition of phosphates **24** - 82 -

2.3.3.2 S1PL inhibition of amino alcohols **31** and **JG** - 87 -

2.3.4 Cell viability (MTT) - 88 -

2.3.5 Lipidomics - 89 -

2.3.5.1 Metabolism of the administered compounds - 89 -

2.3.5.2 Effect on the natural sphingolipidome - 92 -

2.3.6 Computational studies on the inhibition of hS1PL by compounds **24** - 94 -

2.3.7 Conclusions - 99 -

3. SUMMARY AND CONCLUSIONS 103

4. EXPERIMENTAL SECTION 109

4.1 Chemistry - 111 -

4.1.1 General remarks - 111 -

4.1.2 General synthetic methods - 112 -

4.1.3 Vibrational IR and VCD experimental spectra - 115 -

4.1.4 Computational studies - 116 -

4.1.5 Synthesis and characterization of compounds - 116 -

4.2 Biological studies - 141 -

  - 4.2.1 General remarks .... - 141 -
  - 4.2.2 Assays of S1PL enzyme activity .... - 142 -
  - 4.3.3 Lipidomic analyses .... - 143 -

5. REFERENCES 149

6. SUMMARY IN SPANISH 165

7. SUPPORTING INFORMATION (CD) 175

1. INTRODUCTION AND GENERAL OBJECTIVES

1.1 General Introduction

The first time sphingolipids (SLs) were identified was in the 19th century as major constituents of brain tissue by Johan Ludwig Wilhelm Thudichum, who named sphingosine (So), like the sphinx, due to their enigmatic nature at the time.[1] Later, it was found that SLs were universal components of the membranes in eukaryotic cells, as well as in some species of bacteria and fungi.[2] Over the last three decades, these molecules have shown not only structural functions, but also play the role of signalling molecules.[3]

Nowadays, SLs metabolites, such as ceramide (Cer), ceramide-1-phosphate (C1P) and sphingosine-1-phosphate (S1P), have emerged as important signalling molecules that regulate cell growth, survival, immune cell trafficking, vascular and epithelial integrity and are also particularly important in inflammation and cancer (Figure 1.1).[3–5]

An alteration in the metabolism of SLs leads to the establishment of inherit diseases called sphingolipidoses, which are mainly caused by defects in genes encoding proteins involved in the lysosomal degradation of SLs. Most sphingolipidoses are associated with high mortality and are considered as rare disorders, with a collective frequency of 1 in 7000–8000 live births. The development of inhibitors of the enzymes involved in their metabolism may be crucial for establishing new therapeutic strategies for the treatment of these diseases.[6,7]

Thanks to the recent research it is an exciting time to study SLs: firstly, most of the regulatory enzymes involved in their metabolism have been cloned, which allowed the discovery of the physiological functions of SLs metabolites. Besides, the progress in advanced mass spectroscopic techniques has brought the 'omics' revolution to SLs, allowing for the simultaneous analysis and quantification of multiple species. Finally, several SLs signalling protein structures have been solved, allowing a rational drug design and the development of inhibitors of enzymes involved in signalling pathways.[4]

1.2 Structure of the sphingolipids

SLs are characterized by a sphingoid base, which consists of a C18 carbon chain that can be saturated or monounsaturated and a polar 2-amino-1,3-diol head, which can be *N*-acylated with fatty acids of variable length and unsaturations or functionalized at the C1 hydroxyl group to give complex SLs. The structures of the main SLs are shown in Figure 1.1.

Sphinganine (Sa) has two chiral centres (C2 and C3), and D-*erythro* (2*S*,3*R*)-sphinganine is the natural isomer. For So, the same 2*S*,3*R* stereoisomer is found in nature and the double bond has a *trans*-configuration.

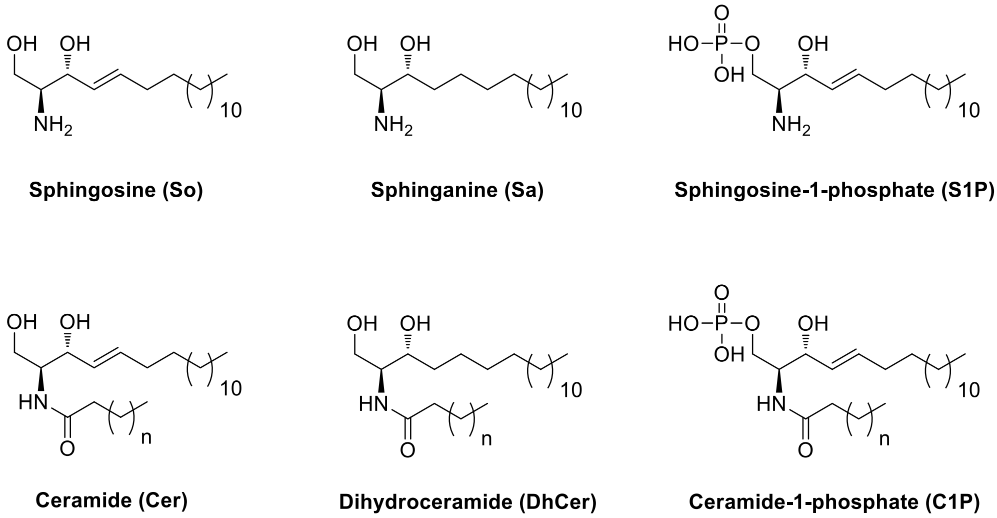

Sphingosine (So) **Sphinganine (Sa)** **Sphingosine-1-phosphate (S1P)**

Ceramide (Cer) **Dihydroceramide (DhCer)** **Ceramide-1-phosphate (C1P)**

Figure 1.1. Structures of the main bioactive sphingolipids (n represents different acyl chain lengths).

1.3 Metabolism of sphingolipids

The SLs metabolism starts with a common metabolic entry point in the endoplasmic reticulum (ER) with the condensation of serine and palmitoyl-CoA by serine palmitoyltransferase (SPT) in the *de novo* pathway (green path in Figure 1.2), and a single exit point mediated by sphingosine-1-phosphate lyase (S1PL), which breaks down S1P irreversibly into phosphoetanolamine (PE) and *trans*-2-hexadecenal (red path in Figure 1.2), which, in turn, can be converted into hexadecenoic acid, which is utilized for the formation of palmitoyl-CoA and subsequently reincorporated into lipid metabolic pathways.[3,4,8]

The intermediate metabolic steps in SLs biosynthesis constitute an interconnected complex network, highly compartmentalized, where Cer and, to a lesser degree, dihydroceramide (DhCer), play a central role in SLs biosynthesis and catabolism, which mainly occurs in the Golgi apparatus. There are two ways to transport Cer from ER to the Golgi: by the ceramide transfer protein (CERT) or by vesicular transport. Cer can also be generated in the plasma membrane, in the lysosome and in the mitochondria by the action of sphingomyelinases (SMases), resulting in compartment-specific Cer generation.[3,4,9] The SLs metabolic pathways above described are detailed in Figure 1.2.

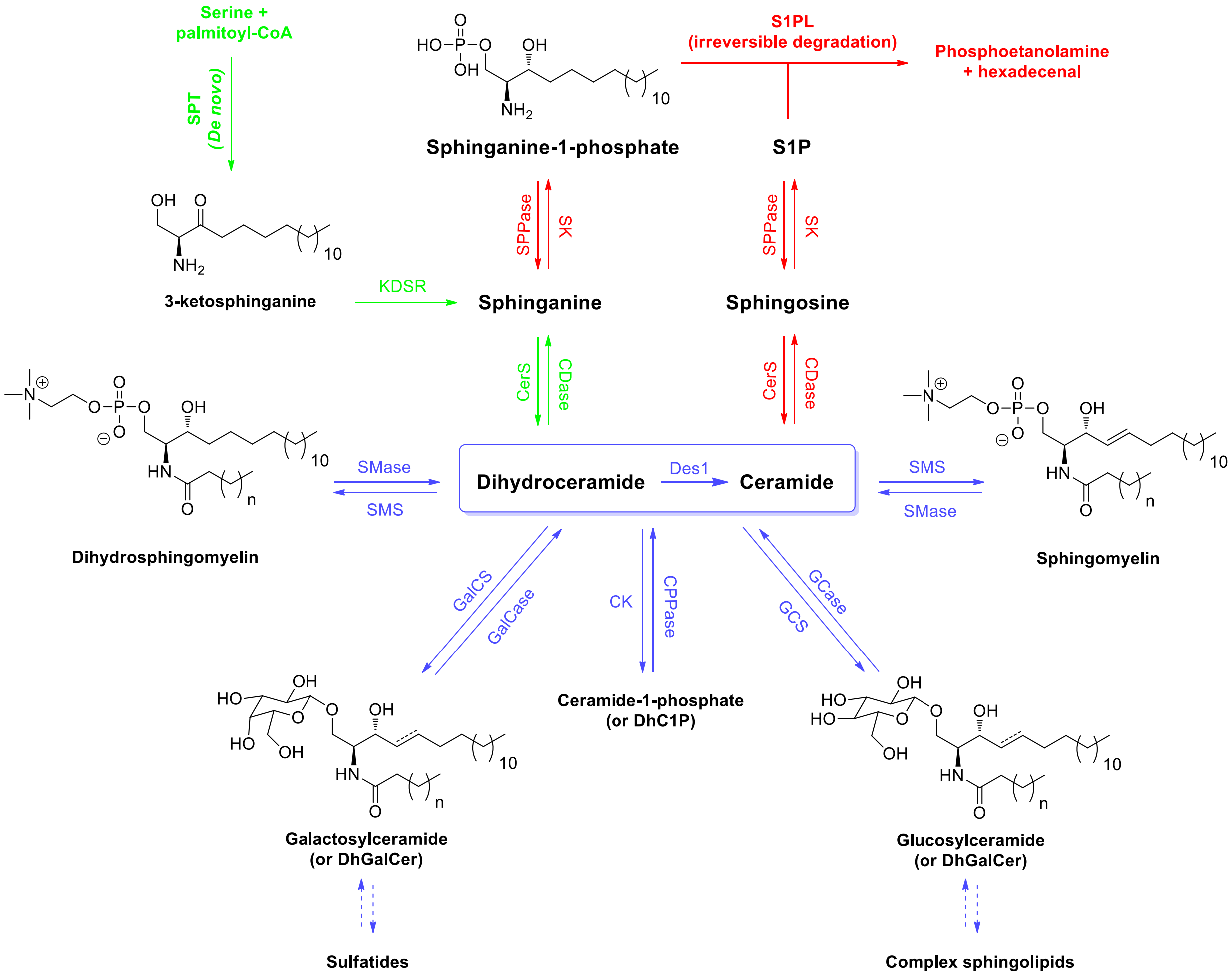
Serine +
palmitoyl-CoA
SPT
(De novo)
3-ketosphinganine
KDSR
Sphinganine
Sphinganine-1-phosphate
SPPase
SK
S1PL
(irreversible degradation)
Phosphoetanolamine
+ hexadecenal
S1P
Sphingosine
CerS
CDase
Dihydroceramide
Des1
Ceramide
SMase
SMS
Dihydrosphingomyelin
Sphingomyelin
GalCS
GalCase
CK
CPPase
GCase
GCS
Ceramide-1-phosphate
(or DhC1P)
Galactosylceramide
(or DhGalCer)
Glucosylceramide
(or DhGalCer)
Sulfatides
Complex sphingolipids

Figure 1.2. The sphingolipid metabolic pathway. CDase (ceramidase), CK (ceramide kinase), CPPase (ceramide phosphate phosphatase), GalCase (galactosyl ceramidase), GalCS (galactosylceramide synthase), GCase (glucosyl ceramidase), GCS (glucosylceramide synthase), KDSR (3-ketosphinganine reductase), S1PL (sphingosine phosphate lyase), SK (sphingosine kinase), SMase (sphingomyelinase), SMS (sphingomyelin synthase), SPPase (sphingosine phosphate phosphatase), SPT (serine palmitoyl transferase).

As mentioned above, defects in proteins of SLs metabolism can cause severe diseases, as for example Gaucher disease, the most common form of the sphingolipidosis, caused by the deficiency of glucosylceramide-β-glucosidase leading to accumulation of glucosylceramide (GlcCer). Another example is Fabry disease, caused by an inborn deficiency of lysosomal α-galactosidase A, which ends up with the accumulation of glycolipids in the affected tissues.[6]

1.4 Sphingolipid signalling

The abundant interconnections in SLs metabolism lead to a complex signalling pathway that the cell can modulate by regulating SLs interconversions, where an increase in the synthesis of one metabolite is linked to the decrease of the levels of another one.[3] For example, the phosphorylation of So increases the levels of S1P and decreases, at the same time, the levels of So. Moreover, the relative levels of Cer, So, and S1P differ tremendously (Figure 1.3). As a result, the phosphorylation of just 1% of So can double the levels of S1P.[3,10]

The changes in the relative concentrations of bioactive SLs bring about functional consequences as, for example, those derived from the balance between Cer and S1P in the so-called "sphingolipid rheostat" that controls cell fate.[3,10,11]

The cell monitors the SLs levels in the plasma membrane by a series of receptor proteins, including metabolism enzymes or transport proteins, among others, that bind mainly to SLs present at low concentrations, such as So or S1P. Alternatively, for SLs present at higher concentrations, changes in the physical properties of the membrane, such as fluidity, thickness or curvature can trigger cell responsiveness.[12]

The regulation of SLs metabolism can be affected by multiple stimuli, like pathogens, oxidative stress and cytokines, that can modulate key SLs metabolic enzymes in a spatial and temporal manner leading to the restricted production of Cer, C1P and S1P on specific compartments that determine a different biological activity.[4,13]

1.4.1 Ceramide (Cer)

Cer is a “hub” in sphingolipid metabolism, serving as a precursor of C1P, SM and complex SLs. Moreover, in the degradative pathway, Cer is the precursor of So, which in turn is the precursor of S1P.

Cer transmits intracellular signalling through the formation of Cer-enriched membrane microdomains, which can be altered ending up with changes in the membrane composition and with interactions of lipids or signalling proteins. These membrane microdomains have been implicated in a variety of signalling cascades.[4]

The implication of Cer as an important second messenger in numerous biological processes, such as regulation of apoptosis, cell growth, diabetes, insulin resistance, inflammation, neurodegenerative disorders and atherosclerosis in various stress responses and growth mechanisms, has been widely studied.[3,7,14,15]

Nonetheless, Cer is not always a proapoptotic or an anti-proliferative metabolite. In fact, it is now clear that Cer can prevent neurons from entering apoptosis.[16,17]

In the last few years, a new paradigm has emerged that integrates significant advances in the field. In the so-called “many ceramides hypothesis”, each Cer species has the potential to elicit a unique cellular response derived from differences in the structure of the bioactive molecule, the protein targets or the subcellular localization.[13]

Thus, given the interconnection of the different lipid metabolites, the interpretation of the signalling pathways caused by Cer becomes a complex process. For example, tumour necrosis factor (TNF) may activate SMase to generate Cer. In a subsequent step, CDase or ceramide kinase (CK) may act on this metabolite to generate So or ceramide-1-phosphate (C1P), respectively. These new metabolites may then mediate their own specific actions, and so on. These interconnections complicate the attempts at analysing the specific pathways of Cer metabolism and functions (Figure 1.2).[13]

1.4.2 Ceramide-1-phosphate (C1P)

So far, the only known enzyme that catalyses the conversion of Cer into C1P in mammalian cells is CK, localized in the Golgi apparatus (Figure 1.3).

C1P is a key regulator of cell proliferation and survival by the inhibition of SMase and Cer accumulation in macrophages. A down-regulation of CK in mammalian cells leads to a reduction of growth and promotion of apoptosis. Subsequently, C1P can regulate the release of arachidonic acid and the production of prostaglandins that give rise to some pro-inflammatory effects.[4,7]

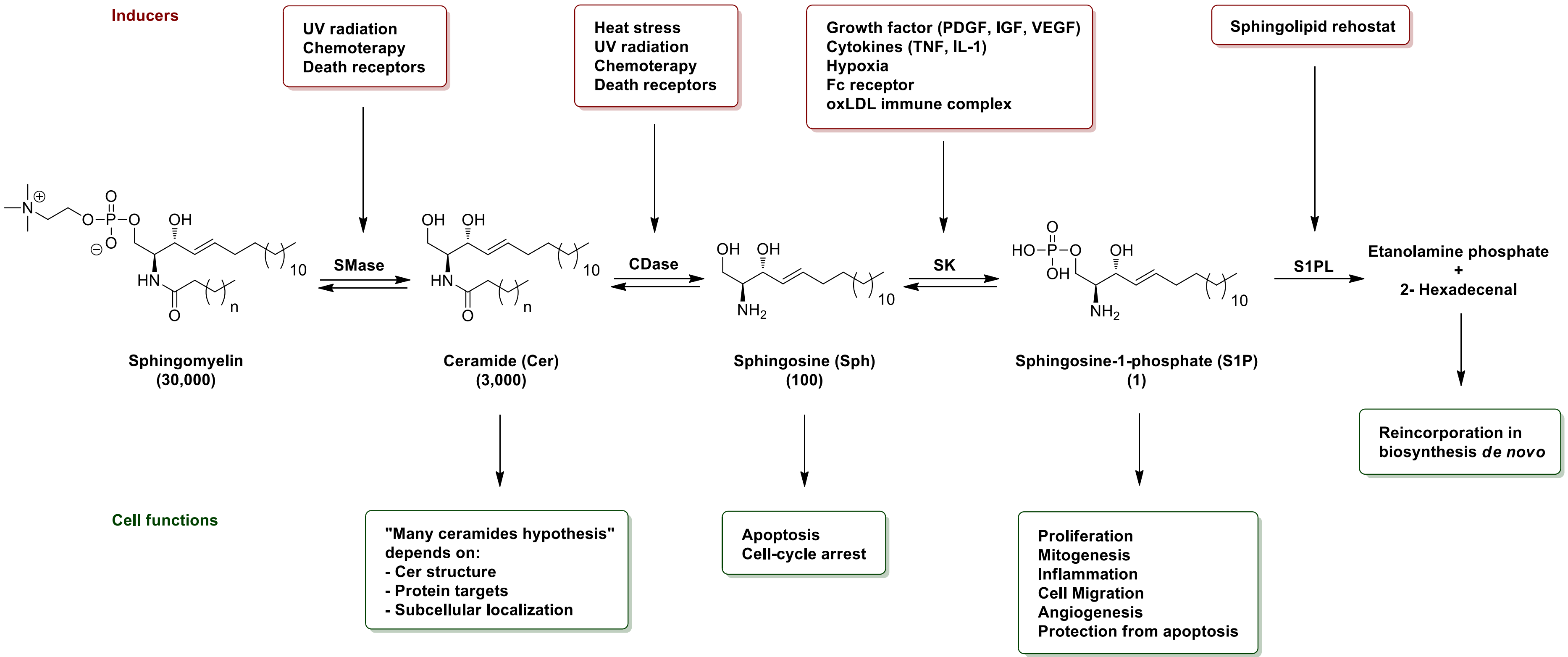
Inducers
UV radiation
Chemoterapy
Death receptors
Heat stress
UV radiation
Chemoterapy
Death receptors
Growth factor (PDGF, IGF, VEGF)
Cytokines (TNF, IL-1)
Hypoxia
Fc receptor
oxLDL immune complex
Sphingolipid rehostat
SMase
CDase
SK
S1PL
Sphingomyelin
(30,000)
Ceramide (Cer)
(3,000)
Sphingosine (Sph)
(100)
Sphingosine-1-phosphate (S1P)
(1)
Etanolamine phosphate
+
2- Hexadecenal
Reincorporation in biosynthesis de novo
Cell functions
"Many ceramides hypothesis" depends on:
- Cer structure
- Protein targets
- Subcellular localization
Apoptosis
Cell-cycle arrest
Proliferation
Mitogenesis
Inflammation
Cell Migration
Angiogenesis
Protection from apoptosis

Figure 1.3. The main role of bioactive SLs cell biological responses. The numbers in brackets indicate the relative levels of these SLs. IL-1, interleukin-1; IGF; insulin-like growth factor; oxLDL, oxidized low-density lipoprotein; PDGF; platelet-derived growth factor; TNF, tumour necrosis factor; VEGF, vascular endothelial.

To date, the intracellular amount of C1P is not exactly known and it varies between cell types, but the basal amounts can be surprisingly high, like in macrophages RAW 264.7, where it accounts for one fourth of the amount of SM and several fold times those of Cer.[18]

1.4.4 Sphingosine-1-phosphate (S1P)

S1P has been implicated in many biological processes, including cell growth, suppression of apoptosis, stress responses, calcium homeostasis, cell migration, angiogenesis, differentiation and vascular maturation (Figure 1.3). [3,4,19–21]

Its intracellular levels are low and tightly regulated by the balance between its synthesis and its degradation. The biosynthesis of S1P is catalysed by sphingosine kinase (SK), an ATP-dependent phosphorylation enzyme. This enzyme is activated by many stimuli, which indicates its central regulating role. The degradation of S1P is mediated by two different pathways: the reversible dephosphorylation to So by specific phosphatases (SPPases) or the irreversible degradation in the ER by the 5'-pyridoxal phosphate (PLP)-dependent S1PL to 2-hexadecenal and PE, which are subsequently reused for the biosynthesis of fatty acids and phosphatidylethanolamine, respectively (Figure 1.2).[3,19]

S1P can be released to the extracellular medium by Spinster homologue 2 (SPNS2) or ATP-binding cassette (ABC) transporters, to become one of the most abundant biologically active lysophospholipids in circulation. Out of the cells, S1P can bind specific lipid G–protein coupled S1PR1–5 receptors or promote a downstream signalling pathway, playing essential roles in vascular development and endothelial integrity, control of cardiac rhythm, and immunity responses, including lymphocyte trafficking and differentiation, cell growth, cell survival, and cytokine and chemokine production, among others.[4,7,22,23]

Recently, specific S1P receptor (S1PR) modulators have been developed and some of them have gained relevance in clinical practice. This is the case of FTY720 (Fingolimod, Gilenya®), a So analogue that can be phosphorylated by SKs to produce the S1PR ligand (*S*)-Fingolimod-P (Figure 1.4). FTY720 was the first orally active drug approved for the treatment of autoimmune diseases, such as multiple sclerosis. It is also use to reduce rejections following organ transplantations, and it is under consideration for other inflammatory and allergic disorders.[7,24–27]

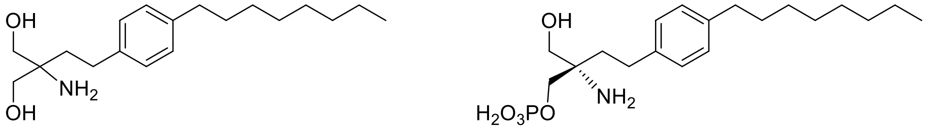
OH
NH$_2$
OH
OH
NH$_2$
H$_2$O$_3$PO

Fingolimod **(*S*)-Fingolimod-P**

Figure 1.4. Structures of Fingolimod and its active phosphorylated metabolite, a S1PR agonist.

As seen in Cer, S1P not always promote cell proliferation and inhibit apoptosis, it depends on the compartment of the cell where S1P is generated. For that two different SK enzymes are described; SK1, located in cytosol, is associate with cell growth and inhibits apoptosis and SK2, located mostly in cell membranes, is related with inhibition of cell growth and a pro-apoptotic response.[28]

These differences according to the compartmentalization of S1P and the metabolism of SLs are summarized in Figure 1.5.

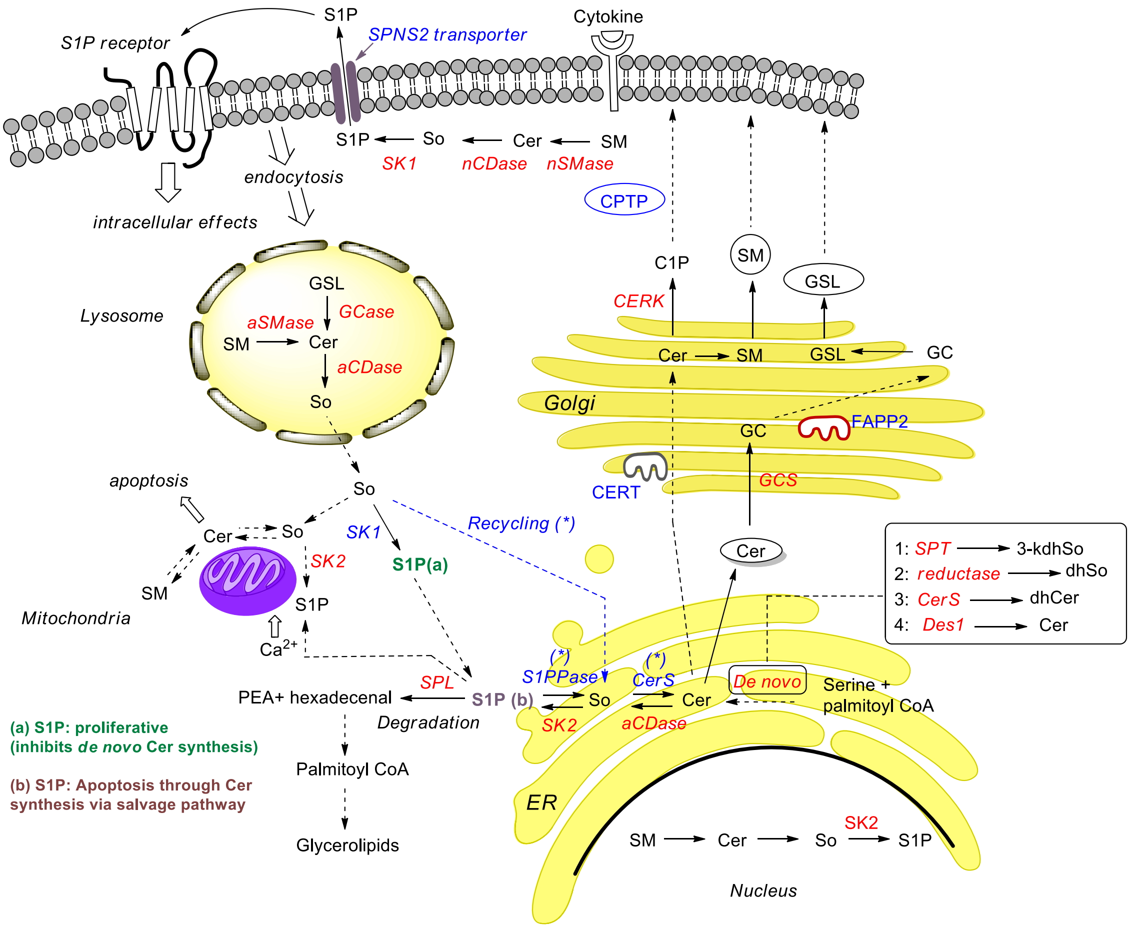
S1P
S1P receptor
SPNS2 transporter
Cytokine
S1P ← So ← Cer ← SM
SK1 nCDase nSMase
endocytosis
intracellular effects
CPTP
C1P
SM
GSL
CERK
Lysosome
GSL
GCase
aSMase
SM → Cer
aCDase
So
Cer → SM GSL ← GC
Golgi
GC
FAPP2
CERT
GCS
apoptosis
So
Cer ⇠ So
SK1
SK2
S1P(a)
Recycling (*)
SM
Mitochondria
S1P
Ca^{2+}
Cer
1: SPT → 3-kdhSo
2: reductase → dhSo
3: CerS → dhCer
4: Des1 → Cer
(*)
S1PPase
(*)
CerS
De novo
Serine + palmitoyl CoA
SPL
PEA+ hexadecenal ← S1P (b) ⇄ So ⇄ Cer
SK2
aCDase
Degradation
Palmitoyl CoA
Glycerolipids
ER
SM → Cer → So → S1P
SK2
Nucleus
(a) S1P: proliferative (inhibits de novo Cer synthesis)
(b) S1P: Apoptosis through Cer synthesis via salvage pathway

Figure 1.5. SK1 and SK2, two very closely related enzymes that use the same substrate and produce the same product, have opposite effects on cell survival and reveal their opposing functions in regulation of sphingolipid metabolism.

1.5 Sphingosine 1-phosphate lyase (S1PL)

As indicated above, S1PL is a key PLP-dependent enzyme of SLs catabolism that catalyses the irreversible cleavage of S1P (Figure 1.3) and the unsaturated sphinganine-1-phosphate (Sa1P).[29] The enzyme is located in the ER and possesses an *N*-terminal lumenal domain, a transmembrane segment and a soluble PLP-binding domain responsible for the catalytic activity. S1PL is active as a dimer, with two catalytic cavities to which each protomer contributes residues simultaneously (Figure 1.6).[21,30]

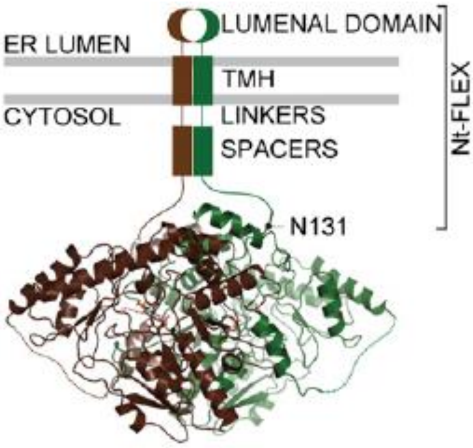

Figure 1.6. Proposed arrangement of the PLP–binding domain of yeast S1PL (Dpl1p).[30]

Together with SK and SPPases, S1PL regulates the intracellular levels of S1P and contributes to the "sphingolipid rheostat", a system that controls the cell fate through the modulation of the ratio of intracellular proliferative S1P and the apoptogenic So and Cer.[7,30–32]

When we started this thesis, at the end of year 2012, the only reported S1PL structures were those of yeast from *Saccharomyces cerevisiae* (Dpl1p)[33] and the prokaryotic homolog from *Symbiobacterium thermophilum* (StS1PL),[30] which were expressed in *E.coli*. In a more recent work, published in 2014, the expression of the human S1PL (hS1PL) in Sf9 insect cells, together with its crystal structure, was reported.[34]

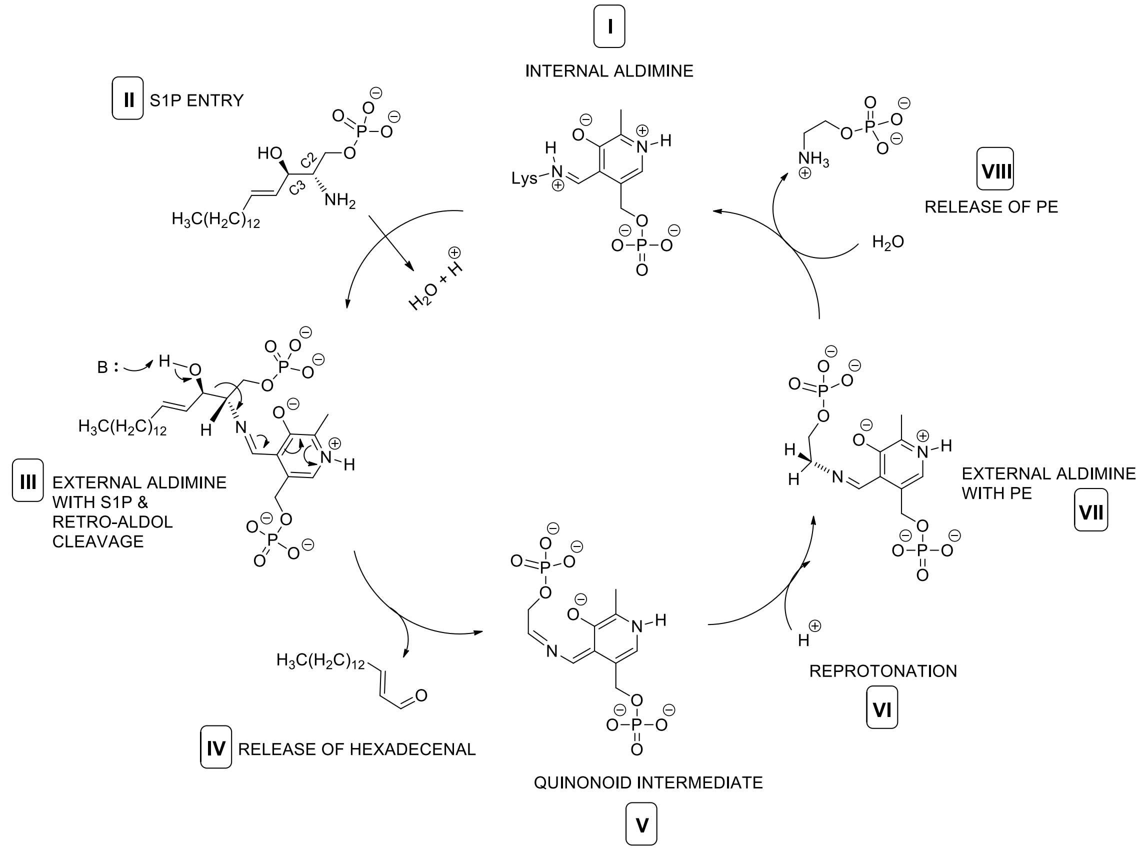
I
INTERNAL ALDIMINE
II
S1P ENTRY
C2
C3
HO
NH₂
H₃C(H₂C)₁₂
H₂O + H⁺
Lys
VIII
RELEASE OF PE
H₂O
NH₃
B :
III
EXTERNAL ALDIMINE WITH S1P & RETRO-ALDOL CLEAVAGE
EXTERNAL ALDIMINE WITH PE
VII
H₃C(H₂C)₁₂
IV
RELEASE OF HEXADECENAL
QUINONOID INTERMEDIATE
V
REPROTONATION
VI
H⁺

Figure 1.7. Described mechanism for the cleavage of S1P by S1PL.

The accepted catalytic mechanism for S1PL is summarized in Figure 1.7. The incoming S1P (step II) replaces the catalytic lysine as Schiff base partner of PLP, forming an external aldimine (step III). Retro-aldol cleavage occurs at the hydroxyl group of C3 of S1P (step III) and 2-hexadecenal is released (step IV). The second external aldimine (step VII) results from reprotonation (step VI) of the quinonoid intermediate (step V). PE is then released (step VIII) and the internal aldimine is reformed (step I): the enzyme is now ready for a second turnover.[30] The same mechanism applies if Sa1P is used as substrate, giving rise to hexadecanal and PE.

Undoubtedly, the development of compounds that are able to specifically target sphingolipid metabolizing enzymes is a promising area of research, which will most likely provide new tools and drugs for the treatment of several disorders. In this context, the inhibition of S1PL has been related with autoimmune disorders, inflammation diseases or cellular deregulation in several types of cancer, among others,[8,26,35,36] and it is considered a promising new target for drug development.

1.5.1 Sphingolipid analogues as S1PL inhibitors

The first reported inhibitor of S1PL was 1-desoxydihydrosphingosine-1-phosphonate (**30**) (Figure 1.8). It was described as a competitive inhibitor, despite the compound behaves also as a substrate with a lower rate of cleavage in comparison with S1P. Due to its haemolytic properties, this phosphonate was proved to be highly toxic when administered intravenously.[37]
The SL analogue 2-vinylsphinganine-1-phosphate (**2VS1P**), described as a mixture of stereoisomers (Figure 1.8) has also been reported as a potent SPL inhibitor.[38] It will be discussed more deeply in section 1.6.
Compound FTY720 (Fingolimod, Gilenya®) (Figure 1.4), initially reported as S1PR 1,3-5 agonist after its phosphorylation, is an immunomodulatory agent that was also reported as S1PL antagonist in vitro.[39] However, this effect is only observed at concentrations around 100-fold higher than those required as S1P agonist.[27]

1.5.2 Functional S1PL inhibitors

The functional S1PL inhibitors reproduce a phenotypic S1PL inhibition *in vivo*, but they are not active on the isolated enzyme on in *in vitro* experiments. In this context, the vitamin B_6 antagonist 4-deoxypyridoxine (DOP) (Figure 1.8) has been reported as a S1PL inhibitor and also as a non-selective inhibitor of PLP-dependent enzymes.[40,41] Although DOP does not inhibit S1PL in either cell-free of cell-based assays,[35,42,43] it induces increased S1P concentrations in various tissues and cause reduction of lymphocyte numbers in circulation when administered *in vivo*,[35,41] suggesting that DOP can act as an indirect S1PL inhibitor. Recently, Ohtoyo *et al*. reported that DOP can be phosphorilated by pyridoxal kinase *in vitro* to 4-deoxypyridoxine 5'-phosphate (DOP-P) (Figure 1.8), which competes with PLP for the active site of apo-S1PL, resulting in the inhibition of the enzymatic activity.[44]
A similar behavior is found for THI and structurally related analogs (Figure 1.8). Oral administration of 2-acetyl-4-tetrahydroxybutylimidazole (THI), originally identified as a minor constituent of caramel color III, caused lymphopenia in rodents,[45] leading to a phenotype similar to that observed in mice expressing reduced levels of S1PL.[35] As for DOP, these compounds only inhibit S1PL *in vivo* and its effect is reversed by excess dietary vitamin B_6.[41]
However, very recently, it has been demonstrated that THI is metabolized to A6770, a metabolic intermediate that can be also phosphorylated to yield the active compound

A6770-P, which inhibits S1PL in the same way as DOP-P does.[46] In addition, derivatives of THI, such as LX2931 and LX2932, have also been described.[35,47] LX2931, was developed for the treatment of rheumatoid arthritis and was the first clinically studied inhibitor of S1PL. After its evaluation in phase I clinical trials in healthy human subjects it failed at phase II, apparently due to sub-therapeutic dosing.[48] All these structures are shown in Figure 1.8.

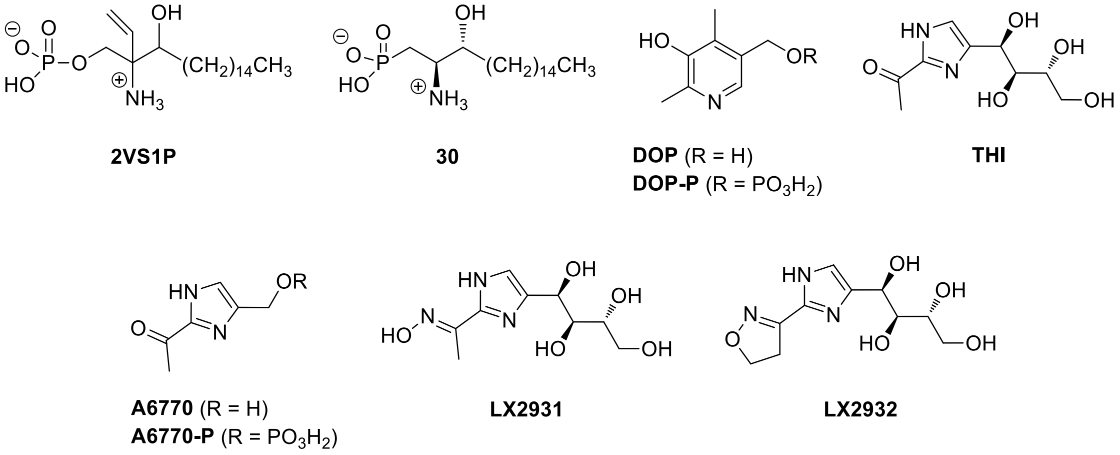
2VS1P
30
DOP (R = H)
DOP-P (R = PO_3H_2)
THI
A6770 (R = H)
A6770-P (R = PO_3H_2)
LX2931
LX2932

Figure 1.8. Functional described S1PL inhibitors.

1.5.3 Non lipidic SPL inhibitors

As a result of extensive HTS experiments, different inhibitors structurally unrelated to S1P have been reported on the last years. This is the case of the oxopyridylpyrimidine **1** (Figure 1.9), which was identified as a hit (IC_{50} = 2.1 µM as S1PL inhibitor) after a HTS performed by Lexicon. Compound **1** increased S1P levels 275 % over controls in HepG2 cells, despite it failed to elicit an *in-vivo* lymphopenic effect, probably because of tight protein binding.[35]

Another massive screening carried out by Novartis ended up with an interesting S1PL inhibitor in the low micromolar range (IC_{50} = 2.4 µM), the piperazinophthalazine derivative **3a**[42,43] (Figure 1.9). Interestingly, (*S*)-**3a** was significantly less potent (IC_{50} > 30 µM). After a lead optimization process, compounds **3b**[43] and **3c**[49] (Figure 1.9) were later reported as improved inhibitors acting in the submicromolar and nanomolar range (IC_{50} values of 0.21 µM and 0.024 µM for **3b** and **3c**, respectively). The reported crystal structure of human S1PL in complex with **3b** demonstrated that the inhibitor is hosted in the substrate binding site.[49,50] Besides, compound **3b** is able to induce lymphopenia and confers protection in animal models of multiple sclerosis.[34]

Kashem and coworkers from Boehringer Ingelheim, reported the development of an HTS experiment which allowed a massive screening that led to the identification of compound **2**, with an IC_{50} value of 1.6 µM, which was selected as an attractive starting point for the development of a new class of immunosuppressive drugs, since it induced dose-dependent lymphopenia in mice, with reduction levels similar than those described for the reference compound FTY720.[34]

Very recently, AbbVie reported the discovery of isoxazolecarboxamide **4a**, which behaved as a low micromolar S1PL inhibitor (*in vitro* IC_{50} = 1 µM, cell IC_{50} = 1.8 µM). Contrary to compound **3a,** the enantiomer (*S*)-**4a** (IC_{50} = 485 nM) was 2-fold more potent than the racemate, while the enantiomer (*R*)-**4a** was inactive. After a hit-to-lead process around **4a**, compounds **4b** and **4c** were reported as potent S1PL inhibitors (for **4b**: *in vitro* IC_{50} = 120 nM, cell IC_{50} = 230 nM; for **4c**: *in vitro* IC_{50} = 590 nM, cell IC_{50} = 240 nM), but with moderate metabolic stability.[51,52] All these structures are shown in Figure 1.9. Likewise, several S1PL potential inhibitors based on a virtual screening approach, have been suggested.[53]

However, Schümann *et al.* reported that both genetic and pharmacologic inhibition of S1PL in rodents resulted in kidney toxicity, skin irritation and platelet activation, among other effects. These results may limit the treatment of autoimmune diseases with S1PL inhibitors, if similar effects are observed in humans.[54]

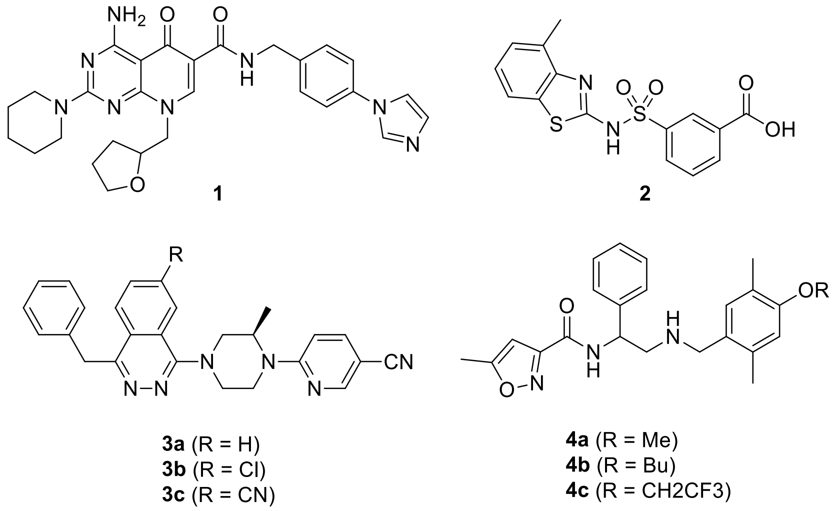

1

2

3a (R = H)
3b (R = Cl)
3c (R = CN)

4a (R = Me)
4b (R = Bu)
4c (R = CH2CF3)

Figure 1.9. Non lipidic S1PL inhibitors.

1.6 Mechanism-based inhibitors

Mechanism-based inhibitors are a type of irreversible inhibitors, generally competitive with the enzyme substrate, that give rise to a prolonged enzyme blockade *via* covalent bond formation. Unlike affinity labelling reagents (that initially bind reversibly to the active site of the enzyme prior undergoing covalent bond formation), mechanism-based inhibitors are unreactive compounds that bear a structural similarity to the substrate of a specific enzyme and are converted by the normal catalytic mechanism of that enzyme into a product that, before its release, inactivates the enzyme. Hence, these compounds act initially as substrates for the target enzyme and are also commonly referred to as suicide substrates.

Mechanism-based inhibitors can be very specific for the target enzyme, or at the very least, highly selective for a family of enzymes that catalyze a common reaction. Therefore, molecules that act through this type of inactivation mechanism can be quite useful in human medicine.[55]

As indicated above, in 1994, Boumendjel and Miller described the S1PL mechanism-based inhibitor **2VS1P**, as a mixture of isomers, with an IC_{50} of 2.4 µM in rat liver microsomal preparations as enzyme source (Figure 1.8).[38] The mechanism of this inhibitor was suggested to be similar to that found for other PLP-dependent enzymes, such as amino acid decarboxylases that are inhibited by α-amino derivatives bearing an unsaturation in the β,γ-position. A classic example of this type of inhibitors is found in Vigabatrin (Structure **5** in Figure 1.10), a GABA amino transferase (GABA-AT) inhibitor approved as antiepileptic drug. By the action of GABA-AT, the resulting intermediate Michael acceptor **7** (Figure 1.10) can irreversibly block the essential Lys329 present at the enzyme active site, thus giving rise to an irreversible enzyme blockade.[56]

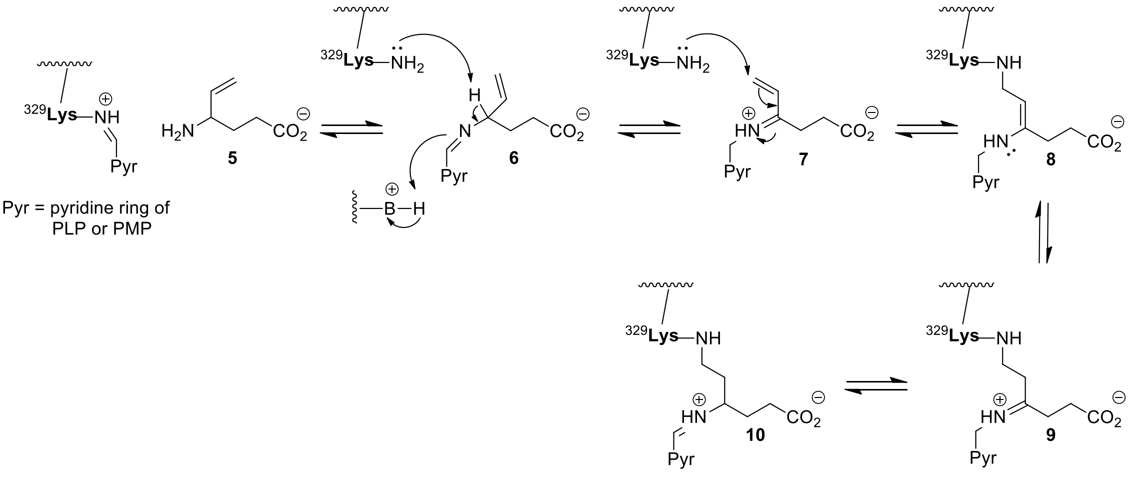

Figure 1.10. Mechanism-based inhibition of GABA-AT by Vigabatrin (**5**).[56]

More recently,[57,58] a series of cyclic analogues of GABA incorporating a fluoro or difluoromethylene unit have corroborated the above mechanism.

1.7 General objectives

Based on these precedents, we reasoned that compounds **24**, which should be regarded as trimmed analogues of **2VS1P** (Figure 1.8)**,** should elicit a mechanism-based inhibition profile towards S1PL. In the light of the above mechanistic considerations, it is conceivable that the presence of the vinyl group gives rise to the highly reactive electrophilic intermediate **26** able to form an irreversible covalent bond by a Michael-type reaction with a nucleophilic residue close to the enzyme active site. The formation of this new bond would account for the irreversible inhibition expected for this family of compounds (Figure 1.11).

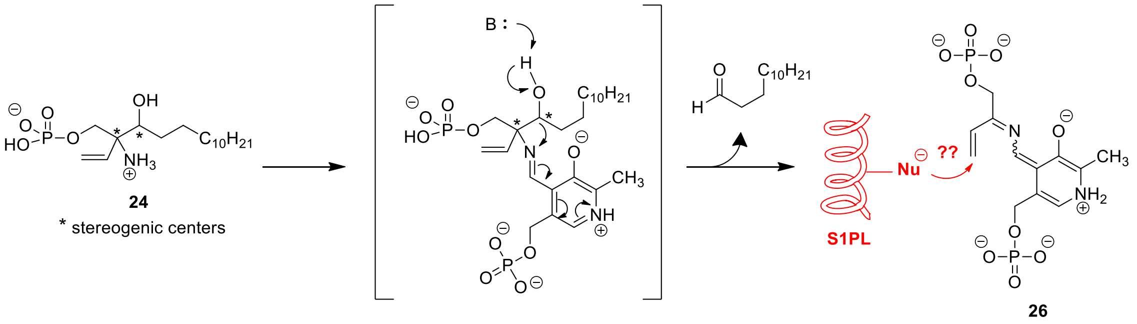

Figure 1.11. Proposed inhibition mechanism for the stereoisomers of **24** on S1PL.

The development of irreversible enzyme inhibitors, apart from their unquestionable use as pharmacological tools, is gaining relevance in drug design to broaden the opportunities provided by targeted covalent inhibitors.[59]

Taking into account all the above considerations, the following objectives for the present doctoral thesis were considered:

A. The synthesis of the four stereoisomers of 2-vinyl phosphates **24** and their corresponding Sa (**31**), So (**JG**) and Cer (**48** and **52**) analogues shown below.

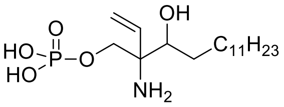
OH
O
HO
HO
P
O
C11H23
NH2

24

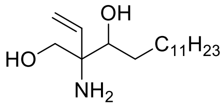
OH
HO
C11H23
NH2

31

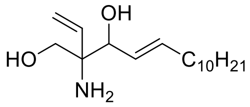
OH
HO
C10H21
NH2

JG

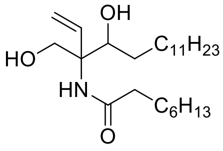
OH
HO
C11H23
HN
C6H13
O

48

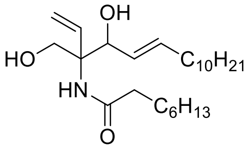
OH
HO
C10H21
HN
C6H13
O

52

B. Study the inhibitory profile of **24, JG** and **31** against bacterial and human S1PL.

C. Analysis of the sphingolipidome profile in selected cell lines for the most relevant analogues obtained in objective A.

2. RESULTS AND DISCUSSION

2.1 Approaches to enantiopure 2-vinyl sphingolipids from non-chiral or racemic precursors

Note: Along this Chapter, for the sake of clarity, we refer to each isomer according to the configuration deduced from the experiments described in detail in sections 2.1.5 and 2.1.10.

2.1.1 Diastereoselective synthesis of (±)-*syn* and (±)-*anti*-2-vinyl aminophosphates 24

The synthesis of enantiomerically pure 2-vinyl sphingolipids required a highly versatile building block to allow the access to all different stereoisomers of the modified sphingoid base. The reported building block **15** (Scheme 2.1.1),[60] which provides the needed functional groups to build the polar head of the sphingolipid scaffold, together with a prostereogenic center, was selected for this purpose. Besides, building block **15** is easily synthesized starting from a cheap and commercially available starting material (Tris), as described in the literature.[61] Thus, a simple and direct synthesis of **15** was carried out by submitting Tris to *tert*-butoxycarbonylation and acetalization in a one-pot process to give alcohol **12**, followed by oxidation to aldehyde **13** in 82% combined yield.[61] Wittig olefination of aldehyde **13** gave **14** in 89% yield, which was converted to diol **15** by acetal hydrolysis in quantitative yield.[60]

The *N*-Boc-protected aminodiol **15** contains the required 2-amino-2-vinyl-1,3-diol polar head of our required sphingolipid analogs. In order to introduce the sphingoid chain, transformation of **15** into aldehyde (±)-**17**, followed by a Grignard reaction with an alkylmagnesium halide was considered. One of the approaches tested for the synthesis of (±)-**17** was the oxidation of the free hydroxyl group of carbamate (±)-**16**, obtained from the intramolecular base-induced cyclization of **15**. Unfortunately, none of the oxidation conditions tested (see Table 2.1.1) afforded the desired aldehyde (±)-**17** and the starting material was recovered in all cases (All these reactions are summarized in Scheme 2.1.1).

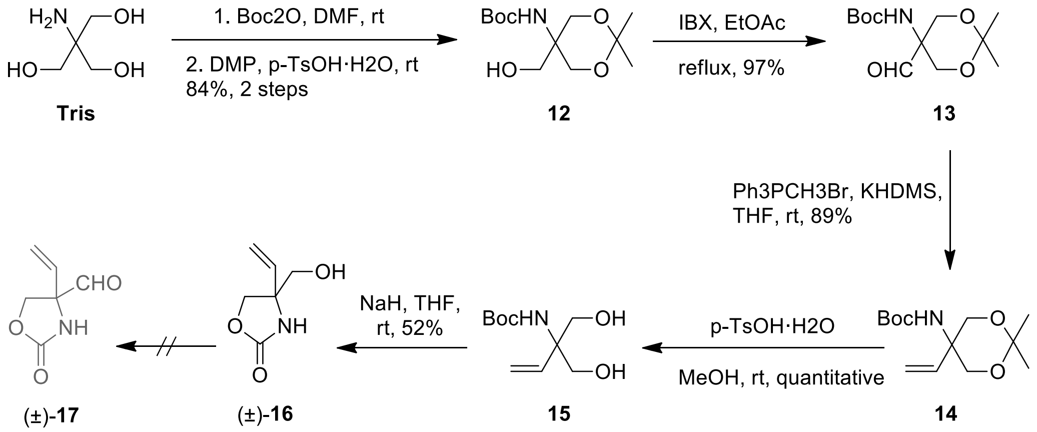
H2N
OH
HO
OH
Tris
1. Boc2O, DMF, rt
2. DMP, p-TsOH·H2O, rt
84%, 2 steps
BocHN
O
HO
O
12
IBX, EtOAc
reflux, 97%
BocHN
O
OHC
O
13
Ph3PCH3Br, KHDMS,
THF, rt, 89%
BocHN
O
O
14
p-TsOH·H2O
MeOH, rt, quantitative
BocHN
OH
OH
15
NaH, THF,
rt, 52%
OH
O
NH
O
(±)-16
CHO
O
NH
O
(±)-17

Scheme 2.1.1. Synthetic route for building block **15** and attempted synthesis of aldehyde (±)-**17**.

Oxidant	Equiv/mol.	Solvent	T (ºC)	Time (h)
IBX	1.5	EtOAc	80	16
IBX	3	EtOAc	80	16
PCC	1.5	CH_2Cl_2	30	16
PDC	2	CH_2Cl_2	30	16
$(COCl)_2$ DMSO	2.5 3	CH_2Cl_2	25	16

Table 2.1.1. Attemps to oxidize alcohol (±)-**16** to aldehyde (±)-**17**.

Due to the lack of reactivity of alcohol (±)-**16**, another synthetic approach was devised. In this case, diol **15** was monosilylated to give (±)-**18** in 84% yield and the resulting free alcohol was subsequently oxidized with IBX to afford aldehyde (±)-**19** in 87% yield (Scheme 2.1.2).

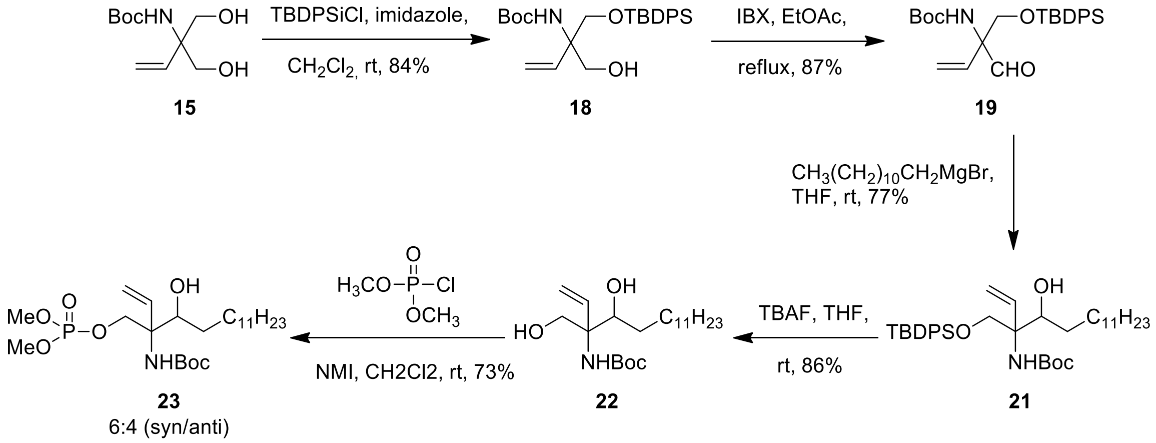
BocHN
OH
OH
15
TBDPSiCl, imidazole,
CH2Cl2, rt, 84%
BocHN
OTBDPS
OH
18
IBX, EtOAc,
reflux, 87%
BocHN
OTBDPS
CHO
19
CH3(CH2)10CH2MgBr,
THF, rt, 77%
TBDPSO
OH
C11H23
NHBoc
21
TBAF, THF,
rt, 86%
HO
OH
C11H23
NHBoc
22
H3CO-P-Cl
O
OCH3
NMI, CH2Cl2, rt, 73%
MeO
MeO
P-O
O
OH
C11H23
NHBoc
23
6:4 (syn/anti)

Scheme 2.1.2. Synthetic route for dimethyl phosphate esters **23**.

In order to optimize the Grignard addition to aldehyde (±)-**19** (Scheme 2.1.2), the commercially available *n*-dodecylmagnesium bromide was used. Despite this leads to a C15 sphingoid base analog (or C17, taking into account the vinyl substituent), we considered not necessary at this point of the project the homologation of the alkyl chain to match the natural sphingolipid chain length. A comparative docking analysis of the C15 *vs* C18 analogs, using the human S1PL (hS1PL) as template,[34] showed comparable results in terms of docking scores (see section 2.3.6).

Addition of a 1M THF solution of commercial dodecylmagnesium bromide to aldehyde (±)-**19** led to the expected sphingoid analog **21** as a mixture of diastereomers in low yield (around 30%), together with large amounts of *n*-dodecanol as a by-product. After several tests, we concluded that *n*-dodecanol was formed by hydrolysis of the corresponding alkoxide, already present (in around 50%) as an oxidation by-product of the Grignard reagent in the commercial solution. The oxidation of Grignard reagents by oxygen is a well-known reaction,[62] which, in our case, could be minimized by using a freshly prepared reagent. This led to a considerable improvement of the reaction yield (around 80% for **21**, obtained as an unseparable 7:3 (±)-*syn/*(±)-*anti* mixture of diastereomers) and the almost negligible presence of *n*-dodecanol in the crude reaction mixtures after protic quenching. Attempts to isolate *syn* and *anti* isomers using semi-preparative HPLC (PDA detector) were not satisfactory. Thus, under isocratic conditions (5:95, H_2O:AcN, 30 mL/min), (±)-*syn*-**21** (Rt: 26.8 min) and (±)-*anti*-**21** (Rt: 24.7 min) could be isolated albeit in low yields (14% and 10%, respectively) with a remaining 76% of mass corresponding to the starting mixture of diastereomers. In light of the low efficiency of this chromatographic separation, the mixture (±)-*syn/*(±)-*anti*-**21** was used in the subsequent synthetic step. In this way, **21** was desilylated to give **22** in 86% yield. Phosphorylation of the primary hydroxyl group of **22** gave the desired dimethyl phosphates **23** in 73% yield as a 6:4 *syn*/*anti* mixture of diastereomers (Scheme 2.1.2), which could be separated by careful flash chromatography, as indicated in the experimental section.

In order to simplify the notation of our vinyl analogs, the *syn*/*anti* stereochemical descriptors will be used throughout the text. According to Masamune,[63] if the two substituents of highest priority are on the same side of the plane in a zig-zag projection, the relative configuration is termed *syn*, whereas if they are on opposite sides, they are called *anti*. In the case of adjacent substituents, the *syn* isomer is equivalent to the *threo* isomer, while the *anti* isomer is equivalent to the *erythro* isomer, as shown in Figure 2.1.1.

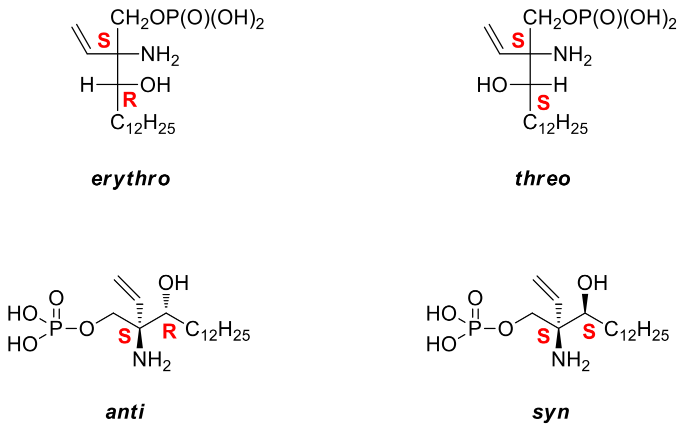

Figure 2.1.1. Designation of the relative configurations of **23** as *syn*/*anti*, according to Masamune.[63]

The chromatographic separation of *N*-Boc phosphate diesters (±)-*syn*-**23** and (±)-*anti*-**23** allowed the synthesis of aminophosphates (±)-*syn*-**24** and (±)-*anti*-**24** in a subsequent step. As shown in Scheme 2.1.3, the simultaneous deprotection of the *N*-Boc and the methyl phosphate diester groups of either (±)-*syn*-**23** or (±)-*anti*-**23** in a one-pot, two-step process with TMSBr,[64] followed by methanolysis, led to aminophosphates **24** in moderate yields. Unfortunately, formation of carbamates **34** (around 30% yield) was also observed as a result of the simultaneous dephosphorylation and cyclization of **23**. The formation of **34** can be explained as shown in Scheme 2.1.3. Our suggested mechanism is based on the ability of the TMS group to bind the P-O oxygen to generate an oxonium cation, followed by intramolecular nucleophilic displacement by the carbonyl *N*-Boc group and subsequent loss of isobutene prior to methanolysis. Interestingly, the formation of carbamates related to **34** had not been observed from substrates lacking the vinyl group, as reported in previous works of our group.[65] Moreover, the propensity of this type of vinyl derivatives to undergo intramolecular cyclizations will be highlighted in section 2.1.5.2 with the formation of the also cyclic structure **33**.

Considering their high polarity and low solubility, the purification of compounds **24** was troublesome. Precipitation of **24**, as reported in the literature for related amino phosphates,[38] was unsuccessful due to co-precipitation with **34**. Fortunately, chromatography using Amberlite™ XAD-4 as support, allowed the isolation of **24** free from the by-products of the deprotection reaction, mainly carbamate **34** and methoxy trimethylsylane (see Scheme 2.1.3).

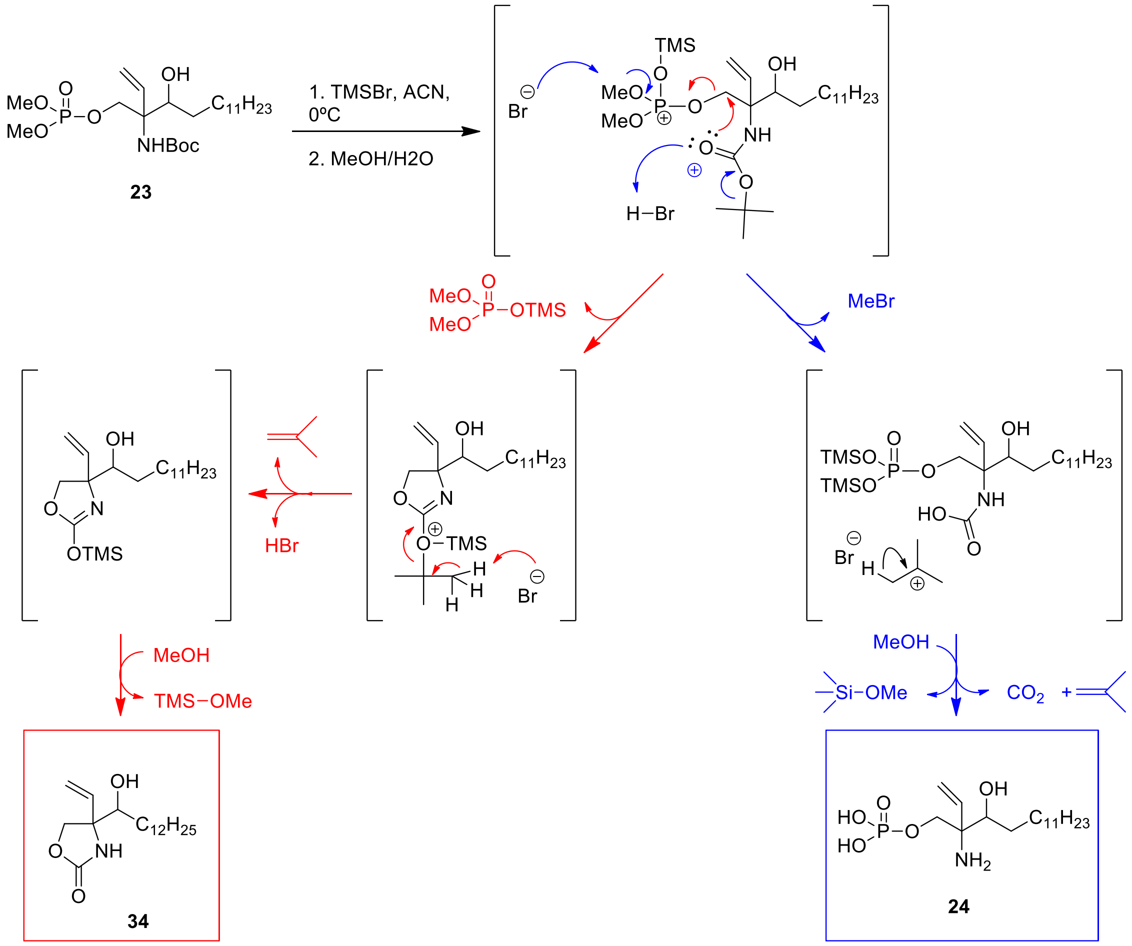

Scheme 2.1.3. Two-step, one-pot deprotection of N-Boc phosphates **23** (*syn* or *anti*) with TMSBr. In blue, the postulated mechanism of phosphate ester dealkylation with TMSBr; in red, our suggested mechanism leading to carbamate **34**.

Other common reported methods to hydrolyze phosphate esters[66] were considered, although they were not tested for several reasons. Thus, the use of benzyl phosphate esters as precursors was also disregarded due to the incompatibility of the required hydrogenolysis with the presence of the vinyl group in our target amino phosphates **24**. On the other hand, the long process to obtain **23** left us with a shortage of product to undertake enough assays in order to optimize the final deprotection.

At this point, we considered of interest the synthesis of the target 2-vinyl dihydrosphingosines analogue **31** (as mixture of isomers) for preliminary biochemical studies. As shown in Scheme 2.1.4. **31** was obtained from **21** (mixture of isomers) by the simultaneous deprotection of the TBDPS and the *N*-Boc groups under mild acidic conditions. Using this protocol, **31·HCl** was obtained as a mixture of isomers in nearly quantitative yield.

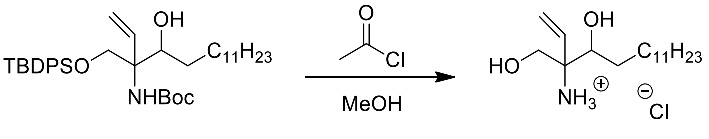

OH
TBDPSO
C₁₁H₂₃
NHBoc
O
Cl
MeOH
HO
NH₃
Cl

21 **31**

Scheme 2.1.4. Synthesis of **31·HCl** from **21** (mixture of isomers).

2.1.2 Use of lipases for the desymmetrization of diol 15

The synthetic sequence described in the previous section, starting from the prochiral diol **15**, would be potentially useful for the synthesis of enantiopure vinyl sphingolipids, provided we were able to carry out an efficient desymmetrization of the starting material. In this context, the use of lipases was considered.

The desymmetrization of prochiral diol **15** is reported in the literature[60] using a *Pseudomonas sp.* from WAKO. Under the described conditions, the kinetic resolution of **15** (Scheme 2.1.5) with vinyl acetate in diisopropyl ether affords the corresponding enantiopure monoaceate **60** in an excellent 97% ee and 94% yield.

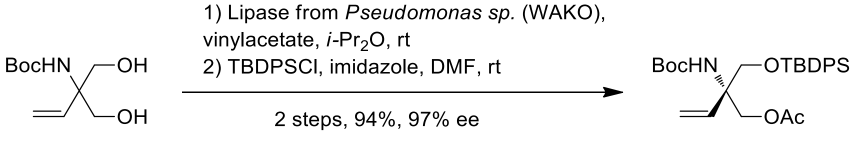

1) Lipase from Pseudomonas sp. (WAKO), vinylacetate, i-Pr₂O, rt
2) TBDPSCl, imidazole, DMF, rt
2 steps, 94%, 97% ee
BocHN
OH
OH
BocHN
OTBDPS
OAc

15 **60**

Scheme 2.1.5. Reported desymmetrization of **15**.

Unfortunately, the described lipase is no longer commercially available and all the different alternative lipases tested gave negative results. 20 mg of lipases from *Thermomyces lanuginosus* (TL) supported on EP100 or *Candida antarctica* lipase B (CALB) were incubated with 12 mg of **15** in 1 mL of diisopropyl ether and 12 μL of vinyl acetate at room temperature under magnetic stirring during 24h. The reaction was monitored by TLC but no desymmetrization was found and less than 50% of the sample was acetylated.

2.1.3 Chemical resolution of synthetic intermediates

After the previous failed attempt of desymmetrization of **15**, the chiral resolution of the monoprotected diol (±)-**18** (Scheme 2.1.6) by chiral HPLC was explored. Several attempts using a series of analytical chiral HPLC columns (columns C, D and E, in mixtures of hexane/isopropanol as eluent, see experimental section) in a PDA detection system were tried. Unfortunately, none of the attempts were promising enough to pursuit the chiral resolution of (±)-**18** at preparative scale using this approach.

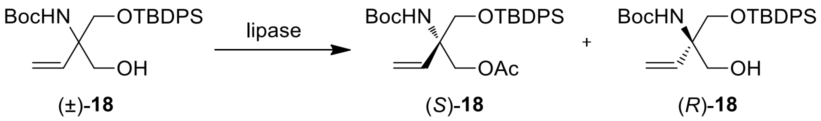

Scheme 2.1.6. Devised kinetic resolution for (±)-**18**.

Hopefully, in our group is being carried out the kinetic resolution of (±)-**18**, which is wanted to be acetylated with lipases that are selective for one of the enantiomers (Scheme 2.1.6). The preliminary results are encouraging and a few lipases with an acceptable resolution ratio have been tested.

Alternatively, the chiral resolution of (±)-*syn*-**23** and (±)-*anti*-**23** was next considered. Several eluting systems were tested using a Daicel Chiralpack IB (5 µm 4.6 x 250 mm) column stationary phase with an ELS detector. The best results were obtained for (±)-*syn*-**23**, for which around 1 minute separation was observed for the two enantiomers under gradient conditions (from 1 to 4 % of isopropanol in 35 min), although the baseline was not reached. In contrast, a much poorer resolution was observed for (±)-*anti*-**23** in the same elution conditions (Figure 2.1.2). These results were considered not good enough for their adaptation to a semipreparative or preparative scale and the approach was abandoned.

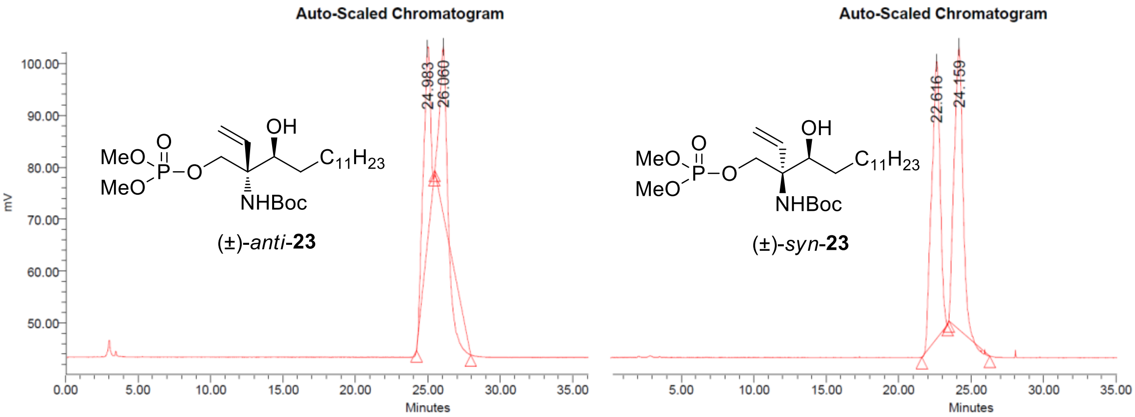

Figure 2.1.2. HPLC-ELS chromatogram of an (±)-*anti*-**23** (left) and (±)-*syn*-**23** (right) (Daicel chiralpack IB (5 µm 4.6 x 250 mm) column, 1 to 4 % isopropanol in hexanes at 1mL/min).

2.1.4 Simultaneous separation and resolution of (±)-*syn* and (±)-*anti*-21 by derivatization as MPA esters

In an attempt to find a chromatographic separation system for (±)-*syn* and (±)-*anti*-**21** (see section 2.1.1), we found that derivatization with (*R*)-α-methoxyphenylacetic acid [(*R*)-MPA] led to esters **25**, which could be partly separated by flash chromatography. Interestingly, the use of (*R*)-MPA as chiral derivatizing reagent should allow the resolution of each enantiomeric pair through the corresponding diastereomeric (*R*)-MPA esters. [67]

The derivatization of **21** was carried out using the standard Steglich esterification conditions in the presence of DMAP (1.1 equiv), as indicated in Scheme 2.1.7.

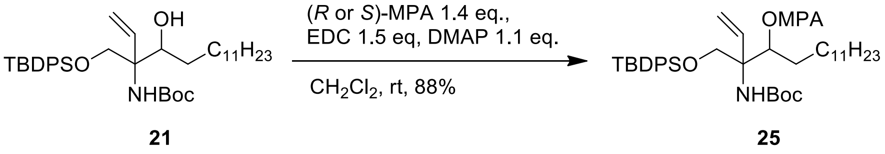

Scheme 2.1.7. General procedure for the derivatization of **21** (mixture of isomers) with (*R*) or (*S*)-MPA.

After several attempts, we were able to find the optimal chromatographic conditions (Hexane/MTBE 95:5, v:v) for the observation of four separate spots on TLC (Figure 2.1.3). However, these conditions were not fully effective for flash chromatography, since only the upper (**25**[(*R*)(-)*anti*-**21**][1], 16 % yield) and the lower (**25**[(*R*)(-)syn-**21**], 19% yield) spots could be isolated as single isomers, as judged by their ^{1}H NMR spectra. The middle fractions were obtained as an inseparable mixture of **25**[(*R*)(+)syn-**21**] and **25**[(*R*)(+)anti-**21**] (28% yield), together with an additional 25% of other unidentified reaction by-products.

---

[1] **25**[(*R*)(-)*anti*-**21**] stands for the isomer of compound **25** resulting from the esterification of (-)-*anti*-**21** with (*R*)-MPA. The same notation is used for the remaning stereoisomers.

Analogously, the use of (*S*)-MPA as chiral derivatizing reagent afforded an identical, *but enantiomeric*, chromatographic pattern in comparison to that observed for the (*R*)-MPA esters. Therefore, as shown in Figure 2.1.3, the combination of both series of MPA esters would allow the chemical resolution of **21** via the corresponding (*R*) or (*S*)-MPA esters **25**, after isolation of the upper and lower spots by flash chromatography and MPA removal. Likewise, the corresponding enantiopure aminoalcohols *syn*-**31** and *anti*-**31** can also be obtained after removal of the derivatization reagent and the protecting groups (Scheme 2.1.8).

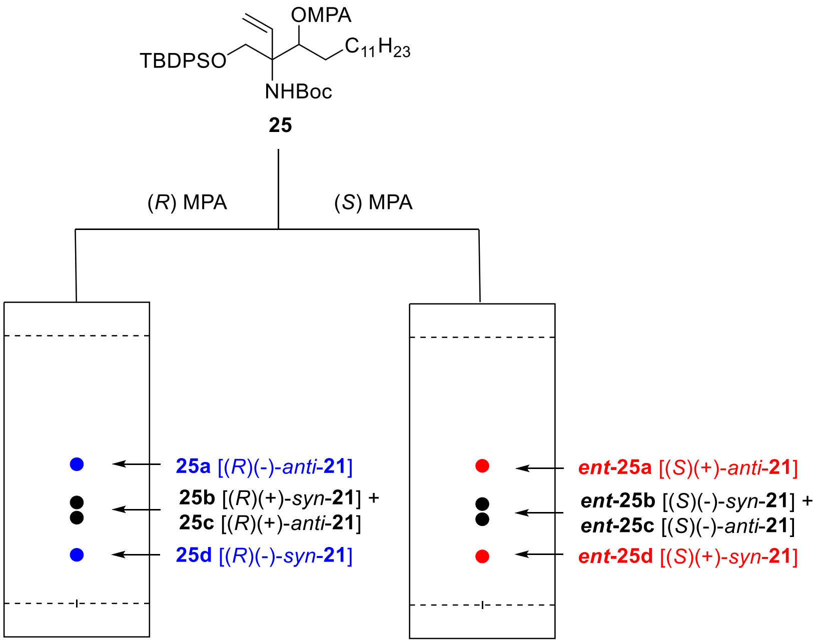

Figure 2.1.3. TLC pattern for the derivatization of **25** as (*R*)-MPA and (*S*)-MPA esters. Isomers corresponding to the blue and red spots could be isolated in pure form, while isomers in black were isolated as mixtures after flash chromatography.

On the other hand, by independently converting each of the middle fractions of mixtures of *syn/anti*-**25** into the easily separable diastereomeric phosphates **23** (see section 2.1.1), the synthesis of enantiomerically pure amino phosphates **24** would be feasible, as indicated in section 2.1.1 for the racemic series. All these transformations are summarized in Scheme 2.1.8.

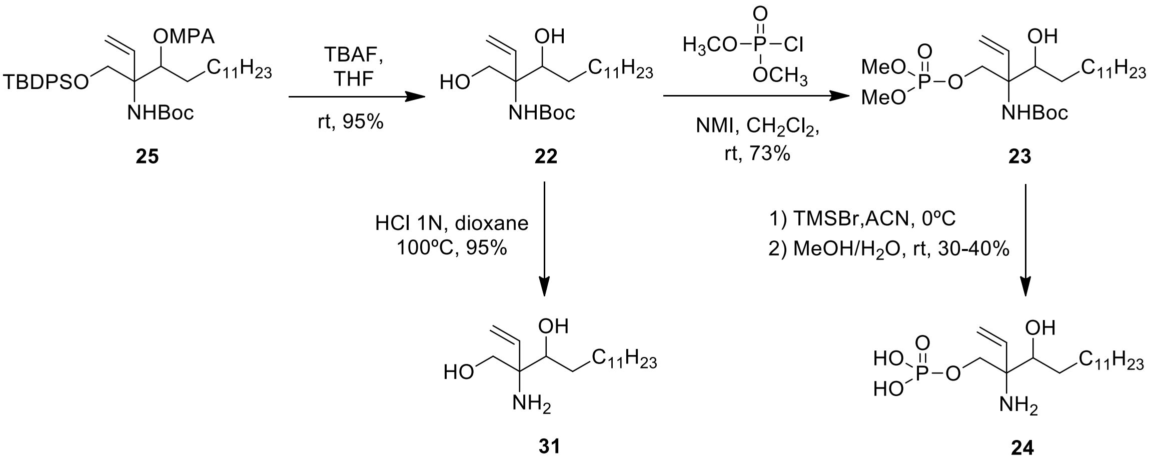
TBDPSO
OMPA
C11H23
NHBoc
25
TBAF, THF
rt, 95%
HO
OH
NHBoc
22
H3CO−P−Cl
OCH3
NMI, CH2Cl2, rt, 73%
MeO
MeO
P−O
23
HCl 1N, dioxane
100ºC, 95%
1) TMSBr,ACN, 0ºC
2) MeOH/H2O, rt, 30-40%
NH2
31
HO
HO
24

Scheme 2.1.8. Transformation of **25** into **31** (2-vinyl dihydrosphingosine) and **24** (2-vinyl dihydrosphingosine-1-phosphate).

Conditions for the simultaneous deprotection of the MPA ester and the TBDPS group of **25** were found by using 2.5 equiv/mol of a 1 M solution of Bu_4NF in THF. Despite the mechanism of the ester removal under these conditions has not been fully elucidated. Zheng *et al.*[68] suggested a E_2 type elimination by means of fluoride promoted abstraction of the acidic carbonyl Cα proton, as shown in Scheme 2.1.9. Likewise, one of the Cα protons of the ammonium salt would play the role of the acid catalyst required to activate the carbonyl ester group for the elimination reaction. This double deprotection afforded the corresponding *N*-Boc diols **22** in excellent yields.

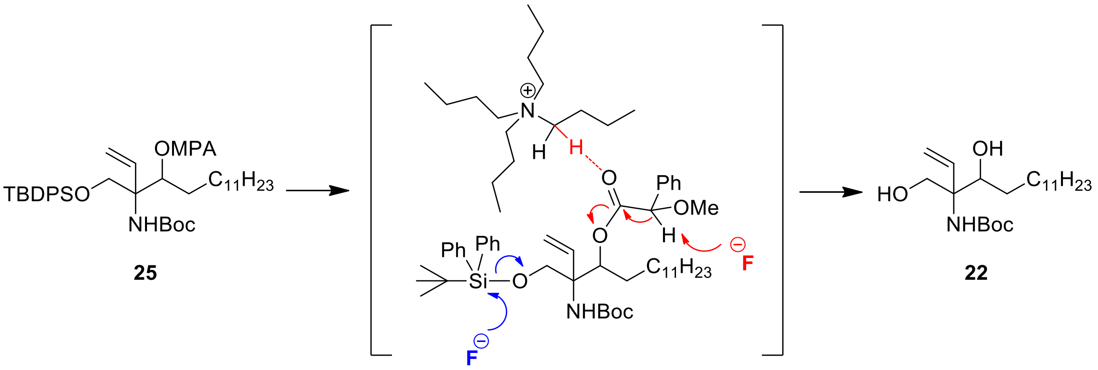
TBDPSO
OMPA
C11H23
NHBoc
25
N
H
H
O
Ph
OMe
H
F
Ph
Ph
Si
O
C11H23
NHBoc
F
HO
OH
C11H23
NHBoc
22

Scheme 2.1.9. In blue, the accepted mechanism for silyl ether deprotection. In red, the proposed mechanism for MPA deacylation of **25** with TBAF.

With enantiomerically pure *N*-Boc amino alcohols **22** in hand, their conversion into free amino diols **31**, amino phosphates **24** (scheme 2.1.8) and ceramides **48** became feasible, as it will be indicated in section 2.1.12. However, although the four enantiomers of **22** could be obtained individually, this route was abandoned due to the poor overall yields of the chromatographic separation and chemical resolution of the MPA esters **25**. Thus, the long, tedious, and low yielding chromatographic separation of **25**, together with its little scalability, encouraged us to seek alternative, more efficient routes, as it will be discussed in section 2.1.7.

Finally, the specific optical rotations for the different stereoisomers of **23**, obtained according to this route, are the following:
anti-(2*S*,3*R*)-**23**: $[\alpha]_D$ +2.4 (c 1, $CHCl_3$)
anti-(2*R*,3*S*)-**23**: $[\alpha]_D$ -2.4 (c 1, $CHCl_3$)
syn-(2*R*,3*R*)-**23**: $[\alpha]_D$ +3.2 (c 1, $CHCl_3$)
syn-(2*S*,3*S*)-**23**: $[\alpha]_D$ -3.6 (c 1, $CHCl_3$)
These values provide evidences that probably no racemization has taken place in this synthetic route, in contrast with that observed in the route described in section 2.1.9 below.

2.1.5. Configurational assignments

The configurational assignment of the reaction intermediates of the above synthetic route was inferred from the configurations of phosphates **23** by the combination of two methods. First, the configuration at C_3 was deduced from application of the Riguera's rules[67] from the (*R*)- and (*S*)-MPA esters **32** (section 2.1.5.1, below). On the other hand, the configuration at C_2 was inferred from NOE experiments carried out on the cyclic carbamate **33**, obtained from an ester **32** of known configuration at C_3 (section 2.1.5.2, below).

2.1.5.1 Configuration at C_3 from phosphates 23

After the chromatographic separation of (±)-*syn* and (±)-*anti* **23**, each enantiomeric pair was derivatized with (S) and (*R*)-MPA, leading, in each case, to a separable mixture of diastereomers **32a,b** or ***ent*-32a,b,** respectively (Scheme 2.1.10). Interestingly, remarkable chemical shift differences for some key protons were observed between the diastereomeric pairs of (*R*) and (*S*)-MPA esters, which allowed the assignment of the absolute configuration at C_3, according to the method described by Riguera and coworkers[67] (Figure 2.1.4). It is worthy of mention that, in our case, the configurational assignment at C_3 from racemic *syn*-**23** could have also been carried out by derivatization with a single (*R*) or (*S*)-MPA, since both enantiomers of *syn*-**32** could be isolated as their corresponding MPA esters. In this way, for example, the ^{1}H-NMR spectrum of **32a** can be compared with that of ***ent*-32b** or with that of the spectroscopically identical **32b** (see Scheme 2.1.10). Along this line, in section 2.1.9 a related configurational assignment is carried out by derivatization with a single MPA ester. The same reasoning is applicable to racemic *anti*-**32.**

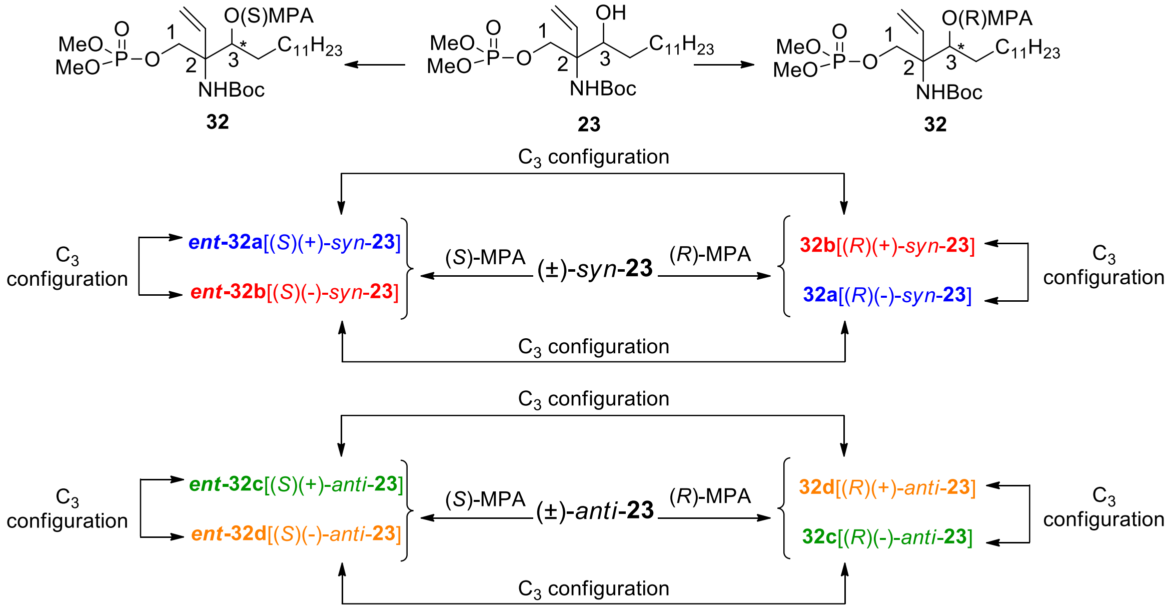
O(S)MPA
MeO
MeO
P
O
1
2
3
*
C11H23
NHBoc
32
OH
23
O(R)MPA
32
C3 configuration
C3 configuration
ent-32a[(S)(+)-syn-23]
ent-32b[(S)(-)-syn-23]
(S)-MPA
(±)-syn-23
(R)-MPA
32b[(R)(+)-syn-23]
32a[(R)(-)-syn-23]
C3 configuration
ent-32c[(S)(+)-anti-23]
ent-32d[(S)(-)-anti-23]
(±)-anti-23
32d[(R)(+)-anti-23]
32c[(R)(-)-anti-23]

Scheme 2.1.10. Conceptual approach for the assignment of the C_3 configuration for (+) and (-)-*syn*-**23**, via derivatization as (*R*) and (*S*)-MPA esters **32**. The configuration at C_3 can be inferred by comparing any of the blue and red pairs indicated in the Scheme. The same approach is also valid for (±)-*anti*-**23**.

Thus, the derivatization of (±)-*syn*-**23** with both (*S*)-MPA and (*R*)-MPA allowed the comparison of **32a** with **ent-32b**. According to the $\Delta\delta^{RS}$ values measured from the ^{1}H-NMR spectra for the protons close to C_3 in both diastereomers, it was deduced that (-)-*syn*-**23** corresponds to the C_3*S* configuration and, consequently, the configuration of (+)-*syn*-**23** must be C_3*R*. The same methodology was applied to the (±)-*anti* isomers. The $\Delta\delta^{RS}$ values of both diastereomers of **32** are collected in Table 2.1.2. This allowed the assignment of the absolute configuration of the secondary alcohol in C_3, as shown in Figure 2.1.4.

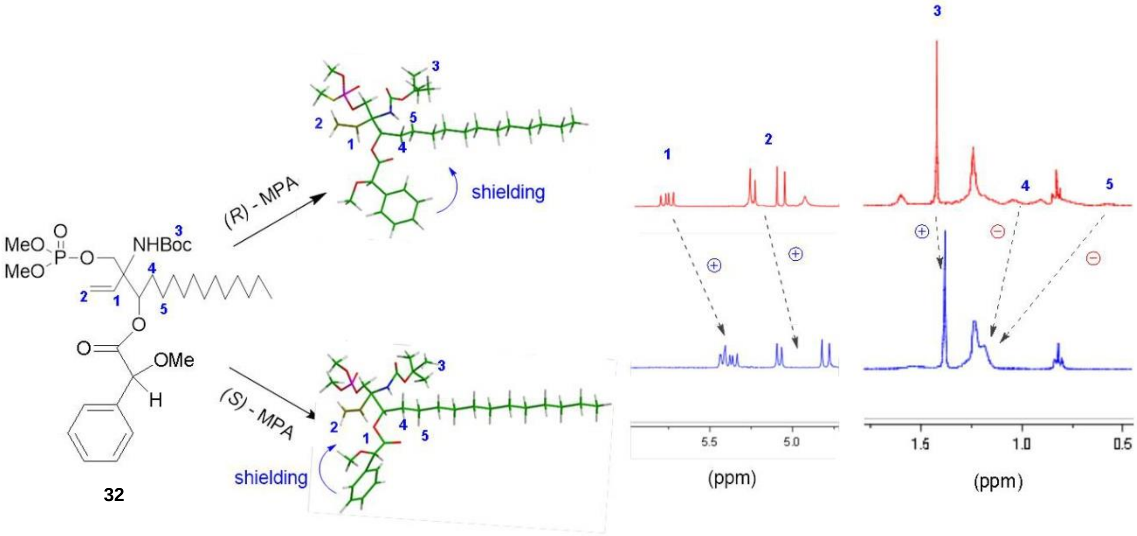
MeO
MeO
P
O
NHBoc
3
4
2
1
5
O
O
OMe
H
(R) - MPA
(S) - MPA
shielding
shielding
1
2
3
4
5
(ppm)
(ppm)
5.5
5.0
1.5
1.0
0.5

32

Figure 2.1.4. MPA effect in chemical shift depending on the enantiomer used in derivatization.

Absolute configuration ***S* at C3 for (-)-*syn*-23**: **32a**-(**ent-32b**)(see Scheme 2.1.10)

	δH_A(*)	δH_B(*)	δH_C(*)	δH_D	δH_E	δH_F	δH_G
32a[(*R*)-(-)-*syn*-**23**]	4.40	5.80	5.16	4.99	1.30	0.66	1.01
ent-32b[(*S*)-(-)-*syn*-**23**]	4.19	5.37	4.82	4.65	1.52	1.20	1.24
$\Delta\delta^{RS}$	+ 0.21	+ 0.43	+ 0.34	+ 0.34	- 0.22	- 0.54	- 0.23

The $\Delta\delta^{RS}$ values for **32b** - (***ent*-32a**) are opposite in sign to the data shown in this table.

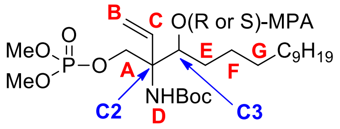
B
C
O(R or S)-MPA
MeO
MeO
P
O
O
A
E
G
C9H19
F
NHBoc
D
C2
C3

32

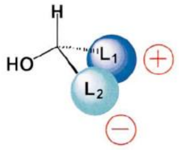

Absolute configuration ***R* at C3 for (+)-*anti*-23**: **32d**-(***ent*-32c**)(see Scheme 2.1.10)

	δH_A(*)	δH_B(*)	δH_C(*)	δH_D	δH_E	δH_F	δH_G
32d[(*R*)-(+)-*anti*-**23**]	4.20	5.38	4.83	4.66	1.57	1.21	1.25
***ent*-32c**[(*S*)-(+)-*anti*-**23**]	4.32	5.81	5.15	4.99	1.41	0.72	1.02
$\Delta\delta^{RS}$	- 0.12	- 0.43	- 0.32	- 0.33	+ 0.16	+ 0.49	+ 0.23

Table 2.1.2. $\Delta\delta^{RS}$ values in ppm of the diastereomers of **32** that allowed the assignment of the configuration at C3. The $\Delta\delta^{RS}$ values for **32c** - (***ent*-32d**) are opposite in sign to the data shown in this table. (*) δ from the center of the system.

2.1.5.2 Configuration at C2 from carbamate *syn*-33

The MPA method described in the previous section did not allow the determination of the absolute configuration of the quaternary center at C_2. In general, the configurational assignment of quaternary centers by NMR methods is not simple, and examples in the literature dealing with this issue are scarce.[69–71] In our case, we tried to solve this problem by carrying out NOE experiments from the cyclic carbamate (-)-*syn*-**33**, obtained accidentally while trying to remove the MPA ester from **32a** to obtain enantiopure (-)-*syn*-**23** (Scheme 2.1.11).

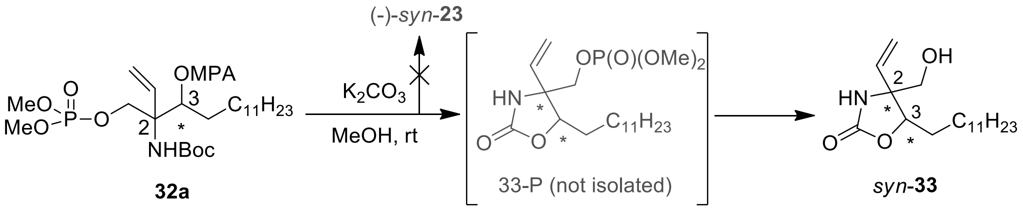

Scheme 2.1.11. Cyclic carbamate *syn*-**33** obtained from the basic hydrolysis of **32a**.

Unfortunately, this cyclization did not take place from the diastereomeric MPA esters in the *anti* series, which precluded, at this stage, an unambiguous configurational assignment at C_2. The regiochemistry of the cyclization step leading to *syn*-**33** was confirmed by analysis of the chemical shifts of the AB system of the -CH_2O- moiety (see Scheme 2.1.12). Thus, the observation of an AB system around 3.6 ppm was in agreement with the proposed structure, by comparison with carbamate **16** (see section 2.1.1). In addition, the AB system around 4.0 ppm, characteristic of carbamate **34** (section 2.1.1), was not observed. Formation of *syn*-**33** (Scheme 2.1.12). can be explained by the initial hydrolysis of the MPA ester and cyclization of the C_3-OH group onto the carbamate moiety, prior to or subsequent to phosphate hydrolysis that will be explained in more detail in section 2.1.6.

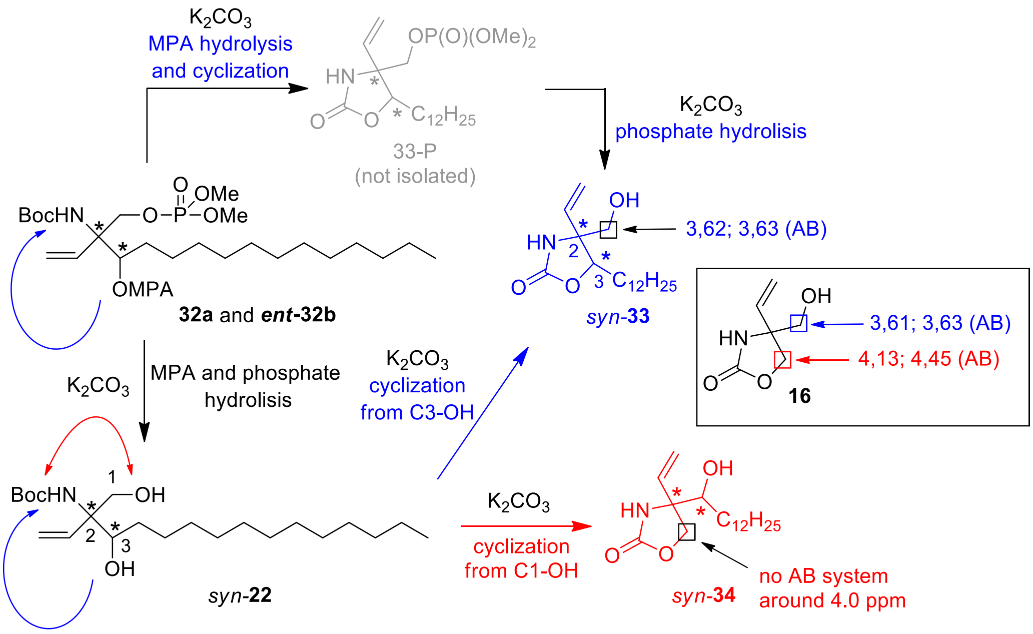
K_2CO_3
MPA hydrolysis
and cyclization
OP(O)(OMe)$_2$
HN
O
O
C$_{12}$H$_{25}$
33-P
(not isolated)
K_2CO_3
phosphate hydrolisis
OMe
BocHN
O-P-OMe
OMPA
32a and ent-32b
HN
OH
3,62; 3,63 (AB)
2
3
C$_{12}$H$_{25}$
syn-33
OH
HN
3,61; 3,63 (AB)
4,13; 4,45 (AB)
16
K_2CO_3
MPA and phosphate
hydrolisis
K_2CO_3
cyclization
from C3-OH
1
BocHN
OH
2
3
OH
syn-22
K_2CO_3
cyclization
from C1-OH
HN
OH
C$_{12}$H$_{25}$
syn-34
no AB system
around 4.0 ppm

Scheme 2.1.12. Postulated reaction pathways for the hydrolysis and cyclization of **32a** under basic hydrolysis.

As indicated above, NOE experiments from *syn*-**33** were performed in order to determine the relative configuration between C_2 and C_3. The observation of a NOE effect between the C_3H and the CH_2OH group at C_2 was indicative of a *cis* relationship between them (Figure 2.1.5). This relative configuration, combined with the 3*S* configuration previously assigned for this isomer by the above MPA method, ***allowed us to unambiguous assign compound syn-33 as the 2S,3S isomer and, hence, to confirm its relative syn configuration***. In agreement with the above correlation, the vinyl group at C_2 showed a weak NOE effect with the aliphatic chain and no correlation with C_3H.

However, since only a weak NOE effect (around 1-2%) was observed for *syn*-**33** and we were not able to obtain *anti*-**33** for comparative purposes, an alternative approach to unambiguously confirm the configuration at C_2 was foreseen.

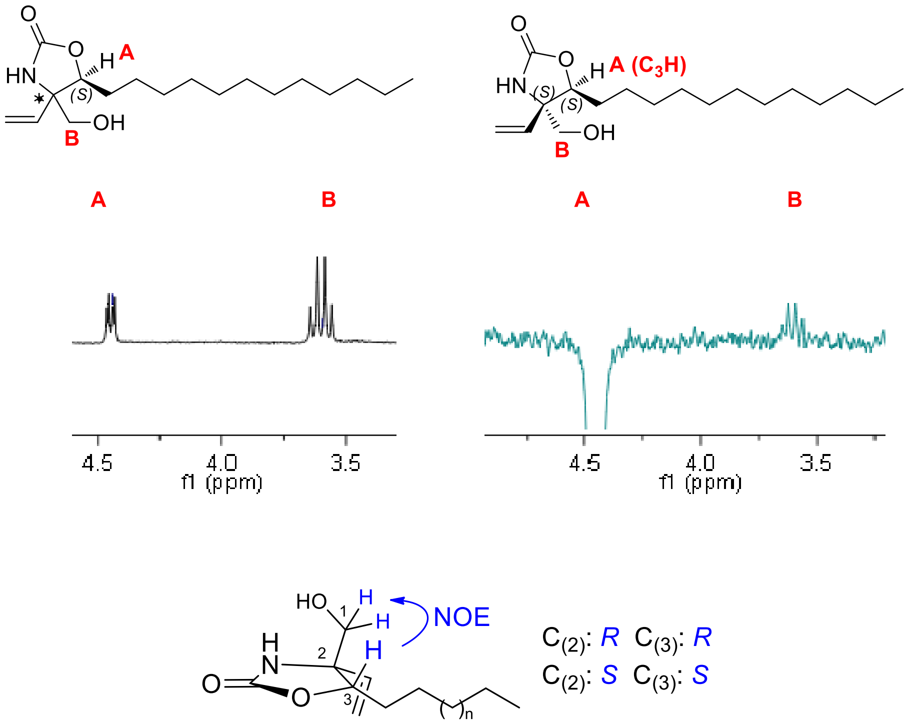

Figure 2.1.5. NOE effect observed between C_3H (A) and the hydroxymethyl group at C_2 (B) in *syn*-**33**, which indicates a *cis* relationship between them.

Thus, in the frame of a collaboration with Dr. Jordi Garcia's group (University of Barcelona, Department of Organic and Inorganic Chemistry), the required *anti*-**33** was synthesized, in a racemic form, by an adaptation of their previously developed methodology leading to the stereocontrolled construction of quaternary centers.[72] In this way, the hydroboration of allene **70** with dicyclohexylborane, followed by the stereoselective addition of the intermediate *Z*-allyborane to *n*-tridecanal, afforded oxazolidinone **71**, with the simultaneous *N*-to *O*- migration of the benzyl protecting group. Removal of the *O*-benzyl protecting group afforded oxazolidinone *anti*-**34**, which isomerized to *anti*-**33** in the presence of sub-stoichiometric amounts of DBU (Scheme 2.1.13).

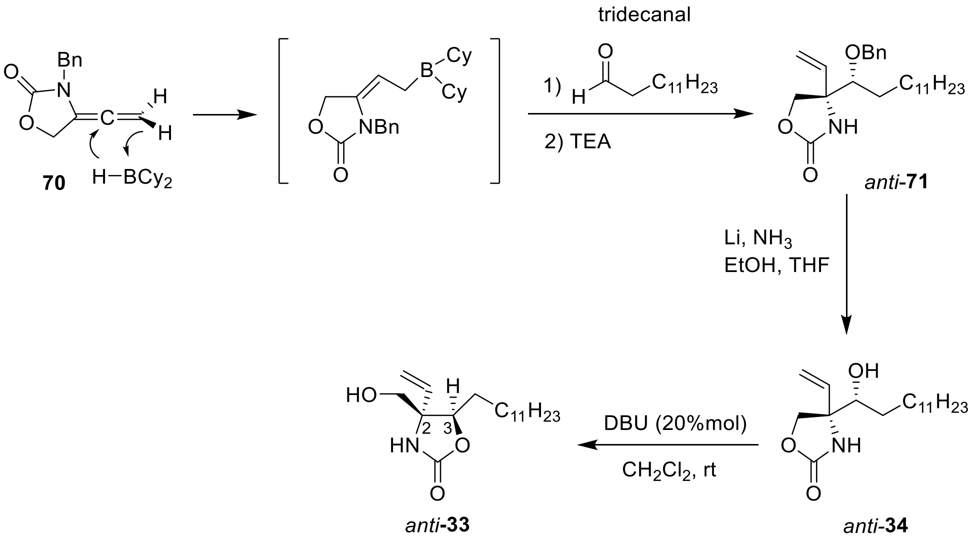
tridecanal
Bn
O
N
H
C
O
H
70
H−BCy2
Cy
B
Cy
O
NBn
O
1)
H
O
C11H23
2) TEA
OBn
C11H23
O
NH
O
anti-71
Li, NH3
EtOH, THF
OH
C11H23
O
NH
O
anti-34
DBU (20%mol)
CH2Cl2, rt
HO
H
C11H23
2
3
HN
O
O
anti-33

Scheme 2.1.13. Synthesis of *anti*-**33** by addition of tridecanal to a *Z*-allenylborane.

In this case, NOE experiments carried out with *anti*-**33** were in agreement with the expected spatial proximity between the C_3H and the vinyl group at C_2. Despite a weak 1% NOE enhancement with the vinyl CH proton was observed, the absence of any other NOE enhancements let us confirm the expected stereochemical assignment for *anti*-**33**.

With this result, the configurational assignments of the different stereoisomers of this synthetic route were confirmed.

2.1.6 Attempts to remove the MPA ester in phosphates 32

As indicated above, the hydrolysis of the MPA ester of phosphate **32a** and **32b** (and their enantiomers) with K_2CO_3 in MeOH led, unexpectedly, to the cyclic carbamate *syn*-**33**. This finding, which allowed the stereochemical assignment reported in section 2.1.5.2, turned out to be a serious drawback that seriously questioned the efficiency of the overall synthetic route, unless we were able to preserve the integrity of the phosphate group in this crucial step. Unfortunately, attempts to carry out the selective hydrolysis of the MPA ester from **32a** and **32b** were fruitless under most of the conditions tested (Table 2.1.3), since the required *syn*-**23** was obtained only in marginal yields in some experiments performed with LiOH as a base (entries 7 and 9).

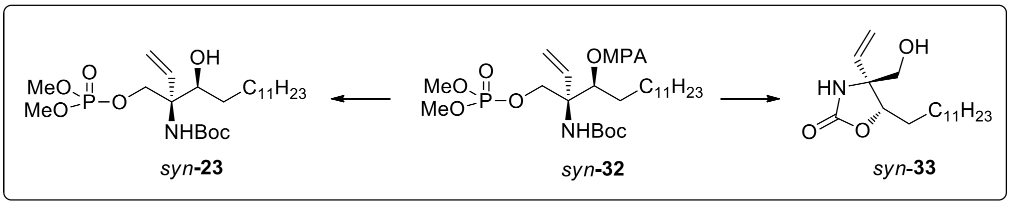

Entry	Reagents	Equiv /mol.	[M]	Compounds
1	K_2CO_3 / MeOH	4.5	0.4	*syn*-**33** (46% yield)
2	K_2CO_3 / MeOH	2	0.4	*syn*-**33** (32 % yield)
3	K_2CO_3 / MeOH	2	0.2	*syn*-**33** (19% yield)
4	1. TmsBr / AcN 2. MeOH / H_2O	9	0.07	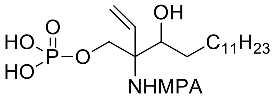
5	$NaBH_4$ / $CaCl_2$ / THF	4:2	0.8	Degradation products.
6	$NaBH_4$ / $CaCl_2$ / THF	4:2	0.3	Degradation products.
7	LiOH / H_2O / THF (5:13)	3	0.8	*syn*-**23** (10 % yield)
8	LiOH / H_2O / THF (5:13)	1.5	0.8	No reaction.
9	LiOH / H_2O / THF (5:13)	4	0.2	*syn*-**23** (20 % yield)
10	TBAF	2	0.04	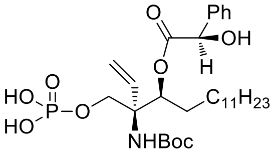

Table 2.1.3. Attempts to hydrolyze the MPA ester in phosphates **32a** and **32b**.

The MPA hydrolysis of the phosphate **32c** and **32d** in some of the above conditions (entries 1-3, 5 and 6) led only to degradation products.

In light of the above drawbacks, the use of lipases for the selective hydrolysis of the ester bond was considered. The following lipases were tested (all of them from Sigma-Aldrich, except otherwise indicated):

Rhizopus arrhizus (Fluka), *Candida rugosa*, *Rhizopus oryzae* (Fluka), *Mucor javanicus* (Fluka), PLE, Amano lipase from *Pseudomonas cepacia*, *Candida cylindracea* VII, Novozyme 871, Novozyme 435, Amano lipase A from *Aspergillus niger* and CAL B (Novozyme).

To a 5.0 mg/mL solution of **32** in dioxane was added 25.0 mg of the corresponding lipase in 2.0 mL of phosphate buffer. The mixture was incubated at 37ºC and stirred at 150 rpm in an orbital water bath for 24 hours. The reaction was monitored by TLC but, unfortunately, none of them were effective and starting **32a** and **32b** were recovered in all cases.

In summary, the results presented are indicative of the difficulties encountered for the chemical resolution of the key advanced intermediates **23**. These results prompted us to look for more efficient synthetic alternatives, which will be discussed in the following section. Nevertheless, this synthetic pathway allowed the assignment of the absolute configurations of the different synthetic intermediates described so far.

2.1.7 Vinyl Garner's aldehyde 42, a new building block for an alternative approach to enantiomerically pure 2-vinyl sphingolipids

Once determined the absolute configuration of some of the key reaction intermediates described in previous sections, an alternative synthetic pathway was designed in order to improve the efficiency of the enantioselective synthesis. In this context, we undertook the synthesis of building block (±)-**44**, an advanced precursor of what we will refer along this thesis dissertation as vinyl Garner's aldehyde (±)-**42** (Scheme 2.1.14). The rationale of this approach was based on the chiral resolution of alcohol (±)-**44**, whose rigidity was expected to be beneficial for the resolution process. Oxidation of enantiopure **44** would allow the access to enantiopure **42** and also to enantiopure 2-vinyl sphingolipids in subsequent steps.

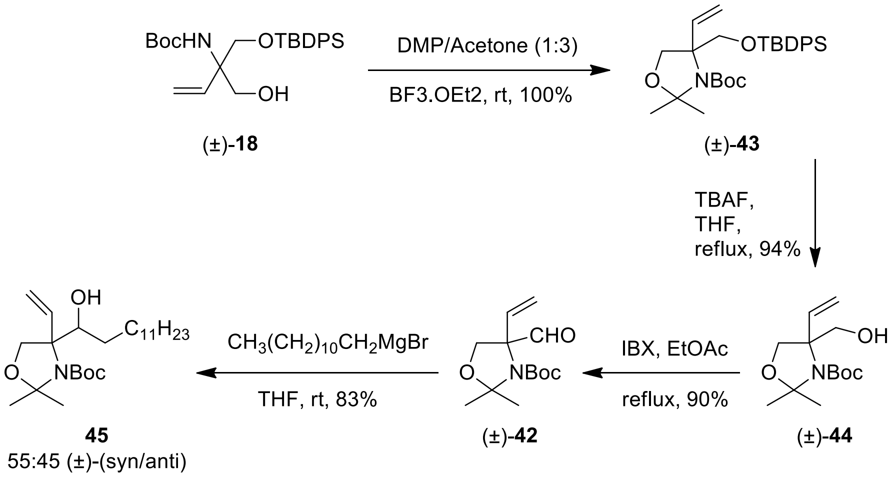
BocHN
OTBDPS
OH
(±)-18
DMP/Acetone (1:3)
BF3.OEt2, rt, 100%
OTBDPS
O
NBoc
(±)-43
TBAF,
THF,
reflux, 94%
OH
O
NBoc
(±)-44
IBX, EtOAc
reflux, 90%
CHO
O
NBoc
(±)-42
CH3(CH2)10CH2MgBr
THF, rt, 83%
OH
C11H23
O
NBoc
45
55:45 (±)-(syn/anti)

Scheme 2.1.14. Synthetic route to the building block (±)-**42** and the introduction of the aliphatic chain to obtain **45**.

Treatment of the monoprotected alcohol (±)-**18** with 2,2-dimethoxypropane (DMP) under acid catalysis afforded (±)-**43** in quantitative yield. This was desilylated to (±)-**44** with TBAF, in 94% yield, and the resulting free alcohol was oxidised with IBX to afford aldehyde (±)-**42** in 90% yield. Addition of *n*-dodecyl magnesium bromide to aldehyde (±)-**42** afforded **45** as a 55:45 mixture of (±)-*syn* and (±)-*anti* diastereomers (Scheme 2.1.14), which could be separated by careful flash chromatography, as indicated in the experimental section.

Although the relative *syn*/*anti* configuration for each diastereomer of **45** was not known at this stage, we use their configurational descriptors for the sake of clarity. Their configurational assignment was confirmed by spectroscopic methods (see section 2.1.10) and later corroborated by transformation of *syn* and *anti*-**45** into a configurationally known stereoisomer of **22** (see figure 2.1.6 and section 2.1.12). The absolute configuration of each of the stereoisomers of **22** had already been carried out as indicated in section 2.1.5.

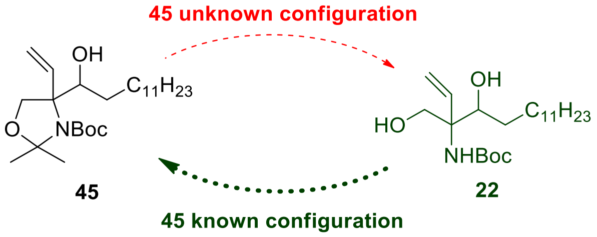
45 unknown configuration
OH
C11H23
O
NBoc
45
OH
HO
C11H23
NHBoc
22
45 known configuration

Figure 2.1.6: Conceptual approach for the configurational assignment of **45** through conversion into compound **22** of known configuration.

The uneventful oxidation of alcohol (±)-**44** into aldehyde (±)-**42** with IBX (Scheme 2.1.14) is in sharp contrast with the failure of alcohol (±)-**16** to undergo oxidation into aldehyde (±)-**17** (see Section 2.1.1 and Scheme 2.1.1). We were intrigued by this different behaviour in light of the structural similarity of (±)-**16** and (±)-**44**. At first glance, the only remarkable difference among them is the possibility of an intramolecular hydrogen bond between the hydroxyl oxygen (acting as donor) and the carbamate NH (acting as acceptor) in carbamate (±)-**16**.

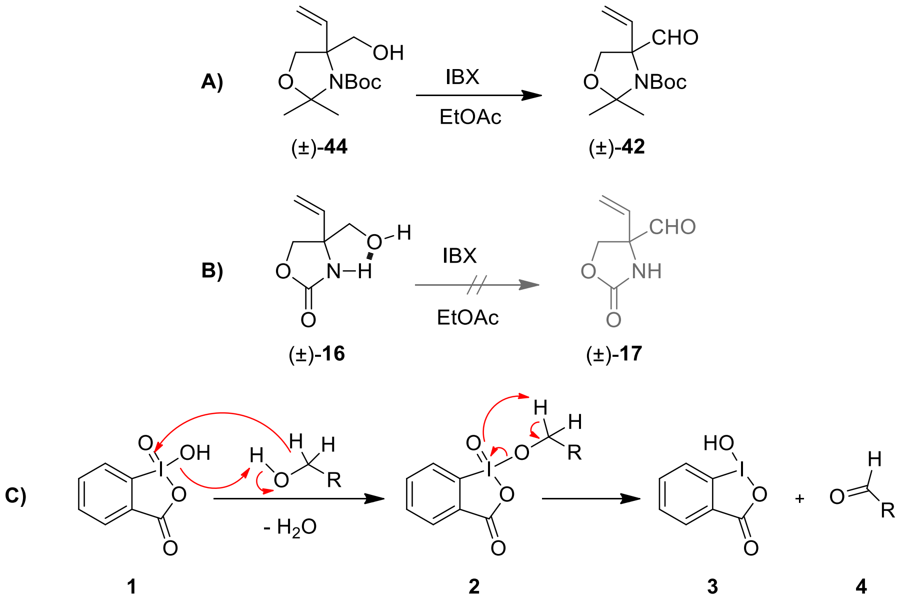

Figure 2.1.7. (A): Oxidation of alcohol (±)-**44** to (±)-**42** and **(B):** failure of alcohol (±)-**16** to undergo oxidation under identical conditions; **(C):** Mechanism of the oxidation of an alcohol to an aldehyde by IBX.

The oxidation by IBX requires the formation of an alkoxy intermediate from the starting alcohol in the coordination sphere of iodine (Figure 2.1.7). In a subsequent step, this intermediate twists to a proper conformation to produce the oxidation product.[73,74] In order to gain insight into the role of the intramolecular hydrogen bonding in (±)-**16** to account for its observed lack of reactivity, a conformational search by MM calculations of **16** and **44** was run (see experimental section for details). The results showed 54 conformers for (*S*)-**16** and 85 for (*S*)-**44** that after an optimization of each conformers with DFT method at a a B3LYP / 6-31G** level, only 48 and 78 conformers were kept respectively.

None of the 48 conformers of (*S*)-**16** showed an intramolecular hydrogen bond, which is, in fact, coherent with its rigid 5-ring structure where the NH and the O groups are arranged in an inappropriate angle to interact among them (Figure 2.1.8).

In contrast, most of conformers of (*S*)-**44** show hydrogen bonds. The one with the lowest energy is form between the oxygen of the carbonyl group and with less strength we find the hydrogen bond with the oxygen of the ester (Figure 2.1.8).

Therefore, we could not explain the lack of reactivity of the primary alcohol of **16** and the higher reactivity of the primary alcohol in **44** through intramolecular interactions and the cause remains unknown.

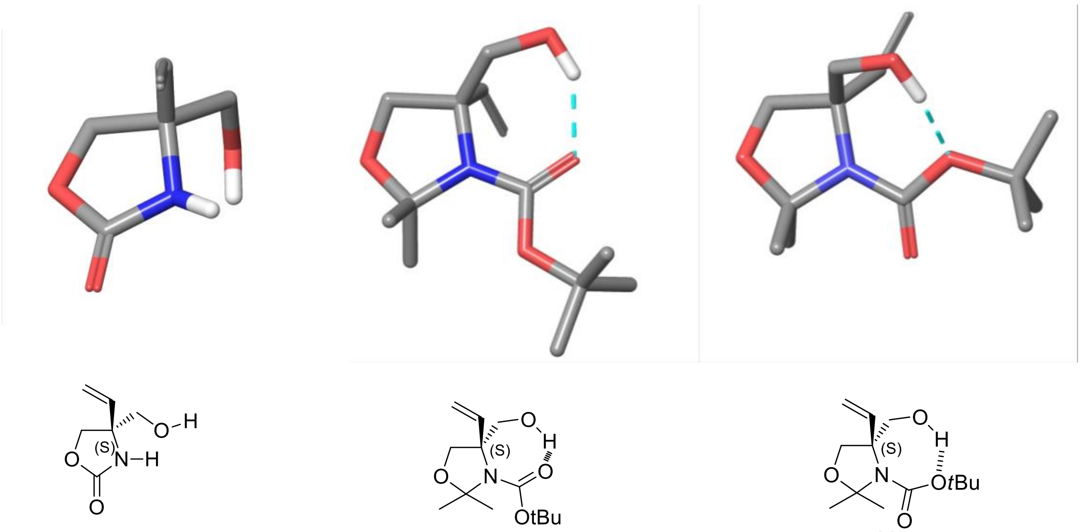

(*S*)-**16** (*S*)-**44** (*S*)-**44**

Figure 2.1.8. Minimized structures for (*S*)-**16** (left) and (*S*)-**44** (the two structures on the right).

2.1.8 Enantioselective approaches to 45 by chemical resolution of synthetic precursors

Initial exploratory attempts were addressed at the chemical resolution of some of the synthetic intermediates indicated in Scheme 2.1.14 by analytical chiral HPLC. Thus, the resolution of silyl alcohol (±)-**43**, the desilylated alcohol (±)-**44**, and the vinyl Garner's aldehyde (±)-**42** was tested under a variety of chromatographic conditions, as indicated in the experimental Section. Unfortunately, none of the attempts proved efficient resolution of the sample and no further experiments were carried out along this line.

The above negative results prompted us to explore the chemical resolution of alcohol (±)-**44** after reaction with a suitable chiral derivatizing agent. Towards this end, alcohol (±)-**44** was esterified with several enantiomerically pure acids and amino acids (Scheme 2.1.15), following the general protocol described in the experimental section, and the resulting crude reaction mixtures were analysed by TLC under different elution conditions (9:1 Hexane/EtOAc, 9:1

Hexane/MTBE and 95:5 CH_2Cl_2/MeOH). The chiral derivatizing agents were selected based on price and availability criteria. Regrettably, none of the selected derivatizing agents led to a clear separation of the two resulting diastereomers by TLC in any of the elution conditions indicated.

The success of the chemical resolution of alcohol (±)-**44** would have been crucial for the enantioselective synthesis of vinyl Garner's aldehyde **42**, a hitherto unreported building block. In addition, the enantiopure (*R*) and (*S*) aldehydes **42** would have allowed the access to the four stereoisomers of **45**, given the already optimized chromatographic separation of the *syn* and *anti* isomers indicated above.

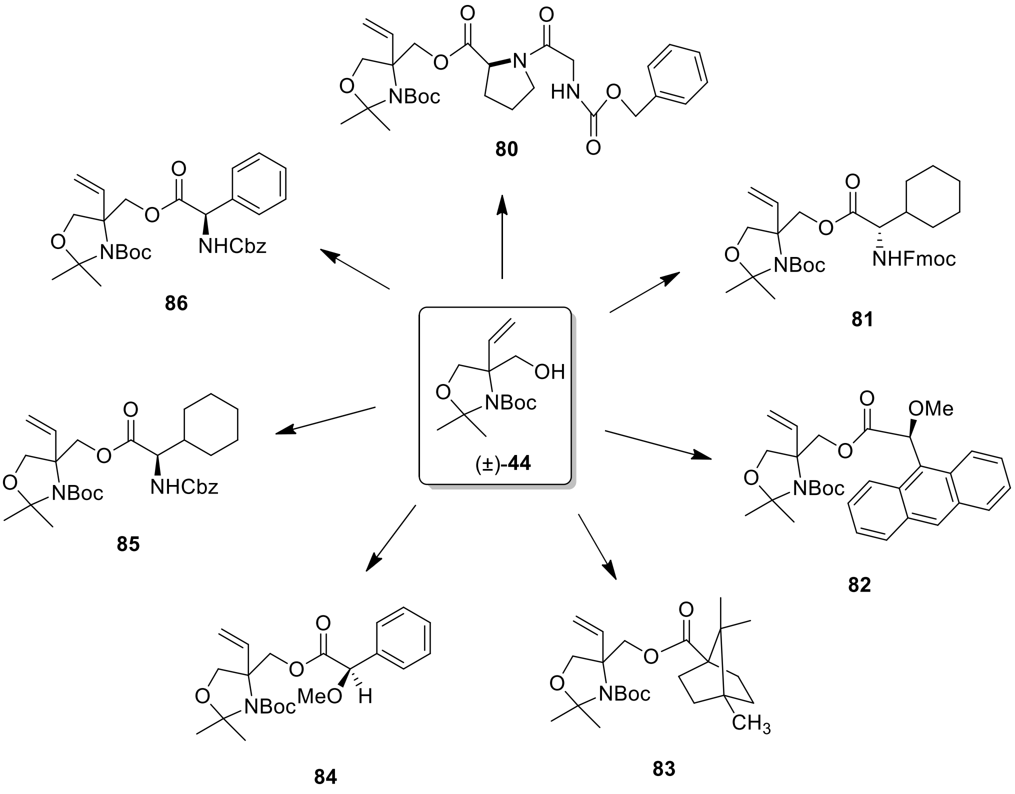

Scheme 2.1.15. Alcohol (±)-**44** was derivatized with Z-Glycyl-L-proline (**80**), Fmoc-3-cyclohexyl-L-alanine (**81**), (*S*)-9-anthrylmethoxyacetic acid (AMA) (**82**), camphanic acid (**83**), (*R*)-MPA (**84**), *N*-Z-D-α-Cyclohexylglycine (**85**) and Z-D-phenylglycine (**86**).

2.1.9 Chemical resolution of (±)-*syn*-45 and (±)-*anti*-45 by derivatization as (*R*)-MPA esters

In light of the above results, a change of strategy was necessary to attempt the resolution of the four enantiomers of **45**. Thus, (±)-*syn*-**45** and (±)-*anti*-**45** were isolated by flash chromatography and independently derivatized as the corresponding (*R*)-MPA esters **46** using the Steglich conditions shown in scheme 2.1.16. The resulting mixtures of diastereomers **46a,b** (from (±)-*syn*-**45**) and **46c,d** (from (±)-*anti*-**45**) could be cleanly isolated by flash chromatography to afford the corresponding MPA esters, which were used to determine the configuration at C_3, as seen in section 2.1.5. In addition, esters **46** should be the precursors of the enantiopure stereoisomers of **45**, after MPA removal.

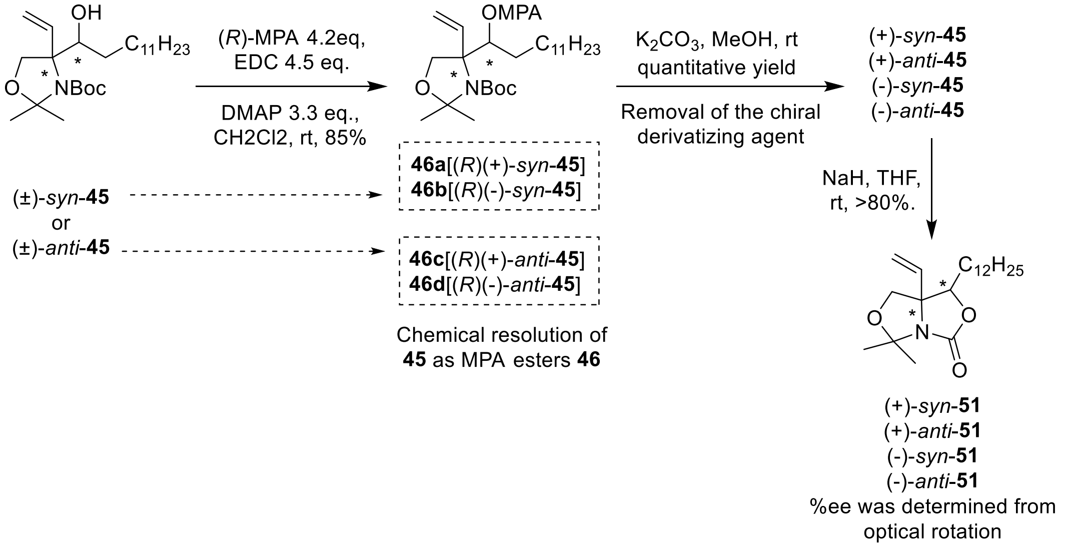
OH
$C_{11}H_{23}$
NBoc
(R)-MPA 4.2eq,
EDC 4.5 eq.
DMAP 3.3 eq.,
CH2Cl2, rt, 85%
OMPA
$C_{11}H_{23}$
NBoc
K$_2$CO$_3$, MeOH, rt
quantitative yield
Removal of the chiral derivatizing agent
(+)-syn-45
(+)-anti-45
(-)-syn-45
(-)-anti-45
(±)-syn-45
or
(±)-anti-45
46a[(R)(+)-syn-45]
46b[(R)(-)-syn-45]
46c[(R)(+)-anti-45]
46d[(R)(-)-anti-45]
Chemical resolution of 45 as MPA esters 46
NaH, THF,
rt, >80%.
$C_{12}H_{25}$
(+)-syn-51
(+)-anti-51
(-)-syn-51
(-)-anti-51
%ee was determined from optical rotation

Scheme 2.1.16. Chemical resolution of **45** through (*R*)-MPA esters **46** and cyclization to bicyclic carbamates **51**.

In order to drive the esterification of compounds **45** with (*R*)-MPA to completion, an excess of acid (4.2 equiv/mol), coupling agent (EDC, 4.5 equiv/mol) and DMAP (3.3 equiv/mol) was required. Despite the chemical yields were excellent in these conditions (around 85%), we were cautious about the possibility of a partial MPA racemization in the presence of excess DMAP, as it had been reported in the literature.[75] The first indication of this possibility was inferred from the low specific rotations observed for each of the enantiomeric pairs of *syn* and *anti*-**45** after MPA removal, for which the following values were obtained:

anti-(2*S*,3*R*)-**45**: $[\alpha]_D$ +1.4 (c 1, CHCl$_3$)

anti-(2*R*,3*S*)-**45**: $[\alpha]_D$ -1.8 (c 1, CHCl$_3$)

syn-(2*R*,3*R*)-**45**: $[\alpha]_D$ +3.4 (c 1, CHCl$_3$)

syn-(2*S*,3*S*)-**45**: $[\alpha]_D$ -3.2 (c 1, CHCl$_3$)

Unfortunately, the presumed partial racemization of (*R*)-MPA in the course of the derivatization step was confirmed by chiral HPLC of the bicyclic derivatives **51**, obtained in high yields from intramolecular cyclization of compounds **45** in NaH/THF (Scheme 2.1.16). As observed in Figure 2.1.9, *anti* isomers were almost completely racemized, the (+)-*syn* isomer was partially racemized, and only the (-)-*syn* isomer was obtained in enantiomerically pure form. In light of these results, it is reasonable to assume that epimerization of MPA esters **46** is a favoured reaction for both *anti* isomers. The possibility that racemization of MPA had taken place prior to ester formation should be ruled out given the different enantiomeric purities found for *syn* and *anti* isomers for bicycles **51**. These rigid structures were submitted to vibrational circular dichroism (VCD) experiments (see chapter 2.2) to fully corroborate the above results.

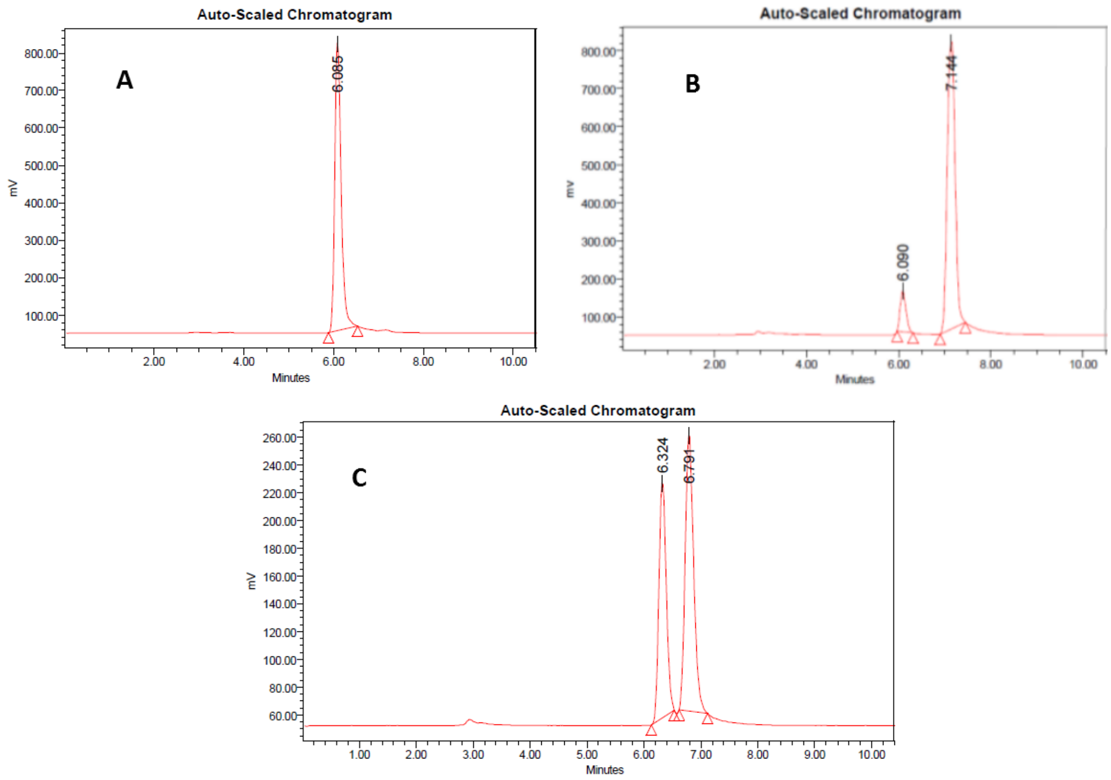

Figure 2.1.9. Chiral HPLC chromatograms (ELS detector, column D, see Experimental Section for details) of (+)-*syn* (2*R*,3*R*)-**51** (A), (-)-*syn* (2*S*,3*S*)-**51** (B) and (+)-*anti* (2*S*,3*R*)-**51** (C), which was practically identical to (-)-*anti* (2*R*,3*S*)-**51**. Compounds were eluted with 10 % isopropanol and hexanes at 1mL/min.

The % ee for (+)-*syn*-**51** was inferred from its optical purity. Thus, by considering that (-)-*syn* (2*S*,3*S*)-**51** is an enantiomerically pure compound [(2*S*,3*S*)-**51**: $[\alpha]_D$ -21.5 (c 3, $CHCl_3$), 100 %ee], a 94%ee can be calculated for (+)-*syn* (2*R*,3*R*)-**51** [$[\alpha]_D$ +20.3 (c 3, $CHCl_3$)]. Unfortunately, the *anti*-isomers were practically obtained as racemic mixtures with optical rotations close to 0 [(2*S*,3*R*)-**51**: $[\alpha]_D$ +0.4 (c 3, $CHCl_3$) and (2*R*,3*S*)-**51**: $[\alpha]_D$ -0.6 (c 3, $CHCl_3$)].

2.1.9.1 Alternatives to the Steglich esterification

The 4-(N,N-dimethylamino)pyridine (DMAP), known as the Steglich catalyst, was first reported by Litvinenko and Kirichenko[76] in 1967 and subsequently by Steglich[77] in 1969. This base has been widely used as a super acylation catalyst for the preparation of esters from carboxylic acid, DCC, and secondary or tertiary alcohols of scarce reactivity.

The Steglich esterification usually requires only 0.1 equiv/mol of DMAP, giving rise to low racemization levels. In our case, the coupling of (*R*)-MPA with compounds **45** under the above classical conditions, either at rt (entry 1, Table 2.1.4), at 60ºC (entry 2) or with an additional 1.0 equiv/mol of TEA (entry 4) was not productive and large amounts of unreacted starting material was recovered, even in the presence of 1.1 equiv/mol of DMAP (entry 3). This forced us to use a larger excess of reagents (EDC and DMAP), which ultimately led to the undesired partial or total racemization observed, as indicated above.

In order to avoid the use of an excess DMAP as coupling partner, several alternatives were explored (see table 2.1.4).

Coupling reactions tested from 45						
Entry	**Coupling reagents**	**Equiv/mol (*)**	**Solvent**	**Δ (ºC)**	**Yield (%)**	**Comments**
1	(*R*)-MPA, EDC, DMAP	1.4/1.5/0.1	ACN	rt	--	No reaction.
2	(*R*)-MPA, EDC, DMAP	1.4/1.5/0.1	ACN	60	--	No reaction.
3	(*R*)-MPA, EDC, DMAP	1.4/1.5/1.1	CH_2Cl_2	rt	--	No reaction.
4	(*R*)-MPA, EDC, DMAP, TEA	1.4/1.5/0.1/ 1.0	ACN	60	--	No reaction.
5	(*R*)-MPA, EDC, HOBt, TEA	1.4/1.5/1.1/ 1.5	ACN	rt	--	No reaction
6	(*R*)-MPA, EDC, HOBt, py	1.1/3.3/1/1	THF	rt	--	Only tested from (±)-*anti*-**45**. No reaction observed.

7	(*R*)-MPA, EDC, HOBt, TEA	1.4/1.5/1.1/ 1.5	ACN	60	--	No reaction.
8	(*R*)-MPA, HATU, DIPEA	2.0/2.5/2.5	DMF	rt	--	No reaction.
9	(*R*)-MPA, HATU, DIPEA	2.0/2.5/2.5	DMF	80	--	No reaction.
10	(*R*)-MPA, HATU, DIPEA	4.0/5.0/5.0	DMF	rt	--	No reaction.
11	(*R*)-MPA, Sc(OTf)$_3$, p-(NO$_2$C$_6$H$_4$CO)$_2$O	1.1/0.1/1.5	CH_3NO_2	rt	--	Only tested from (±)-*anti*-**45**. No reaction observed.
12	(*R*)-MPA, Sc(OTf)$_3$, p-(NO$_2$C$_6$H$_4$CO)$_2$O	1.1/0.1/1.5	CH_3NO_2	50	--	Only tested from (±)-*anti*-**45**. No reaction observed.
13	(*R*)-MPA, PFP-TFA, TEA	1.0/1.2/3	CH_2Cl_2	rt	--	Only tested from (±)-*anti*-**45**. No reaction observed.
14	(*R*)-MPA chloride, DMAP, TEA	1.3/0.1/3.0	CH_2Cl_2	rt	--	No reaction.
15	(*R*)-MPA chloride, DMAP, TEA	1.3/1.0/3.0	CH_2Cl_2	rt	83	Reaction observed with (±)-*syn*-**45**. (±)-*Anti*-**45** remained unreacted.
16	(*R*)-MPA fluoride, DIPEA	3.0/2.0	CH_2Cl_2	rt	62	Reaction observed with (±)-*syn*-**45**. (±)-*Anti*-**45** remains unreactive.
17	(*R*)-MPA fluoride, TBAF	1.5/0.5	THF	rt	--	No reaction observed. Only tested with (±)-*anti*-**45**.
18	MTPA, EDC, DMAP	1.4/1.5/0.1	CH_2Cl_2	rt	--	No reaction.
19	MTPA, EDC, DMAP	1.4/1.5/1.0	CH_2Cl_2	rt	--	No reaction.
20	MTPA, EDC, DMAP	2.8/3.0/2.0	CH_2Cl_2	rt	--	No reaction.
21	MTPA, EDC, DMAP	2.8/3.0/2.0	CH_2Cl_2	40	--	No reaction.
22	MTPA chloride, DMAP, TEA	1.5/1.0/3.0	CH_2Cl_2	rt	86	Reaction observed with (±)-*syn*-**45**. (±)-*Anti*-**45** leads only 10% yield. The chromatographic resolution is not possible.
23	MTPA chloride, DMAP, TEA	3.0/2.0/6.0	CH_2Cl_2	rt	10	Only tested from (±)-*anti*-**45** that leads 10% yield.

(*) relative to **45**

Table 2.1.4. Different coupling reactions tested from compound **45** in order to avoid racemization. If not specified, the reaction was tested with both (±)-*syn* and (±)-*anti*-**45**.

The use of catalysts, such as HOBt, HATU, scandium(III) triflate[78] or pentafluorophenyl trifluoroacetate, has been reported[79] to reduce the extent of racemization. However, none of these catalysts proved efficient in our case (entries 5 to 13).

In another approach, (*R*)-MPA was used as the corresponding acyl chloride in the presence of DMAP (entry 15). Only (±)-*syn*-**45** was reactive under these conditions (83% yield), while the most prone to racemization (±)-*anti*-**45** isomers remained unreactive. A similar trend was observed with the acyl fluoride of (*R*)-MPA, (entries 16 and 17).

The use of MTPA (Mosher's acid), as an alternative derivatization reagent, was also considered. In this case, unlike MPA, the presence of a quaternary centre at the α-position of the carboxylic acid prevents the epimerization of the reagent. However, no reaction was observed under any of the conditions tested (entries 18-21). By using the corresponding acyl chloride (entries 22 and 23), some reactivity was observed but the chromatographic separation of the resulting diastereomers was not possible.

2.1.10 Configurational assignments

2.1.10.1 Configuration at C_3 from MPA esters 46

The ^{1}H-NMR spectra of esters **46** displayed challenging features. Thus, the spectra of each of the four stereoisomers appeared to be a mixture of two different species, a fact that complicated their analysis (see, for example, Figure 2.1.10). The possibility of cross contamination with other stereoisomers was initially disregarded, since none of the minor signals in a given spectrum matched those corresponding to any of the remaining stereoisomers. For this reason, we assumed the presence of rotamers in the conditions of the ^{1}H-NMR experiment. This was confirmed by 1D gradient NOE experiments, following the protocol of Hu *et al.*[80] Thus, the signal at 5.57 ppm (B) in **46a** was sensitive to the irradiation of the $C_{16}H$ resonance signal at 5.39 ppm (A) (Figure 2.1.11), which confirmed that (A) and (B) belong to two rotamers of the same diastereomer and not to different diastereomers. If this were the case, one diastereomer would not be able to transfer spin information, *via* chemical exchange, to the other diastereomer if it were present in the NMR sample.

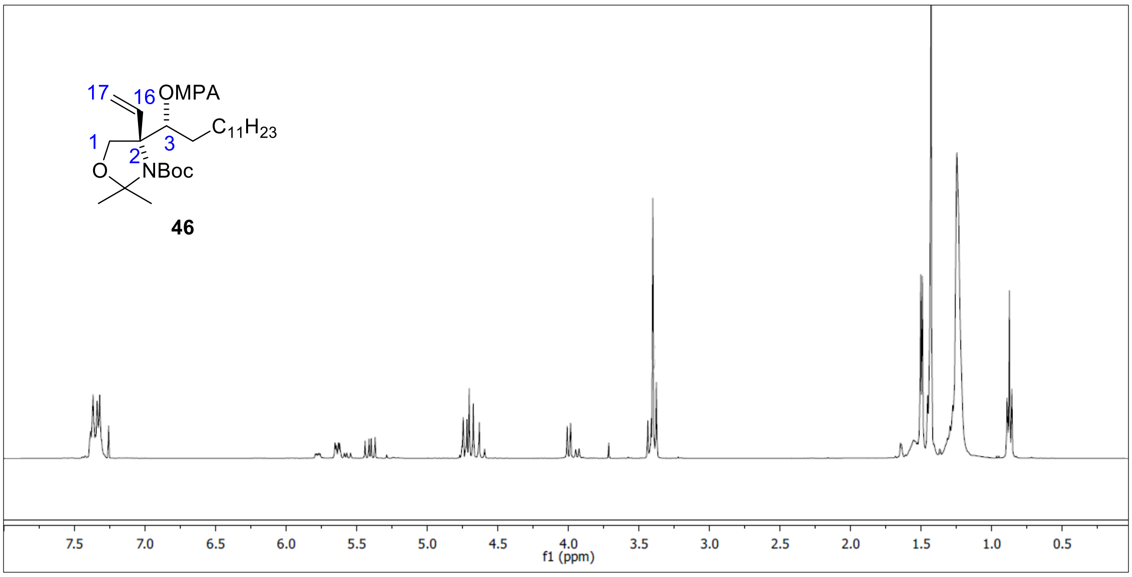

Figure 2.1.10. ^{1}H NMR spectra of the mixture of rotamers **46a**[(*R*)(+)*syn*-**45**] (see Scheme 2.1.16).

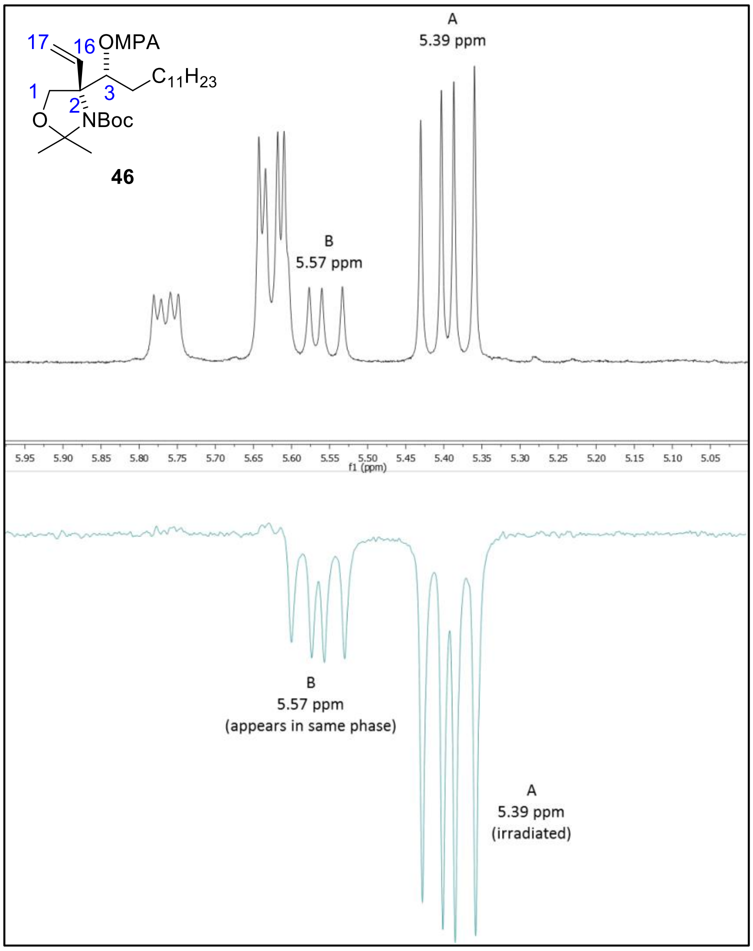

Figure 2.1.11. Example of 1D gradient NOE that confirms that signals A and B, in **46a**, belong to the same proton of two rotamers of the same diastereomer.

Once completed the signal assignment for the different diastereomers of **46**, the configuration at C_3 was deduced from application of Riguera's rules[67] from the corresponding (*R*)-MPA esters **46a-d.** In this case, we only used the (*R*)-MPA ester to determine the absolute configuration at C_3 by comparison of the ^{1}H-NMR spectra of **46a/46b** (for *syn* isomers), and **46c/46d** (for *anti* isomers) (See Table 2.1.5). Derivatization of (±)-*syn*-**45** with (*R*)-MPA, led to a mixture of diastereomers **46a** and **46b**, which could be isolated by chromatographic methods. According to the $\Delta\delta^{RS}$ values from the two ^{1}H-NMR spectra, it was deduced that (+)-*syn*-**45** corresponds to the C_3R configuration and, consequently, the configuration of (-)-*syn*-**45** is C_3S. The same approach was applied to the (±)-*anti*-**45** isomers. In this case, (-)-*anti*-**45** is C_3S and (+)-*anti*-**45** is C_3R. The $\Delta\delta^{RS}$ values of **46a-d** are collected in Table 2.1.5.

Configuration **C_3 *S*** for (-)*anti*-**45** (**46d-46c**)						
	δH_A(*)	δH_B(*)	δH_C(*)	δH_D(*)	δH_E	δH_F
46d[(*R*)(-)-*anti*-**45**]	4.11	3.94	5.33	6.02	0.98	0.71
46c[(*R*)(+)-*anti*-**45**]	4.01	3.88	5.19	5.91	1.17	1.12
$\Delta\delta^{RS}$	+ 0.10	+ 0.06	+ 0.14	+ 0.11	- 0.19	- 0.41

The $\Delta\delta^{RS}$ values for **46c** – **46d** are opposite in sign to the data shown in this table.

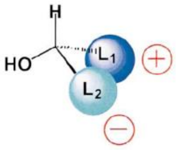

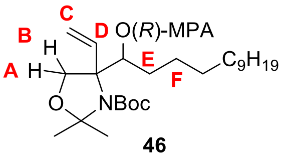

46

Configuration **C_3 *R*** for (+)*syn*-**45** (**46a-46b**)						
	δH_A(*)	δH_B(*)	δH_C(*)	δH_D(*)	δH_E	δH_F
46a[(*R*)(+)-*syn*-**45**]	3.99	3.43	4.69	5.41	1.60	1.24
46b[(*R*)(-)-*syn*-**45**]	4.16	3.82	5.06	5.86	1.28	1.05
$\Delta\delta^{RS}$	- 0.17	- 0.39	- 0.37	- 0.45	+ 0.32	+ 0.19

Table 2.1.5. $\Delta\delta^{RS}$ values in ppm that allowed the assignment of the C_3 configuration for the four stereoisomers of **45**. The $\Delta\delta^{RS}$ values for **46b** – **46a** are opposite in sign to the data shown in this table. (*) δ from the center of the system.

2.1.10.2 Configuration at C_2 from bicyclic carbamates 51

The relative configuration at the quaternary C_2 centre was carried out by NOE experiments from bicycle **51**. Thus, for *syn*-**51**, the irradiation at C_3H gave a 1 % NOE enhancement with one of the C_1H protons. A similar NOE enhancement was observed with the vinyl CH proton after irradiation at C_3H for *anti*-**51**, as shown in Figure 2.1.12.

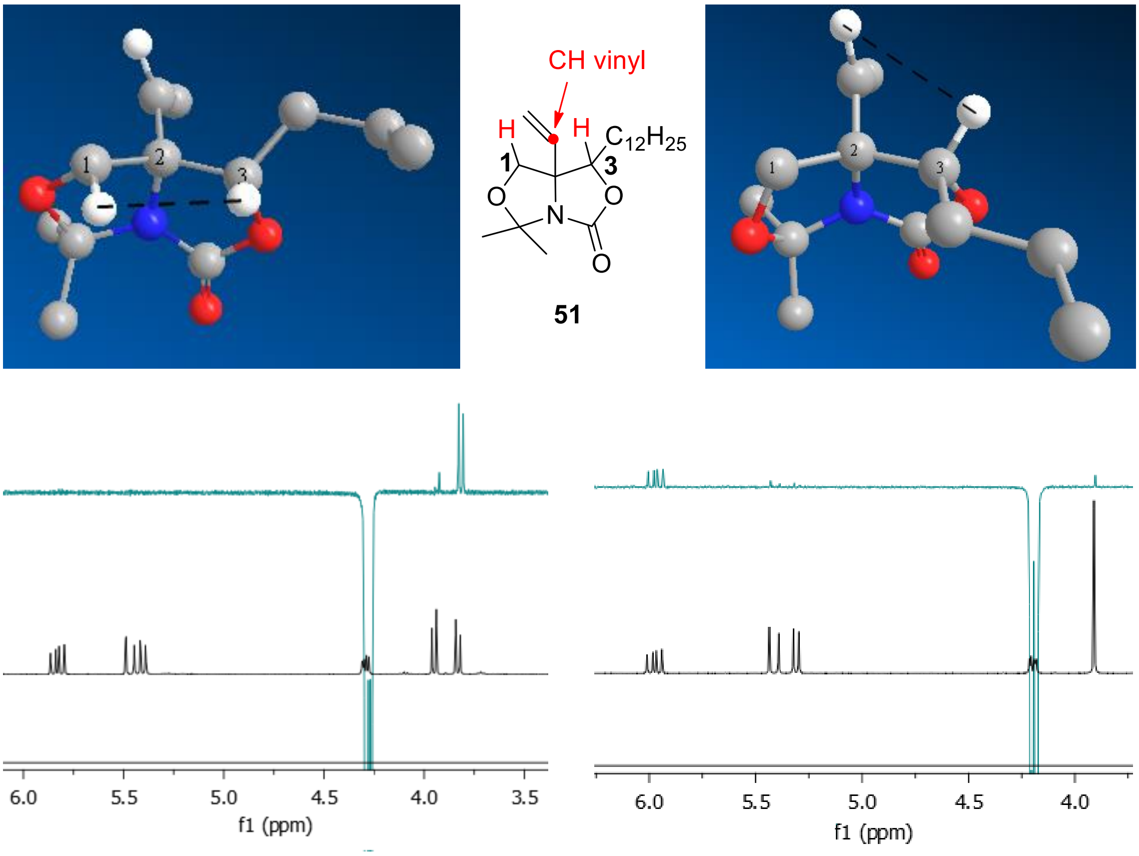

Figure 2.1.12. NOE experiments by irradiation at C_3H in *syn* and *anti*-**51** (downfield signal). Left: *syn*-**51**; Right: *anti*-**51**. A *cis* relationship between C_3H and the vinyl CH is found for *anti*-**51** and a cis relationship between C_3H and one of the two C_1H for the *syn*-**51**.

This relative configuration at C_2, combined with that assigned above for C_3 by the MPA method, allowed us to unambiguously assign the absolute configuration of compounds **51** and, hence, those of the precursors **45**. In agreement with these correlations, conversion of **45** into *N*-Boc amino diols **22** (Scheme 2.1.17) afforded compounds of relative *syn* and *anti* configurations identical to those already determined by the method described in section 2.1.5.

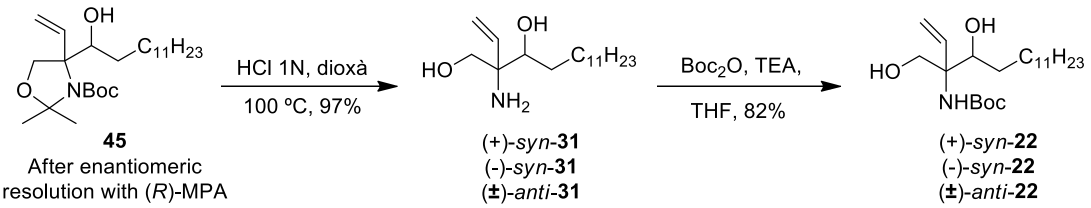

Scheme 2.1.17. Transformation of **45** into **22** *via* amino diols **31**.

2.1.11 X-ray diffraction trials

Despite the good correlations described above, the results are based in the application of an empirical model (Riguera's rules[67]) and the observation of a weak (around only 1 %) NOE enhancement between pairs of selected protons. For this reason, we looked for an alternative method to confirm the configurational assignments described in the previous section. In this context, we considered the potential of X-ray diffraction analysis. This technique is a tool generally used to identify the atomic and molecular structure of a crystal. It has the capacity to distinguish between the enantiomorphs of a chiral crystal structure and the enantiomers of a chiral molecule. The determination of the absolute configuration depends on the ability of the technique to identify small diffraction intensity differences between two crystal structure models of opposite chirality. With compounds containing only light atoms, a significant difference between enantiomers is not guaranteed.[81] This is not the case when a heavy atom, such as bromine, is present in the crystal.[82] For this reason, we undertook the synthesis of (-)-*syn*-**50** (Scheme 2.1.18), with a *p*-bromoacetamide moiety that can be useful to analyze the small differences between enantiomers.

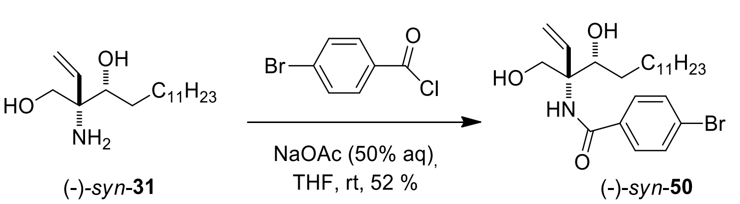

Scheme 2.1.18. Synthesis of (-)-*syn*-**50** from (-)-*syn*-**31** through a Schotten-Baumann reaction.

A sample of (-)-*syn*-**50** was carefully crystallized in order to obtain a suitable crystal for X-ray diffraction analysis. Among the different methods reported in the literature,[83] the best results were obtained by evaporation of the sample from a THF/Hexane (1:1) mixture. However, the small colourless needle-shaped crystals obtained were not suitable for X-ray diffraction and other alternatives were sought (see Chapter 2.2).

2.1.12 Synthesis of 2-vinyl dihydrosphingolipids

Despite the racemization problems found in the *anti* series, as it will be corroborated in Chapter 2.2 by VCD, we decided to proceed with their transformation into the corresponding target vinyl sphingolipid analogues.

Several conditions were tested from (-) and (+)-*syn*-**45** and (±)-*anti*-**45** to selectively cleave the isopropylidene group to afford compounds **22** (Scheme 2.1.19). Acidic conditions, such as *p*-TsOH in MeOH (from 0.2 to 5 equiv/mol of acid), aq AcOH (even at 50ºC)[84] or also in the presence of LiCl)[85] or DCA in MeOH led, in all cases, to the recovery of starting material. For this reason, it was decided to obtain **22** in two steps, starting from **45**, with the simultaneous removal of the isopropylidene and *N*-Boc groups, followed by the reintroduction of the *N*-Boc group in amino diols **31**. However, the deprotection of **45** was not devoid of problems. Initial attempts (acetyl chloride in MeOH) from (+)-*syn*-**45** and (±)-*anti*-**45** led to the oxazolidines **80** and **81** as the only reaction products. However, the use of stronger acidic conditions (1*N* HCl in dioxane) led to the required vinyl amino diols **31** in high yields. In a subsequent step, amino diols **31** were converted in high yields into **22** by reaction with Boc_2O in THF. Compounds **22** are the precursors of the vinyl amino phosphates **24**, as already indicated (section 2.1.4)

In parallel, compounds **31** were acylated to the ceramide analogues **48**. Initial attempts from (-)-*syn*-**31** and (±)-*anti*-**31** using octanoic acid in the presence of HOBt as coupling partner led to oxazolines **82**, whose formation can be interpreted as a result of an intramolecular cyclization of the C_3OH group onto the initially formed amide carbonyl group. Gratifyingly, the use of octanoyl chloride, under the classical Schotten-Baumann conditions,[86] led to ceramides **48**. All these reactions are summarized in Scheme 2.1.19.

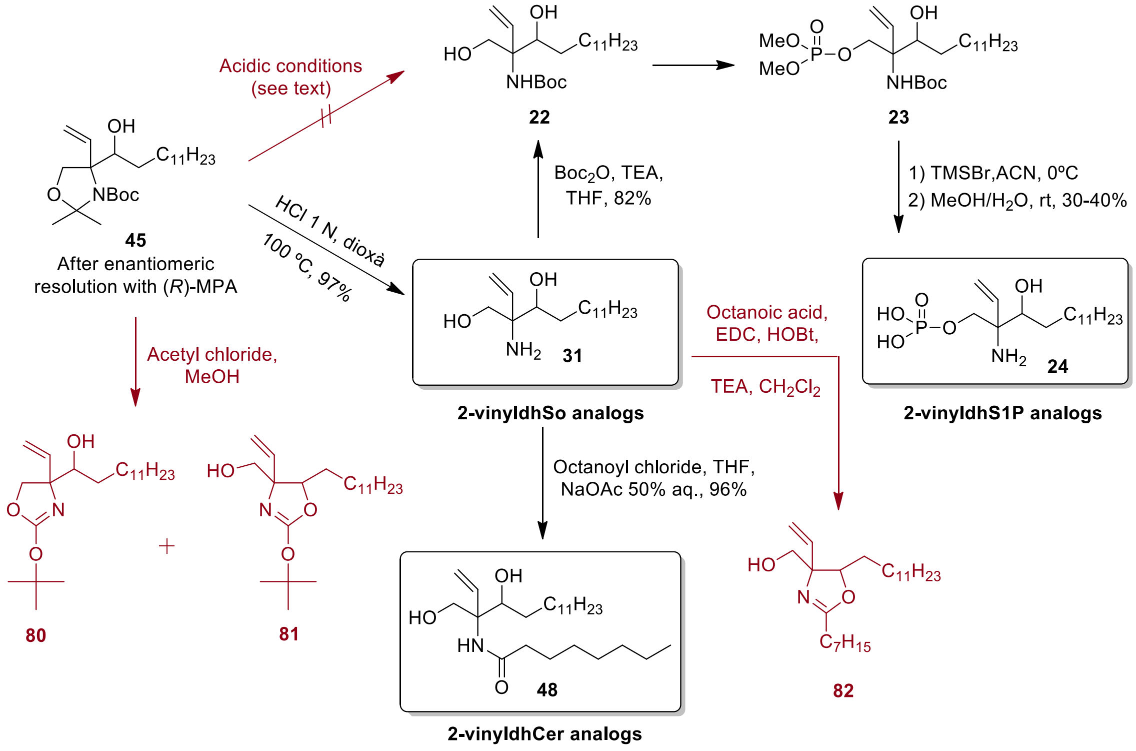
Acidic conditions
(see text)
OH
$C_{11}H_{23}$
HO
NHBoc
22
MeO
O
P
O
MeO
OH
$C_{11}H_{23}$
NHBoc
23
OH
$C_{11}H_{23}$
O
NBoc
45
After enantiomeric
resolution with (R)-MPA
HCl 1 N, dioxa
100 °C, 97%
Boc_2O, TEA,
THF, 82%
1) TMSBr,ACN, 0°C
2) MeOH/H_2O, rt, 30-40%
HO
OH
$C_{11}H_{23}$
NH_2
31
2-vinyldhSo analogs
Octanoic acid,
EDC, HOBt,
TEA, CH_2Cl_2
HO
O
P
O
HO
OH
$C_{11}H_{23}$
NH_2
24
2-vinyldhS1P analogs
Acetyl chloride,
MeOH
OH
$C_{11}H_{23}$
O
N
O
80
+
HO
$C_{11}H_{23}$
N
O
O
81
Octanoyl chloride, THF,
NaOAc 50% aq., 96%
HO
OH
$C_{11}H_{23}$
HN
O
48
2-vinyldhCer analogs
HO
$C_{11}H_{23}$
N
O
C_7H_{15}
82

Scheme 2.1.19. In black, synthetic route from **45** to 2-vinyldhS1P (**24**), 2-vinylSa (**31**) and 2-vinyldhCer (**48**) analogues. In red, by-products arising from unexpected reactions.

2.1.13 Synthesis of 2-vinyl sphingolipids

These compounds were obtained in the wake of collaboration with Dr. Jordi Garcia's group (University of Barcelona, Department of Organic and Inorganic Chemistry).

The synthetic route used was an adaptation of their previously developed methodology[72] leading to the stereocontrolled construction of quaternary centres. This one-pot process that is based on the hydroboration of the allene with $(c\text{-}C_6H_{11})_2BH$ at the less hindered face of the terminal double bond to generate an allylborane which could be added *in situ* to an aldehyde, was seen previously in Scheme 2.1.13, section 2.1.5.2.

Allene **72** (Scheme 2.1.20), obtained from but-2-yn-1,4-diol in 61% yield,[87] in which the easier removable *N*-benzoyl group is used as *N*-protecting group.[88] We envisaged that the addition of allene **72** to (*E*)-2-tridecenal would provide access to 2-vinyl sphingoid analogs **75** (Scheme 2.1.20), structurally related to sphingosine.

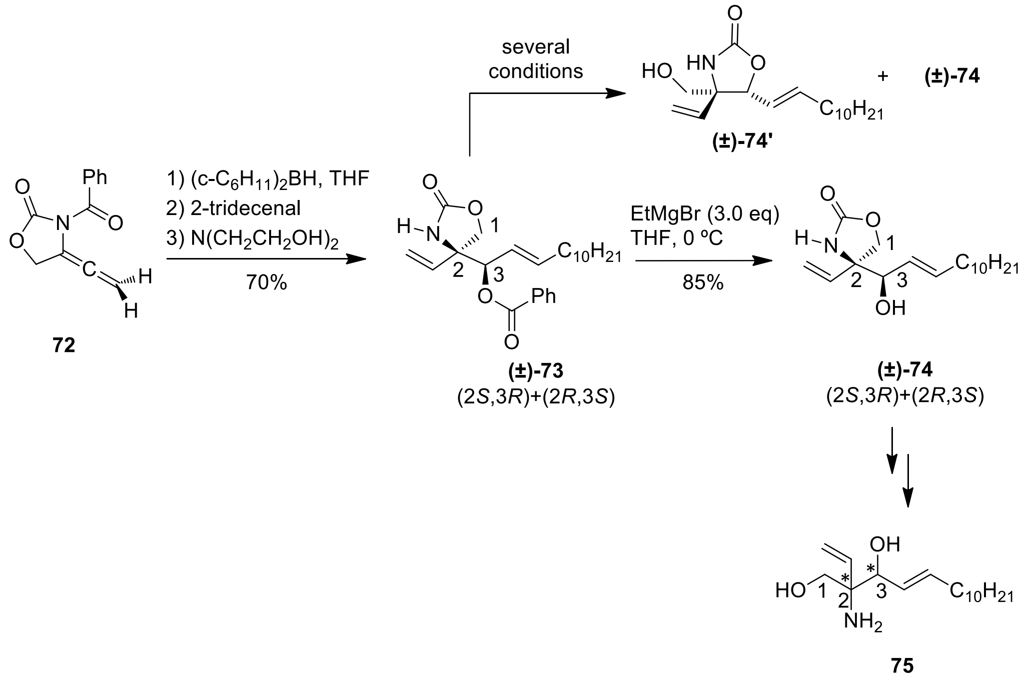

Scheme 2.1.20. Synthesis of sphingoid precursor (±)-**74** from allene **72** and attempts of selective hydrolysis of benzoate (±)-**73**.

As expected, hydroboration of **72** with (c-C_6H_{11})$_2$BH, in CH_2Cl_2 at 0 ºC followed by addition of (*E*)-2-tridecenal, afforded carbamate (±)-**73** in very high stereochemical purity (>95:5 by ^{1}H-NMR) after a hydrolytic work-up with triethanolamine. It should be remarked that a complete migration of the benzoyl protecting group from the nitrogen atom to the newly formed secondary alcohol was observed, avoiding in this way the isomerization of **73** to the inner carbamate (±)-**74’** (Scheme 2.1.20). Thus, compound (±)-**73** was obtained in an acceptable 75% yield, after chromatographic purification, as a single isomer.

Hydrolysis of the benzoate group in (±)-**73** to the desired alcohol (±)-**74** avoiding the isomerization to the inner carbamate was not a trivial task. A number of hydrolytic treatments with different basic (K_2CO_3, LiOH) or acidic (H_2SO_4, HCl) aqueous or methanolic media, as well as reductive treatment of (±)-**73** with $LiBH_4$ in THF, were performed leading to mixtures of both carbamates arising from the primary or the secondary alcohol ((±)-**74** and (±)-**74'**). Gratifyingly, the use of EtMgBr in THF at 0 ºC afforded the required alcohol (±)-**74** in good yield with negligible isomerization. Since we were interested in the influence of the different stereoisomers of 2-vinyl sphingosines in the sphingolipid metabolism, we next faced the resolution of (±)-**74**. This goal was accomplished by transformation of (±)-**74** into a mixture of the corresponding diastereomeric esters **76** derived from (*R*)-methoxyphenylacetic acid [(*R*)-MPA][89] using EDC in the presence of cat. DMAP as coupling reagent. Esters **76** were then easily isolated by column chromatography and their configuration at C3 was inferred from Δδ between selected pair of protons, following the empirical method of Riguera *et al*,[90] as indicated in Table 2.1.6. Since the relative configuration between C2 and C3 had already been established based on mechanistic grounds,[72] the absolute configuration at both stereogenic centers in esters **76** was thus assigned.

C3*S* configuration assigned from Δδ [(2*R*,3*S*)-(2*S*,3*R*)] (*R*)-MPA esters								
	δH_C(*)	δH_D(*)	δH_E	δH_F	δH_G(*)	δH_H	δH_I(*)	δH_J
2*R*3*S*	1.16	1.88	5.59	5.18	5.83	5.28	4.11	5.90
2*S*3*R*	1.29	2.02	5.91	5.30	5.62	5.06	3.85	5.72
$\Delta\delta^{SR}$	-0.13	-0.14	-0.32	-0.12	+0.21	+0.22	+0.26	+0.18

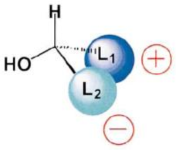

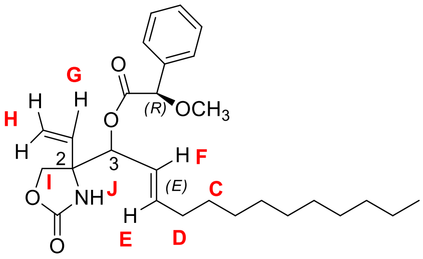

76

C3*R* configuration assigned from Δδ [(2*R*,3*R*)-(2*S*,3*S*)] (*R*)-MPA esters								
	δH_C(*)	δH_D(*)	δH_E	δH_F	δH_G(*)	δH_H	δH_I(*)	δH_J
2*R*3*R*	1.32	2.01	5.82	5.29	5.62	5.16	3.90	5.42
2*S*3*S*	1.01	1.80	5.24	5.09	5.81	5.34	4.17	5.78
$\Delta\delta^{RS}$	+0.31	+0.21	+0.58	+0.20	-0.19	-0.18	-0.27	-0.36

Table 2.1.6. $\Delta\delta^{RS}$ values in ppm that allowed the configurational assignment at C3 position of (*R*)-MPA esters **76**. (*) δ from the center of the system.

Enantiopure (2*S*,3*R*)-**76** and (2*R*,3*S*)-**76** we independently treated in basic hydro-alcoholic media to obtain free aminodiols (2*S*,3*R*)-**JG** and (2*R*,3*S*)-**JG**, respectively, in good yields (Scheme 2.1.21).

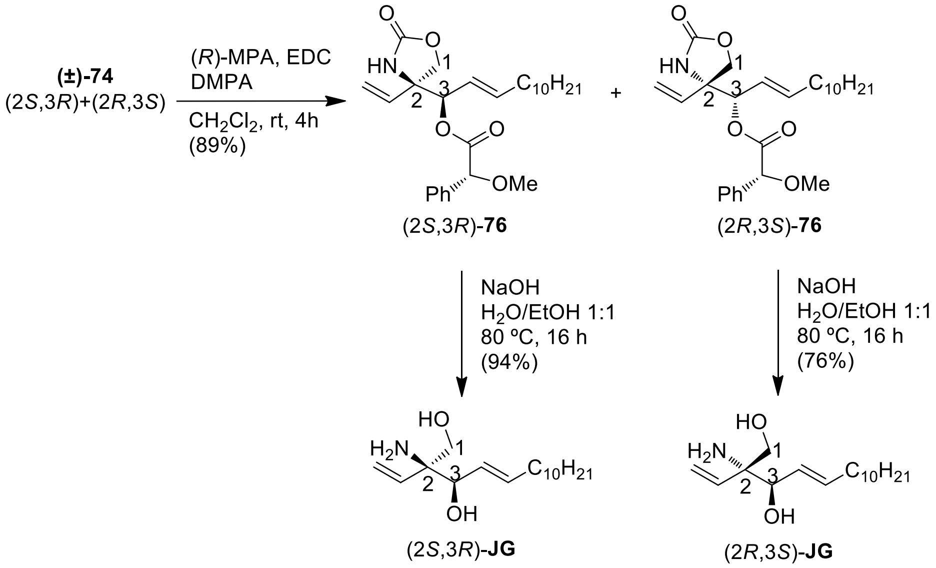

Scheme 2.1.21. Resolution of (±)-**74** and conversion of enantiopure esters **76** into (2*S*,3*R*)-**JG** and (2*R*,3*S*)-**JG**.

Regarding the preparation of the enantiomeric series, (2*S*,3*S*) and (2*R*,3*R*), we first attempted a direct inversion of the secondary alcohol in (±)-**74** by a Mitsunobu reaction, using benzoate as nucleophile, without success. Then, we turned our attention to a redox two-step process based on the oxidation of (±)-**74** to ketone (±)-**78**, followed by reduction. In practice, the Dess-Martin oxidation of (±)-**74** gave ketone (±)-**78**, which was used without further purification. The reduction of (±)-**78** under Luche conditions (Ce(III)/$NaBH_4$)[91] turned out to be scarcely stereoselective, since a roughly 1:1 mixture of the corresponding diastereomeric alcohols **79** in a satisfactory 63% yield (two steps) (Scheme 2.1.22). Unfortunately, we were not able to isolate efficiently both diastereomeric racemates by column chromatography. Thus, we attempted the resolution of the mixture of alcohols **79** through the formation of the corresponding diastereomeric esters **76** derived from (*R*)-MPA (Scheme 2.1.22). To our satisfaction, the four stereoisomeric esters were shown separately enough by TLC. After column chromatographic isolation of (2*R*,3*R*)-**76** and (2*S*,3*S*)-**76**, the amino diols (2*R*,3*R*)-**JG** and (2*S*,3*S*)-**JG** were obtained in 85% and 65% yield, respectively, by basic hydrolysis. Again, the configuration at C3 of the diasteromeric esters (2*R*,3*R*)-**76** and (2*S*,3*S*)-**76** was inferred by the method of Riguera *et al*, based on the Δδ values indicated in Table 2.1.6.

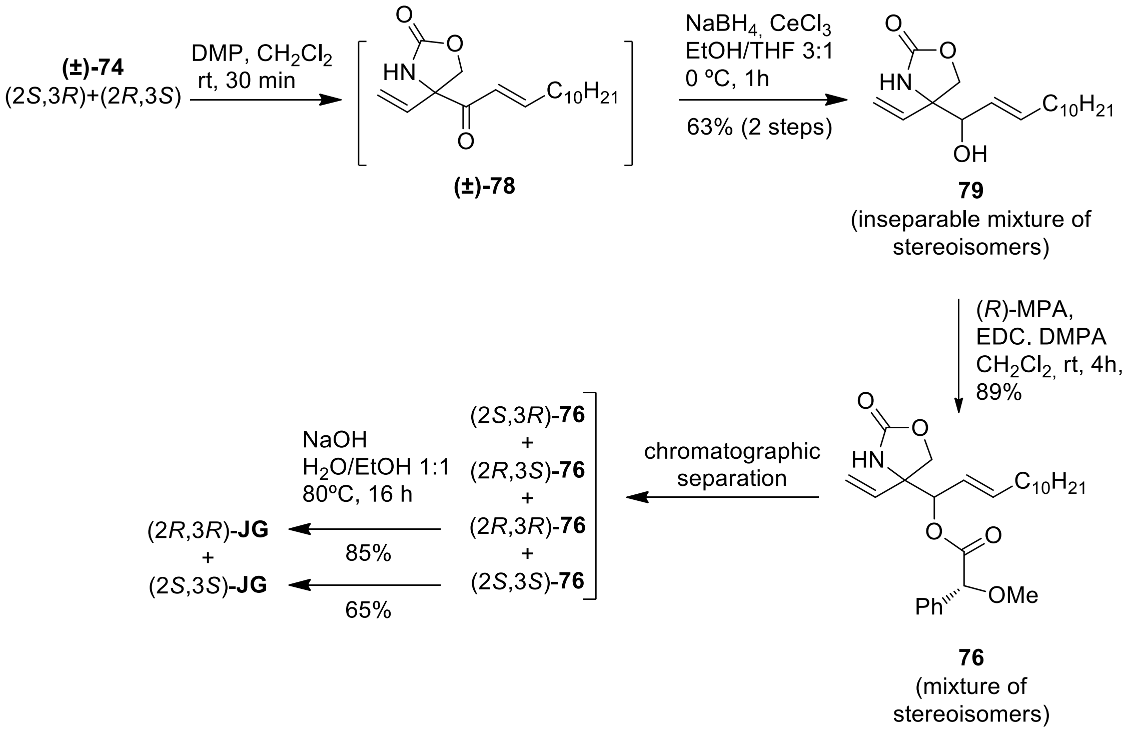
(±)-74
(2S,3R)+(2R,3S)
DMP, CH2Cl2
rt, 30 min
HN
O
C10H21
(±)-78
NaBH4, CeCl3
EtOH/THF 3:1
0 ºC, 1h
63% (2 steps)
OH
79
(inseparable mixture of stereoisomers)
(R)-MPA,
EDC. DMPA
CH2Cl2, rt, 4h,
89%
Ph
OMe
76
(mixture of stereoisomers)
chromatographic separation
(2S,3R)-76
+
(2R,3S)-76
+
(2R,3R)-76
+
(2S,3S)-76
NaOH
H2O/EtOH 1:1
80ºC, 16 h
(2R,3R)-JG
+
(2S,3S)-JG
85%
65%

Scheme 2.1.22. Resolution of (±)-**78** and preparation of (2*S*,3*S*) and (2*R*,3*R*) **76** and **JG**.

In regard to the synthesis of amides **52**, the different stereoisomers of **JG**, except (2*S*,3*S*)-**JG** due to the small amount obtained in the previously described synthesis, were acylated with octanoyl chloride in THF/NaOAc$_{aq.}$ with a Schotten-Baumann classic conditions (Scheme 2.1.23) in the same way as **48** (Scheme 2.1.19, Section 2.1.12).

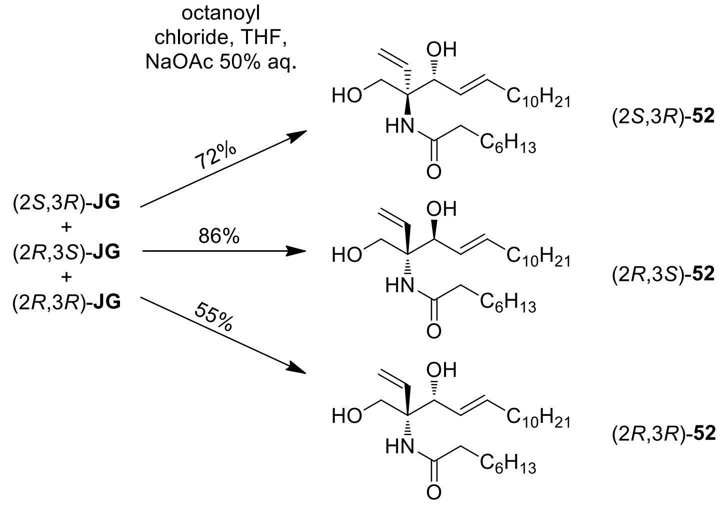
octanoyl chloride, THF, NaOAc 50% aq.
(2S,3R)-JG
+
(2R,3S)-JG
+
(2R,3R)-JG
72%
86%
55%
HO
OH
HN
O
C10H21
C6H13
(2S,3R)-52
(2R,3S)-52
(2R,3R)-52

Scheme 2.1.23. Synthesis of different stereoisomers of Ceramide analogues **52** from **JG**.

2.1.14 Conclusions

- The (±)-*syn* and (±)-*anti* aminophosphate **24** was synthesized through intermediate **21** in Section 2.1.1, as well as the racemic mixture of aminodiol **31**.

- Several desymmetrization and chiral resolution experiments have been carried out without success.

- Resolution of **21** with chiral auxiliary MPA was undertaken with evidences that probably no racemization has taken place, but because of the low efficiency of the process is abandoned. See section 2.1.4.

- A more practical synthetic route was developed with cyclic structure **45** as an intermediate but *anti* isomers racemization was faced. See section 2.1.9.

- Different approaches to obtain enantiomeric pure vinylic Garner's alcohol **44** were tried with no results, although kinetic resolution of (±)-**18** is being carried out in our group with promising results.

- Finally, dhCers analogs **48**, aminodiols **31** and aminophosphates **24** were achieved with racemic *anti*- and enantiomerically pure *syn*- compounds and the unsaturated aminodiols **JG** and Cers **52** analogues as final products were obtained enantiomerically pure for the four **JG** and for three of **52**.

2.2 Vibrational circular dichroism (VCD) studies to confirm the absolute configuration of 51

2.2.1 Introduction

As we have discussed along this thesis dissertation, different techniques have been tried to determine the absolute configuration of our chiral compounds. In sections 2.1.5 and 2.1.10, we discussed on the use of configurationally defined MPA esters and the application of the Riguera's rules[67] to determine the absolute configuration of the nearby stereogenic centres in alcohols and amines.

On the other hand, X-ray crystallography is considered as the most reliable technique for configurational analysis, provided a good quality single crystal can be grown and at least one heavy atom is present. As indicated in Section 2.1.11, we tried this approach on compound (-)-*syn*-**50**, albeit without success.

In this context, VCD is a technique that complements X-ray and NMR methods, since it does not require a single crystal, it does not entail derivatization reactions or the addition of adjuvants for intermolecular interactions[92], and it is suitable for samples in liquid, solid, and even in gas phase[93].

The vibrational optical activity (VOA) is a spectroscopic measure that detects the differential response of a chiral molecule to the left versus the right circularly polarized radiation during a vibrational transition[94]. It is the extension of circular dichroism spectroscopy into the infrared and near infrared ranges and is known as VCD and vibrational Raman optical activity, known as ROA. The determination of the absolute configuration of a chiral molecule is made by comparing the experimental VCD spectra with the simulated one, using *ab initio* calculations. Thus, VCD is a powerful technique that allows the identification of the absolute configurations of small molecules in solution.

If the sign and relative intensity of the observed bands in the experimental VCD spectrum of a sample are the same as those of the calculated spectrum, the absolute configuration of the sample corresponds to that arbitrarily chosen for the *ab initio* calculation. On the contrary, if the experimental and the calculated bands are opposite, the initially chosen absolute configuration must be reversed.[93]

For flexible molecules, the first step for VCD calculation is to carry out a conformational analysis, usually by molecular mechanics, to determine the lower energy conformers and their relative population. In order to simplify the study, the bicyclic derivatives **51** (Scheme 2.2.1) were synthesized, as described in Section 2.1.9, to reduce the conformational flexibility, which is now limited to the alkyl side chain. The experimental VCD spectra for **51** were compared with the calculated VCD spectra for the simplified analogues **52**, whose side chain has been replaced with a methyl group in order to remove any conformational flexibility and, hence, to simplify the calculation of the theoretical VCD spectra.

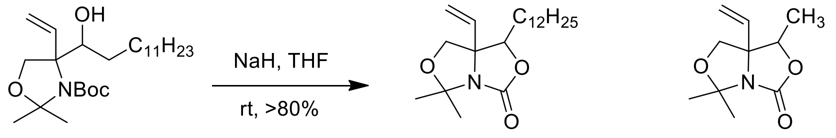

(+)-*syn*-(2*R*,3*R*)-**45**
(-)-*syn*-(2*S*,3*S*)-**45**
(+)-*anti*-(2*S*,3*R*)-**45**
(-)-*anti*-(2*R*,3*S*)-**45**

(+)-*syn*-(2*R*,3*R*)-**51**
(-)-*syn*-(2*S*,3*S*)-**51**
(+)-*anti*-(2*S*,3*R*)-**51**
(-)-*anti*-(2*R*,3*S*)-**51**

52
Model structure
of **51** to perform the
conformational search

Scheme 2.2.1. Synthesis of the four enantiomers of **51** from the corresponding enantiomer of **45**.

2.2.2 Conformational search

All the theoretical calculations were carried out in the laboratories of the Department of Physical and Analytical Chemistry of the University of Jaén by Professors Manuel Montejo Gámez and Juan Jesús López González, whose contribution to this part of the project has been crucial.

Taking **52** as simplified models, the strategy of "relaxed scan" was used to study the sequential rotation of the vinyl group at a B3LYP / 6-31+G* level of calculation. In the case of (2*S*,3*S*)-**52**, the results showed two conformers of minimum energy (Figure 2.2.1). It is interesting to note that the global minimum is characterized by the occurrence of a hydrogen bonding between one of the vinyl hydrogen atoms and the nitrogen atom.

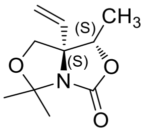

(2S,3S)-**52**

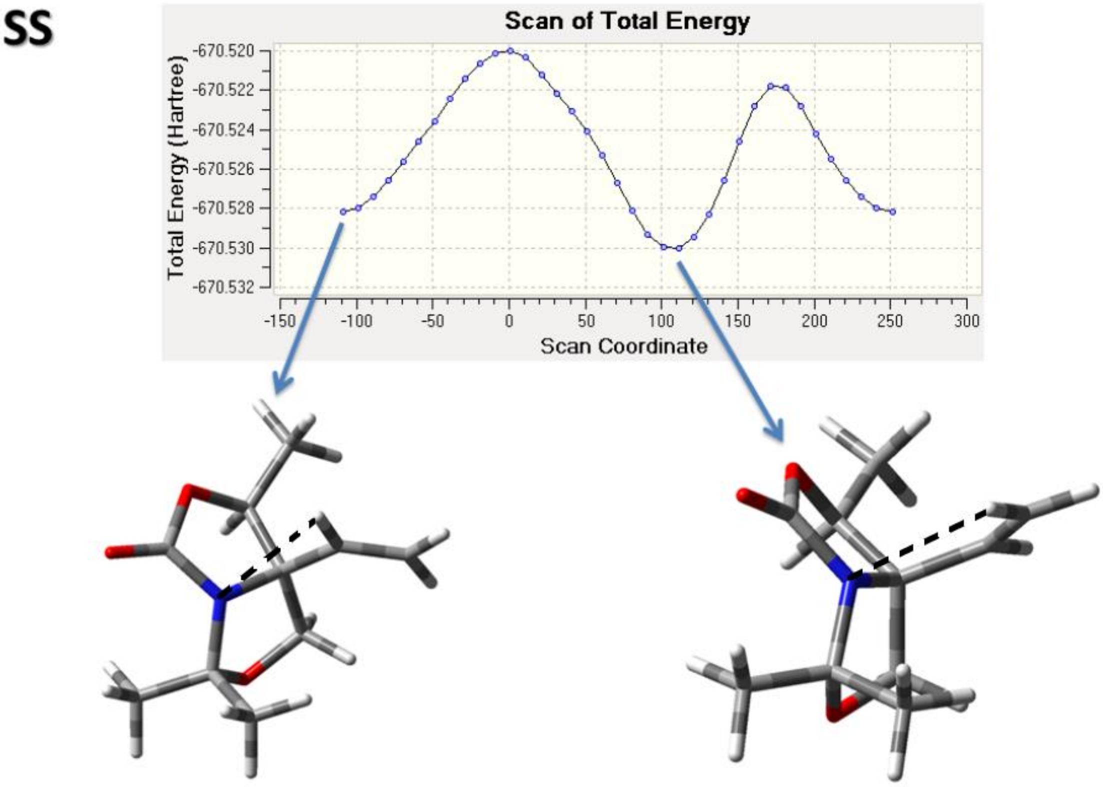

Figure 2.2.1. Relaxed scan of the position of the vinyl group in (2*S*,3*S*)-**52**.

The same strategy was applied to the *anti* diastereomer (2*S*,3*R*)-**52**, leading to the location of three minimum energy conformers, from which the global minimum is again characterized by the existence of an intramolecular hydrogen bonding, as shown in Figure 2.2.2.

The two minimum energy localized structures for (2*S*,3*S*)-**52**, together with the three other ones for (2*S*,3*R*)-**52** could be confirmed as minim, in their respective potential energy surfaces, by calculation of their vibrational spectra (B3LYP / 6-31+G*), which were free from negative frequencies.

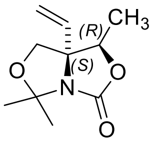

(2*S*,3*R*)-**52**

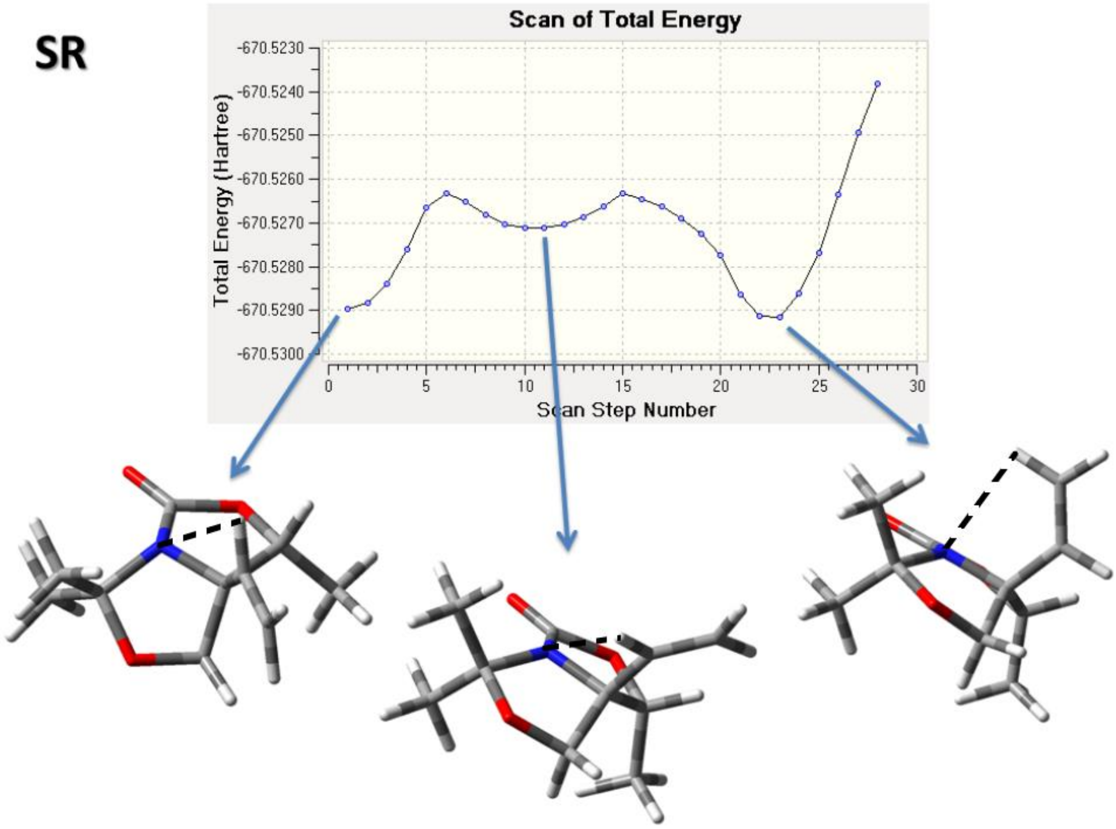

Figure 2.2.2. Relaxed scan of the position of the vinyl group in diastereomer (2*S*,3*R*)-**52**.

Taking the optimized structures obtained for the simplified model **52**, the research proceeded with the study of a conformational search space for diastereomers **51**, bearing the dodecyl side chain. In the case of *syn*-(2*S*,3*S*)-**51**, two models differing only in the orientation of the vinyl group were taken as starting point. By using molecular mechanics (force field MMFF implemented in Spartan08), a MonteCarlo type search resulting from free rotation of all the dihedral angles of the molecule led to up to 10,000 different structures, from which only the 20 of minimum energy were considered. The same protocol, when applied to the alternative model differing in the orientation of the vinyl group, led to an additional set of 20 minimum energy conformers. The combined 40 conformers were confirmed as a minimum surface potential by subsequent geometric optimization and calculation of the vibrational frequencies at B3LYP / 6-31+G* level. In this step, the presence of the solvent used in the experimental studies was considered (CCl_4), in agreement with the PCM model. Of the total of conformers obtained, only the 12 of lower energy were kept, which represented more than 90% of the conformational composition of the species in solution, according to their calculated Boltzmann populations. A geometric optimization (PCM-B3LYP/cc-pVTZ) of these 12 structures was carried out, calculating also their IR and VCD vibrational spectra.

The individual value of E_0 (E_e+ZPE) for each species, their relative values relating to global minimum (conformer 11, Figure 2.2.3) and the theoretical calculated Boltzmann populations are collected in Table 2.2.1.

Conf.	**E_0 B3LYP/ccpVTZ - PCM (H)**	**Δ E_0 (Kcal mol^{-1})**	**Boltzmann population**
11	**-1102,807360**	**0,00**	**23,8**
12	-1102,806837	0,33	13,7
1	-1102,806820	0,34	13,4
4	-1102,806815	0,34	13,3
6	-1102,806273	0,68	7,5
3	-1102,805804	0,98	4,6
2	-1102,805779	0,99	4,5
5	-1102,805717	1,03	4,2
9	-1102,805686	1,05	4,0
7	-1102,805656	1,07	3,9
8	-1102,805599	1,11	3,7
10	-1102,805556	1,13	3,5

Table 2.2.1. Boltzmann populations for the 12 lowest energy conformers of (2*S*,3*S*)-**51**, which represented more than 90% of the conformational composition of the species in solution.

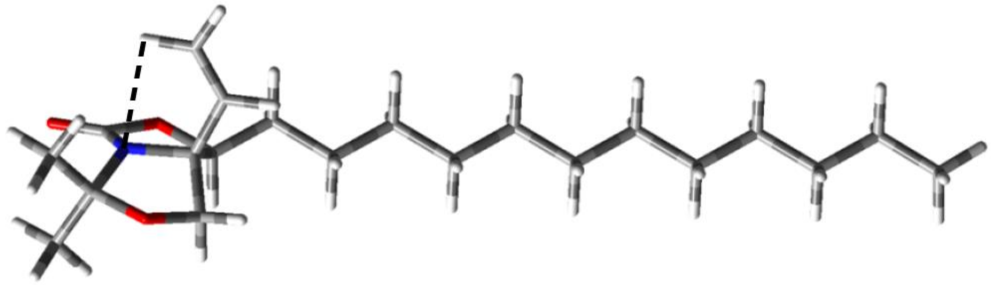

Figure 2.2.3. Conformer **11**, showing the global minimum energy for (2*S*,3*S*)-**51**.

As shown in Figure 2.2.3, the global minimum for (2*S*,3*S*)-**51** corresponds to the linear conformation of the alkyl chain. Furthermore, the hydrogen bond between the nitrogen atom and one of the vinyl hidrogen atoms is still present.

For the *anti* isomer (2*S*,3*R*)-**51**, a similar methodology was followed, except that three optimized structures (instead of the two structures used for the *syn* isomer) were taken as starting point in the experiments carried out with the simplified model **52**. Thus, 60 (20 x 3) structures were obtained by molecular mechanics. In this case, only five of them represented more than 90% of the theoretical conformational composition of the species in solution (PCM-B3LYP / 6-31+G*).

The individual value of E_0 (E_e+ZPE) for each species, their relative values relating to the global minimum (conformer 1, Figure 2.2.4) and the theoretical calculated Boltzmann populations are collected in Table 2.2.2.

Conf.	**E_0 B3LYP/ccpVTZ - PCM (H)**	**Δ E_0 (Kcal mol^{-1})**	**Boltzmann population**
1	**-1102,807547**	**0,00**	**47,4**
2	-1102,807181	0,23	32,1
3	-1102,806046	0,94	9,7
4	-1102,805553	1,25	5,7
5	-1102,805440	1,32	5,1

Table 2.2.2. Boltzmann populations for the five lowest energy conformers of (2*S*,3*R*)-**51**, which represented more than 90% of the conformational composition of the species in solution.

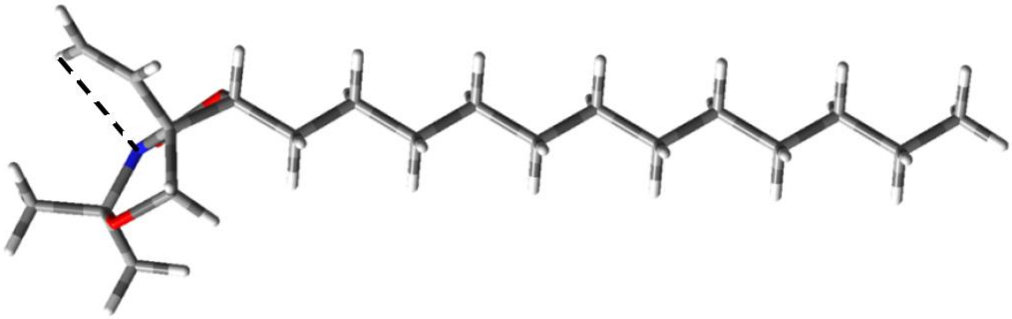

Figure 2.2.4. Conformer 1 representing the global minimum energy of (2*S*,3*R*)-**51**.

As shown again in Figure 2.2.4, the global minimum conformer for (2*S*,3*R*)-**51** also corresponds to a linear side chain conformation and is characterized by the occurrence of an intramolecular hydrogen bond.

2.2.3 Vibrational IR and VCD spectra

The theoretical IR and VCD spectra for each diastereomer were determined from the contribution of each of the generated conformers of minimum energy (12 for the *syn* diastereomer and 5 for the *anti* diastereomer). These contributions were weighted according to their respective calculated Boltzmann populations, as indicated above (B3LYP /cc-pVTZ level) taking into account the presence of the solvent, according to the PCM model.

As shown below, despite some discrepancies in the relative intensities of some vibrational bands, a good overall correlation between the theoretical and the experimental IR for both diastereomers was obtained (see Figure 2.2.5 for the *syn* diastereomer , and Figure 2.2.6 for the *anti* diastereomer). Deviations between calculated and experimentally observed wavenumbers are within the range of what is expected when the vibrational frequencies are calculated under the harmonic approximation. Moreover, as expected, both the experimental and the theoretical IR spectra for each of the enantiomeric pairs (2*S*,3*S*)-**51**, (2*R*,3*R*)-**51** and (2*S*,3*R*)-**51**, (2*R*,3*S*)-**51** are coincident.

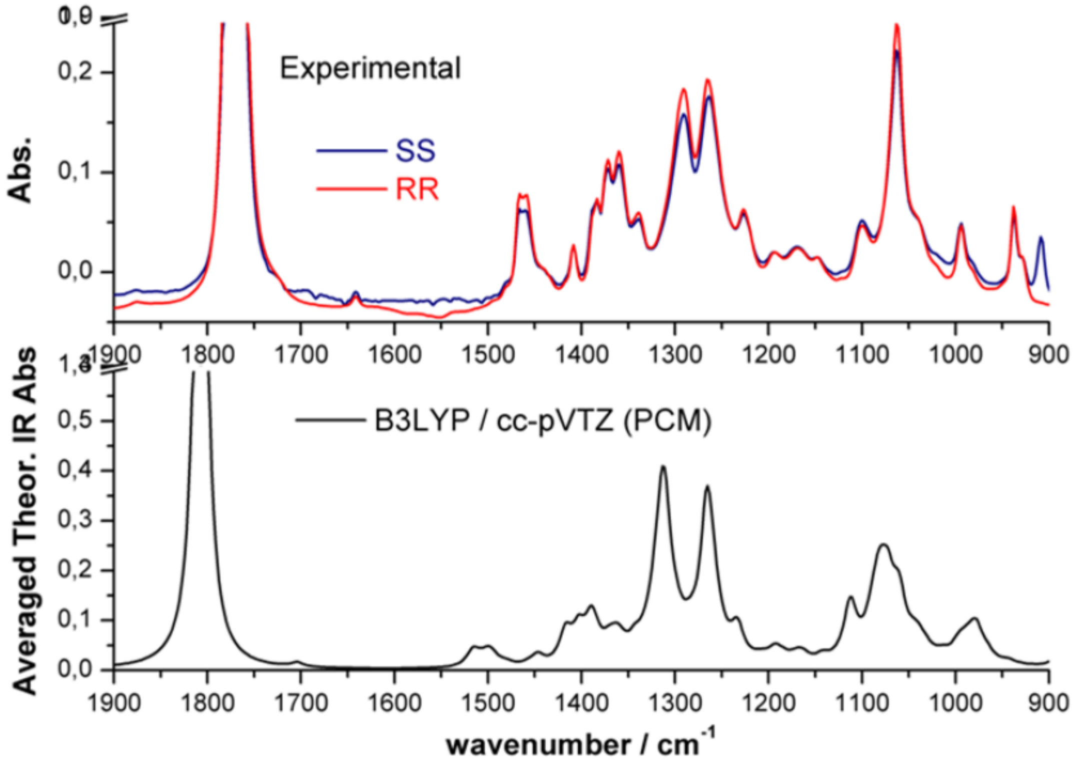

Figure 2.2.5. Theoretical and experimental comparison of IR spectra for the *syn* pair of enantiomers.

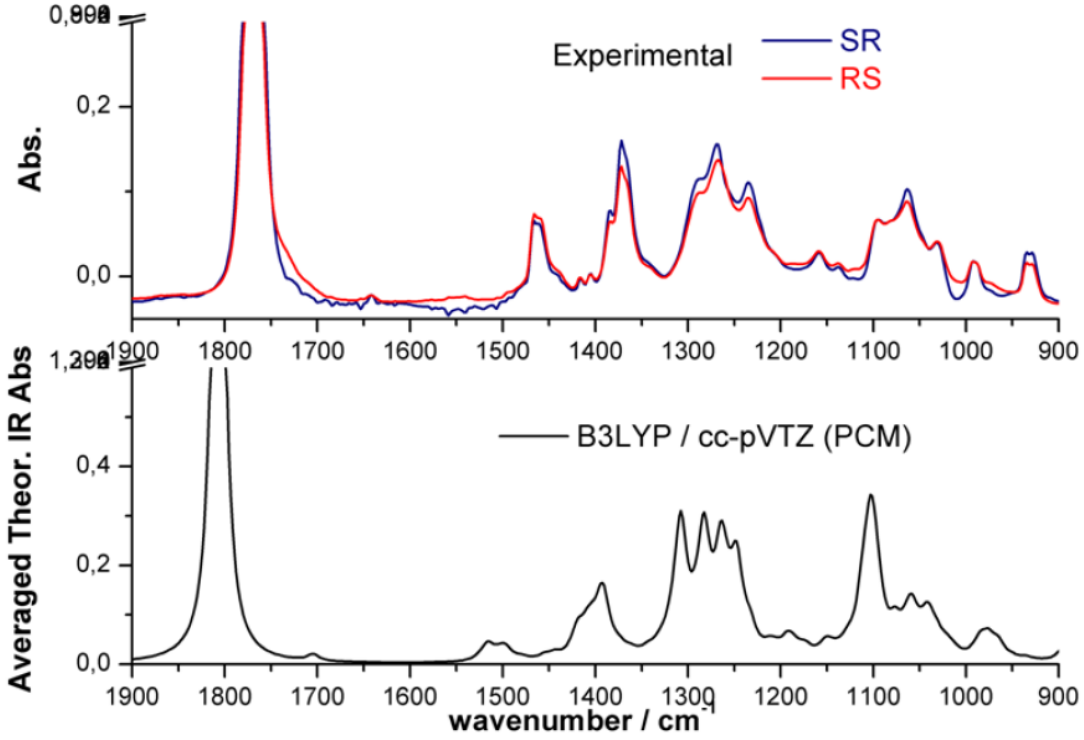

Figure 2.2.6. Theoretical and experimental comparison of IR spectra of the *anti* pair of enantiomers.

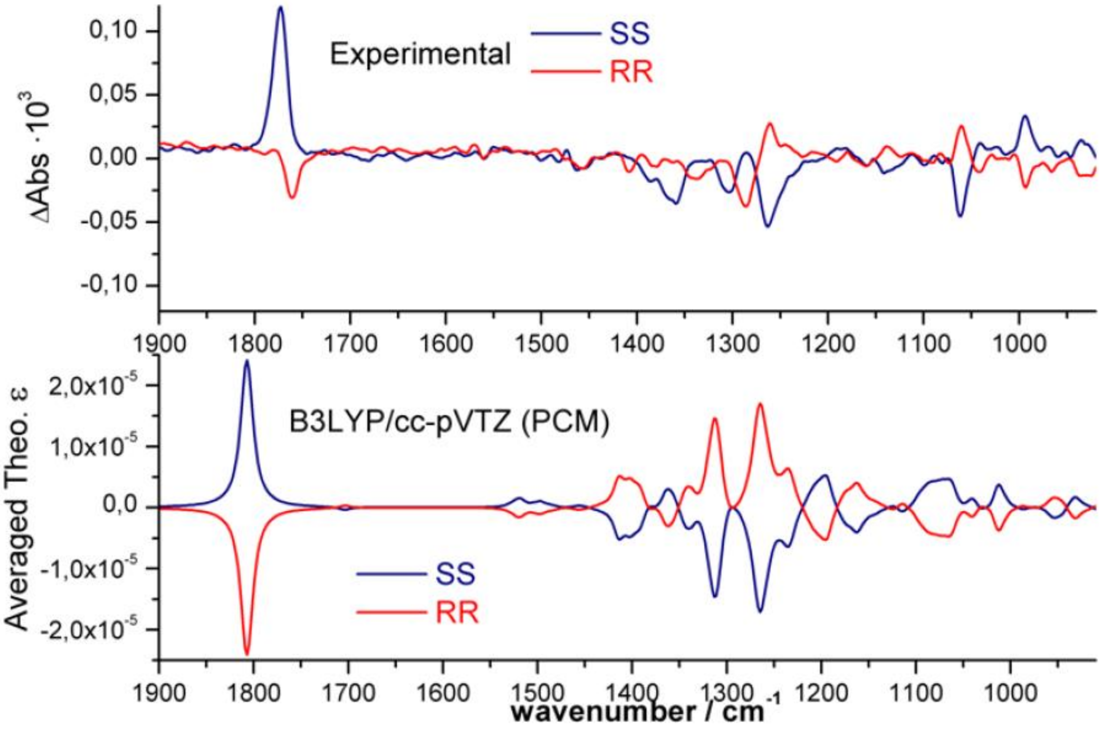

Figure 2.2.7. Experimental (up) and theoretical (down) VCD spectra for the enantiomers of *syn*-**51**.

Concerning the VCD spectra, the results obtained for the *syn* enantiomers are reasonably reproduced by the theoretical model, as shown in Figure 2.2.7, especially for (2*S*,3*S*)-**51**. Regarding *syn*-(2*R*,3*R*)-**51** (Figure 2.2.7), despite its profile is close to the mirror image of (2*S*,3*S*)-**51**, the intensity of the VCD signal is significantly lower. Since both spectra were carried out at the same concentrations, it is conceivable to assume that (2*R*,3*R*)-**51** is partially racemized. This assumption is reinforced by the fact that the IR spectra of both enantiomers have similar intensities (Figure 2.2.5), this rule out any possible contamination of the sample with other species. Moreover, this observation is in agreement with the HPLC experiments described in section 2.1.9, where a significant racemization of (2*R*,3*R*)-**51** was observed. Even so, in the sample there is an enantiomeric excess of 94 % of (2*R*,3*R*)-**51**, calculated from optical rotation.

Concerning the *anti* diastereomers, the experimental VCD spectra are characterized by the absence of a clear signal. As shown in Figure 2.2.8, the profiles obtained for both species are nearly coincident, showing a relatively high noise level and the absence of clear bands. The good agreement between the theoretical and the experimental IR profiles, together with the absence of clear VCD signals, confirm the presence of the two enantiomers in similar amounts and, hence, that extensive racemization has taken place. These results are in agreement with those reported in section 2.1.9 and confirm the racemization of the *anti* isomers under the esterification conditions with (*R*)-MPA.

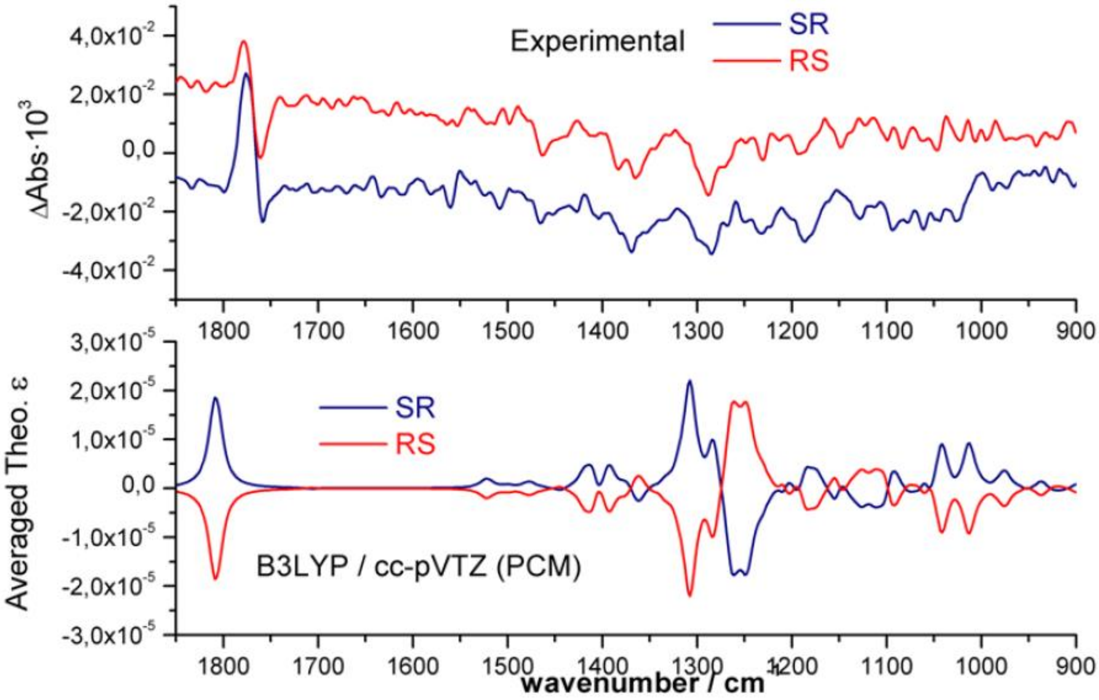

Figure 2.2.8. Theoretical-experimental comparison of VCD spectra of the *anti* pair of enantiomers.

2.2.4 Conclusions

- A conformational study for **51** and its simplified analogue **52** were carried out in order to calculate their Boltzmann population.

- The theoretical IR and VCD spectra for each diastereomer were determined from the calculated Boltzmann population.

- The experimental IR and VCD spectra for each diastereomer were measured and compared with the theoretical ones.

- The enantiopurity pattern established in Chapter 2 was confirmed through intermediate **51** and its precursor **45** by experiments of VCD.

2.3 Biological assays

2.3.1 Introduction

One of the main objectives of this doctoral thesis was to discern the stereoselectivity of S1PL towards the different stereoisomers of 2-vinylsphinganines **24**. As stated in section 2.1.9, the *anti* diastereomers were obtained as racemic mixtures. For this reason, in this chapter we will consider three different chemical entities, consisting of enantiopure (2*S*,3*S*)-**24**, enantioenriched (2*R*,3*R*)-**24**, and racemic (±)-*anti*-**24**. The stereoselectivity of the bacterial (StS1PL) and the recombinant human (hS1PL) lyases towards compounds **24**, **31** and **JG**, has been studied using a fluorogenic assay developed in our group[95,96] (see below). Moreover, toxicity (cell viability) and the effect of our compounds on the cellular lipidome have also been considered. These two additional studies have also been extended to vinylsphinganines **31** and vinyldihydroceramides **48**, both sharing the same enantiopurity pattern as **24**. In addition, enantiopure vinylsphingosines **JG** and vinylceramides **52** were included in this study (Figure 2.3.1). These compounds, obtained as a result of a collaboration with Dr. Jordi Garcia's group (University of Barcelona, Department of Organic and Inorganic Chemistry), were considered given the close structural relationship with our target sphingolipid analogues.

Regarding the evaluation of S1PL inhibitors, several assays have been reported in the literature.[95,96] Those amenable to "on-plate" analysis are particularly interesting for their application to HTS protocols. In this context, our group developed the fluorogenic probe RBM13,[97] a S1PL substrate that releases the fluorescent reporter umbelliferone, after a base-promoted retro-Michael decomposition of the intermediate aldehyde product (Scheme 2.3.1).

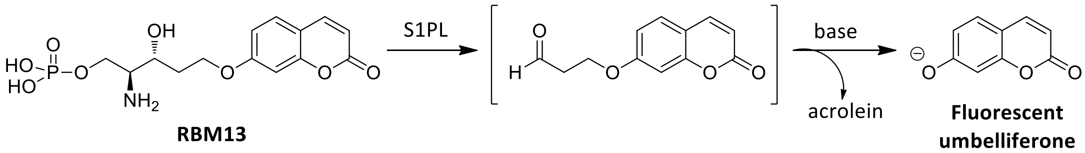

Scheme 2.3.1. Spontaneous release of umbelliferone from RBM13 after reaction with S1PL.

This substrate was initially used in both fluorogenic assays, with StS1PL and hS1PL. More recently, the new fluorogenic substrate **RBM7-148**, showing higher S1PL affinity, was synthesized within the frame of the doctoral Thesis of Pol Sanllehí. This substrate has also been used in this thesis, as it is detailed in section 2.3.3

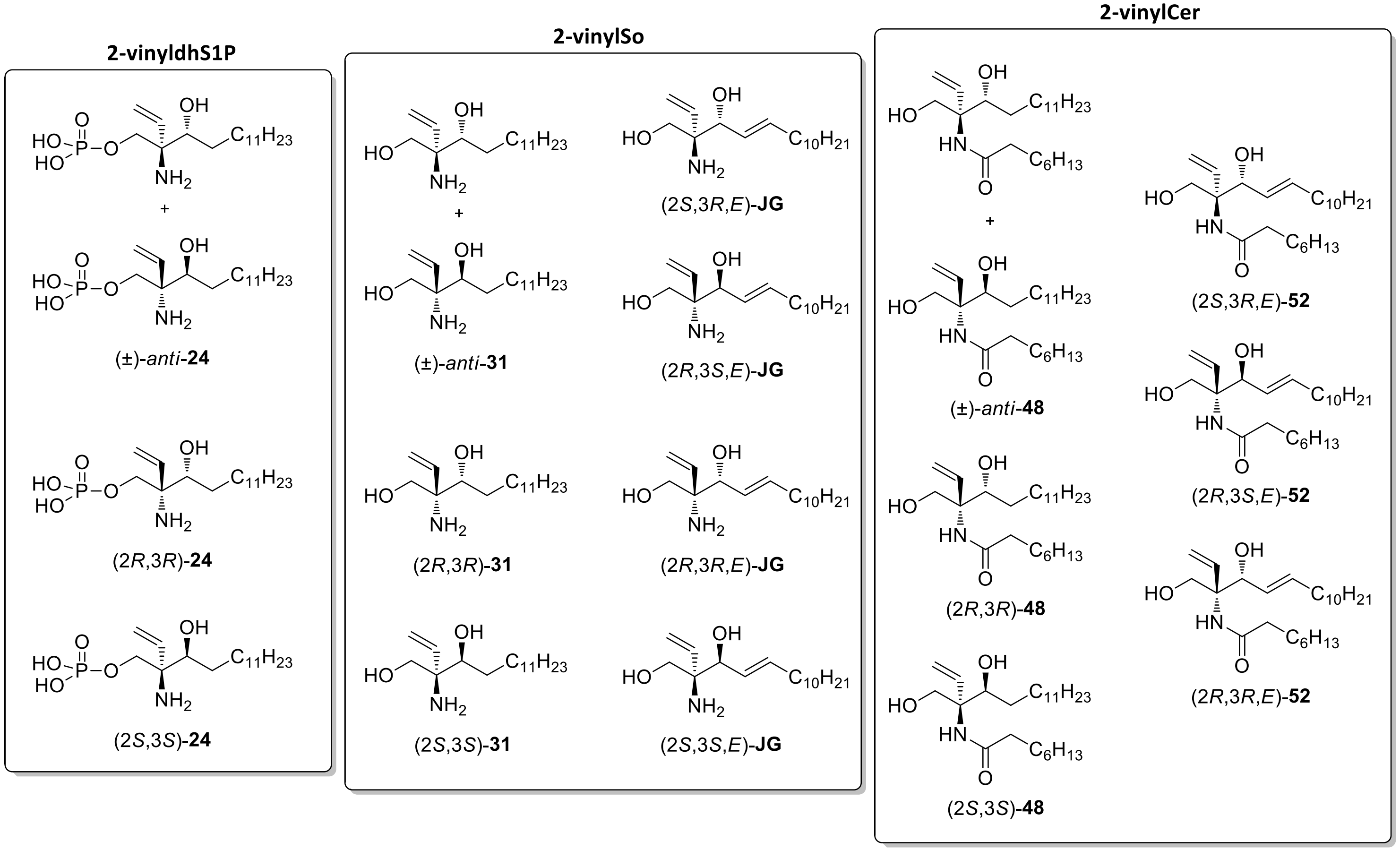
2-vinyldhS1P
(±)-anti-24
(2R,3R)-24
(2S,3S)-24
2-vinylSo
(±)-anti-31
(2R,3R)-31
(2S,3S)-31
(2S,3R,E)-JG
(2R,3S,E)-JG
(2R,3R,E)-JG
(2S,3S,E)-JG
2-vinylCer
(±)-anti-48
(2R,3R)-48
(2S,3S)-48
(2S,3R,E)-52
(2R,3S,E)-52
(2R,3R,E)-52

Figure 2.3.1. Summary of all the compounds tested in the biological assays.

2.3.2 Inhibition of StS1PL using RBM13 as substrate

At the beginning of this doctoral thesis, only recombinant S1PL from *Symbiobacterium thermophilum* (StS1PL)[98,99] was available in our group. This enzyme was used in our fluorescence assay using **RBM13** as a substrate (Scheme 2.3.1).[97]

Initially, phosphates **24** (mixture of isomers) were tested in the inhibition assay, which allowed the determination of the IC_{50} value as proof of concept. An IC_{50} of 2.4 µM in lisosomal rat liver preparation, as enzyme source, has been reported for the analogue **2VS1P**[38] (Figure 2.3.2) (see section 1.5.1).

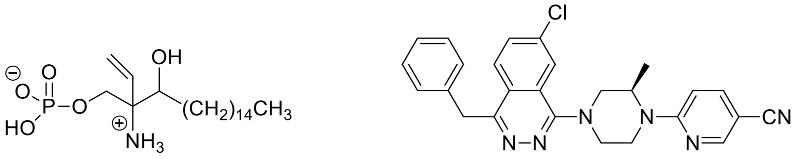

2VS1P **3b**

Figure 2.3.2. Described S1PL inhibitors: **2VS1P** (1994) and **3b** (2014).

As seen in Figure 2.3.3, the results obtained were promising, as **24** (mixture of isomers) showed a 95% of inhibition of StS1PL activity at 250 µM after 4h of incubation. Furthermore, results illustrate a progressive decrease of enzyme activity along the incubation time, which could be indicative of an irreversible inhibition.

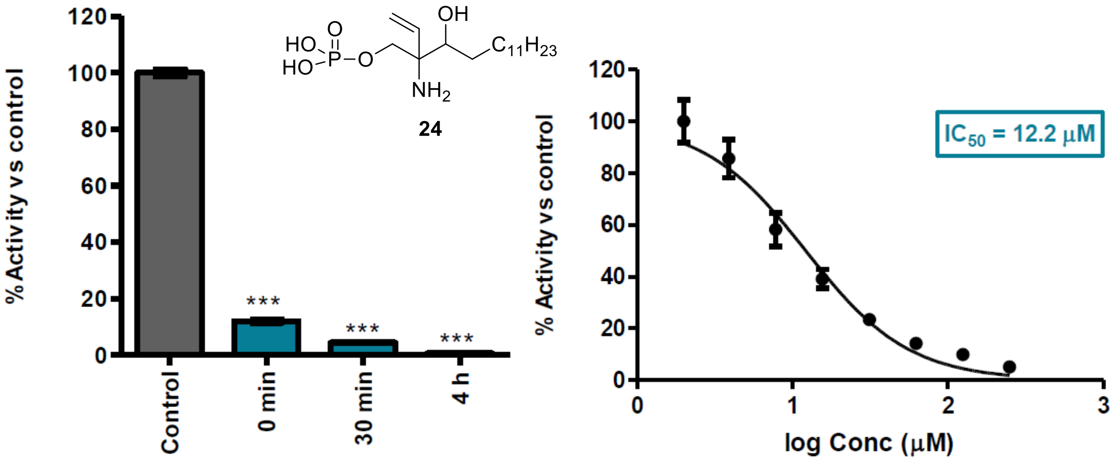

Figure 2.3.3. Left: %Activity of StS1PL versus control in the presence of 250 µM of **24** (mixture of isomers) after different preincubation times (0, 30 and 240 min). Data were analyzed by one way ANOVA following by Dunnet's multiple comparison post-test if ANOVA P < 0.0001. Right: IC_{50} of **24** (mixture of isomers) after 30 min of preincubation. Values of both experiments are means±SD of determinations from two independent experiments with triplicates.

An IC_{50} value of 12.2 µM was determined for the mixture **24**, after 30 min of incubation in StS1PL. This time was considered optimum, since longer or shorter incubation times led to enzyme inactivation or low substrate conversion, respectively. Given the different nature of our experiment, our IC_{50} value is not comparable to that described by Boumendjel and Miller for **2VS1P** in their original work.[38]

2.3.3 Inhibition of hS1PL using RBM7-148 as substrate

In 2014, Weiler *et al.* reported on a recombinant human S1PL (hS1PL) expressed in Sf9 insect cells.[34] Thanks to a kind donation of Prof. Andreas Billich (Novartis), we were able to use this enzyme to test the stereoisomers of **24** (Figure 2.3.1). In addition, our improved fluorogenic substrate **RBM7-148** (Scheme 2.3.2) was used in these experiments. The combination of hS1PL as enzyme source and a better fluorogenic substrate improved the assay conditions in terms of reaction sensitivity and substrate requirements, in comparison to the initial combination of StS1PL as enzyme source and **RBM13** as substrate.

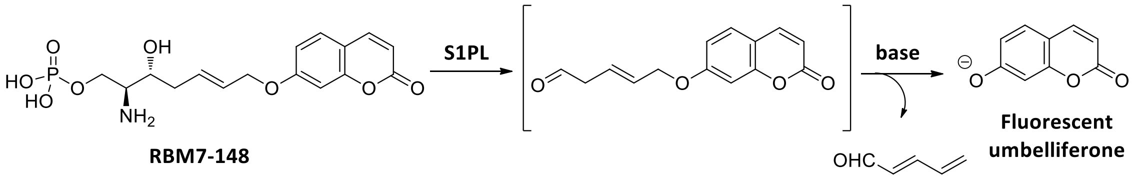

Scheme 2.3.2. Umbelliferone release from **RBM7-148** after reaction with S1PL, followed by treatment with a base.

Furthermore, the recently reported hS1PL inhibitor **3b**[34] (see section 1.5.3) was used as a positive control. Again, we are deeply acknowledged to Prof. Andreas Billich (Novartis) by a kind donation of a sample of **3b** (Figure 2.3.2).

2.3.3.1 S1PL inhibition of phosphates 24

Results of inhibition of hS1PL for the different stereoisomers of **24** (Figure 2.3.4), showed (2*S*,3*S*)-**24** as the most potent isomer, with an around 85% inhibition ($p<0.001$) *versus* control at 250 µM. Under these conditions, **3b** (10 µM) displayed an almost complete enzyme inhibition. No pre-incubation time was set for these experiments.

By using a pre-incubation time from 15 to 60 min, higher inhibition was obtained, albeit lower fluorescence values for the control were observed. As a result, smaller fluorescence differences between control and blank experiments were observed, which represented a serious drawback in terms of assay sensitivity. For this reason the use of preincubation time for these experiments was discarded.

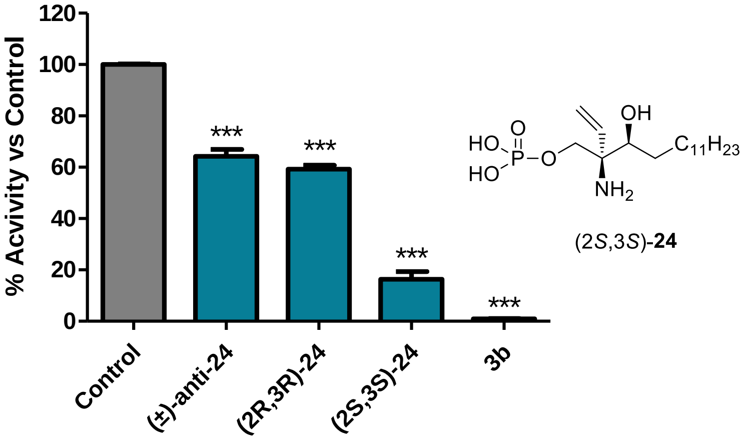

Figure 2.3.4. % Activity versus control of hS1PL of stereoisomers of compounds **24.** **3b** inhibitor is taken as positive control of inhibition. Compound **RBM7-148** was used as substrate at a final concentration of 125 µM. Data are the mean ± SD of four independent experiments with duplicates. Data were analyzed by one way ANOVA following by Dunnet's multiple comparison post-test if ANOVA ($p< 0.0001$).

An IC_{50} of 33.4 ± 8.6 µM was calculated for (2*S*,3*S*)-**24**, the eutomer in hS1PL. An optimum incubation time of 180 min was set, since longer times led to a loss of the enzyme activity. This data was obtained from three independent experiments with duplicates. No pre-incubation time was set for these experiments.

In these assays, we observed again that the inhibitory activity of (2*S*,3*S*)-**24** increased through the time (data not shown), which could be indicative of an irreversible inhibition. For this reason, irreversibility assays were attempted in order to confirm this assumption.

The irreversibility of an inhibition can be determined by measuring the recovery of the enzyme activity after a rapid and large dilution of the putative enzyme-inhibitor complex. A convenient method consists of incubating the target enzyme at a concentration of 100-fold over the concentration required for the activity assay, with an inhibitor concentration equivalent to 10-fold the IC_{50}. After a reasonable equilibration time (typically 15–30 minutes), this mixture is diluted 100-fold into reaction buffer containing the enzyme substrates to initiate reaction. The progress curve for this sample is then measured and compared to that of a similar sample of enzyme incubated and diluted in the absence of inhibitor. For reversible inhibitors the enzyme activity is recovered with time. On the contrary, irreversible or tight binding inhibitors display slow or no recovery of the activity of the enzyme.[55]

As shown in Figure 2.3.5, after testing (2*S*,3*S*)-**24** under the above conditions, a clear pattern of irreversibility or tight binding inhibition was observed, since the enzyme activity could not be recovered after 180 min. This was not observed in the control experiment (DMSO), from which S1PL activity was recovered in a linear way.

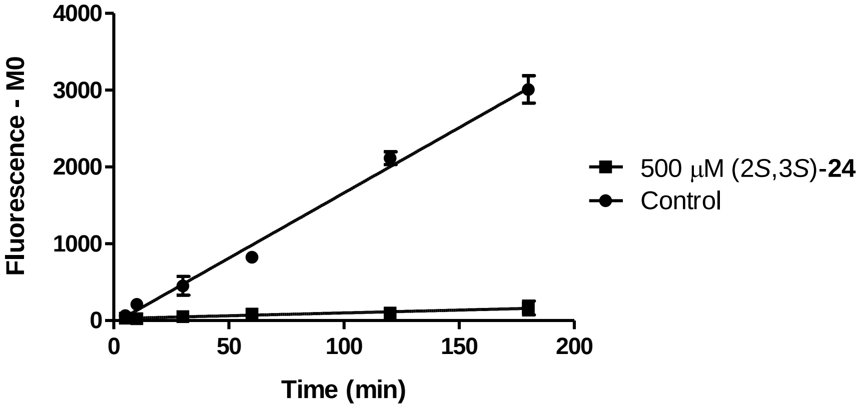

Figure 2.3.5. Lack of recovery of enzyme activity with (2*S*,3*S*)-**24** in a dilution assay. Compound **RBM7-148** was used as substrate at a final concentration of 125 μM. Data are the mean ± SD of two independent experiments with duplicates.

Based on the above results and on the proposed mechanism for S1PL,[98] it is conceivable to assume that **24** behaves as a mechanism-based inhibitor, which gives rise to a reactive intermediate (**26**) able to irreversibly bind to a nucleophilic centre of the enzyme active site (Figure 2.3.6). This was corroborated by ESI-MS experiments that revealed an increase of the mass protein corresponding to **26**, as explained below.

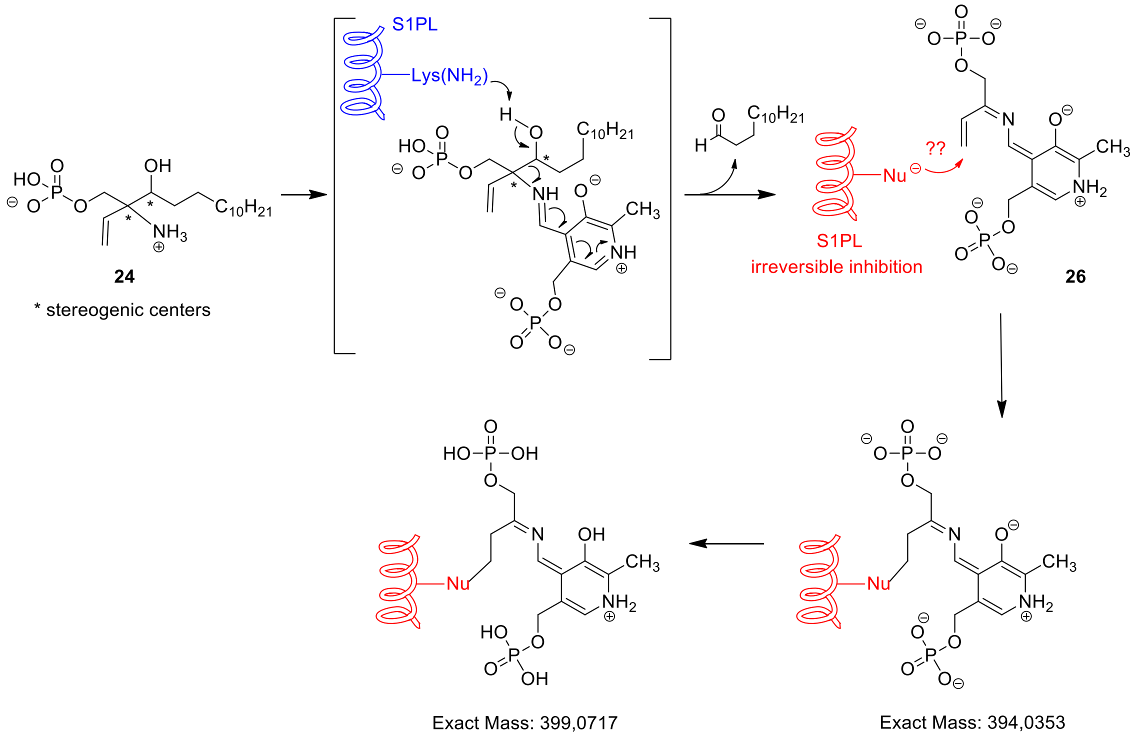

Figure 2.3.6. Postulated mechanism for the irreversible inhibition of S1PL by **24**. The protein should increase the mass with if an irreversible inhibition with **26** takes place.

ESI-MS experiments carried out in Max Planck Institute (Düsseldorf, Germany), thanks to the kindness of Dra. Gemma Triola, corroborated the above assumption. As depicted in Figure 2.3.7, the control sample (A) containing StS1PL in a buffer solution gave a major peak with a mass of 55437 Da, that is two units more than the described mass reported by Bourquin[10] (p 87), which is consider within the error range given the experimental conditions. This peak corresponds to the mass of the protein sequence (without the *N*-terminal methionine). Although they described two different populations, without cofactor (mass of 55435) and with PLP (55665), we only saw the mass of the enzyme without PLP (called apo-form).

After incubation of **24** for 1h with StS1PL at 37ºC, ESI-MS of the sample showed a major peak corresponding to the apo-form of the enzyme (55435 Da), together with a minor peak of 55834 Da. Interestingly, the observed mass increment (399) for this minor peak was in agreement with the expected mass of the protein after Michael addition to the quinonimine **26** (Figure 2.3.6). Unfortunately, we have not been able to reproduce these results using hS1PL as enzyme source under similar experimental conditions since any clear peak could be identified, including that of the protein without inhibitor.

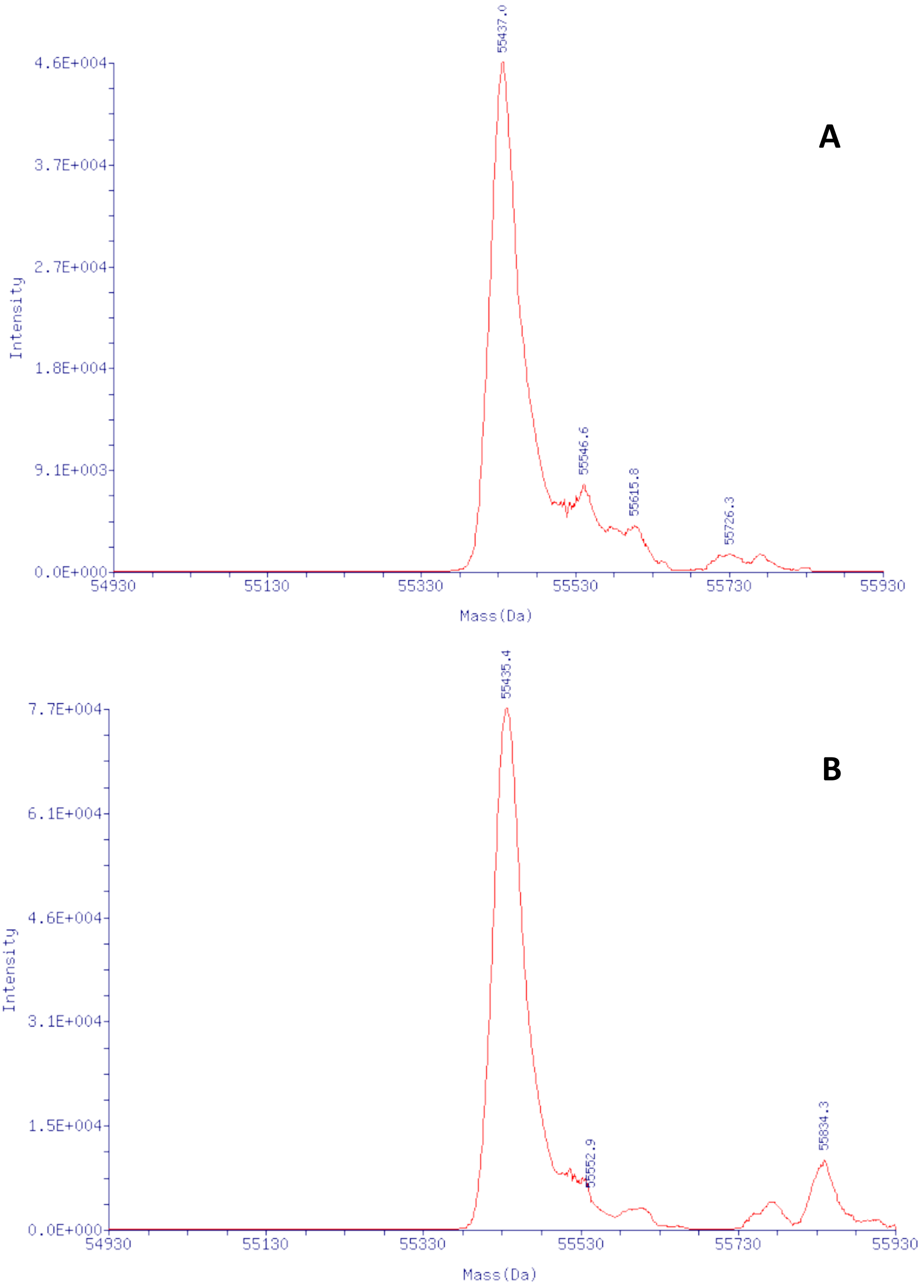

Figure 2.3.7. ESI-MS of **A:** control, StS1PL without inhibitor. The major pick sows the mass of the enzyme; 55437. **B:** StS1PL incubated 1h with **24**. It shows the mass of the control; 55435 and a peak with an increase of mass of 399 that corresponds to the **26**; 55834.

2.3.3.2 S1PL inhibition of amino alcohols 31 and JG

Results of inhibition of hS1PL for the stereoisomers of **31** and **JG** (Figure 2.3.8), showed (±)-*anti*-**31** and (2*S*,3*R*)-**JG** as the more potent isomers, with more than 80% inhibition (p<0.001) *versus* the control at 200 µM.

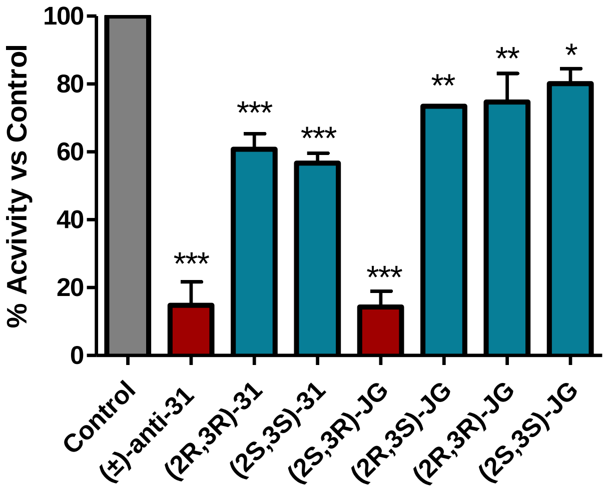

Figure 2.3.8. % Activity versus control in hS1PL for different stereoisomers of compounds **31** and **JG**. Compound **RBM7-148** was used as substrate at a final concentration of 125 µM. Data are the mean ± SD of three independent experiments with duplicates. Data were analyzed by one way ANOVA following by Dunnet's multiple comparison post-test if ANOVA ($p < 0.0001$).

An IC_{50} for (2*S*,3*R*)-**JG** of 89.4 µM was determined. This data was calculated from three independent experiments, with duplicates and with 60 min of incubation time. No pre-incubation time was set for these experiments.

It was not possible to determine the IC_{50} for (±)-*anti*-**31**, due the impossibility to adjust the dose-response curves. This abnormal behaviour could be attributed to the racemic nature of the mixture.

The above results suggest that the phosphate group at C1 is not necessary for hS1PL inhibition, although it confers a slightly higher potency. However, hS1PL shows a different stereoselectivity for each type of inhibitors. Thus, while amino phosphate (2*S*,3*S*)-**24** is the most potent inhibitor, amino alcohol (2*S*,3*R*)-**JG** is the most potent of this series.

2.3.4 Cell viability (MTT)

The cytotoxicity of these compounds was determined in A549 cells, showing the LD_{50} values shown in Table 2.3.1.

Compound	Configuration	LD_{50} (µM)
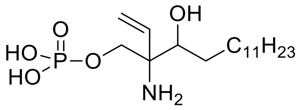	(±)-*anti*-**24**	50.5 ± 9.3
	(2*R*,3*R*)-**24**	36.9 ± 5.7
	(2*S*,3*S*)-**24**	55.8 ± 8.5
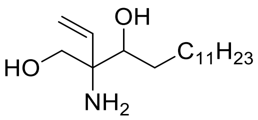	(±)-*anti*-**31**	21.9 ± 3.3
	(2*R*,3*R*)-**31**	24.0 ± 2.5
	(2*S*,3*S*)-**31**	19.6 ± 1.9
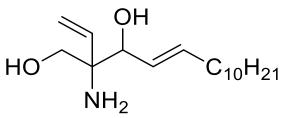	(2*S*,3*R*)-**JG**	30.3 ± 2.9
	(2*R*,3*S*)-**JG**	26.4 ± 2.4
	(2*R*,3*R*)-**JG**	34.1 ± 3.6
	(2*S*,3*S*)-**JG**	29.5 ± 3.0
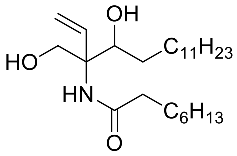	(±)-*anti*-**48**	72.8 ± 6.8
	(2*R*,3*R*)-**48**	66.0 ± 8.9
	(2*S*,3*S*)-**48**	60.1 ± 5.4
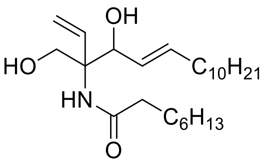	(2*S*,3*R*)-**52**	60.9 ± 9.3
	(2*R*,3*S*)-**52**	61.5 ± 7.9
	(2*R*,3*R*)-**52**	54.0 ± 6.0

Table 2.3.1. Cytotoxicity of the different stereoisomers of **24** (DMSO as a vehicle), **31**, **48**, **JG** and **52** (MeOH as a vehicle). A549 cells were treated with different concentrations of these compounds or the vehicles for 24 h and the number of viable cells was determined by the MTT test. Data correspond to the average ± SD of three independent experiments with triplicates.

All the tested compounds showed LD_{50} values in the mid µM range. Amino diols **31** and **JG** were slightly more cytotoxic than ceramides **48** and **52,** whereas amino phosphates **24** were moderately cytotoxic.

Regrettably, the IC_{50} value of the different calculated isomers is proximate or above of their LD_{50} values.

2.3.5 Lipidomics

2.3.5.1 Metabolism of the administered compounds

The metabolism of configurationally defined vinylSos **JG** and vinylCers **52** was evaluated in A549 cells at sub-toxic concentrations for 24 hours. Among compounds **JG**, only the 2*S*,3*R* diastereomer was *N*-acylated (Figure 2.3.9 A,B). Interestingly, only the C22, C24 and C24:1 acyl derivatives were formed (Figure 2.3.9A). Since A549 cells produce also Cers with other *N*-acyl chains, with C16 being also very abundant,[100,101] this result suggests that (2*S*,3*R*)-**JG** is a substrate of ceramide synthase 2 (CerS2), which produces long chain Cers, but it is not substrate of CerS5 and CerS6, which catalyze the formation of C16 Cer.[102] This is the first example of a sphingoid base selectively used by a specific CerS. On the other hand, (2*S*,3*R*)-**JG** and, to a significantly lower extent, (2*S*,3*S*)-**JG** are phosphorylated at hydroxyl at C1 (Figure 2.3.9C), which supports that, despite the presence of the vinyl group, the natural stereochemistry at C2 is essential for sphingosine kinase activity, with preferential activity over the compound having the natural (2*S*,3*R*) configuration.

The results obtained with the *N*-octanoylamides derived from **JG** (compounds **52**) are in agreement with those found with the free aminodiols (**JG**). Among the compounds tested, only (2*S*,3*R*)-**52** was metabolized to amides with other *N*-acyl chains, which included only long chain derivatives (C22:0, C24:0 and C24:1) (Figure 2.3.9D,E). Furthermore, the corresponding free bases (**JG**) were detected in the extracts, albeit at lower levels than those of the administered amides **52** (Figure 2.3.9F). These results indicate that compounds **52** are hydrolyzed by CDase, and that the released (2*S*,3*R*)-**JG**, but not the other diastereomers, is then acylated by CerS2. Which one of the 5 different CDases[103] is responsible for the hydrolysis of Cers **52** is so far unknown. Phosphates (**JG**-PO_3) were not detected in extracts from cells treated with **52**, except for the (2*S*,3*R*) isomer. Nevertheless, peak areas were very low and an accurate quantification could not be carried out. This is not unexpected considering the phosphorylation conversion levels, the low amounts of substrate (2*S*,3*R*)-**JG** generated from (2*S*,3*R*)-**52** and the detection limit of the technique for sphingoid base phosphates.

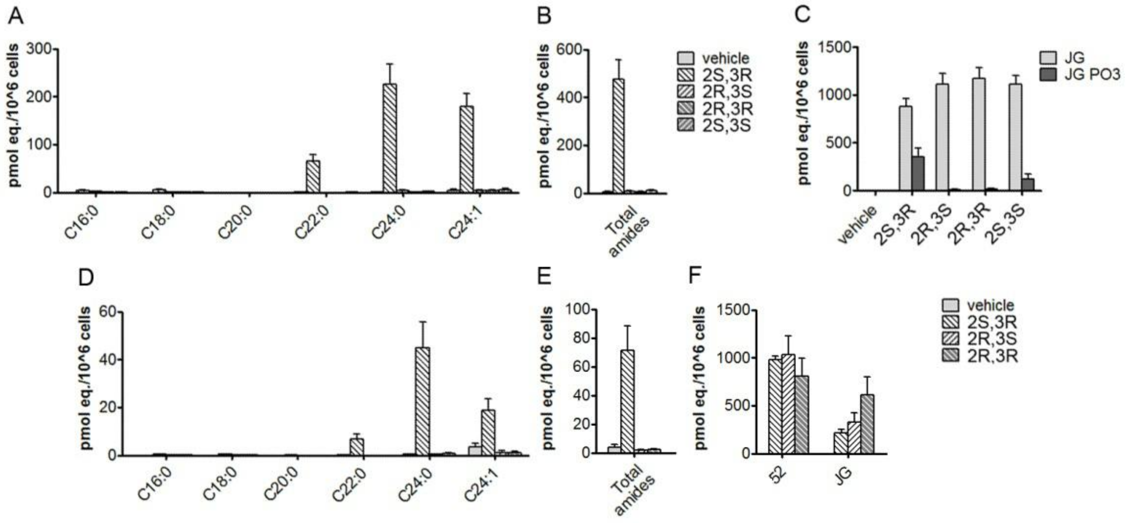

Figure 2.3.9. Metabolism of compounds **JG** and **52.** Cells were incubated with: A-C, **JG** (15 µM) and D-F, **52** (30 µM) for 24 h. Lipid analysis was carried out by UPLC/TOF MS in ESI + (free bases and amides) or ESI – (phosphates). A-C, amounts of amides (A,B) and phosphates (C) present in cells treated with the different **JG** stereoisomers. D-F, amounts of amides (D,E), incorporated **52** (F) and **JG** (E) formed form **52**. Data were obtained from two independent experiments with triplicates.

Analysis of lipid extracts from A549 cells incubated with (±)-*anti*-**31** showed a higher level of phosphorylation than enantiomerically enriched (2*R*,3*R*)-**31** and enantiomerically pure (2*S*,3*S*)-**31**. Phosphorylation levels were higher at 24 h than at 1 h. Likewise, (±)-*anti*-**31** was *N*-acylated, while (2*R*,3*R*)-**31** and (2*S*,3*S*)-**31** were not. Interestingly, only the long chain derivatives (C22:0, C24:0 and C24:1) were formed, suggesting that CerS2 exhibits stereoselectivity for the vinyl bases. Similarly to phosphorylation, higher levels of *N*-acylation occurred at 24 h than at 1 h. Whether only one enantiomer (2*S*,3*R* or 2*R*,3*S*) of **31** or both are phosphorylated and *N*-acylated needs to be investigated with the pure enantiomers. All these results are resumed in Figure 2.3.10, below.

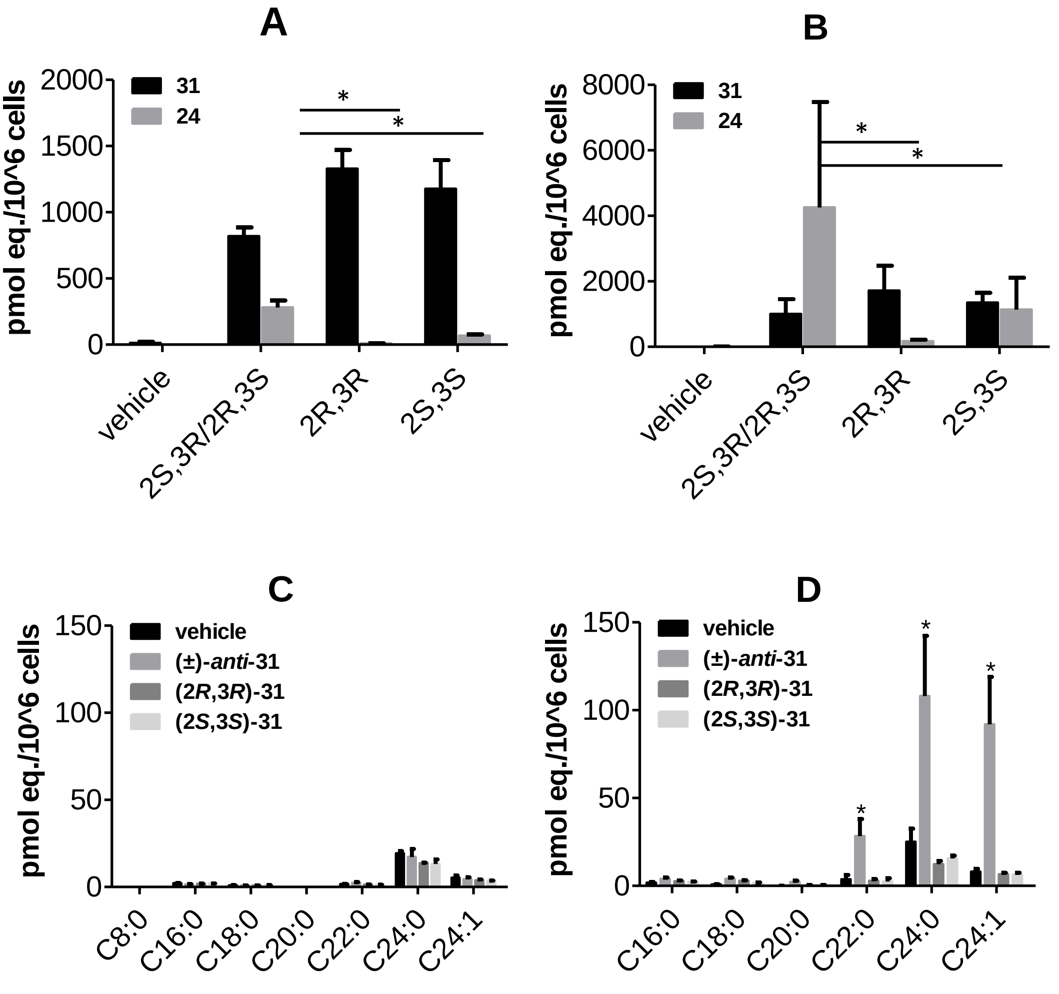

Figure 2.3.10. Metabolism of **31** (10 µM) to the C1-O-phosphate **24** (A and B) and N-acylderivatives (C and D) in A549 cells treated with the compounds for 1 h (A and C) and 24 h (B and D). Data are the mean ± SD of two experiments with triplicates. In A and B, means are statistically different between groups when indicated. (*, $p < 0.05$; unpaired two tailed t test). In C and D means are statistically different from vehicle when indicated (*, $p < 0.05$; unpaired two tailed t test).

Analysis of lipid extracts from cells treated with **48** showed that the (±)-*anti*-**48** was transacylated only at 24 h after treatment, likely by CDase hydrolysis and further CerS-catalyzed reacylation (Figure 2.3.11). In agreement with the results found with **31**, only the long chain derivatives (C22:0, C24:0 and C24:1) were formed. In contrast, and also in accordance with the results found with **31**, (2*R*,3*R*)-**48** and (2*S*,3*S*)-**48** were not transacylated. Whether only one enantiomer (2*S*,3*R* or 2*R*,3*S*) or both are transacylated needs to be investigated with the pure enantiomers.

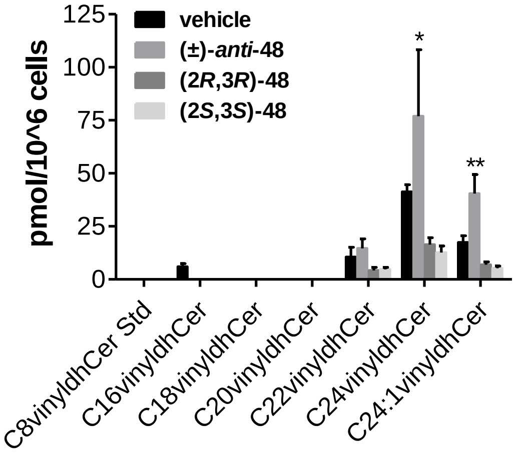

Figure 2.3.11. Transacylation of **48** (40 µM) in A549 cells treated with the compounds for 24 h. Data are the mean ± SD of two experiments with triplicates. Means are statistically different from vehicle when indicated. *, p< 0.05; **, p<0.01 (unpaired two tailed t test)

2.3.5.2 Effect on the natural sphingolipidome

Analysis of natural sphingolipids showed that **31** (10 µM/24h) had no effect of the amounts of ceramides , sphingomyelins and glucosylceramides (GlcCers) as compared to vehicle treated cells (data not shown). In contrast, all stereoisomers of **48** (40 µM/24h) provoked a significant decrease in Cers, SMs and GlcCers over controls (Figure 2.3.12). These results suggest that these vinylceramides may inhibit the ceramide *de novo* pathway, serine palmitoyltransferase (SPT) being a potential target.

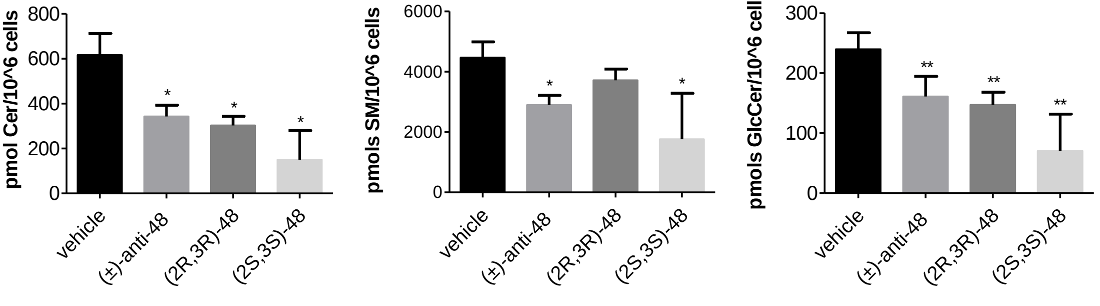

Figure 2.3.12. Effect of **48** on Cers, SMs and GlcCers in A549 cells after 24 h treatment. Data are the mean ± SD of two experiments with triplicates. Means are statistically different from vehicle when indicated. *, p< 0.001; **, p<0.01 (unpaired two tailed t test)

Cells treated with compounds **JG** (15 µM/24 h) did not experience any remarkable change in the natural sphingolipids content. In contrast, cells exposed to ceramides **52** (30 µM/24 h) contained significantly lower total Cer levels than vehicle treated controls (Figure 2.3.13A). This reduction is translated into significantly lower levels of GlcCers (Figure 2.3.13B) and SMs (Figure 2.3.13C). All the different *N*-acyl species are similarly reduced upon exposure to **52** (data not shown).

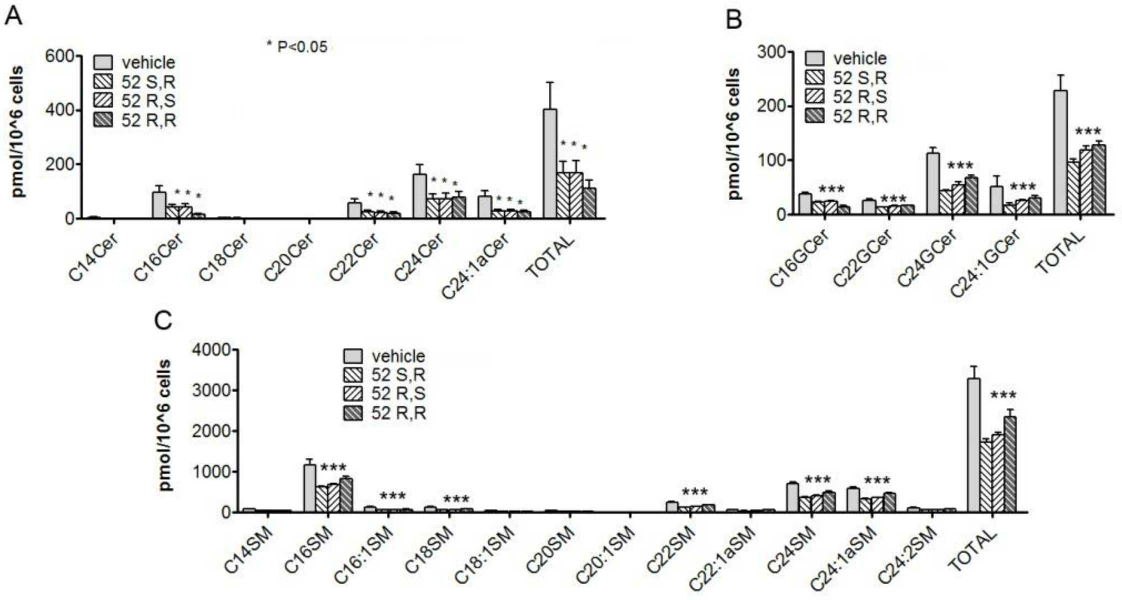

Figure 2.3.13. Effect of compound **52** on the sphingolipidome**.** Cells were incubated with **52** (30 µM) for 24 h. Lipid analysis was carried out by UPLC/TOF MS. A: amounts of natural ceramides; B: amounts of glucosyl ceramides; C: amounts of sphingomyelins formed from the different stereoisomers of **52**. Data were obtained from two independent experiments with triplicates. Asterisks indicate statistical difference with vehicle (control) (unpaired, two-tail *t* test).

As observed for amides **48**, these results are consistent with inhibition of Cer synthesis *de novo*. Since inhibition of CerS results in an increase in long chain bases and their phosphates[104,105] and either Sa, So or their phosphates are not detected in extracts after cell treatment with **52**, we suggest that SPT, the rate-limiting enzyme in Cer synthesis *de novo*, is a likely candidate to be affected by **52**. Although the three stereoisomers of **52** are *N*-deacylated, the resulting compounds **JG** have no effect on Cer, GlcCer and SM levels, which argues against their involvement in the observed inhibition. On the other hand, the fact that the three diastereomers of **52** produce similar decreases in Cer, GlcCer and SM levels, while only the 2*S*,3*R* isomer is reacylated is against the reacylation products being the inhibitory species. Collectively, our data support that amides **48** and **52** could be responsible for the putative SPT inhibition.

2.3.6 Computational studies on the inhibition of hS1PL by compounds 24

These studies have been carried out by Dr. Jordi Bujons (IQAC-CSIC) within the frame of a current collaboration with our group.

In an attempt to elucidate a putative interaction model for the stereoisomers of **24** with the active site of hS1PL (PDB code 4Q6R), a computational study was carried out. Based on the described mechanism for S1P cleavage by S1PL[30] (See section 1.4), we hypothesized the general irreversible inhibition mechanism for **24** shown in Figure 2.3.14, already seen in Section 2.3.3.1.

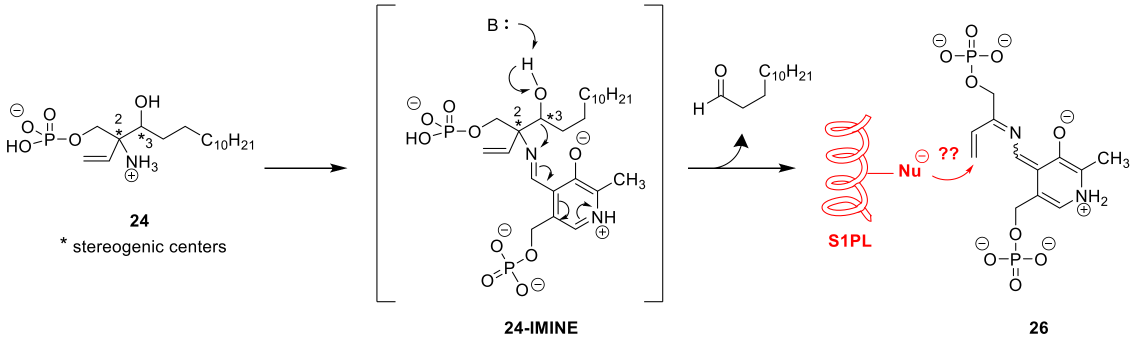

Figure 2.3.14. Proposed inhibition mechanism for the stereoisomers of **24** on S1PL.

According to our mechanistic model, compounds **24** would be able to form an external aldimine with PLP. Following a retro-aldol cleavage, tridecanal would be released and the intermediate quinonimines **26** would be ready to react in a Michael-type reaction with a nearby nucleophile, thus forming a covalent bond at the enzyme active site to account for the presumed irreversible inhibition. This mechanism is conceptually similar to that reported for related mechanism-based irreversible inhibitors of GABA-T, another PLP-dependent enzyme.[56] In our case, the higher hS1PL inhibitory activity observed for enantiopure (2*S*,3*S*)-**24** in comparison with the corresponding enantioenriched (2*R*,3*R*) enantiomer (see Section 2.3.3.1), reveals a putative enzyme stereoselectivity towards these vinyl derivatives.

Computational models of the complexes of **24** bound into the active site of hS1PL were generated using the Schrodinger Suite software.[106] After removing the bound ligands from the 4Q6R structure of hS1PL, the imine bond between the essential Lys353 and the PLP cofactor was cleaved and the external aldimine structures from **24** (all four stereoisomers) were manually build on the resulting PLP moiety considering the 3–hydroxypyridine and the imino groups of the PLP prosthetic group in their ionized state. Figure 2.3.15 shows the minimized structures of the four hS1PL-aldimine complexes, exhibiting a similar arrangement for the different stereoisomers of **24**. For each isomer, the aliphatic chain is placed along the narrow hydrophobic access channel that communicates the active site of the protein with the surface. In addition, the phosphate group can establish strong interactions with the anion binding site of hS1PL formed by residues T148, Y150, H174 and K359, confirming that the presence of the phosphate moiety is essential for the binding and orientation of the molecules in the enzyme active site. On the other hand, the reactive C3(OH) group is oriented towards the PLP-phosphate and the side chain of H242, with which in most cases establishes hydrogen bond interactions either as H-bond donor (with phosphate) or acceptor (with H242).

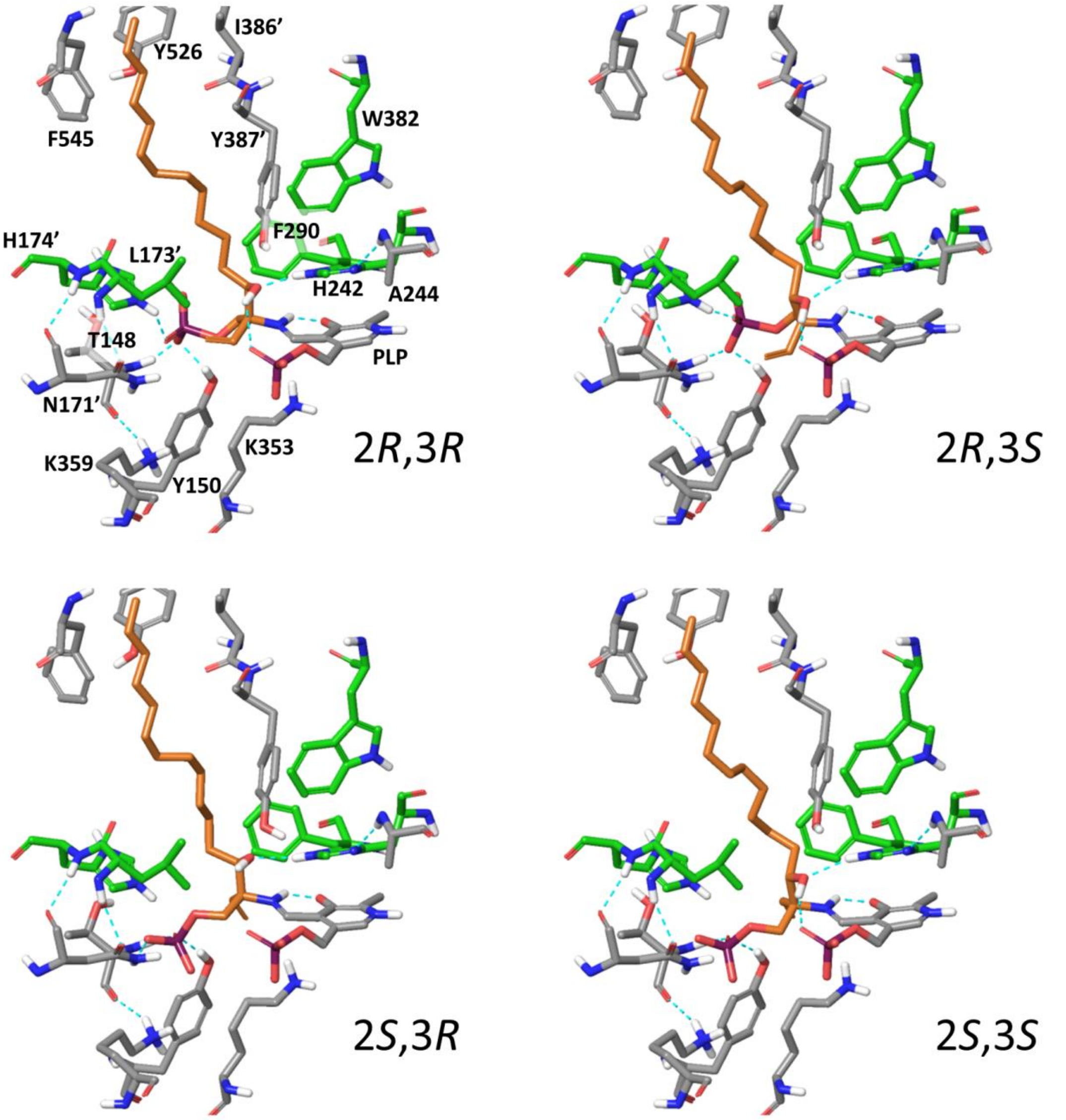

Figure 2.3.15. Minimized structures of the modelled aldimines (orange) of the four stereoisomers of **24** in the hS1PL active site. Residues forming a hydrophobic patch close to the PLP-binding site are highlighted in green.

A more in depth analysis of these interactions using molecular dynamics simulations in explicit water (50ns, 300 K, periodic boundary conditions, NPT ensemble) was carried out. In all cases, the simulations showed that the structures were mostly stable after an initial slight and normal rearrangement of the whole protein, with Cα-RMSD values around 1.5 Å relative to the starting structures.

Aldimines from (2*R*,3*S*)-**24** and (2*S*,3*R*)-**24** showed a similar hydrogen bond association pattern. Thus, in both cases the C3(OH) group was hydrogen-bonded to the terminal O-atoms of the PLP-phosphate during ≥ 95% of the simulation time and to H242, although this last interaction was established for 94% of the simulation time for (2*R*,3*S*)-**24** and only for about 53% for (2*S*,3*R*)-**24**, as shown in Figure 2.3.16. This would suggest that the PLP-phosphate could act as base, capturing the proton from the C3(OH), the first step of the retro-aldol cleavage of these compounds, and that the interaction with H242 could serve to increase the acidity of this hydroxyl group.

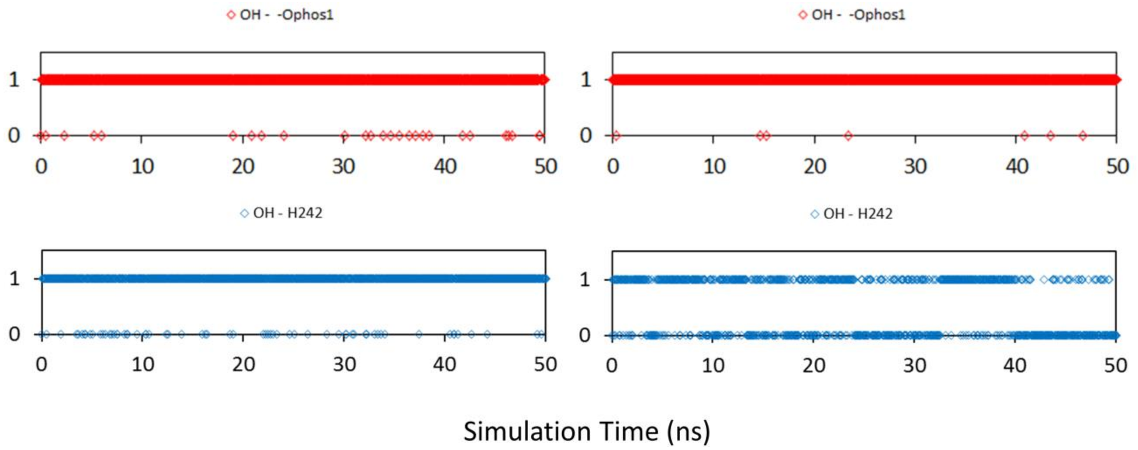

Figure 2.3.16. Time dependence of the hydrogen bond interactions for the C3(OH) of the aldimines from (2*R*,3*S*)-**24** (left) and (2*S*,3*R*)-**24** (right) with the terminal O-atoms of the PLP-phosphate (red) and the ε-NH of H242 (blue).

Similarly, the aldimine from (2*S*,3*S*)-**24** established a H-bond interaction between its C3(OH) group and H242 for about 95 % of the simulation, but almost no direct interaction with the PLP-phosphate was observed (Figure 2.3.17). However, looking at the minimum distance between the H-atom of the C3(OH) and the terminal O-atoms of the PLP-phosphate it came out that, on average, both atoms were separated by only 3.6 ± 0.4 Å throughout the simulation, and that indeed a H-bond interaction was established for most of the time through a mediating water molecule. Thus, it could be speculated that in this case the PLP-phosphate could also promote the proton abstraction from the C3(OH) through that water molecule.

In contrast, for the aldimine from (2*R*,3*R*)-**24** a conformational shift was observed after the first 13 ns of simulation. Due to this change, the C3(OH) went from being H-bonded to H242 to adopt a disposition close to the C1-phosphate, establishing a H-bond with the O-atom of the C1(O)-phosphate group (P-O-C) for the rest of the simulation (Figure 2.3.17). This would suggest that in this case it could be that phosphate, rather than the PLP-phosphate, the one that could abstract the proton from the C3(OH). Since this proton abstraction is crucial for the initiation of the retro-aldol cleavage of the substrates, the different interactions found for each stereoisomer could account for the observed differences between them as enzyme inhibitors.

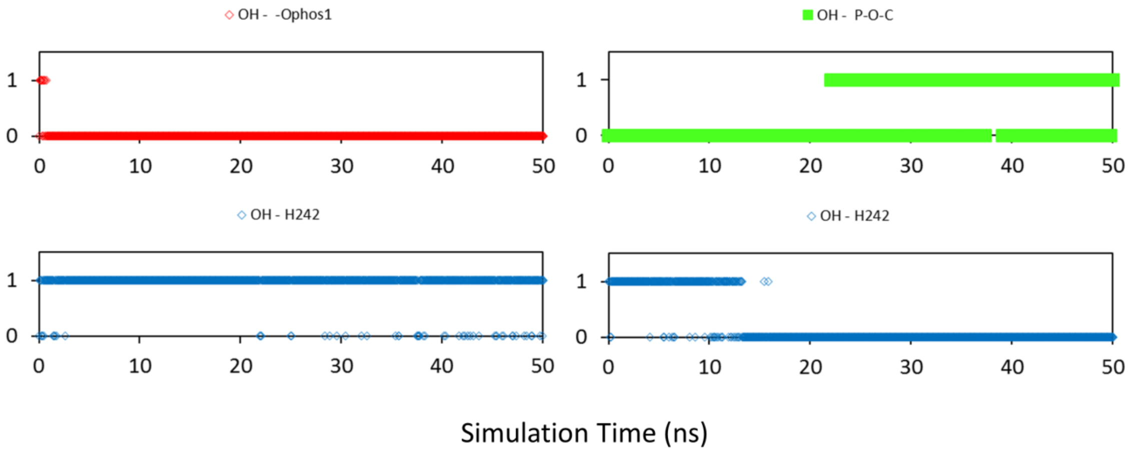

Figure 2.3.17. Time dependence of the hydrogen bond interactions for the C3(OH) of the aldimines from (2*S*,3*S*)-**24** (left) and (2*R*,3*R*)-**24** (right) with the terminal O-atoms of the PLP-phosphate (red), the ε-NH of His242 (blue) and the O-atom of the C1(O)-phosphate group (green).

Concerning the reaction products, and assuming a concerted E2 mechanism for the elimination step[30], two stereoisomeric quinonimines (***E*-26** and ***Z*-26**) would be expected, depending on the configuration at C2 of the intermediate aldimines arising from **24** (Figure 2.3.18). Interestingly, the orientation of the PLP moiety, which is determinant for the configuration of the resulting quinomimines **26**, is imposed by the steric restrictions of the enzyme active site, where both phosphate groups are close in space. Likewise, it is worth mentioning that the configuration at C3 is irrelevant for the stereochemical outcome of the resulting quinonimines **26**.

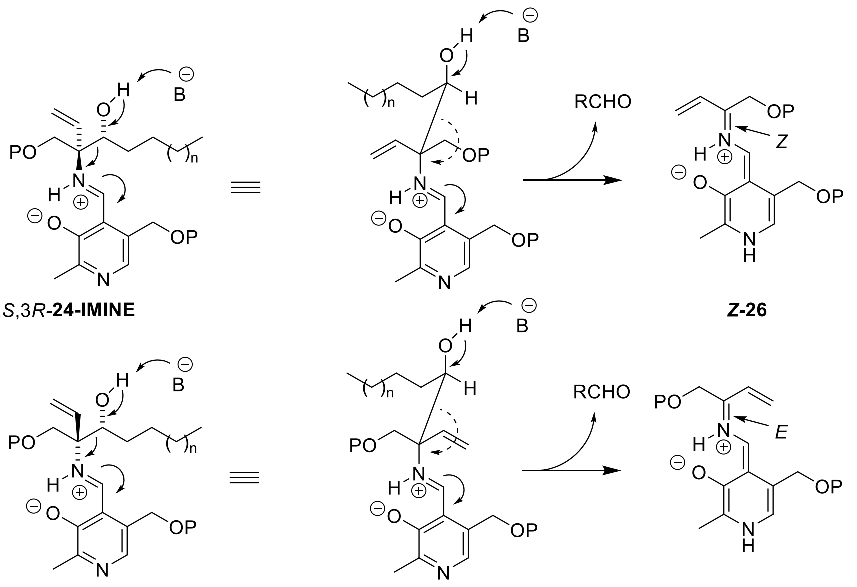

2*S*,3*R*-**24-IMINE**

***Z*-26**

2*R*,3*R*-**24-IMINE**

***E*-26**

Figure 2.3.18. A suggested E2-elimination pathway for the reaction of aldimines from **24** with hS1PL.

The molecular models of each quinonimine at the hS1PL active site revealed a different disposition for each stereoisomer. Thus, ***Z*-26**, arising from the C2(*S*) aldimines, places the reactive vinyl moiety at about 5 Å from the ε-amino group of the essential L353. This suggests that this group could be the nucleophile for the Michael-type addition postulated in Figure 2.3.14, which would be responsible for the irreversible type of inhibition postulated for these compounds. Another potential nucleophile could be the thiol group from C317. However, since this is around 10 Å away from the vinyl group, some conformational rearrangement of the complex would be required to bring the S-atom and the vinyl group close enough for the nucleophilic attack. On the other hand, in the complex of ***E*-26**, arising from the C(2*R*) aldimines, the vinyl moiety is located between L353 and L359, also at around 5 Å from each ε-amino group. All these interactions are depicted in Figure 2.3.19.

With this data in hand, it is difficult to postulate any of both of the lysine residues as potential nucleophiles. However, looking at the interactions of both groups, it comes out that the ε-amino group of L359 is strongly hydrogen bonded to residues T148 and H352, while L353 can interact with D350. These interactions would make more difficult that both potential nucleophiles could get close enough to the reactive vinyl group, and this would correlate with the lower activity observed for the (2*R*)-**24** stereroisomers.

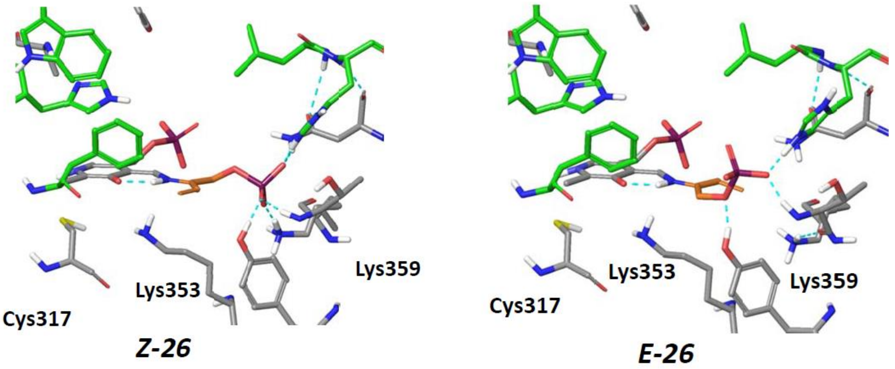

Figure 2.3.19. Molecular models of the two quinonimines ***Z*-26** and ***E*-26** in the hS1PL active site.

2.3.7 Conclusions

- The IC_{50} of **24** was calculated *in vitro* for purified enzyme: the racemic mixture on StS1PL presents an IC_{50}= 12.2 µM with RBM13 as a substrate and experiments on hS1PL with RBM7-148 as a substrate reveal that the eutomer is (2*S*,3*S*)-**24** with an IC_{50}= 33.4 µM.

- The dilution assay and the ESI-MS experiments shown the typical behaviour of irreversible or tight binding inhibitor.

- The aminodiols analogues **JG** and saturated **31** showed a moderate inhibitor activity towards hS1PL where natural configuration (2*S*,3*R*) seems the most potent in both cases ((±)-*anti* mixture for **31**). It suggests then that the phosphate is not strictly necessary to inhibit hS1PL, although it confers more potency.

- The LD_{50} values of different isomers of **24**, **31**, **JG**, **48** and **52** have been calculated. Regrettably, the IC_{50} value of the different calculated isomers is proximate or above of their LD_{50} values.

- Lipidomics experiments suggests that (2*S*,3*R*)-**JG** and (±)-*anti*-**31** are substrate of CerS2, which produces long chain Cers, but it is not substrate of CerS5 and CerS6, which catalyze the formation of C16 Cer. It is the first time that a selective CerS2 substrate is found. Besides, both **48** and **52** are hydrolysed by CDases and only the corresponding natural configuration of the free aminodiol base was acylated again in agreement with **JG** and **31** results.

- Related to the effects on natural sphingolipidome, all diastereomers of vinylCers **48** and **52** seems to inhibit the Cer *de novo* pathway, beeing Serine palmitoyltransferase (SPT) a potential target, since a decrease of Cers, SMs and GlcCer was found.

- In computational studies and molecular dynamics simulations, suggest that the PLP-phosphate could act as base, capturing the proton from the C3(OH), the first step of the retro-aldol cleavage of these compounds except from (2*R*,3*R*)-**24** that it could be the C1-phosphate the one that could abstract the proton.

- Also, the formed quinonimines after the aliphatic chain removal by the enzyme will be different if they come from C2(*S*) aldimines (ending up with ***Z*-26**) or from C2(*R*) aldimines (***E*-26**). For ***Z*-26**, the most likely nucleophile that could attack the vinyl group is L353 at about 5 Å, and for ***E*-26**, the vinyl moiety is located between L353 and L359, also at around 5 Å from each ε-amino group.

3. SUMMARY AND CONCLUSIONS

The most remarkable conclusions derived from each of the topics presented in the present doctoral thesis are highlighted in this section. A detailed analysis of the conclusions derived from each of the topics presented in this dissertation is outlined at the end of the corresponding sections.

- In chapter 1 the development of compounds that are able to specifically target sphingolipid metabolizing enzymes is a promising area of research was shown, which will most likely provide new tools and drugs for the treatment of several disorders. In this context, the inhibition of S1PL has been related with autoimmune disorders, inflammation diseases or cellular deregulation in several types of cancer, among others, and it is considered a promising new target for drug development.

- In chapter 2 were displayed several synthetic route to obtain enantiomerically pure saturated sphingolipid analogues, but unfortunately only the enantiopure (-)-*syn*, enantiorich (+)-*syn* and the (±)-*anti* as a racemic mixture were achieved for aminophosphate **24**, aminodiol **31** and dhCers analogs **48**. For the unsaturated series, the four aminodiols **JG** and three Cers **52** were achieved as enantiomerically pure compounds. The absolute configuration for the mentioned compounds was determined for all synthetic routes used.

- In chapter 3 the enantiopurity found in chapter 2 of intermediates **51** and their precursors **45** were confirmed through experiments of VCD.

- In chapter 4 the IC_{50} of **24**, both on StS1PL and hS1PL, was calculated. The eutomer on hS1PL is (2*S*,3*S*)-**24** with an IC_{50}= 33.4 µM, that shows the typical behaviour of irreversible or tight binding inhibitors. The aminodiols analogues (2*S*,3*R*)-**JG** and saturated (±)-*anti*-**31** showed a moderate inhibitor activity towards hS1PL too, what suggests that the phosphate is not strictly necessary to inhibit hS1PL, although it confers more potency. Regrettably, the IC_{50} value of the different calculated isomers is proximate or above of their LD_{50} values.
- Lipidomics experiments suggests that (2*S*,3*R*)-**JG** and (±)-*anti*-**31** are substrate of CerS2 and the vinylCer **48** and **52** seems to inhibit the Cer *de novo* pathway, beeing Serine palmitoyltransferase (SPT) a potential target.

- In computational studies and molecular dynamics simulations, suggest that the PLP-phosphate could act as base, capturing the proton from the C3(OH), the first step of the retro-aldol cleavage of these compounds except from (2*R*,3*R*)-**24** that it could be the C1-phosphate the one that could abstract the proton.

4. EXPERIMENTAL SECTION

4.1 Chemistry

4.1.1 General remarks

All reagents were purchased from commercial suppliers and were used without further purification. Reactions were monitored by TLC pre-coated SiO_2 aluminium plates, ALUGRAM® SIL G/UV_{254} (Machery-Nagel). Compounds were purified with the indicated solvents using flash column chromatography employing silica gel 60 Å (37-70 µm) (Chromagel) as stationary phase. Phosphates were purified with polymeric resin Amberlite® XAD4 20-60 mesh (100 Å). Yields refer to chromatographically and spectroscopically pure compounds, unless otherwise stated.

Nuclear Magnetic Resonance (NMR) experiments were carried out on a Varian Mercury 400 instrument (400MHz for ^1H, 101 MHz for ^{13}C, 162 MHz ^{31}P and 376 MHz ^{19}F). The chemical shifts (δ) are reported in ppm relative and coupling constants (J) are reported in Hertz (Hz). Signal assignments were confirmed, in some instances, using various 2D NMR spectra, including ^1H-^1H gDQCOSY and ^1H-^{13}C gHSQC. The following abbreviations were used for ^1H NMR assignments: s = singlet, d = doublet, t = triplet, q = quartet, dd = doublet of doublets, dt = doublet of triplets, td = triplet of doublets, ddd = double doublet of doublets, ddt = double doublet of triplets, m = multiplet and br = broad signal.

HRMS (High Resolution Mass Spectrometry) analyses were carried out using a UPLC-ESI-TOF equipment [Acquity UPLC® coupled to a LCT Premier orthogonal accelerated time-of-flight mass spectrometer (Waters)]. Compound characterization was carried out in Flow Injection Analysis (FIA) mode using CH_3CN/water (70:30) mixture as mobile phase.

Specific optical rotations ($[\alpha]_D$) were recorded on a digital Perkin-Elmer 34 polarimeter at 25 ºC in 1-dm 1-mL cell, using a sodium light lamp (λ = 589 nm, sodium D line), expressed in 10^{-1} deg cm^3 g^{-1}, and concentrations (*c*) are reported in g/100 mL of solvent.

HPLC analyses were performed in an Alliance HPLC system, consisting of a 2695 Separation Module (Waters) coupled to a 2996 PDA detector (Waters) and a light scattering ELS-1000 detector (Polymer Laboratories) using different columns with the following elution systems:

- Column A: Kromasil C18 (C18, 5µm, 4 x 150 mm, Tracer). Water and acetonitrile were used as a mobile phase, flowing at 1 mL/min (unless otherwise indicated).
- Column B: Halo C18 (C18, 5µm, 4.6 x 100 mm, Teknokroma). Water and acetonitrile were used as a mobile phase, flowing at 1 mL/min (unless otherwise indicated).

Chiral HPLC analyses:

- Column C: Daicel chiralpack IB (5 µm 4.6 x 250 mm). Compounds were eluted with isopropanol and hexanes at 1mL/min. Each sample was run for up to 15-30 minutes and the injection volume was set at 10 µL (unless otherwise indicated).
- Coumn D: Lux amylose (5 µm 4.6 x 250 mm, Phenomenex). Compounds were eluted with isopropanol and hexanes at 1mL/min. Each sample was run for up to 15-30 minutes and the injection volume was set at 10 µL (unless otherwise indicated).
- Column E: Chiralpack IA ((5 µm 4.6 x 250 mm). Compounds were eluted with isopropanol and hexanes at 1mL/min. Each sample was run for up to 15-30 minutes and the injection volume was set at 10 µL (unless otherwise indicated).

Semipreparative HPLC (Waters prepLC system®) coupled to Waters Prep LC controller and Waters 2489 UV/Vis detector were used.

- Column F: Kromasil C18 (XBridge, 5 µm 19 x 250 mm) were used for the separation of (±)-*syn* and (±)-*anti*-**21**.
- Column G: Halo C18 (C18, 5 µm 21.2 x 250 mm, Teknokroma) were used for the separation of (±)-*syn* and (±)-*anti*-**21**.

4.1.2 General synthetic methods

General procedure 1: Oxidation of an alcohol to an aldehyde with IBX:

A mixture of the starting alcohol (1.0 mmol) and IBX (1.5 mmol) was suspended in EtOAc (30.0 mL) under argon atmosphere. The mixture was refluxed with stirring 15 h and then cooled down in an ice-water bath. The white precipitate was filtered through a Celite® pad and washed with cool EtOAc (3 x 10.0 mL). The organic filtrates were concentrated under vacuum and the residue was purified by flash chromatography with the conditions indicated below, to afford the desired aldehyde.

General procedure 2: Grignard reaction

A solution of the starting aldehyde (1.0 mmol) and freshly prepared dodecylmagnesium bromide (1.5 mmol) in THF 0.5M was stirred for 3 h at rt under argon atmosphere. The mixture was next diluted in Et_2O (5.0 mL), washed with NH_4Cl (3 x 7.0 mL), dried over $MgSO_4$ and concentrated under reduced pressure. The crude residue was purified by flash chromatography, as indicated in each particular case.

General procedure 3: Selective phosphorylation of a primary alcohol

To a solution of the starting alcohol (1.0 mmol) in anhydrous CH_2Cl_2 (20.0 mL), neat NMI (3.0 mmol) was added dropwise at rt. The reaction was next cooled down to 0 ºC, followed by dropwise addition of neat dimethyl chlorophosphate (1.2 mmol) under argon atmosphere. The mixture was warmed to rt and stirred for additional 2h. The reaction was next quenched by addition of aq NH_4Cl (5.0 mL) and extracted with CH_2Cl_2 (3 x 10.0 mL). The combined organic extracts were dried over MgSO4, filtered and concentrated under reduced pressure. The resulting crude was purified by flash chromatography, as indicated in each particular case.

General procedure 4: Simultaneous deprotection of dimethyl phosphate esters and *N*-Boc group

Neat TMSBr (3.2 mmol) was added dropwise over a solution of the starting *N*-Boc phosphate dimethyl ester (1.0 mmol) in anhydrous ACN (25.0 mL) at 0 ºC under argon atmosphere. The reaction mixture was vigorously stirred at rt for 3h and concentrated next under reduced pressure. The crude residue was taken up in 95:5 MeOH/H2O (10.0 mL), and vigorously stirred for 1h. Evaporation under reduced pressure afforded a residue, which was purified as indicated in each case to obtain the desired product.

General procedure 5: Steglich esterification

A solution of the required carboxylic acid (1.4 mmol) and EDC (1.5 mmol) in anhydrous CH_2Cl_2 (10.0 mL) was stirred for 30 min. To this mixture, a solution of the starting alcohol (1.0 mmol) and DMAP (1.1 mmol) in CH_2Cl_2 (10.0 mL) was added dropwise. After stirring 15h at rt, the mixture was diluted with CH_2Cl_2 (10.0 mL) and washed successively with HCl 1.0 N, water, $NaHCO_3$ and water (10.0 mL each). The organic layer was dried over $MgSO_4$, filtered and concentrated under reduced pressure. The resulting crude was purified by flash chromatography, as indicated in each case.

General procedure 6: Schotten-Baumann amidation

A solution of the starting aminodiol (1.0 mmol) in THF (5.0 mL) was added at 0 °C to 10.0 mL of a 50% aqueous solution of NaOAc under stirring. After 10 min, a solution of the required acid chloride (1.5 mmol) in THF (5.0 mL) was added dropwise, and stirring was continued at rt for 5h. The reaction mixture was next diluted with $CHCl_3$ (10.0 mL), and the organic layer was washed with brine, and dried over $MgSO_4$. The solvent was removed under vacuum to furnish a crude residue, which was purified by flash chromatography, as indicated in each case.

General procedure 7: Preparation of acid chlorides

To a solution of the starting carboxylic acid (1.0 mmol) in hexanes was added dropwise neat oxalyl chloride (4.0 mmol) and DMF (5 µL, equivalent to 0.1 mmol) under argon atmosphere. The mixture was stirred at rt for 4h or until the complete disappearance of the white precipitate. Then, the solution was transferred, under inert atmosphere, to an oven-dried round-bottom flask *via* cannula and evaporated under reduced pressure. The residue was taken up in anhydrous THF (5.0 mL) and used for the next reaction without further purification.

General procedure 8: Intramolecular base-induced cyclization of carbamates

Sodium hydride (7.0 mmol from a 60% dispersion in mineral oil) was added portionwise under argon atmosphere to a solution of the starting alcohol (1.0 mmol) in anhydrous THF (35.0 mL). The mixture was warmed to 50ºC and refluxed with stirring for 15 h. The reaction was next quenched by addition of water (20.0 mL) and extracted with EtOAc (3 x 15.0 mL). The combined organic extracts were dried over anhydrous Mg_2SO_4 and concentrated *in vacuo*. The resulting crude was purified by flash chromatography, as indicated in each case.

General procedure 9: Cleavage of silyl ethers

A solution of TBAF (2.0 mmol, 1.0 M in THF) was added dropwise to a solution of the starting silyl ether (1.0 mmol) in anhydrous THF (30.0 mL) under argon atmosphere. After stirring at rt 15h, the reaction was quenched with water (20.0 mL) and extracted with EtOAc (3 x 15.0 mL). The combined organic extracts were dried over $MgSO_4$ and concentrated under reduced pressure to give a crude residue, which was purified by flash chromatography, as indicated in each case.

General procedure 10: *N*-Boc protection

To a solution of the starting amine (1.0 mmol) in anhydrous THF (15.0 mL), TEA (2.5 mmol) was added dropwise and the reaction was stirred for 15 min at rt. Next, Boc_2O (1.2 mmol) was added and stirring was continued for 48h. The resulting mixture was evaporated under reduced pressure and the crude residue was purified by flash chromatography as indicated in each case.

General procedure 11: MPA ester hydrolysis under basic conditions

To a solution of the starting MPA ester (1.0 mmol) in MeOH (13.0 mL) was added neat K_2CO_3 (4.5 mmol) and the reaction was stirred at rt for 15h. The reaction was next quenched by addition of HCl 1N (5.0 mL) and extracted with CH_2Cl_2 (3 x 10.0 mL). The combined organic extracts were dried over $MgSO_4$, filtered and concentrated under reduced pressure. The resulting crude was purified by flash chromatography, as indicated in each case.

4.1.3 Vibrational IR and VCD experimental spectra

The IR and VCD were recorded by the group of Prof. Juan Jesús López and Dr. Manuel Montejo (University of Jaén) in the laboratories of the European Centre for Chirality (EC2) at the University of Antwerp using a spectrophotometer Fourier transform BioTools dual-PEM ChiralIR-2X, equipped with a MCTV detector cooled to the temperature of nitrogen liquid, using standard liquid cells with an optical step of 100 microns and BaF_2 windows. The spectral resolution was 4 cm^{-1} and 20000 scans were accumulated (6h 30 min acquisition time) in each measure. The concentration of the samples (0.1 M) allowed obtaining IR absorbances in the recommended range of 0.1 to 0.7. The baseline correction of the spectra was performed by subtracting the spectrum of the solvent (carbon tetrachloride) in the same experimental conditions.

4.1.4 Computational studies

Computational studies were carried out by Dr. Jordi Bujons (IQAC-CSIC, Barcelona) using the Schrödinger Suite 2016.1,[106] through its graphical interface Maestro.[107] Coordinates of hS1PL (PDB 4Q6R)[34] were obtained from the Protein Data Bank at Brookhaven National Laboratory. The protein X–ray structures were prepared using the Protein Preparation Wizard[108] included in Maestro to remove solvent molecules and ions, adding hydrogens, setting protonation states[109] and minimizing the energies. Ligands were manually set up and minimized with Macromodel[110] using the OPLS3 forcefield.[111] From these, simulation systems for molecular dynamics were built using the System Builder of the Maestro-Desmond interface,[112] which automatically assigns parameters to all atom. Each protein-aldimine complex was immersed in a 120 x 120 x 120 Å cubic box of TIP3P water with enough Cl^- anions to achieve neutrality (~52000 water molecules, ~170000 atoms in total). Molecular dynamics simulations (50 ns, 2 fs time step, PBC, NPT ensemble, 300 K and 1.0 bar) were performed with the program Desmond[113–116] using the OPLS3 force field.

4.1.5 Synthesis and characterization of compounds

Dodecylmagnesium bromide (11):

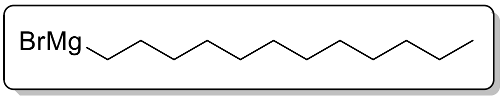

In an oven-dried round-bottom flask, a mixture of 1-bromododecane (1.0 mmol, from a 0.5 M solution in THF) and magnesium turnings (2.0 mmol) was stirred for 1h under argon atmosphere. The reaction was initiated with the help of a ultrasonic bath and kept under stirring until the reflux stopped and a cloudy solution appeared. This solution was used immediately, without further manipulation.

tert-Butyl (5-(hydroxymethyl)-2,2-dimethyl-1,3-dioxan-5-yl)carbamate (12)

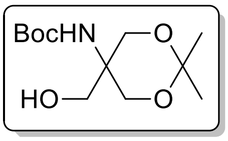

To a suspension of tris(hidroxymethyl) aminomethane (20.0 g, 165.2 mmol) in DMF (0.3 L) was added Boc_2O (40.0 g, 183.3 mmol), and the mixture was stirred at room temperature for 1 h. 2,2-Dimethoxypropane (25.0 mL, 204.0 mmol) and *p*-toluenesulfonic acid monohydrate (1.6 g, 8.3 mmol) were next added to the mixture, and stirring was continued for 15h. The reaction mixture was diluted with Et_2O, washed with saturated $NaHCO_3$ and brine, dried, and concentrated. Recrystallization of the residue from Et_2O-hexanes afforded **12** (36.2 g, 84%) as colourless crystals. The physical and spectroscopic data of compound **12** were identical to those reported in the literature.(61)

^{1}H NMR (400 MHz, $CDCl_3$) δ 5.33 (br s, 1H), 4.25 (br s, 1H), 3.84 (d, *J* = 11.4 Hz, 2H), 3.80 (d, *J* = 11.4 Hz, 2H), 3.72 (s, 2H), 1.45 (s, 12H), 1.43 (s, 3H).

tert-Butyl (5-formyl-2,2-dimethyl-1,3-dioxan-5-yl)carbamate (13)

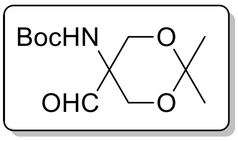

This compound was obtained as described in the general procedure 1, starting from **12** (103.0 mmol). Compound **13** (25.9 g, 97%) was obtained as a white solid and used without further purification. The physical and spectroscopic data of **13** were identical to those reported in the literature.(61)

^{1}H NMR (400 MHz, $CDCl_3$) δ 9.63 (s, 1H), 5.56 (br s, 1H), 4.06 (d, *J* = 11.9 Hz, 2H), 3.95 (d, *J* = 11.8 Hz, 2H), 1.46 (s, *J* = 9.4 Hz, 15H).

tert-Butyl (2,2-dimethyl-5-vinyl-1,3-dioxan-5-yl)carbamate (14)

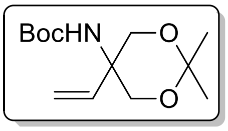

To a solution of Ph_3PCH_3Br (51.3 g, 115.7 mmol) in THF (200.0 mL) was added KHMDS (23.0 g, 115.7 mmol) at 0 °C under argon atmosphere. The mixture was stirred for 30 min at this temperature and then treated with a solution of **13** (15.0 g, 57.8 mmol) in THF (100.0 mL). The reaction mixture was stirred at rt for 5h, and then quenched with a saturated aqueous NH_4Cl solution (0.1 L). The aqueous phase was extracted with EtOAc (3 x 0.2 L) and the combined organic extracts were dried over anhydrous Mg_2SO_4 and concentrated *in vacuo*. Flash chromatography (hexanes/EtOAc, from

0% to 10% of EtOAc) afforded **14** (13.3 g, 89%) as a white solid. The physical and spectroscopic data of compound **14** were identical to those reported in the literature.(60)

^{1}H NMR (400 MHz, $CDCl_3$) δ 5.85 (dd, *J* = 17.7, 11.1 Hz, 1H), 5.20 (dd, *J* = 5.8, 5.2 Hz, 2H), 5.16 (br d, *J* = 0.6 Hz, 1H), 3.87 (d, *J* = 11.6 Hz, 2H), 3.79 (d, *J* = 11.7 Hz, 2H), 1.42 (s, 3H), 1.41 (s, 12H).

***tert*-Butyl (1-hydroxy-2-(hydroxymethyl)but-3-en-2-yl)carbamate (15)**

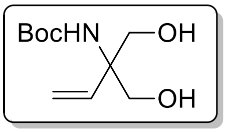

A solution of **14** (3.0 g, 11.9 mmol) in MeOH (0.6 L) was treated with *p*-TsOH·H_2O (0.4 g, 2.3 mmol). The resulting solution was stirred at rt for 15h. The reaction was next quenched with a saturated aqueous $NaHCO_3$ solution (0.3 L), and extracted with EtOAc (3 x 0.2 L). The combined organic extracts were dried over anhydrous Mg_2SO_4 and concentrated *in vacuo*. Flash chromatography (1:1 hexanes/EtOAc) afforded **15** (2.5 g, quantitative) as a white solid. The physical and spectroscopic data of compound **15** were identical to those reported in the literature.(60)

^{1}H NMR (400 MHz, $CDCl_3$) δ 5.85 (dd, *J* = 17.4, 10.8 Hz, 1H), 5.32 (d, *J* = 10.8 Hz, 1H), 5.30 (s, 1H), 5.25 (d, *J* = 17.4 Hz, 1H), 3.69 (m, 4H), 3.41 (br s, 2H), 1.45 (s, 9H).

(±)-4-(Hydroxymethyl)-4-vinyloxazolidin-2-one (16)

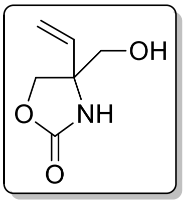

To a solution of **15** (0.5 g, 1.9 mmol) in THF (40.0 mL) was added NaH (195.0 mg of a 60% dispersion in mineral oil, equivalent to 4.9 mmol) at 0ºC under argon atmosphere. The reaction mixture was allowed to warm to rt and stirred until complete conversion (typically 15h) of the starting material was observed (Rf CH_2Cl_2/MeOH 95:5 (v:v): 0.33). The reaction was next quenched with brine and extracted with EtOAc (3 x 15.0 mL). The combined organic extracts were dried over anhydrous Mg_2SO_4 and concentrated *in vacuo*. Flash chromatography (CH_2Cl_2/MeOH, from 0% to 5% of MeOH) afforded **16** (145.0 mg, 52%) as a pale yellow solid.

HRMS (ESI+) calcd. for $C_6H_9NO_3$ $[M+Na]^+$ *(m/z)*: 166.0480, found 166.0472. **^{1}H NMR** (400 MHz, $CDCl_3$) δ 6.71 (br s, 1H, N*H*), 5.84 (dd, *J* = 17.4, 10.8 Hz, 1H, =C*H*), 5.35 (dd, *J* = 24.7, 14.0 Hz, 2H, =C*H*$_2$), 4.45 (d, *J* = 8.4 Hz, 1H, C*H*HO), 4.13 (d, *J* = 8.4 Hz, 1H, CH*H*O), 3.62 (dd, *J* = 34.7, 11.9 Hz, 2H, C*H*$_2$OH), 3.48 (br s, 1H, O*H*). **^{13}C NMR** (101 MHz, CDCl$_3$) δ 160.46 (C), 136.57 (CH), 117.10 (CH$_2$), 72.35 (CH$_2$), 66.17 (CH$_2$), 63.64 (C). **mp** 64-68 ºC.

(±)-*tert*-Butyl (1-((*tert*-butyldiphenylsilyl)oxy)-2-(hydroxymethyl)but-3-en-2-yl)carbamate (18)

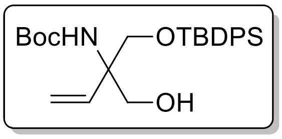

A mixture of **15** (0.9 g, 4.2 mmol), imidazole (565.0 mg, 8.3 mmol) and TBDPSiCl (1.1 g, 4.2 mmol) in CH$_2$Cl$_2$ (60.0 mL) was stirred for 5h at rt or until complete conversion of the starting material by TLC (Rf, hexanes/EtOAc 9:1 (v:v): 0.4). The reaction mixture was concentrated under reduced pressure and the residue was purified by flash chromatography (hexanes/EtOAc from 0 to 10% of EtOAc) to give **18** (1.6 g, 84%) as a colourless oil.

HRMS (ESI+) calcd. for $C_{26}H_{37}NO_4Si$ [M+Na]$^+$ *(m/z)*: 478.2390, found 478.2385. **^{1}H NMR** (400 MHz, CDCl$_3$) δ 7.68 – 7.63 (m, 4H, Ar*H*), 7.48 – 7.37 (m, 6H, Ar*H*), 5.86 (dd, *J* = 17.4, 10.8 Hz, 1H, =C*H*), 5.31 (s, 1H, N*H*), 5.25 (dd, *J* = 19.0, 14.2 Hz, 2H, =C*H*$_2$), 4.13 (br s, 1H, O*H*), 3.84 – 3.63 (m, 4H, C*H*$_2$O), 1.46 (s, 9H, C(C*H*$_3$)$_3$), 1.08 (s, 9H, SiC(C*H*$_3$)$_3$). **^{13}C NMR** (101 MHz, CDCl$_3$) δ 156.24 (C), 137.50 (CH), 135.77 (CH), 135.65 (CH), 132.93 (C), 132.71 (C), 130.06 (CH), 130.04 (CH), 127.95 (CH), 127.92 (CH), 115.77 (CH$_2$), 80.04 (C), 66.81 (CH$_2$), 66.73 (CH$_2$), 28.47 (CH$_3$), 26.95 (CH$_3$).

(±)-*tert*-Butyl (1-((*tert*-butyldiphenylsilyl)oxy)-2-formylbut-3-en-2-yl)carbamate (19)

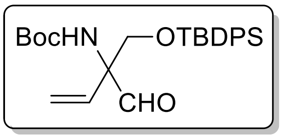

This compound was obtained as described in general procedure 1, starting from **18** (1.8 g, 3.9 mmol). Flash chromatography on Hexanes/EtOAc as eluent (from 0 to 10% EtOAc) to give 1.5 g of **19** (87% yield) as a colourless oil. (Rf, hexanes/EtOAc 9:1 (v:v): 0.63)

HRMS (ESI+) calcd. for $C_{26}H_{35}NO_4Si$ [M+Na]$^+$ *(m/z)*: 476.2200, found 476.2201. **^{1}H NMR** (400 MHz, CDCl$_3$) δ 9.37 (br s, 1H, C*H*O), 7.68 – 7.56 (m, 4H, Ar*H*), 7.48 – 7.33 (m, 6H, Ar*H*), 5.87 (dd, *J* = 17.5, 10.8 Hz, 1H, =C*H*), 5.57 (br s, 1H, N*H*), 5.33 (dd, *J* = 29.9, 14.2 Hz, 2H, =C*H*$_2$), 4.05 (dd, *J* = 22.2, 14.4 Hz, 2H, C*H*$_2$O), 1.47 (s, 9H, C(C*H*$_3$)$_3$), 1.05 (s, 9H, SiC(C*H*$_3$)$_3$). **^{13}C NMR** (101 MHz,

$CDCl_3$) δ 196.51 (C), 154.98 (C), 135.68 (C), 135.64 (C), 132.93 (CH), 130.09 (CH), 127.97 (CH), 118.49 (CH_2), 80.33 (C), 68.86 (C), 64.55 (CH_2), 28.42 (CH_3), 26.87 (CH_3).

(±)-*syn* and (±)-*anti*-*tert*-Butyl[3-[[(*tert*-butyldiphenylsilyl)oxy]methyl]-4-hydroxyhexadec-1-en-3-yl) carbamate (21)

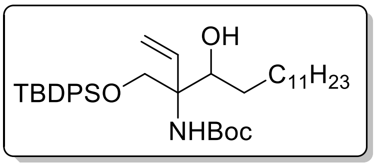

These compounds were obtained, as described in the general procedure 2, starting from aldehyde (±)-**19** (2.6 mmol). The reaction mixture was purified by flash chromatography on Hexanes/EtOAc (from 0 to 5% EtOAc) to give 1.2 g of **21** (77% yield, as an inseparable 7:3 mixture of (±)-*syn*/*anti*) as a colourless oil (Rf, hexanes/EtOAc 9:1 (v:v): 0.76). For characterization purposes, semi-preparative HPLC on a reverse phase column (Column G) using an isocratic method (5:95, H_2O:CH_3CN, 30 mL/min) afforded isomer (±)-*syn*-**21** in 14% yield (Rt: 26.8 min) and isomer (±)-*anti*-**21** in 10% yield (Rt: 24.7 min).

Isomer (±)-*syn*-**21**: **HRMS** (ESI+) calcd. for $C_{38}H_{61}NO_4Si$ $[M+H]^+$ *(m/z)*: 624.4448, found 624.4472. **^{1}H NMR** (400 MHz, $CDCl_3$) δ 7.68 – 7.61 (m, 4H, Ar*H*), 7.47 – 7.34 (m, 6H, Ar*H*), 5.77 (dd, *J* = 17.7, 11.1 Hz, 1H, =C*H*), 5.26 (br s, 1H, N*H*), 5.14 (dd, *J* = 55.9, 14.4 Hz, 2H, =C*H*$_2$), 4.29 (br s, 1H, O*H*), 4.10 (d, *J* = 10.2 Hz, 1H, C*H*HO), 3.91 (d, *J* = 10.3 Hz, 1H, CH*H*O), 3.73 (dd, *J* = 14.8, 8.3 Hz, 1H, C*H*OH), 1.57 (s, 2H, C*H*$_2$CHOH), 1.44 (s, 9H, C(C*H*$_3$)$_3$), 1.35 – 1.19 (br m, 20H, $C_{10}H_{20}$), 1.06 (s, 9H, SiC(C*H*$_3$)$_3$), 0.88 (t, *J* = 6.9 Hz, 3H, CH_3). **^{13}C NMR** (101 MHz, $CDCl_3$) (major rotamer) δ 156.13 (C), 138.29 (CH), 135.83 (CH), 135.68 (CH), 133.15 (C), 129.99 (CH), 129.98 (CH), 127.93 (CH), 127.90 (CH), 115.22 (CH_2), 79.80 (C), 76.33 (CH), 66.71 (CH_2), 32.08 (CH_2), 31.44 (C), 29.84 (CH_2), 29.82 (CH_2), 29.80 (CH_2), 29.79 (CH_2), 29.51 (CH_2), 28.51 (CH_3), 26.99 (CH_3), 26.49 (CH_2), 22.85 (CH_2), 19.47 (CH_2), 19.41 (CH_2), 14.28 (CH_3).

Isomer (±)-*anti*-**21**: **HRMS** (ESI+) calcd. for $C_{38}H_{61}NO_4Si$ $[M+Na]^+$ *(m/z)*: 646.4268, found 646.4282. **^{1}H NMR** (400 MHz, $CDCl_3$) δ 7.67 – 7.60 (m, 4H, Ar*H*), 7.48 – 7.35 (m, 6H, Ar*H*), 5.82 (dd, *J* = 17.4, 10.8 Hz, 1H, =C*H*), 5.45 (br s, 1H, N*H*), 5.18 (dd, *J* = 42.8, 14.2 Hz, 2H, =C*H*$_2$), 3.96 (br d, *J* = 9.3 Hz, 1H, O*H*), 3.87 (d, *J* = 9.9 Hz, 1H, C*H*HO), 3.75 (d, *J* = 8.4 Hz, 1H, CH*H*O), 3.54 – 3.47 (m, 1H, C*H*OH), 1.61 (d, *J* = 9.8 Hz, 2H, C*H*$_2$CHOH), 1.44 (s, 9H, C(C*H*$_3$)$_3$), 1.36 – 1.17 (br m, 20H, $C_{10}H_{20}$), 1.07 (s, 9H, SiC(C*H*$_3$)$_3$), 0.88 (t, *J* = 6.9 Hz, 3H, CH_3). **^{13}C NMR** (101 MHz, $CDCl_3$) (major rotamer) δ 155.90 (C) 138.14 (CH), 135.83 (CH), 135.75 (CH), 132.82 (C), 130.12 (CH), 130.11 (CH), 127.99 (CH), 127.95 (CH), 114.91 (CH_2), 81.09 (C), 75.72 (CH), 66.08 (CH_2), 32.08 (CH_2), 31.37 (C), 29.84 (CH_2), 29.83 (CH_2), 29.81 (CH_2), 29.74 (CH_2), 29.51 (CH_2), 28.51 (CH_3), 27.02 (CH_3), 26.76 (CH_2), 22.85 (CH_2), 19.41 (CH_2), 14.28 (CH_3).

(±)-*syn* and (±)-*anti*-*tert*-Butyl[4-hydroxy-3-(hydroxymethyl)hexadec-1-en-3-yl]carbamate (22)

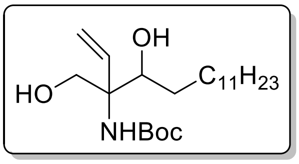

These compounds were obtained, as described in general procedure 9, in quantitative yield from the diastereomeric mixture of **21** (0.7 mmol), as an inseparable mixture of isomers or from (±)-*syn*-**31** (0.8 mmol, 83% yield) or (±)-*anti*-**31** (0.7 mmol, 86% yield), as described in general procedure 10. In all cases, the compounds were purified by flash chromatography, using Hexanes/EtOAc as eluent (from 0 to 10% EtOAc) to give a colourless oil. (Rf, hexanes/EtOAc 9:1 (v:v): 0.16).

Isomer (±)-*syn*-**22**: **HRMS** (ESI+) calcd. for $C_{22}H_{43}NO_4$ $[M+H]^+$ *(m/z)*: 386.3270, found 386.3278. **^{1}H NMR** (400 MHz, $CDCl_3$) δ 5.85 (dd, *J* = 17.5, 11.0 Hz, 1H, =C*H*), 5.27 (d, *J* = 11.0 Hz, 1H, =C*H*H), 5.20 (s, 1H, N*H*), 5.15 (d, *J* = 5.4 Hz, 1H, =CH*H*), 4.02 (d, *J* = 10.9 Hz, 1H, C*H*HOH), 3.89 (br s, 1H, O*H*), 3.68 (d, *J* = 12.2 Hz, 1H, CH*H*OH), 3.64 (s, 1H, C*H*OH), 1.54 (dd, *J* = 23.1, 14.5 Hz, 2H, CH_2CHOH), 1.44 (s, 9H, $C(CH_3)_3$), 1.36 – 1.13 (br m, 20H, $C_{10}H_{20}$), 0.87 (t, *J* = 6.8 Hz, 3H, CH_3). **^{13}C NMR** (101 MHz, $CDCl_3$) δ 156.88 (C), 137.56 (CH), 115.56 (CH_2), 80.52 (C), 75.60 (CH), 66.37 (CH_2), 64.56 (C), 32.05 (CH_2), 31.46 (CH_2), 29.81 (CH_2), 29.79 (CH_2), 29.78 (CH_2), 29.75 (CH_2), 29.72 (CH_2), 29.69 (CH_2), 29.49 (CH_2), 28.43 (CH_3), 26.53 (CH_2), 22.82 (CH_2), 14.25 (CH_3).

Enantiopure or enantioenriched *syn*-isomers were similarly obtained by the route described in section 2.1.12:

syn-(2*R*,3*R*)-**22**, obtained from *syn*-(2*R*,3*R*)-**31**: **$[\alpha]_D$** = +3.3 (*c* = 3.0, $CHCl_3$)

syn-(2*S*,3*S*)-**22**, obtained from *syn*-(2*S*,3*S*)-**31**: **$[\alpha]_D$** = -4.6 (*c* = 3.0, $CHCl_3$)

Isomer (±)-*anti*-22: **HRMS** (ESI+) calcd. for $C_{22}H_{43}NO_4$ $[M+Na]^+$ *(m/z)*: 408.3090, found 408.3089. **^{1}H NMR** (400 MHz, $CDCl_3$) δ 5.91 (dd, *J* = 17.4, 10.8 Hz, 1H, =C*H*), 5.32 (d, *J* = 10.8 Hz, 1H, =C*H*H), 5.22 (br s, 1H, N*H*), 5.18 (d, *J* = 17.5 Hz, 1H, =CH*H*), 4.22 (br s, 1H, O*H*), 3.79 – 3.71 (m, 1H, C*H*HOH), 3.68 – 3.55 (m, 2H, CH*H*OH, C*H*OH), 3.03 (br d, *J* = 4.7 Hz, 1H, O*H*), 1.58 (s, 2H, CH_2CHOH), 1.45 (s, 9H, $C(CH_3)_3$), 1.39 – 1.12 (br m, 20H, $C_{10}H_{20}$), 0.88 (t, *J* = 6.8 Hz, 3H, CH_3). **^{13}C NMR** (101 MHz, $CDCl_3$) δ 156.87 (C), 137.55 (CH), 115.59 (CH_2), 80.59 (C), 73.52 (CH), 66.48

(CH_2), 64.56 (C), 32.08 (CH_2), 30.88 (CH_2), 29.86 (CH_2), 29.83 (CH_2), 29.81 (CH_2), 29.80 (CH_2), 29.78 (CH_2), 29.75 (CH_2), 29.72 (CH_2), 29.51 (CH_2), 28.46 (CH_3), 26.60 (CH_2), 22.84 (CH_2), 14.27 (CH_3).

Enantiopure or enantioenriched *anti*-isomers were similarly obtained by the route described in section 2.1.12:

anti-(2*R*,3*S*)-**22**, obtained from *anti*-(2*R*,3*S*)-**31**: **[α]$_D$** = -1.6 (*c* = 3.0, $CHCl_3$)

anti-(2*S*,3*R*)-**22**, obtained from *anti*-(2*S*,3*R*)-**31**: **[α]$_D$** = +0.4 (*c* = 3.0, $CHCl_3$)

(±)-*syn* and (±)-*anti*-*tert*-Butyl [3-[[(dimethoxyphosphoryl)oxy]methyl]-4-hydroxyhexadec-1-en-3-yl]carbamate (23)

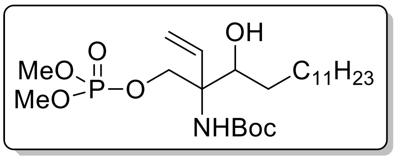

These compounds were obtained as described in general pocedure 3, starting from (±)-*syn*-**22** (0.2 mmol) or (±)-*anti*-**22** (0.2 mmol). The compounds were purified by flash chromatography using Hexanes/EtOAc as eluent (from 0 to 35% of EtOAc) to give (±)-*syn*-**23** (74.0 mg, 73% yield) or (±)-*anti*-**23** (78.0 mg, 74% yield) as a colourless oils. (Rf, hexanes/EtOAc 7:3 (v:v): 0.08).

Isomer (±)-*syn*-**23**: **HRMS** (ESI+) calcd. for $C_{24}H_{48}NO_7P$ $[M+H]^+$ *(m/z)*: 494.3247, found: 494.3257. **^{1}H NMR** (400 MHz, $CDCl_3$) δ 5.81 (dd, *J* = 17.6, 11.1 Hz, 1H, =C*H*), 5.26 (dd, *J* = 30.3, 14.4 Hz, 2H, =CH_2), 5.04 (br s, 1H, N*H*), 4.43 (dd, *J* = 10.4, 6.2 Hz, 1H, C*H*HOP), 4.32 (dd, *J* = 10.4, 6.7 Hz, 1H, CH*H*OP), 3.76 (dd, *J* = 11.1, 1.7 Hz, 6H, $(OCH_3)_2$), 3.62 (d, *J* = 8.9 Hz, 1H, C*H*OH), 1.55 (dd, *J* = 18.0, 8.1 Hz, 2H, CH_2CHOH), 1.42 (s, 9H, $C(CH_3)_3$), 1.23 (br s, 20H, $C_{10}H_{20}$), 0.86 (t, *J* = 6.9 Hz, 3H, CH_3). **^{13}C NMR** (101 MHz, $CDCl_3$) δ 156.17 (C), 137.24 (CH), 116.14 (CH_2), 80.45 (C), 73.98 (CH), 68.48 (CH_2), 68.42 (CH_2), 63.56 (C), 63.49 (C), 54.64 (CH_3), 54.58 (CH_3), 32.04 (CH_2), 30.79 (CH_2), 29.80 (CH_2), 29.79 (CH_2), 29.76 (CH_2), 29.74 (CH_2), 29.71 (CH_2), 29.66 (CH_2), 29.47 (CH_2), 28.39 (CH_3), 26.52 (CH_2), 22.81 (CH_2), 14.23 (CH_3). **^{31}P NMR** (162 MHz, $CDCl_3$) δ 1.64.

Enantiopure or enantioenriched *syn*-isomers were similarly obtained from the corresponding precursors:

Obtained by the route described in section 2.1.4:

syn-(2*R*,3*R*)-**23**: [α]$_D$ +3.2 (c 1, $CHCl_3$) and *syn*-(2*S*,3*S*)-**23**: [α]$_D$ -3.6 (c 1, $CHCl_3$).

Obtained by the route described in section 2.1.12:

syn-(2*R*,3*R*)-**23**: [α]$_D$ +11 (c 3, $CHCl_3$) and *syn*-(2*S*,3*S*)-**23**: [α]$_D$ -15 (c 3, $CHCl_3$).

Isomer (±)-*anti*-**23**: **HRMS** (ESI+) calcd. for $C_{24}H_{48}NO_7P$ $[M+Na]^+$ *(m/z)*: 516.3066, found 516.3075. **^{1}H NMR** (400 MHz, $CDCl_3$) δ 5.84 (dd, *J* = 17.5, 10.9 Hz, 1H, =C*H*), 5.26 (dd, 2H, =C*H*$_2$), 5.17 (br s, 1H, N*H*), 4.32 (dd, *J* = 6.1, 3.4 Hz, 2H, C*H*$_2$OP), 3.78 (dd, *J* = 11.1, 1.3 Hz, 6H, (OC*H*$_3$)$_2$), 3.61 (d, *J* = 8.3 Hz, 1H, C*H*OH), 1.68 – 1.57 (m, 1H, C*H*HCHOH), 1.56 – 1.47 (m, 1H, CH*H*CHOH), 1.44 (s, 9H, C(C*H*$_3$)$_3$), 1.25 (br s, 20H, $C_{10}H_{20}$), 0.87 (t, *J* = 6.8 Hz, 3H, C*H*$_3$). **^{13}C NMR** (101 MHz, $CDCl_3$) δ 155.55 (C), 136.25 (CH), 116.33 (CH_2), 77.36(C), 74.19 (CH), 68.03 (CH_2), 67.97 (CH_2), 54.76 (CH_3), 54.76 (CH_3), 54.70 (CH_3), 54.70 (CH_3), 32.07 (CH_2), 31.65 (CH_2), 29.82 (CH_2), 29.80 (CH_2), 29.79 (CH_2), 29.76 (CH_2), 29.74 (CH_2), 29.50 (CH_2), 28.45 (CH_3), 26.77 (CH_2), 22.83 (CH_2), 14.26 (CH_3). **^{31}P NMR** (162 MHz, $CDCl_3$) δ 1.57.

Enantiopure or enantioenriched *anti*-isomers were similarly obtained from the corresponding precursors:

Obtained by the route described in section 2.1.4:

anti-(2*S*,3*R*)-**23**: $[\alpha]_D$ +2.4 (c 1, $CHCl_3$) and *anti*-(2*R*,3*S*)-**23**: $[\alpha]_D$ -2.4 (c 1, $CHCl_3$).

Obtained by the route described in section 2.1.12:

anti-(2*S*,3*R*)-**23**: $[\alpha]_D$ +0.6 (c 3, $CHCl_3$) and *anti*-(2*R*,3*S*)-**23**: $[\alpha]_D$ -1.7 (c 3, $CHCl_3$)

(±)-*syn* and (±)-*anti*-2-Amino-3-hydroxy-2-vinylpentadecyl dihydrogen phosphate (24)

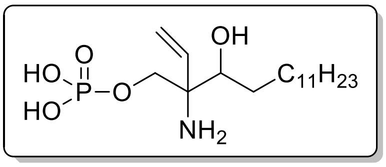

These compounds were obtained as described in general procedure 4, starting from (±)-*syn*-**23** (0.3 mmol) or (±)-*anti*-**23** (0.3 mmol). Purification was carried out by chromatography on XAD-4 resin, using water/ACN as eluent (from 0 to 100% of ACN) followed by lyophilization to give (±)-*syn*-**24** (37.0 mg, 36% yield) or (±)-*anti*-**24** (33.0 mg, 33% yield) as a white solids. Dephosphorylated aminoalcohol (±)-*syn*-**34** (29.0 mg, 33% yield) or (±)-*anti*-**34** (26.0 mg, 29% yield) were also obtained.

Isomer (±)-*syn*-**24**: **HRMS** (ESI+) calcd. for $C_{17}H_{36}NO_5P$ $[M+Na]^+$ *(m/z)*: 388.2229, found 388.2257. **^{1}H NMR** (400 MHz, CD_3OD) δ 5.90 (dd, *J* = 17.9, 11.5 Hz, 1H, =C*H*), 5.45 (dd, *J* = 39.2, 14.7 Hz, 2H, =C*H*$_2$), 4.04 (ddd, *J* = 24.6, 11.5, 5.6 Hz, 2H, C*H*$_2$OP), 3.79 (d, *J* = 10.7 Hz, 1H, C*H*OH), 1.57 (d, *J* = 5.5 Hz, 2H, C*H*$_2$CHOH), 1.35 (br d, *J* = 44.3 Hz, 20H, $C_{10}H_{20}$), 0.90 (t, *J* = 6.9 Hz, 3H, C*H*$_3$. **^{13}C NMR** (101 MHz, CD_3OD) δ 133.18 (CH), 119.68 (CH_2), 72.24 (CH), 66.53 (CH_2), 66.48 (CH_2), 65.31 (CH_2), 65.23 (CH_2), 33.08 (CH_2), 32.30 (CH_2), 30.81 (CH_2), 30.78 (CH_2), 30.76

(CH_2), 30.76 (CH_2), 30.61 (CH_2), 30.48 (CH_2), 27.30 (CH_2), 23.74 (CH_2), 14.43 (CH_3). **^{31}P NMR** (162 MHz, CD_3OD) δ 0.64.

Enantiopure or enantioenriched *syn*-isomers were similarly obtained from the corresponding precursors by the route described in section 2.1.12:

syn-(2*R*,3*R*)-**24**: [α]D +14.4 (c 0.5, DMSO) and *syn*-(2*S*,3*S*)-**24**: [α]D -15 (c 0.5, DMSO)

Isomer (±)-*anti*-**24**: **HRMS** (ESI+) calcd. for $C_{17}H_{36}NO_5P$ $[M+H]^+$ *(m/z)*: 366.2409, found 366.2400. **^{1}H NMR** (400 MHz, CD_3OD) δ 5.95 (dd, *J* = 17.9, 11.4 Hz, 1H, =C*H*), 5.47 (dd, *J* = 28.5, 14.7 Hz, 2H, =C*H*$_2$), 4.23 (dd, *J* = 9.6, 3.5 Hz, 1H, C*H*HOP), 3.93 (dd, *J* = 10.8, 4.2 Hz, 1H, CH*H*OP), 3.73 (d, *J* = 9.0 Hz, 1H, C*H*OH), 1.62 (d, *J* = 8.2 Hz, 1H, C*H*HCHOH), 1.48 (dd, *J* = 17.9, 10.5 Hz, 1H, CH*H*CHOH), 1.29 (br s, 20H, $C_{10}H_{20}$), 0.90 (t, *J* = 6.8 Hz, 3H, C*H*$_3$). **^{13}C NMR** (101 MHz, CD_3OD) δ 134.28 (CH), 119.58 (CH_2), 72.99 (CH), 65.81 (CH_2), 65.77 (CH_2), 64.87 (CH_2), 64.80 (CH_2), 33.07 (CH_2), 31.60 (CH_2), 30.80 (CH_2), 30.77 (CH_2), 30.76 (CH_2), 30.73 (CH_2), 30.70 (CH_2), 30.47 (CH_2), 30.45 (CH_2), 27.49 (CH_2), 23.73 (CH_2), 14.43 (CH_3). **^{31}P NMR** (162 MHz, CD_3OD) δ 0.84.

Enantiopure or enantioenriched *anti*-isomers were similarly obtained from the corresponding precursors by the route described in section 2.1.12:

anti-(2*S*,3*R*)-**24**: [α]D +7 (c 0.5, DMSO) and *anti*-(2*R*,3*S*)-**24**: [α]D -3.8 (c 0.5, DMSO)

MPA esters (25) for the simultaneous separation and resolution of compounds 21

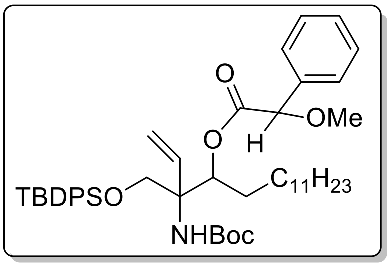

These compounds were obtained as described in general procedure 5, starting from a mixture of (±)-*syn* and (±)-*anti*-**21** and reaction with (*R*)-MPA or (*S*)-MPA (see Figure 2.1.3, Section 2.1.4). Purification by flash chromatography using Hexanes/MTBE as eluent (from 0 to 5% of MTBE) gave the corresponding isomers of **25**.

From (*R*)-MPA:

Isomer **25a** [(*R*)(-)-*anti*-**21**] (210.0 mg, 19% yield) as a colourless oil. (Rf, Hexanes/MTBE 95:5 (v:v): 0.68). **HRMS** (ESI-) calcd. For $C_{47}H_{69}NO_6Si$ $[M-H]^+$ *(m/z)*: 770.4816, found 770.4858. **^{1}H NMR** (400 MHz, $CDCl_3$) δ 7.67 – 7.49 (m, 5H, Ar*H*), 7.48 – 7.28 (m, 7H, Ar*H*), 7.22 (dd, *J* = 5.1, 2.0 Hz, 3H, Ar*H*), 5.77 (dd, *J* = 17.5, 10.9 Hz, 1H, =C*H*), 5.55 (dd, *J* = 10.7, 2.3 Hz, 1H, C*H*O), 4.91 (d, *J* = 10.9 Hz, 1H, =C*H*H), 4.71 (s, 1H, C*H*OMe), 4.67 (s, 1H, =CH*H*), 4.57 (s, 1H, N*H*), 4.09 (d, *J* =

9.8 Hz, 1H, C*H*HO), 3.52 (d, *J* = 10.3 Hz, 1H, CH*H*O), 3.39 (s, 3H, OC*H*$_3$), 1.68 – 1.58 (m, 1H, C*H*HCHOH), 1.54 – 1.43 (m, 1H, CH*H*CHOH), 1.37 (s, 9H, C(C*H*$_3$)$_3$), 1.32 – 1.22 (br m, 18H, C$_9$*H*$_{18}$), 1.21 – 1.09 (m, 2H, C*H*$_2$CH$_2$), 1.03 (s, 9H, SiC(C*H*$_3$)$_3$), 0.89 (t, *J* = 6.8 Hz, 3H, CH$_2$C*H*$_3$). **^{13}C NMR** (101 MHz, CDCL$_3$) δ 169.66 (C), 136.50 (CH), 136.35 (CH), 135.83 (CH), 133.41 (C), 133.15 (C), 129.80 (CH), 128.77 (CH), 128.61 (CH), 127.77 (CH), 127.75 (CH), 127.31 (CH), 114.99 (CH$_2$), 82.72 (CH), 75.60 (CH), 65.14 (CH$_2$), 63.21 (C), 57.49 (CH$_3$), 32.07 (CH$_2$), 29.82 (CH$_2$), 29.80 (CH$_2$), 29.78 (CH$_2$), 29.71 (CH$_2$), 29.63 (CH$_2$), 29.54 (CH$_2$), 29.51 (CH$_2$), 29.13 (CH$_2$), 28.44 (CH$_3$), 27.03 (CH$_3$), 26.05 (CH$_2$), 22.84 (CH$_2$), 19.42 (CH$_2$), 14.27 (CH$_3$).

Isomers **25b** [(*R*)(+)-*syn*-**21**] and **25c** [(*R*)(+)-*anti*-**21**]: 155.0 mg diastereomer 1 (*R*)(+)-*syn*-**25**, Rf Hexanes/MTBE 95:5 (v:v): 0.62), 28% yield as an inseparable mixture with diastereomer 2 (*R*)(+)-*anti*-**25** (Rf Hexanes/EtOAc 95:5 (v:v): 0.57) as a colourless oil. **HRMS** (ESI-) calcd. For C$_{47}$H$_{69}$NO$_6$Si [M-H]$^+$ *(m/z)*: 770.4816, found 770.4858. **^{1}H NMR** (400 MHz, CDCl$_3$, as an inseparable mixture of diastereomers 1 and 2) δ 7.67 – 7.62 (m, 3H, Ar*H,* 1 and 2), 7.61 – 7.57 (m, 3H, Ar*H*, 1 and 2), 7.47 – 7.27 (m, 9H, Ar*H*, 1 and 2), 6.00 (dd, *J* = 17.5, 10.9 Hz, 1H, =C*H*, 2), 5.58 (d, *J* = 7.5 Hz, 1H, C*H*O, 1), 5.53 (d, *J* = 10.4 Hz, 1H, C*H*O, 2), 5.39 (dd, *J* = 17.6, 11.2 Hz, 1H, =C*H,* 1), 5.18 (d, *J* = 11.0 Hz, 1H, =C*H*H, 2), 5.09 (d, *J* = 17.4 Hz, 1H, =CH*H*, 2), 4.97 (d, *J* = 10.9 Hz, 1H, =C*H*H, 1), 4.92 (s, 1H, N*H*, 2), 4.72 (s, 1H, N*H*, 1), 4.65 (d, *J* = 17.9 Hz, 1H, =CH*H*, 1), 4.22 (br s, 1H, C*H*HO, 2), 3.93 (br s, 1H, C*H*HO, 1), 3.70 (d, *J* = 10.3 Hz, 1H, CH*H*O, 1 and 2), 3.41 (s, 3H, OC*H*$_3$, 1), 3.34 (s, 3H, OC*H*$_3$, 2), 1.58 – 1.47 (m, 2H, C*H*$_2$, 1), 1.47 – 1.39 (m, 2H, C*H*$_2$, 1), 1.37 (d, *J* = 10.9 Hz, 9H, C(C*H*$_3$)$_3$, 1 and 2), 1.35 – 1.12 (br m, 18H, C$_9$*H*$_{18}$, 1 and 2), 1.07 (d, *J* = 4.3 Hz, 9H, SiC(C*H*$_3$)$_3$, 1 and 2), 0.89 (dt, *J* = 10.4, 5.0 Hz, 3H, CH$_2$C*H*$_3$, 1 and 2), 0.68 (s, *J* = 18.1 Hz, 2H, C*H*$_2$, 2). **^{13}C NMR** (101 MHz, CDCl$_3$, as an inseparable mixture of diastereomers 1 and 2) δ 171.25 (C, 1), 169.95 (C, 2), 136.42 (CH, 2), 136.33 (CH, 1), 135.84 (CH, 1 and 2), 135.82 (CH, 1 and 2), 135.79 (CH, 2), 135.76 (CH, 1), 133.29 (C, 1), 133.26 (C, 2), 132.96 (C, 1 and 2), 129.92 (CH, 1 and 2), 129.87 (CH, 1), 128.91 (CH, 1 and 2), 128.79 (CH, 2), 128.67 (CH, 1), 128.60 (CH, 2), 127.84 (CH, 1), 127.83 (CH, 1), 127.81 (CH, 2), 127.80 (CH, 2), 127.51 (CH, 1), 127.31 (CH, 2), 115.84 (CH$_2$, 1), 115.03 (CH$_2$, 2), 76.17 (CH, 1 and 2), 63.25 (CH$_2$, 1 and 2), 57.52 (CH$_3$, 2), 57.39 (CH$_3$, 1), 32.06 (CH$_2$, 1 and 2), 29.83 (CH$_2$, 1 and 2), 29.81 (CH$_2$, 1 and 2), 29.79 (CH$_2$, 1 and 2), 29.75 (CH$_2$, 1 and 2), 29.69 (CH$_2$, 1 and 2), 29.64 (CH$_2$, 1), 29.56 (CH$_2$, 2), 29.52 (CH$_2$, 1), 29.50 (CH$_2$, 1), 29.44 (CH$_2$, 2), 29.37 (CH$_2$, 2), 29.08 (CH$_2$, 1 and 2), 28.50 (CH$_3$, 1), 28.46 (CH$_3$, 2), 27.04 (CH$_2$, 1 and 2), 26.98 (CH$_3$, 1 and 2), 26.12 (CH$_2$, 1), 25.50 (CH$_2$, 2), 22.83 (CH$_2$, 1 and 2), 19.45 (CH$_2$, 1 and 2), 14.26 (CH$_3$, 1 and 2).

Isomer **25d** [(*R*)(-)-*syn*-**21**]: (177.0 mg, 16% yield) as a colourless oil. (Rf, Hexanes/MTBE 95:5 (v:v): 0.52). **HRMS** (ESI-) calcd. For $C_{47}H_{69}NO_6Si$ $[M-H]^+$ *(m/z)*: 770.4816, found 770.4858. **^{1}H NMR** (400 MHz, $CDCl_3$) δ 7.64 (ddd, *J* = 7.1, 4.5, 1.7 Hz, 3H, Ar*H*), 7.47 – 7.26 (m, 12H, Ar*H*), 5.78 (dd, *J* = 17.7, 11.1 Hz, 1H, =C*H*), 5.49 (d, *J* = 9.6 Hz, 1H, C*H*O), 5.20 (d, *J* = 11.0 Hz, 1H, =C*H*H), 4.98 (d, *J* = 17.9 Hz, 1H, =CH*H*), 4.73 (s, 1H, N*H*), 4.06 (br s, 1H, C*H*HO), 3.76 (d, *J* = 10.3 Hz, 1H, CH*H*O), 3.42 (s, *J* = 11.8 Hz, 3H, OCH_3), 1.40 (s, *J* = 11.7 Hz, 9H, $C(CH_3)_3$), 1.35 – 1.13 (br m, 18H, C_9H_{18}), 1.08 (d, *J* = 2.6 Hz, 9H, $SiC(CH_3)_3$), 1.01 – 0.92 (m, 2H, CH_2), 0.89 (t, *J* = 6.9 Hz, 3H, CH_2CH_3), 0.84 – 0.71 (m, 1H, C*H*HCHOH), 0.70 – 0.57 (m, 1H, CH*H*CHOH). **^{13}C NMR** (101 MHz, $CDCL_3$) δ 154.67 (C), 136.39 (CH), 135.83 (CH), 135.76 (CH), 133.26 (C), 132.94 (C), 129.91 (CH), 128.85 (CH), 128.65 (CH), 127.85 (CH), 127.30 (CH), 116.00 (CH_2), 82.78 (CH), 76.41 (CH), 63.60 (CH_2), 63.06 (C), 57.46 (CH_3), 32.08 (CH_2), 29.84 (CH_2), 29.81 (CH_2), 29.79 (CH_2), 29.74 (CH_2), 29.57 (CH_2), 29.52 (CH_2), 29.45 (CH_2), 29.38 (CH_2), 29.17 (CH_2), 28.52 (CH_2), 28.46 (CH_3), 27.00 (CH_3), 25.53 (CH_2), 22.84 (CH_2), 19.47 (CH_2), 14.27 (CH_3).

From (*S*)-MPA, similar yields were obtained. As above, three fractions were collected after flash chromatography using Hexanes/MTBE as eluent (from 0 to 5% of MTBE).

Isomer ***ent*-25a** [(*S*)(+)-*anti*-**21**] was chromatographic and spectroscopically identical to **25a** [*R*)(-)-*anti*-**21**]

The mixture of ***ent*-25b** [(*S*)(-)-*syn*-**21**] and ***ent*-25c** [(*S*)(-)-*anti*-**21**] was chromatographic and spectroscopically identical to the above mixture of **25b** [(*R*)(+)-*syn*-**21**] and **25c** [(*R*)(+)-*anti*-**21**].

Isomer ***ent*-25d** [(*S*)(+)-*syn*-**21**] was chromatographic and spectroscopically identical to 25d [(*R*)(-)-*syn*-**25**].

(±)-*syn* and (±)-*anti*-2-Amino-2-vinylpentadecane-1,3-diol (31)

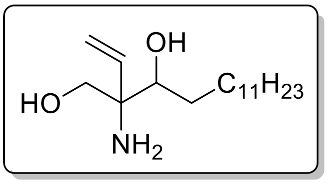

To a solution of (±)-*syn*-**45** (1 g, 2.4 mmol) or (±)-*anti*-**45** (360.0 mg, 0.8 mmol) in dioxane (40.0 µM) was added HCl 1.0 N (9.0 and 3.5 mL respectively) and the mixture was refluxed with stirring for 2.5h. After that time, complete conversion of the starting material was observed by TLC (Rf, CH_2Cl_2/MeOH 9:1 (v:v): 0.13 (±)-*syn*-**31** and CH_2Cl_2/MeOH 9:1 (v:v): 0.16 (±)-*anti*-**31**). The mixture was cooled down, diluted with Et_2O and washed successively with NaOH (2N) and brine. The organic layer was dried over $MgSO_4$, filtered and concentrated under reduced pressure. The resulting crude was purified by flash chromatography with CH_2Cl_2/MeOH (from 0 to 10% of MeOH) to give (±)-*syn*-**31** (0.7 g, 97% yield) and (±)-*anti*-**31** (235.0 mg, 97% yield) as a white wax.

Isomer (±)-*syn*-**31**: **HRMS** (ESI+) calcd. for $C_{17}H_{36}NO_2$ $[M+H]^+$ *(m/z)*: 286.2746, found 286.2754. ^{1}**H NMR** (400 MHz, $CDCl_3$) δ 5.76 (dd, *J* = 17.5, 10.9 Hz, 1H, =C*H*), 5.34 – 5.22 (m, 2H, =C*H*$_2$), 3.68 (d, *J* = 11.6 Hz, 1H, C*H*HOH), 3.59 (d, *J* = 9.8 Hz, 1H, C*H*OH), 3.50 (d, *J* = 11.1 Hz, 1H, CH*H*OH), 2.93 (br d, *J* = 28.7 Hz, 4H, (O*H*)x2 and N*H*$_2$), 1.52 (br d, *J* = 6.7 Hz, 1H, C*H*HCHOH), 1.44 – 1.35 (br m, 1H, CH*H*CHOH), 1.24 (br s, 20H, $C_{10}H_{20}$), 0.87 (t, *J* = 6.8 Hz, 3H, C*H*$_3$). ^{13}**C NMR** (101 MHz, $CDCl_3$) δ 139.48 (CH), 115.69 (CH_2), 110.16 (C), 75.19 (CH), 68.25 (CH_2), 61.69 (C), 32.06 (CH_2), 31.89 (CH_2), 29.83 (CH_2), 29.81 (CH_2), 29.79 (CH_2), 29.50 (CH_2), 26.51 (CH_2), 22.83 (CH_2), 14.25 (CH_3).

Enantiopure or enantioenriched *syn*-isomers were similarly obtained from the corresponding precursors by the route described in section 2.1.12:

syn-(2*R*,3*R*)-**31**: [α]D +7 (c 3, $CHCl_3$) and *syn*-(2*S*,3*S*)-**31**: [α]D -11 (c 3, $CHCl_3$)

Isomer (±)-*anti*-**31**: **HRMS** (ESI+) calcd. for $C_{17}H_{36}NO_2$ $[M+H]^+$ *(m/z)*: 286.2746, found 286.2754. ^{1}**H NMR** (400 MHz, $CDCl_3$) δ 5.88 (dd, *J* = 17.6, 10.9 Hz, 1H, , =C*H*), 5.34 – 5.22 (m, 2H, =C*H*$_2$), 3.80 (d, *J* = 11.0 Hz, 1H, C*H*HOH), 3.49 (d, *J* = 11.1 Hz, 1H, CH*H*OH), 3.46 – 3.41 (m, 1H, C*H*OH), 2.82 (br d, *J* = 20.0 Hz, 4H, (O*H*)x2 and N*H*$_2$), 1.65 – 1.43 (m, 2H, C*H*$_2$CHOH), 1.25 (br s, 20H, $C_{10}H_{20}$), 0.86 (t, 3H, C*H*$_3$). ^{13}**C NMR** (101 MHz, $CDCl_3$) δ 139.80 (CH), 115.96 (CH_2), 110.17 (C), 66.33 (CH_2), 60.82 (C), 32.07 (CH_2), 31.51 (CH_2), 29.83 (CH_2), 29.81 (CH_2), 29.80 (CH_2), 29.50 (CH_2), 27.04 (CH_2), 22.83 (CH_2), 14.26 (CH_3).

Enantiopure or enantioenriched *anti*-isomers were similarly obtained from the corresponding precursors by the route described in section 2.1.12:

anti-(2*S*,3*R*)-**31**: [α]D +0.8 (c 3, $CHCl_3$) and *anti*-(2*R*,3*S*)-**31**: [α]D -2.2 (c 3, $CHCl_3$)

MPA esters (32) for the configurational assignment of the C(3) position of phosphates 23

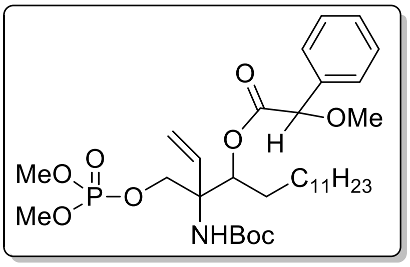

These compounds were obtained as described in general procedure 5, starting from the corresponding isomer (±)-*syn* or (±)-*anti*-**23** and (*R*)-MPA or (*S*)-MPA (see Scheme 2.1.10, section 2.1.5.1). The residue was purified by flash chromatography using Hexanes/EtOAc as eluent (from 0 to 35% EtOAc) to give the corresponding isomers of **32** (92% yield).

Isomer **32a** [(*R*)(-)-*syn*-**23**] (45.0 mg, 27% yield) as a colourless oil. (Rf, Hexanes/EtOAc 7:3 (v:v): 0.12). **HRMS** (ESI+) calcd. for $C_{33}H_{56}NO_9P$ $[M+H]^+$ *(m/z)*: 642.3771, found 642.3769. **^{1}H NMR** (400 MHz, $CDCl_3$) δ 7.49 – 7.28 (m, 5H, Ar*H*), 5.78 (dd, *J* = 17.8, 11.2 Hz, 1H, =C*H*), 5.33 (s, 1H, C*H*O), 5.21 (dd, *J* = 64.6, 14.5 Hz, 2H, =CH_2), 4.99 (br s, 1H, N*H*), 4.79 (s, 1H, C*H*OMe), 4.39 (br s, 1H, C*H*HOP), 4.26 (dd, *J* = 10.2, 4.4 Hz, 1H, CH*H*OP), 3.76 (dd, *J* = 11.1, 4.6 Hz, 6H, $P(OCH_3)_2$), 3.43 (s, 3H, OCH_3), 1.41 (s, 9H, $C(CH_3)_3$), 1.25 (br s, *J* = 11.7 Hz, 16H, C_8H_{16}), 1.10 – 1.00 (br m, 2H, $CH_2CH_2CH_2CHO$), 0.97 – 0.92 (br m, 2H, CH_2CH_2CHO), 0.88 (t, *J* = 6.8 Hz, 3H, CH_2CH_3), 0.83 – 0.72 (br m, 1H, C*H*HCHO), 0.65 (br m, 1H, CH*H*CHO). **^{13}C NMR** (101 MHz, $CDCl_3$) δ 170.96 (C), 154.37 (C), 136.29 (C), 134.92 (CH), 128.97 (CH), 128.72 (CH), 127.35 (CH), 116.97 (CH_2), 82.68 (CH), 75.64 (CH), 66.92 (CH_2), 61.91 (C), 57.47 (CH_3), 54.68 (CH_3), 54.54 (CH_3), 32.06 (CH_2), 31.57 (CH_2), 29.84 (CH_2), 29.79 (CH_2), 29.77 (CH_2), 29.73 (CH_2), 29.54 (CH_2), 29.50 (CH_2), 29.38 (CH_2), 29.22 (CH_2), 29.09 (CH_2), 28.45 (CH_3), 25.22 (CH_2), 22.83 (CH_2), 14.26 (CH_3).

Isomer **32b** [(*R*)(+)-*syn*-**23**]: (50.0 mg, 28% yield) as a colourless oil. (Rf, Hexanes/EtOAc 7:3 (v:v): 0.18). **HRMS** (ESI+) calcd. for $C_{33}H_{56}NO_9P$ $[M+H]^+$ *(m/z)*: 642.3771, found 642.3769. **^{1}H NMR** (400 MHz, $CDCl_3$) δ 7.50 – 7.29 (m, 5H, Ar*H*), 5.42 (dd, *J* = 10.5, 2.3 Hz, 1H, =C*H*), 5.37 (d, *J* = 6.5 Hz, 1H, C*H*O), 5.08 (d, *J* = 11.2 Hz, 1H, =C*H*H), 4.80 (d, *J* = 17.7 Hz, 1H, =CH*H*), 4.75 (s, 1H, C*H*OMe), 4.65 (s, 1H, N*H*), 4.19 (br d, *J* = 3.5 Hz, 2H, CH_2OP), 3.72 (ddd, *J* = 11.1, 4.7, 0.7 Hz, 6H, $P(OCH_3)_2$), 3.40 (s, *J* = 0.6 Hz, 3H, , OCH_3), 1.57 – 1.45 (br m, 2H, CH_2CHOH), 1.37 (s, 9H, $C(CH_3)_3$), 1.22 (br d, *J* = 17.8 Hz, 20H, $C_{10}H_{20}$), 0.87 (dd, *J* = 6.9, 6.4 Hz, 3H, CH_2CH_3). **^{13}C NMR** (101 MHz, $CDCl_3$) δ 170.66 (C), 154.03 (C), 136.31 (C), 134.07 (CH), 131.07 (CH), 129.06 (CH), 128.79 (CH), 127.57 (CH), 116.98 (CH_2), 82.59 (CH), 75.12 (CH), 66.29 (CH_2), 62.01 (C), 57.39 (CH_3), 54.59 (CH_3), 54.50 (CH_3), 32.04 (CH_2), 29.78 (CH_2), 29.76 (CH_2), 29.74 (CH_2), 29.64 (CH_2), 29.57 (CH_2), 29.47 (CH_2), 29.37 (CH_2), 28.96 (CH_2), 28.42 (CH_3), 25.84 (CH_2), 22.81 (CH_2), 14.24 (CH_3).

Isomer **32c** [(*R*)(-)-*anti*-**23**] (47.0 mg, 14% yield) as a colourless oil. (Rf, Hexanes/EtOAc 7:3 (v:v): 0.14). **HRMS** (ESI+) calcd. for $C_{33}H_{56}NO_9P$ $[M+H]^+$ *(m/z)*: 642.3771, found 642.3769. **^{1}H NMR** (400 MHz, $CDCl_3$) δ 7.49 – 7.30 (m, 5H, Ar*H*), 5.62 (dd, *J* = 16.1, 9.4 Hz, 1H, =C*H*), 5.43 (dd, *J* = 10.6, 1.9 Hz, 1H, C*H*O), 5.05 (d, *J* = 11.0 Hz, 1H, =C*H*H), 4.80 (d, *J* = 14.2 Hz, 1H, =CH*H*), 4.74 (s, 1H, C*H*OMe), 4.57 (br s, 1H, N*H*), 4.26 – 4.18 (br m, 1H, C*H*HOP), 3.85 – 3.77 (br m, 1H, CH*H*OP), 3.73 – 3.67 (m, 6H, $P(OCH_3)_2$), 3.41 (s, *J* = 0.7 Hz, 3H, OCH_3), 1.71 – 1.61 (m, 2H,

CH_2CH_2CHOH), 1.54 – 1.46 (m, 2H, CH_2CHOH), 1.41 (s, 9H, $C(CH_3)_3$), 1.23 (br d, *J* = 17.8 Hz, 18H, C_9H_{18}), 0.88 (t, *J* = 6.7 Hz, 3H, CH_2CH_3). **^{13}C NMR** (101 MHz, $CDCl_3$) δ 170.42 (C), 152.37 (C), 134.62 (CH), 129.04 (CH), 128.87 (CH), 127.45 (CH), 116.51 (CH_2), 82.65 (CH), 72.49 (CH), 67.36 (CH_2), 57.50 (CH_3), 54.52 (CH_3), 32.08 (CH_2), 29.80 (CH_2), 29.70 (CH_2), 29.62 (CH_2), 29.51 (CH_2), 28.41 (CH_3), 22.85 (CH_2), 18.02 (CH_2), 14.28 (CH_3).

Isomer **32d** [(*R*)(+)-*anti*-**23**] (55.0 mg, 11% yield) as a colourless oil. (Rf, Hexanes/EtOAc 7:3 (v:v): 0.10). **HRMS** (ESI+) calcd. for $C_{33}H_{56}NO_9P$ $[M+H]^+$ *(m/z)*: 642.3771, found 642.3769. **^{1}H NMR** (400 MHz, $CDCl_3$) δ 7.48 – 7.28 (m, 5H, Ar*H*), 5.87 (dd, *J* = 17.6, 11.0 Hz, 1H, =C*H*), 5.40 (d, *J* = 10.3 Hz, 1H, C*H*O), 5.21 (dd, *J* = 46.4, 14.3 Hz, 2H, $=CH_2$), 4.75 (s, 1H, C*H*OMe), 4.51 (dd, *J* = 10.0, 4.0 Hz, 1H, , C*H*HOP), 4.32 (br s, 1H, N*H*), 4.18 – 4.10 (m, 1H, , CH*H*OP), 3.75 (ddd, *J* = 5.9, 4.1, 1.4 Hz, 6H, $P(OCH_3)_2$), 3.42 (s, 3H, OCH_3), 1.43 (br s, *J* = 3.7 Hz, 9H, $C(CH_3)_3$), 1.25 (s, 16H, C_8H_{16}), 1.14 – 1.04 (br m, 2H, $CH_2CH_2CH_2CHO$), 1.04 – 0.94 (br m, 2H, CH_2CH_2CHO), 0.88 (t, *J* = 6.7 Hz, 3H, CH_2CH_3), 0.85 – 0.80 (br m, 1H, C*H*HCHO), 0.74 – 0.63 (br m, 1H, CH*H*CHO). **^{13}C NMR** (101 MHz, $CDCl_3$) δ 170.36 (C), 154.12 (C), 136.42 (C), 134.96 (CH), 128.74 (CH), 127.34 (CH), 126.76 (CH), 116.22 (CH_2), 82.76 (CH), 74.53 (CH), 67.52 (CH_2), 62.10 (C), 57.20 (CH_3), 54.43 (CH_3), 29.80 (CH_2), 29.52 (CH_2), 29.43 (CH_2), 28.43 (CH_3), 22.85 (CH_2), 14.28 (CH_3).

Equivalent yields and spectra were obtained for reaction of (±)-*syn*-**23** and (±)-*anti*-**23** with (*S*)-MPA to give ***ent*-32a**, ***ent*-32b**, ***ent*-32c** and ***ent*-32d** (see Scheme 2.1.10, section 2.1.5.1).

(±)-*syn*-5-dodecyl-4-(hydroxymethyl)-4-vinyloxazolidin-2-one (33)

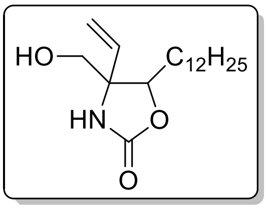

This compound was obtained by treatment of (±)-*syn*-**32** (70.0 mg, 0.1 mmol) in MeOH (1.5 mL) with K_2CO_3 (70.0 g, 0.5 mmol) at rt with stirring during 7h. The reaction mixture was concentrated under reduced pressure and the residue was purified by flash chromatography (hexanes/EtOAc from 0 to 30% of EtOAc) to give (±)-*syn*-**33** (15.0 mg, 34%) as a white solid (Rf, hexanes/EtOAc 7:3 (v:v): 0.20).

Isomer (±)-*syn*-**33**: **HRMS** (ESI+) calcd. for $C_{18}H_{33}NO_3$ $[M+H]^+$ *(m/z)*: 334.2358, found 334.2344. **^{1}H NMR** (400 MHz, $CDCl_3$) δ 5.93 (br s, 1H, N*H*), 5.73 (dd, *J* = 17.5, 10.5 Hz, 1H, =C*H*), 5.41 (dd, *J* = 14.1, 3.1 Hz, 2H, $=CH_2$), 4.47 (dd, *J* = 10.0, 3.3 Hz, 1H, C*H*O), 3.62 (dd, *J* = 23.1, 11.5 Hz, 2H, CH_2OH), 1.65 – 1.49 (m, 2H, CH_2CHO), 1.48 – 1.37 (m, 2H, CH_2CH_2CHO), 1.27 (br d, *J* = 18.7 Hz, 18H, C_9H_{18}), 0.88 (t, *J* = 6.8 Hz, 3H, C*H*$_3$). **^{13}C NMR** (101 MHz, $CDCl_3$) δ 159.27 (C), 133.88 (CH), 118.27 (CH_2), 81.91 (CH), 66.72 (CH_2), 66.13 (C), 32.07 (CH_2), 31.55 (CH_2), 29.81 (CH_2), 29.79 (CH_2), 29.76 (CH_2), 29.68 (CH_2), 29.59 (CH_2), 29.50 (CH_2), 25.99 (CH_2), 22.84 (CH_2), 14.27 (CH_3).

(±)-*syn* and (±)-*anti*-4-(1-hydroxytridecyl)-4-vinyloxazolidin-2-one (34)

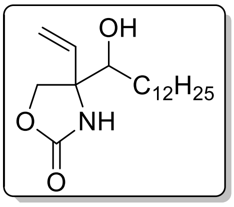

These compounds were obtained as described in general procedure 4, as a by-product, starting from the corresponding isomer of **23**. Purification was carried out by chromatography on XAD-4 resin, using water/ACN as eluent (from 0 to 100% of ACN) followed by lyophilization to give (±)-*syn*-**34** (29.0 mg, 33% yield) or (±)-*anti*-**34** (26.0 mg, 29% yield) as a white solids.

Isomer (±)-*syn*-**34**: **HRMS** (ESI+) calcd. for $C_{18}H_{33}NO_3$ $[M+H]^+$ *(m/z)*: 312.2539, found 312.2530. **^{1}H NMR** (400 MHz, CD_3OD) δ 5.97 (dd, *J* = 17.3, 10.7 Hz, 1H, =C*H*), 5.31 (ddd, *J* = 14.0, 11.6, 0.8 Hz, 2H, =C*H*$_2$), 4.48 (d, *J* = 8.4 Hz, 1H, C*H*HO), 4.06 (d, *J* = 8.4 Hz, 1H, CH*H*O), 3.47 (dd, *J* = 10.0, 2.3 Hz, 1H, C*H*OH), 1.64 – 1.40 (br m, 2H, C*H*$_2$CHOH), 1.29 (br s, *J* = 14.3 Hz, 20H, $C_{10}H_{20}$), 0.90 (t, *J* = 6.9 Hz, 3H, C*H*$_3$). **^{13}C NMR** (101 MHz, CD_3OD) δ 162.01 (C), 139.55 (CH), 115.43 (CH_2), 75.47 (CH), 73.78 (CH_2), 67.61 (C), 33.07 (CH_2), 32.17 (CH_2), 30.79 (CH_2), 30.77 (CH_2), 30.76 (CH_2), 30.73 (CH_2), 30.71 (CH_2), 30.58 (CH_2), 30.47 (CH_2), 27.42 (CH_2), 23.73 (CH_2), 14.44 (CH_3).

Isomer (±)-*anti*-**34**: **HRMS** (ESI+) calcd. for $C_{18}H_{33}NO_3$ $[M+H]^+$ *(m/z)*: 312.2539, found 312.2530. **^{1}H NMR** (400 MHz, CD_3OD) δ 6.08 (dd, *J* = 17.4, 10.8 Hz, 1H, =C*H*), 5.37 – 5.29 (m, 2H, =C*H*$_2$), 4.45 (d, *J* = 8.7 Hz, 1H, C*H*HO), 4.10 (d, *J* = 8.7 Hz, 1H, CH*H*O), 3.54 – 3.49 (m, 1H, C*H*OH), 1.65 – 1.40 (m, 2H, C*H*$_2$CHOH), 1.29 (s, *J* = 13.5 Hz, 20H, $C_{10}H_{20}$), 0.90 (t, *J* = 6.9 Hz, 3H, C*H*$_3$). **^{13}C NMR** (101 MHz, CD_3OD) δ 161.80 (C), 137.85 (CH), 115.85 (CH_2), 76.70 (CH), 74.59 (CH_2), 67.01 (C), 33.07 (CH_2), 32.57 (CH_2), 30.79 (CH_2), 30.77 (CH_2), 30.76 (CH_2), 30.74 (CH_2), 30.70 (CH_2), 30.59 (CH_2), 30.47 (CH_2), 27.17 (CH_2), 23.73 (CH_2), 14.43 (CH_3).

(±)-*tert*-butyl 4-formyl-2,2-dimethyl-4-vinyloxazolidine-3-carboxylate (42)

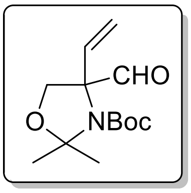

This compound was obtained as described in general procedure 1, starting from (±)-**44** (6.9 g, 26.8 mmol). Flash chromatography on Hexanes/EtOAc as eluent (from 0 to 10% EtOAc) afforded 6.2 g of (±)-**42** (90% yield) as a pale yellow oil. (Rf, hexanes/EtOAc 9:1 (v:v): 0.47).

HRMS (ESI+) calcd. for $C_{13}H_{21}NO_4$ $[M+Na]^+$ *(m/z)*: 278.1368, found 278.1380. ^{1}**H NMR** (400 MHz, CDCl$_3$, as a mixture of rotamers) δ 9.49 (s, 1H, C*H*O, minor), 9.40 (s, *J* = 33.4 Hz, 1H, C*H*O, major), 6.23 – 6.09 (m, *J* = 17.4, 11.1 Hz, 1H, =C*H*, both), 5.36 – 5.15 (m, 2H, =C*H*$_2$, both), 4.04 – 3.95 (m, 1H, C*H*HO, both), 3.79 (dd, *J* = 9.3 Hz, 1H, CH*H*O, both), 1.64 (s, 3H, C*H*$_3$, major), 1.58 (d, *J* = 8.8 Hz, 3H, C*H*$_3$, both), 1.45 (s, 9H, C(C*H*$_3$)$_3$, minor), 1.33 (s, 9H, C(C*H*$_3$)$_3$, major). ^{13}**C NMR** (101 MHz, CDCl$_3$, as a mixture of rotamers) δ 196.67 (CH, minor), 196.43 (CH, major), 151.64 (C, minor), 150.56 (C, major), 134.00 (CH, major), 133.46 (CH, minor), 116.31 (CH$_2$, minor), 115.96 (CH$_2$, major), 96.18 (C, major), 95.19 (C, minor), 81.34 (C, both), 69.18 (CH$_2$, major), 68.81 (CH$_2$, minor), 28.16 (CH$_3$, minor), 27.98 (CH$_3$, major), 26.14 (CH$_3$, minor), 25.57 (CH$_3$, minor), 25.27 (CH$_3$, major), 24.39 (CH$_3$, major).

(±)-*tert*-butyl 4-((*tert*-butyldiphenylsilyl)oxy)-2,2-dimethyl-4-vinyloxazolidine-3-carboxylate (43)

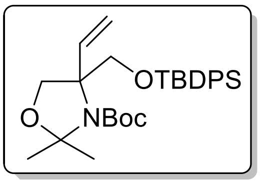

To a solution of (±)-**18** (1.8 g, 4.0 mmol) in DMP/acetone (3:9 mL) was added dropwise BF_3·OEt_2 (25.0 µL, 0.2 mmol). The resulting red solution was next vigorously stirred at rt for 2h and quenched next with Et_3N (60.0 µL) to give a colourless solution. The crude reaction mixture was concentrated under reduced pressure and purified by flash chromatography using Hexanes/EtOAc as eluent (from 0 to 5% EtOAc) to afford compound (±)-**43** (2.0 g, quantitative yield) as a pale yellow oil. (Rf, hexanes/EtOAc 9:1 (v:v): 0.72).

HRMS (ESI+) calcd. for $C_{28}H_{39}NO_4Si$ $[M+H]^+$ *(m/z)*: 496.2883, found 496.2749. ^{1}**H NMR** (400 MHz, CDCl$_3$, as a mixture of rotamers) δ 7.74 – 7.60 (m, 4H, Ar*H*, both), 7.48 – 7.33 (m, 6H, Ar*H*, both), 5.99 (dt, *J* = 17.2, 11.2 Hz, 1H, =C*H*, both), 5.24 – 5.13 (m, 2H, =C*H*$_2$, both), 4.33 (d, *J* = 8.9 Hz, 1H, C*H*HOTBDPS, major), 4.28 (d, *J* = 8.6 Hz, 1H, C*H*HOTBDPS, minor), 4.21 (d, *J* = 9.9 Hz, 1H, C*H*HO, minor), 3.90 (d, *J* = 9.7 Hz, 1H, C*H*HO, major), 3.87 (d, *J* = 9.0 Hz, 1H, CH*H*OTBDPS, major), 3.81 (d, *J* = 8.6 Hz, 1H, CH*H*OTBDPS, minor), 3.77 (d, *J* = 9.5 Hz, 1H, CH*H*O, major), 3.72 (d, *J* = 10.1 Hz, 1H, CH*H*O, minor), 1.61 (d, *J* = 2.8 Hz, 3H, C*H*$_3$, both), 1.55 (d, *J* = 4.0 Hz, 3H, C*H*$_3$, both), 1.49 (s, 9H, C(C*H*$_3$)$_3$, minor), 1.24 (s, 9H, C(C*H*$_3$)$_3$, major), 1.06 (d, *J* = 7.5 Hz, 9H, SiC(C*H*$_3$)$_3$). **^{13}C NMR** (101 MHz, CDCl$_3$, as a mixture of rotamers) δ 151.69 (C, major), 151.33 (C,minor), 138.21 (CH, major), 137.49 (CH,minor), 135.83 (CH, both), 135.77 (CH, both), 135.71 (CH, both), 129.90 (CH, both), 129.89 (CH, both), 129.78 (CH, both), 129.75 (CH, both), 127.85 (CH, both), 127.82 (CH, both), 127.75 (CH, both), 114.76 (CH$_2$, minor), 114.58 (CH$_2$, major), 95.95 (C, major), 95.15 (C,minor), 79.97 (C,minor), 79.86 (C, major), 72.91 (C, both), 71.84 (CH$_2$, major), 70.62 (CH$_2$, minor), 65.48 (CH$_2$, major), 63.23 (CH$_2$, minor), 28.60 (CH$_3$, minor), 28.58 (CH$_3$, major), 28.36 (CH$_3$, both), 26.98 (CH$_3$, major), 26.90 (CH$_3$, minor), 25.77 (CH$_3$, minor), 25.43 (CH$_3$, major), 25.12 (CH$_3$, both).

Elution conditions for the chemical resolution of (±)-43:

Compound (±)-**43** was eluted in column C, coupled to a PDA detector, ranging from 10:90 to 0:100 IPA/Hexane and flow rates between 0.5 to 1 mL/min. After several runs, no apparent resolution of the sample was observed.

(±)-*tert*-butyl 4-(hydroxymethyl)-2,2-dimethyl-4-vinyloxazolidine-3-carboxylate (44)

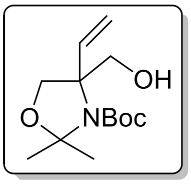

This compound was obtained as described in general procedure 9, starting from (±)-**43** (14.3 g, 28.9 mmol). Flash chromatography on Hexanes/EtOAc as eluent (from 0 to 10% EtOAc) to give 7.0 g of (±)-**44** (94% yield) as a pale yellow oil. (Rf, hexanes/EtOAc 9:1 (v:v): 0.14).

HRMS (ESI+) calcd. for $C_{13}H_{23}NO_4$ $[M+Na]^+$ *(m/z)*: 280.1525, found 280.1502. **^{1}H NMR** (400 MHz, CDCl$_3$) δ 5.94 (dd, *J* = 17.1, 10.8 Hz, 1H, =C*H*), 5.25 (dd, *J* = 35.5, 14.0 Hz, 2H, =C*H*$_2$), 4.42 (d, *J* = 5.5 Hz, 1H, C*H*HO), 4.07 (br s, 1H, O*H*), 3.81 (d, *J* = 8.9 Hz, 1H, C*H*HOH), 3.78 (s, 1H, CH*H*O), 3.72 (d, *J* = 9.3 Hz, 1H, CH*H*OH), 1.56 (d, *J* = 23.4 Hz, 6H, C(C*H*$_3$)$_2$), 1.47 (d, *J* = 18.7 Hz, 9H, C(C*H*$_3$)$_3$). **^{13}C NMR** (101 MHz, CDCl$_3$) δ 153.60 (C), 136.70 (CH), 115.57 (CH$_2$), 95.78 (C), 81.37 (C), 71.13 (CH$_2$), 66.61 (CH$_2$), 28.48 (CH$_3$), 26.53 (CH$_3$), 25.81 (CH$_3$).

(±)-*syn* and (±)-*anti*-*tert*-butyl 4-(1-hydroxytridecyl)-2,2-dimethyl-4-vinyloxazolidine-3-carboxylate (45)

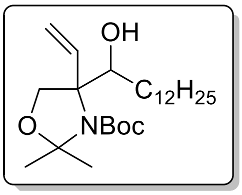

These compounds were obtained as described in general procedure 2, starting from (±)-**42** (3.8 g, 14.9 mmol). Flash chromatography on Hexanes/MTBE as eluent (from 0 to 6 % of MTBE) afforded (±)-*syn*-**45** (2.8 g, 44% yield) or (±)-*anti*-**45** (2.5 g, 39% yield) as a colourless oils. (Rf, hexanes/EtOAc 9:1 (v:v): 0.58 (±)-*anti*-**45** and 0.51 (±)-*syn*-**45**). These compounds are also obtained from the corresponding isomer of **46** as described in general procedure 11. Flash chromatography on Hexanes/EtOAc as eluent (from 0 to 5 % of EtOAc) afforded the corresponding isomer of **45** in quantitative yields.

Isomer (±)-*syn*-**45**: **HRMS** (ESI+) calcd. for $C_{25}H_{47}NO_4$ $[M+H]^+$ *(m/z)*: 426.3583, found 426.3574. **^{1}H NMR** (400 MHz, $CDCl_3$) δ 6.16 (dd, *J* = 17.4, 10.8 Hz, 1H, =C*H*), 5.25 (dd, *J* = 38.7, 14.2 Hz, 2H, =CH_2), 4.14 (br s, 1H, O*H*), 3.97 – 3.86 (m, 1H, C*H*OH), 3.85 (s, 1H, CH_2O), 1.55 (d, *J* = 25.1 Hz, 6H, C(CH_3)$_2$), 1.52 (s, 2H, CH_2CH$_2$CHOH), 1.49 (s, 9H, C(CH_3)$_3$), 1.45 – 1.38 (m, 2H, CH_2CHOH), 1.25 (br s, 18H, C_9H_{18}), 0.87 (t, *J* = 6.9 Hz, 3H, CH_3). **^{13}C NMR** (101 MHz, $CDCl_3$) δ 153.78 (C), 135.40 (CH), 115.71 (CH$_2$), 95.69 (C), 81.45 (C), 75.77 (CH), 69.90 (CH$_2$), 32.07 (CH$_2$), 29.82 (CH$_2$), 29.79 (CH$_2$), 29.77 (CH$_2$), 29.50 (CH$_2$), 28.56 (CH$_3$), 27.08 (CH$_2$), 26.56 (CH$_3$), 25.57 (CH$_3$), 22.83 (CH$_2$), 14.26 (CH$_3$).

Enantiopure or enantioenriched *syn*-isomers were similarly obtained from the corresponding precursors:

syn-(2*R*,3*R*)-**45**: [α]D +3.4 (c 1, $CHCl_3$) and *syn*-(2*S*,3*S*)-**45**: [α]D -3.2 (c 1, $CHCl_3$)

Isomer (±)-*anti*-**45**: **HRMS** (ESI+) calcd. for $C_{25}H_{47}NO_4$ $[M+H]^+$ *(m/z)*: 426.3583, found 426.3574. **^{1}H NMR** (400 MHz, $CDCl_3$) δ 6.02 (dd, *J* = 17.2, 10.8 Hz, 1H, =C*H*), 5.20 (dd, *J* = 26.5, 14.0 Hz, 2H, =CH_2), 4.28 (d, *J* = 7.6 Hz, 1H, O*H*), 3.84 (s, 2H, CH_2O), 3.81 – 3.68 (m, 1H, C*H*OH), 1.69 – 1.59 (m, 1H, CH_2CHOH), 1.55 (d, *J* = 14.4 Hz, 6H, C(CH_3)$_2$), 1.48 (s, 9H, C(CH_3)$_3$), 1.25 (br s, 20H, $C_{10}H_{20}$), 0.87 (t, *J* = 6.8 Hz, 3H, CH_3). **^{13}C NMR** (101 MHz, $CDCl_3$) δ 153.58 (C), 138.03 (CH), 114.11 (CH$_2$), 95.91 (C), 81.26 (C), 73.77 (CH), 71.20 (CH$_2$), 32.06 (CH$_2$), 29.82 (CH$_2$), 29.80 (CH$_2$), 29.78 (CH$_2$), 29.77 (CH$_2$), 29.50 (CH$_2$), 28.53 (CH$_3$), 26.86 (CH$_2$), 26.33 (CH$_3$), 25.59 (CH$_3$), 22.83 (CH$_2$), 14.26 (CH$_3$).

Enantiopure or enantioenriched *anti*-isomers were similarly obtained from the corresponding MPA esters **46** :

anti-(2*S*,3*R*)-**45**: [α]D +1.4 (c 1, $CHCl_3$) and *anti*-(2*R*,3*S*)-**45**: [α]D -1.8 (c 1, $CHCl_3$)

Chemical resolution of (±)-*syn*-45 and (±)-*anti* 45 by derivatization as (*R*)-MPA esters 46

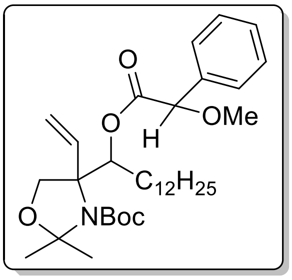

Compounds **46a**[(*R*)(+)-*syn*-**45**] and **46b**[(*R*)(-)-*syn*-**45**] were obtained as described in general procedure 5, starting from (±)-*syn*-**45** and (*R*)-MPA Compounds **46c**[(*R*)(-)-*anti*-**45**], and **46d**[(*R*)(+)-*anti*-**45**] required an extra 2.0 eq of carboxylic acid, EDC and DMAP to complete the reaction, which was followed by TLC until the complete conversion of **45** (see Scheme 2.1.16, Section 2.1.9). The residue was purified by flash chromatography on Hexanes/MTBE as eluent (from 0 to 6 % MTBE) to give the corresponding isomers of **46** (85% yield).

Isomer **46a**[(*R*)(+)-*syn*-**45**] : (620.0 mg, 41% yield) as a colourless oil. (Rf, Hexanes/EtOAc 9:1 (v:v): 0.51). **HRMS** (ESI+) calcd. For $C_{34}H_{55}NO_6$ $[M+Na]^+$ *(m/z)*: 596.3927, found 596.3958. **^{1}H NMR** (400 MHz, $CDCl_3$, as a mixture of rotamers) δ 7.35 (dddd, *J* = 18.9, 6.5, 5.1, 1.7 Hz, 5H, Ar*H*, both), 5.78 (dd, *J* = 8.9, 4.0 Hz, 1H, C*H*O, minor), 5.64 (dd, *J* = 9.8, 3.4 Hz, 1H, C*H*O, major), 5.61 – 5.53 (m, 1H, =C*H*, minor), 5.41 (dd, *J* = 17.4, 10.9 Hz, 1H, =C*H*, major), 4.80 – 4.57 (m, 3H, =CH_2 and C*H*OMe, both), 4.00 (d, *J* = 9.6 Hz, 1H, C*H*HO, major), 3.94 (d, *J* = 9.7 Hz, 1H, C*H*HO, minor), 3.47 – 3.35 (m, 4H, CH*H*O and OCH_3, both), 1.61 – 1.53 (m, 2H, CH_2CHO, both), 1.50 (d, *J* = 4.8 Hz, 6H, C(CH_3)$_2$, both), 1.43 (s, 9H, C(CH_3)$_3$, both), 1.37 – 1.11 (br s, 20H, $C_{10}H_{20}$, both), 0.88 (t, *J* = 6.8 Hz, 3H, CH_3, both). **^{13}C NMR** (101 MHz, $CDCl_3$, as a mixture of rotamers) δ 170.01 (C, major), 169.36 (C, minor), 151.23 (C, both), 137.08 (CH, major), 136.27 (CH, minor), 129.00 (CH, major), 128.93 (CH, minor), 128.69 (CH, major), 128.65 (CH, minor), 127.56 (CH, minor), 127.41 (CH, major), 114.37 (CH_2, both), 96.05 (C, major), 95.23 (C, minor), 82.65 (CH, both), 80.73 (CH, major), 80.51 (CH, minor), 75.92 (CH, both), 69.15 (CH_2, major), 68.27 (CH_2, minor), 67.74 (C, minor), 67.11 (C, major), 57.47 (CH_3, major), 57.37 (CH_3, minor), 32.05 (CH_2, both), 29.80 (CH_2, both), 29.78 (CH_2, both), 29.74 (CH_2, minor), 29.68 (CH_2, major), 29.64 (CH_2, minor), 29.54 (CH_2, minor), 29.49 (CH_2, major), 29.43 (CH_2, minor), 29.22 (CH_2, minor), 29.09 (CH_2, major), 28.54 (CH_3, major), 28.49 (CH_3, minor), 26.81 (CH_2, minor), 26.13 (CH_2, major), 25.77 (CH_3, minor), 25.62 (CH_3, minor), 25.36 (CH_3, major), 24.76 (CH_3, major), 22.83 (CH_2, both), 14.26 (CH_3, both).

Isomer **46b**[(*R*)(-)-*syn*-**45**]: (490.0 mg, 32% yield) as a colourless oil. (Rf, Hexanes/EtOAc 9:1 (v:v): 0.39). **HRMS** (ESI+) calcd. For $C_{34}H_{55}NO_6$ $[M+Na]^+$ *(m/z)*: 596.3927, found 596.3958. **^{1}H NMR** (400 MHz, $CDCl_3$, as a mixture of rotamers) δ 7.49 – 7.28 (m, 5H, Ar*H*, both), 6.00 (dd, *J* = 17.5, 11.0 Hz, 1H, =C*H*, minor), 5.86 (dd, *J* = 17.5, 10.9 Hz, 1H, =C*H*, major), 5.77 (dd, *J* = 10.5, 2.5 Hz, 1H, C*H*O, minor), 5.67 (dd, *J* = 10.9, 2.4 Hz, 1H, C*H*O, major), 5.12 – 4.99 (m, 2H, =C*H*$_2$, both), 4.67 (s, 1H, C*H*OMe, both), 4.16 (d, *J* = 9.6 Hz, 1H, C*H*HO, major), 4.08 (d, *J* = 9.6 Hz, 1H, C*H*HO, minor), 3.82 (d, *J* = 9.6 Hz, 1H, CH*H*O, major), 3.47 – 3.34 (m, 3H, OC*H*$_3$, both), 1.53 (d, *J* = 6.1 Hz, 6H, C(C*H*$_3$)$_2$, major), 1.48 (d, *J* = 8.4 Hz, 6H, C(C*H*$_3$)$_2$, minor), 1.43 (s, 1.61 – 1.37 (m, 9H, C(C*H*$_3$)$_3$, both), 1.35 – 1.16 (m, 16H, C_8H_{16}, both), 1.10 (t, *J* = 6.6 Hz, 2H, C*H*$_2$CH$_2$CHO, both), 1.04 – 0.93 (m, 2H, C*H*$_2$CHO, both), 0.91 – 0.81 (m, 3H, C*H*$_3$, both), 0.73 (m, 2H, C*H*$_2$CH$_2$CH$_2$CHO, both). **^{13}C NMR** (101 MHz, $CDCl_3$) δ 170.23 (C, major), 169.66 (C, minor), 151.19 (C, both), 138.05 (CH, major), 137.20 (CH, minor), 128.84 (CH, both), 128.66 (CH, minor), 128.60 (CH, major), 128.52 (CH, both), 128.19 (CH, both), 128.05 (CH, minor), 128.01 (CH, major), 127.67 (CH, both), 114.63 (CH_2, major), 114.54 (CH_2, minor), 96.03 (C, major), 95.25 (C, minor), 86.21 (C, both), 82.82 (CH, major), 82.35 (CH, minor), 80.69 (C, major), 80.44 (C, minor), 75.77 (CH, minor), 75.63 (CH, major), 69.50 (CH_2, major), 68.71 (CH_2, minor), 67.78 (CH_2, minor), 67.09 (CH_2, major), 57.41 (CH_3, both), 31.99 (CH_2, both), 29.76 (CH_2, both), 29.72 (CH_2, both), 29.70 (CH_2, major), 29.65 (CH_2, minor), 29.47 (CH_2, both), 29.43 (CH_2, major), 29.40 (CH_2, major), 29.38 (CH_2, minor), 29.32 (CH_2, minor), 29.21 (CH_2, minor), 29.17 (CH_2, major), 28.49 (CH_3, both), 28.43 (CH_2, both), 26.51 (CH_3, minor), 25.84 (CH_3, minor), 25.46 (CH_3, major), 25.13 (CH_3, major), 24.86 (CH_2, both), 22.76 (CH_2, both), 14.19 (CH_3, both).

Isomer **46c**[(*R*)(+)-*anti*-**45**]**:** (210.0 mg, 19% yield) as a colourless oil. (Rf, Hexanes/EtOAc 9:1 (v:v): 0.56). **HRMS** (ESI+) calcd. For $C_{34}H_{55}NO_6$ $[M+Na]^+$ *(m/z)*: 596.3927, found 596.3958. **^{1}H NMR** (400 MHz, $CDCl_3$, as a mixture of rotamers) δ 7.47 – 7.27 (m, 5H, Ar*H*, both), 6.19 (dd, *J* = 16.5, 12.0 Hz, 1H, =C*H*, minor), 5.95 (dd, *J* = 17.5, 10.9 Hz, 1H, =C*H*, major), 5.87 (d, *J* = 8.4 Hz, 1H, C*H*O, minor), 5.75 (d, *J* = 8.7 Hz, 1H, C*H*O, major), 5.31 – 5.13 (m, 2H, =C*H*$_2$, both), 4.70 (s, 1H, C*H*OMe, both), 4.03 (d, *J* = 8.7 Hz, 1H, C*H*HO, both), 3.89 (d, *J* = 8.5 Hz, 1H, CH*H*O, both), 3.36 (s, *J* = 8.1 Hz, 3H, OC*H*$_3$, both), 1.52 (d, *J* = 17.7 Hz, 6H, C(C*H*$_3$)$_2$, both), 1.40 (s, *J* = 18.2 Hz, 9H, C(C*H*$_3$)$_3$, both), 1.24 (br s, 18H, C_9H_{18}, both), 1.15 (br s, 2H, C*H*$_2$CHO, both), 1.11 (br s, 2H, C*H*$_2$CH$_2$CHO, both), 0.86 (t, *J* = 6.9 Hz, 3H, C*H*$_3$, both). **^{13}C NMR** (101 MHz, $CDCl_3$, as a mixture of rotamers) δ 170.02 (C, major), 169.32 (C, minor), 151.11 (C, both), 136.58 (CH, major), 136.08 (CH, minor), 128.94 (CH, minor), 128.74 (CH, major), 127.66 (CH, minor), 127.49 (CH, major), 115.89 (CH_2, major), 115.77 (CH_2, minor), 96.18 (C, major), 95.13 (C, minor), 83.57 (CH, both), 80.73 (C, major), 80.10 (C, minor), 73.23 (CH, major), 72.92 (CH, minor), 68.02 (CH_2, major), 67.79 (CH_2, minor), 57.60 (CH_3, major), 57.38 (CH_3, minor), 32.00 (CH_2, major), 31.74 (CH_2, minor), 29.73 (CH_2, both), 29.72 (CH_2, both), 29.69 (CH_2, both), 29.58 (CH_2, both), 29.43 (CH_2, both), 29.41 (CH_2, both), 29.37 (CH_2, both), 28.41 (CH_3, minor), 28.17 (CH_3, major), 26.49 (CH_2, both), 26.33 (CH_2, both), 23.70 (CH_2, both), 22.77 (CH_2, both), 14.20 (CH_3, both).

Isomer **46d**[(*R*)(-)-*anti*-**45**]**:** (210.0 mg, 19% yield) as a colourless oil. (Rf, Hexanes/EtOAc 9:1 (v:v): 0.48). **HRMS** (ESI+) calcd. For $C_{34}H_{55}NO_6$ $[M+Na]^+$ *(m/z)*: 596.3927, found 596.3958. **^{1}H NMR** (400 MHz, $CDCl_3$, as a mixture of rotamers) δ 7.47 – 7.28 (m, 5H, Ar*H*, both), 6.23 (dd, *J* = 17.9, 11.0 Hz, 1H, =C*H*, minor), 5.99 (dd, *J* = 17.4, 10.9 Hz, 1H, =C*H*, major), 5.87 (d, *J* = 9.5 Hz, 1H, C*H*O, minor), 5.73 (d, *J* = 8.9 Hz, 1H, C*H*O, major), 5.39 – 5.18 (m, 2H, $=C\mathit{H}_2$, both), 4.70 (s, 1H, C*H*OMe, both), 4.09 (d, *J* = 9.0 Hz, 1H, C*H*HO, major), 4.01 (dd, *J* = 30.0, 9.2 Hz, 2H, $C\mathit{H}_2O$, minor), 3.92 (d, *J* = 9.0 Hz, 1H, CH*H*O, major), 3.42 (d, *J* = 10.9 Hz, 3H, $OC\mathit{H}_3$, both), 1.61 (d, *J* = 16.2 Hz, 6H, $C(C\mathit{H}_3)_2$, major), 1.53 (d, *J* = 9.9 Hz, 6H, $C(C\mathit{H}_3)_2$, minor), 1.48 (d, *J* = 12.3 Hz, 9H, $C(C\mathit{H}_3)_3$, both), 1.25 (br s, 16H, C_8H_{16}, both), 1.12 – 1.03 (m, 2H, $C\mathit{H}_2CH_2CHO$, both), 1.02 – 0.93 (m, 2H, $C\mathit{H}_2CHO$, both), 0.88 (t, *J* = 6.9 Hz, 3H, $C\mathit{H}_3$, both), 0.78 – 0.58 (m, 2H, $C\mathit{H}_2CH_2$ CH_2CHO, both). **^{13}C NMR** (101 MHz, $CDCl_3$, as a mixture of rotamers) δ 169.80 (C, both), 151.36 (C, both), 136.72 (CH, major), 136.64 (CH, minor), 128.85 (CH, minor), 128.72 (CH, major), 127.43 (CH, minor), 127.32 (CH, major), 116.02 (CH_2, both), 96.11 (C, both), 82.68 (CH, both), 81.06 (C, both), 73.03 (CH, both), 68.43 (CH_2, major), 68.09 (CH_2, minor), 57.71 (CH_3, major), 57.64 (CH_3, minor), 32.07 (CH_2, both), 31.38 (CH_2, both), 29.80 (CH_2, both), 29.78 (CH_2, both), 29.75 (CH_2, both), 29.56 (CH_2, minor), 29.51 (CH_2, major), 29.35 (CH_2, major), 29.24 (CH_2, minor), 28.59 (CH_2, major), 28.54 (CH_2, minor), 28.28 (CH_3, both), 26.45 (CH_3, both), 24.44 (CH_3, both), 22.84 (CH_2, both), 14.27 (CH_3, both).

(±)-*syn* and (±)-*anti*-N-(4-hydroxy-3-(hydroxymethyl)hexadec-1-en-3-yl)octanamide (48)

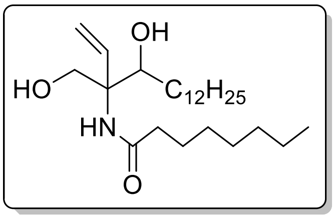

These compounds were obtained as described in general procedure 6, starting from the corresponding isomer of **31** (80.0 mg, 0.2 mmols). Flash chromatography on CH_2Cl_2/MeOH as eluent (from 0 to 3 % of MeOH) afforded (±)-*syn*-**48** (105.0 mg, 91% yield) or (±)-*anti*-**48** (110.0 mg, 96% yield) as a colourless oils. (Rf, CH_2Cl_2/MeOH 95:5 (v:v): 0.62 for (±)-*anti*-**48** and 0.50 for (±)-*syn*-**48**).

Isomer (±)-*syn*-**48**: **HRMS** (ESI+) calcd. for $C_{25}H_{49}NO_3$ $[M+H]^+$ *(m/z)*: 412.3791, found 412.3814. ^{1}**H NMR** (400 MHz, $CDCl_3$) δ 5.98 (s, 1H, N*H*), 5.89 (dd, *J* = 17.5, 10.9 Hz, 1H, =C*H*), 5.24 (dd, *J* = 52.1, 14.2 Hz, 2H, =C*H*$_2$), 4.24 (br s, 2H, O*H*), 3.99 (d, *J* = 11.7 Hz, 1H, C*H*HOH), 3.65 (d, *J* = 11.7 Hz, 1H, CH*H*OH), 3.63 (d, *J* = 6.9 Hz, 1H, C*H*OH), 2.31 – 2.25 (m, 2H, C*H*$_2$C(O)NH), 1.69 – 1.60 (m, 2H, C*H*$_2$ CH_2C(O)NH), 1.58 – 1.46 (m, 2H, C*H*$_2$CHOH), 1.41 – 1.14 (br m, 28H, $C_{14}H_{28}$), 0.98 – 0.75 (m, 6H, C*H*$_3$). ^{13}**C NMR** (101 MHz, $CDCl_3$) δ 174.95 (C), 137.19 (CH), 115.78 (CH_2), 74.98 (CH), 66.54 (C), 66.09 (CH_2), 37.52 (CH_2), 32.06 (CH_2), 31.81 (CH_2), 31.50 (CH_2), 29.81 (CH_2), 29.79 (CH_2), 29.78 (CH_2), 29.76 (CH_2), 29.74 (CH_2), 29.68 (CH_2), 29.49 (CH_2), 29.27 (CH_2), 29.12 (CH_2), 26.51 (CH_2), 26.06 (CH_2), 22.82 (CH_2), 22.73 (CH_2), 14.19 (CH_3).

Enantiopure or enantioenriched *syn*-isomers were similarly obtained from the corresponding precursors **45**: *syn*-(2*R*,3*R*)-**48**: [α]D +3.3 (c 3, $CHCl_3$) and *syn*-(2*S*,3*S*)-**48**: [α]D -3.2 (c 3, $CHCl_3$)

Isomer (±)-*anti*-**48**: **HRMS** (ESI+) calcd. for $C_{25}H_{49}NO_3$ $[M+H]^+$ *(m/z)*: 412.3791, found 412.3814. ^{1}**H NMR** (400 MHz, $CDCl_3$) δ 6.07 (s, 1H, N*H*), 5.92 (dd, *J* = 17.4, 10.7 Hz, 1H, =C*H*), 5.21 (dd, *J* = 83.4, 14.1 Hz, 2H, =C*H*$_2$), 4.76 (br s, 2H, O*H*), 3.71 (d, *J* = 12.0 Hz, 1H, C*H*HOH), 3.64 (dd, *J* = 9.0, 2.9 Hz, 1H, C*H*OH), 3.56 (d, *J* = 12.0 Hz, 1H, CH*H*OH), 2.29 (t, 2H, C*H*$_2$C(O)NH), 1.81 – 1.43 (m, 4H, C*H*$_2$ CH_2C(O)NH and C*H*$_2$CHOH), 1.43 – 1.09 (br m, 28H, $C_{14}H_{28}$), 0.95 – 0.74 (m, 6H, C*H*$_3$). ^{13}**CNMR** (101 MHz, $CDCl_3$) δ 174.91 (C), 137.06 (CH), 115.58 (CH_2), 73.12 (CH), 67.11 (C), 65.95 (CH_2), 37.30 (CH_2), 32.06 (CH_2), 31.82 (CH_2), 30.94 (CH_2), 29.82 (CH_2), 29.80 (CH_2), 29.78 (CH_2), 29.77 (CH_2), 29.75 (CH_2), 29.49 (CH_2), 29.32 (CH_2), 29.13 (CH_2), 26.56 (CH_2), 26.10 (CH_2), 22.82 (CH_2), 22.74 (CH_2), 14.25 (CH_2), 14.19 (CH_3).

Enantiopure or enantioenriched *anti*-isomers were similarly obtained from the corresponding precursors **45**: *anti*-(2*S*,3*R*)-**48**: [α]D +0.4 (c 3, $CHCl_3$) and *anti*-(2*R*,3*S*)-**48**: [α]D -2.2 (c 3, $CHCl_3$)

(2*S*,3*S*)-4-bromo-N-(4-hydroxy-3-(hydroxymethyl)hexadec-1-en-3-yl)benzamide (50)

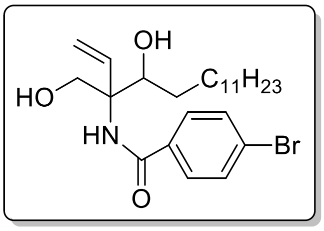

This compounds was obtained as described in general procedure 6, starting from the corresponding isomer of **31** (90.0 mg, 0.3 mmols). Flash chromatography on Hexanes/EtOAc as eluent (from 0 to 20% EtOAc) afforded **50** (77.0 mg, 52% yield) as a colourless crystals. (Rf, Hexanes/EtOAc 7:3 (v:v): 0.30).

Isomer (*2S,3S*)-**50**: **HRMS** (ESI+) calcd. for $C_{21}H_{37}NO_3$ $[M+H]^+$ *(m/z)*: 468.2113, found 468.2127. **^{1}H NMR** (400 MHz, CD_3OD) δ 7.96 – 7.90 (m, 1H, , Ar*H*), 7.80 – 7.71 (m, 1H, Ar*H*), 7.71 – 7.59 (m, 2H, Ar*H*), 5.98 (dd, *J* = 17.5, 10.9 Hz, 1H, =C*H*), 5.32 – 5.14 (m, 2H, =CH_2), 3.94 (d, *J* = 11.4 Hz, 1H, C*H*HOH), 3.89 (d, *J* = 9.4 Hz, 1H, C*H*OH), 3.84 (d, *J* = 11.3 Hz, 1H, CH*H*OH), 1.67 – 1.54 (m, 2H, CH_2CH_2CHOH), 1.37 (m, 2H, CH_2CHOH), 1.34 – 1.18 (m, 18H, C_9H_{18}), 0.89 (t, *J* = 6.8 Hz, 3H, CH_3). **^{13}CNMR** (101 MHz, CD_3OD) δ 169.7 (C), 137.7 (CH), 135.1 (C), 132.8 (CH), 132.8 (CH), 132.5 (CH), 130.2 (CH), 127.2 (C), 115.8 (CH_2), 74.5 (CH), 67.8 (C), 65.2 (CH_2), 33.1 (CH_2), 32.6 (CH_2), 30.8 (CH_2), 30.8 (CH_2), 30.8 (CH_2), 30.7 (CH_2), 30.6 (CH_2), 30.5 (CH_2), 27.5 (CH_2), 23.7 (CH_2), 14.4 (CH_3).

(±)-*syn* and (±)-*anti*-1-dodecyl-5,5-dimethyl-7a-vinyldihydro-1H-oxazolo[3,4-c]oxazol-3(5H)-one (51)

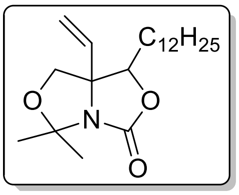

These compounds were obtained as described in general procedure 8, starting from the corresponding (±)-*syn*- **45** or (±)-*anti*- **45** (60.0 mg, 0.1 mmols). Flash chromatography on Hexanes/EtOAc as eluent (from 0 to 6% EtOAc) afforded (±)-*syn*-**51** (50.0 mg, quantitative yield) or (±)-*anti*-**51** (40.0 mg, 80% yield) as a white waxy solid. (Rf, Hexanes/EtOAc 9:1 (v:v): 0.37 for (±)-*anti*-**51** and 0.32 for (±)-*syn*-**51**).

Isomer (±)-*syn*-**51**: **HRMS** (ESI+) calcd. for $C_{21}H_{37}NO_3$ $[M+H]^+$ *(m/z)*: 352.2852, found 352.2814. **^{1}H NMR** (400 MHz, $CDCl_3$) δ 5.85 (dd, *J* = 17.0, 10.5 Hz, 1H, =C*H*), 5.45 (dd, *J* = 25.5, 13.8 Hz, 2H, =CH_2), 4.31 (dd, *J* = 8.8, 4.4 Hz, 1H, C*H*O), 3.97 (d, *J* = 8.8 Hz, 1H, C*H*HO), 3.85 (d, *J* = 8.8 Hz, 1H, CH*H*O), 1.70 (s, 3H, $C(CH_3)_2$), 1.68 – 1.47 (m, 2H, CH_2CHO), 1.44 (s, 3H, $C(CH_3)_2$), 1.25 (s, 20H,

$C_{10}H_{20}$), 0.87 (t, *J* = 6.8 Hz, 3H, C*H*$_3$). **^{13}C NMR** (101 MHz, $CDCl_3$) δ 156.88 (C), 134.78 (CH), 117.76 (CH_2), 95.14 (C), 85.23 (CH), 72.59 (CH_2), 32.04 (CH_2), 30.56 (CH_2), 29.77 (CH_2), 29.75 (CH_2), 29.72 (CH_2), 29.62 (CH_2), 29.50 (CH_2), 29.47 (CH_2), 29.44 (CH_2), 26.83 (CH_3), 25.86 (CH_2), 24.06 (CH_3), 22.81 (CH_2), 14.25 (CH_3).

Enantiopure or enantioenriched *syn*-isomers were similarly obtained from the corresponding precursors:

syn-(2*S*,3*S*)-**51**: $[\alpha]_D$ -21.5 (c 3, $CHCl_3$) and *syn*-(2*R*,3*R*)-**51**: $[\alpha]_D$ +20.3 (c 3, $CHCl_3$)

Isomer (±)-*anti*-**51**: **HRMS** (ESI+) calcd. for $C_{21}H_{37}NO_3$ $[M+H]^+$ *(m/z)*: 352.2852, found 352.2814. **^{1}H NMR** (400 MHz, $CDCl_3$) δ 5.98 (dd, *J* = 17.2, 10.6 Hz, 1H, =C*H*), 5.36 (dd, *J* = 41.5, 13.9 Hz, 2H, =C*H*$_2$), 4.20 (dd, *J* = 9.6, 3.9 Hz, 1H, C*H*O), 3.91 (s, 2H, CH_2O), 1.68 (s, 3H C(C*H*$_3$)$_2$), 1.65 – 1.49 (m, 2H, C*H*$_2$CHO), 1.47 (s, 3H C(C*H*$_3$)$_2$), 1.25 (br s, 20H, $C_{10}H_{20}$), 0.87 (t, *J* = 6.8 Hz, 3H, C*H*$_3$). **^{13}CNMR** (101 MHz, $CDCl_3$) δ 156.95 (C), 139.90 (CH), 115.61 (CH_2), 95.46 (C), 81.50 (CH), 72.29 (C), 67.38 (CH_2), 32.04 (CH_2), 31.14 (CH_2), 29.83 (CH_2), 29.76 (CH_2), 29.75 (CH_2), 29.71 (CH_2), 29.61 (CH_2), 29.50 (CH_2), 29.47 (CH_2), 29.37 (CH_2), 27.95 (CH_3), 25.77 (CH_2), 24.05 (CH_3), 22.82 (CH_2), 14.25 (CH_3).

Enantiopure or enantioenriched *anti*-isomers were similarly obtained from the corresponding precursors:

anti-(2*S*,3*R*)-**51**: $[\alpha]_D$ +0.4 (c 3, $CHCl_3$) and *anti*-(2*R*,3*S*)-**51**: $[\alpha]_D$ -0.6 (c 3, $CHCl_3$)

(2*R*,3*S*), (2*S*,3*R*), and (2*R*,3*R*)-(*E*)-*N*-(4-hydroxy-3-(hydroxymethyl)hexadeca-1,5-dien-3-yl)octanamide (52)

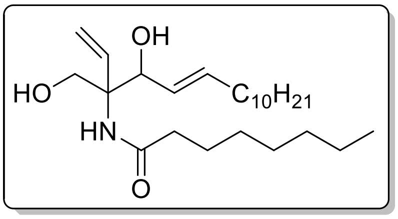

These compounds were obtained as described in general procedure 6, starting from the corresponding isomer of **JG** (40.0 mg, 0.1 mmols). Flash chromatography on CH_2Cl_2/MeOH as eluent (from 0 to 3 % of MeOH) afforded (2*R*,3*S*)-**52** (50.0 mg, 86% yield), (2*S*,3*R*)-**52** (42.0 mg, 72% yield) or (2*R*,3*R*)-**52** (47.0 mg, 83% yield) as colourless oil. (Rf, CH_2Cl_2/MeOH 95:5 (v:v): 0.55 for (±)-*anti*-**52** and 0.46 for (±)-*syn*-**52**).

Isomer (±)-*syn*-**52**: **HRMS** (ESI+) calcd. for $C_{25}H_{47}NO_3$ $[M+H]^+$ *(m/z)*: 410.3634, found 410.3595. **^{1}H NMR** (400 MHz, $CDCl_3$) δ 6.07 (br s, 1H, N*H*), 5.86 (dd, *J* = 17.4, 10.8 Hz, 1H, =C*H*), 5.84 –

5.74 (m, 1H, =C*H*$C_{10}H_{21}$), 5.47 – 5.39 (m, 1H, =C*H*CHOH), 5.36 – 5.14 (m, 2H, =C*H*$_2$), 4.19 (d, *J* = 6.5 Hz, 1H, C*H*OH), 3.94 (d, *J* = 12.0 Hz, 1H, C*H*HO), 3.67 (d, *J* = 12.0 Hz, 1H, CH*H*O), 2.30 – 2.25 (m, 2H, C*H*$_2$C(O)), 2.05 (dd, *J* = 14.0, 7.0 Hz, 2H, =CHC*H*$_2$), 1.65 (dt, *J* = 14.9, 7.6 Hz, 2H, C*H*$_2$ CH_2C(O)), 1.46 – 1.13 (br m, 24H, $C_{12}H_{24}$), 0.94 – 0.83 (m, 6H, C*H*$_3$). **^{13}C NMR** (101 MHz, $CDCl_3$) δ 174.86 (C), 135.85 (CH), 135.74 (CH), 126.61 (CH), 116.61 (CH_2), 75.97 (CH), 66.34 (CH_2), 66.10 (CH_2), 37.60 (CH_2), 32.54 (CH_2), 32.06 (CH_2), 31.82 (CH_2), 29.78 (CH_2), 29.62 (CH_2), 29.49 (CH_2), 29.37 (CH_2), 29.31 (CH_2), 29.25 (CH_2), 29.15 (CH_2), 26.09 (CH_2), 22.83 (CH_2), 22.75 (CH_2), 14.26 (CH_3), 14.20 (CH_3).

syn-(2*R*,3*R*)-**52**: **[α]$_D$** = -10.5 (*c* = 1.5, $CHCl_3$)

Isomer (±)-*anti*-**52**: **HRMS** (ESI+) calcd. for $C_{25}H_{47}NO_3$ $[M+H]^+$ *(m/z)*: 410.3634, found 410.3595. **^{1}H NMR** (400 MHz, $CDCl_3$) δ 6.04 (br s, 1H, N*H*), 5.93 (dd, *J* = 17.3, 10.7 Hz, 1H, =C*H*), 5.79 – 5.66 (m, 1H, =C*H*$C_{10}H_{21}$), 5.38 (ddd, *J* = 7.6, 7.0, 1.7 Hz, 1H, =C*H*CHOH), 5.24 (dd, *J* = 82.8, 14.0 Hz, 2H, =C*H*$_2$), 4.45 (br s, 1H, CH_2O*H*), 4.07 (d, *J* = 7.4 Hz, 1H, C*H*OH), 3.74 (s, 1H, CHO*H*), 3.60 (ddd, *J* = 15.4, 12.0, 4.3 Hz, 2H, C*H*$_2$OH), 2.31 – 2.24 (m, 2H, C*H*$_2$C(O)), 2.04 (dd, *J* = 14.5, 7.0 Hz, 2H, =CHC*H*$_2$), 1.65 (dt, *J* = 14.9, 7.6 Hz, 2H, C*H*$_2$ CH_2C(O)), 1.45 – 1.17 (br m, 24H, $C_{12}H_{24}$), 0.88 (td, *J* = 6.8, 2.6 Hz, 6H, C*H*$_3$). **^{13}C NMR** (101 MHz, $CDCl_3$) δ 174.85 (C), 136.56 (CH), 136.31 (CH), 126.55 (CH), 116.17 (CH_2), 74.72 (CH), 66.87 (CH_2), 65.98 (CH_2), 37.32 (CH_2), 32.54 (CH_2), 32.04 (CH_2), 31.82 (CH_2), 29.77 (CH_2), 29.76 (CH_2), 29.61 (CH_2), 29.47 (CH_2), 29.37 (CH_2), 29.35 (CH_2), 29.23 (CH_2), 29.14 (CH_2), 26.09 (CH_2), 22.82 (CH_2), 22.74 (CH_2), 14.25 (CH_3), 14.19 (CH_3).

anti-(2*R*,3*S*)-**52**: **[α]$_D$** = -6.7 (*c* = 1.5, $CHCl_3$) and *anti*-(2*S*,3*R*)-**52**: **[α]$_D$** = +7.9 (*c* = 1.5, $CHCl_3$)

The experimental data for compounds from **72** to **77** and **JG** will be published elsewhere (manuscript in preparation).

4.2 Biological studies

4.2.1 General remarks

Cell cultures

A549 (human lung carcinoma cells), purchased in American type culture collections, were maintained in F-12 HAM medium supplemented with 10% FBS, 100 IU/ml penicillin, 100 µgr/ml streptomycin and 2mM of Glutamine. Cells were grown routinely without reaching high confluence.

All cells were kept at 37°C in humidified atmosphere, 95% air-5% CO2.

Cell viability

Cell viability was determined by the colorimetric 3-(4,5-dimethylthiazol-2-yl)-2,5-diphenyl tetrazolium bromide (MTT) assay. Cells were seeded in 96-well plates by adding 100 µl/well of cell suspension (A549 in F-12 HAM) and allowed to grow for 24 hours. Medium was replaced with fresh medium and the specific treatments were added. All compounds were dissolved in MeOH or DMSO and control experiments were performed with the correspondent solvent. Plates were incubated 24 hours; after that 10 µl of MTT reactive (5 mg/ml) was added and incubated during 3 hours. Subsequently the medium was removed and the formazan precipitate was solubilized in 100 µl of DMSO. Absorbance was measured at 570 nm with a Spectramax Plus Reader (Molecular Device Corporation).

ESI-MS

Electrospray ionization mass spectrometry (ESI-MS) measurements were performed on a Bruker Daltonics Esquire 3000 Plus (Düsseldorf, Germany) ion trap mass spectrometer with a C4 analytical column (300 Å). Mass spectra were recorded both in positive and negative ionization mode in the m/z 700–2000 range. The enzyme concentration was of 1 µM/100 µL (50 µL of Buffer solution A described above and 50 µL of AcN with 0.5% of TFA). The inhibitor concentration was 250 µM. Samples were infused into the mass spectrometer using a syringe pump, in a flow rate of 4L/min with an water:AcN gradient. The deconvolution of the mass spectra were undertook with ProMass Deconvolution Software.

Statistical analysis

Data were analysed by Student's *t* test or one-way ANOVA test followed by Bonferroni's or Dunnet's multiple comparison test.

4.2.2 Assays of S1PL enzyme activity

Fluorogenic assay of StS1PL enzyme activity with RBM13 as a substrate

In a 96-well plate, 5 µL of putative inhibitors (added from stock solutions in DMSO; final DMSO: 2.5 %) were preincubated with recombinant bacterial StS1PL (45 µL from stock solutions in buffer A, final concentration: 25 µg/mL) at 37 ºC for 30 min. Subsequently, 50 µL of RBM13 (added from a stock solution 0.5 M in buffer A; final concentration: 125 µM) was added, ending up with a final volume of 100 µL. Buffer solution A correspond to a 1 mM potassium phosphate buffer, pH 7.2, containing 100 mM NaCl, 1 mM EDTA, 1 mM DTT, 10 µM pyridoxal 5'-phosphate. The mixture was incubated at 37 ºC for 1 h and the enzymatic reaction was stopped by the addition of 50 µL of MeOH. Finally, 100 µL of a 200 mM glycine-NaOH buffer, pH 10.6, were added to the resulting solution and the mixture was incubated for 20 additional min at 37 ºC in order to complete the β-elimination reaction. The amount of umbelliferone formed was determined on SpectraMax M5 (Molecular Devices) microplate reader (λex/em = 355/460 nm), using a calibration curve. IC50 values were determined by plotting percent activity versus log [I] and fitting the data to the log(inhibitor) vs. response equation in Prism 5 (GraphPad Software, La Jolla). Settings for curve adjustments were kept with their default values.

Fluorogenic assay of hS1PL enzyme activity with RBM7-148 as a substrate

The protocol of the assay with the new substrate is similar, but considering RBM7-148 more affine to the hS1PL, a less concentration of enzyme is necessary to obtain a better fluorogenic response. Furthermore, no preincubation time was set for this assay.

Human S1PL (50 µL from stock solutions in buffer B, final concentration: 0.8 µg/mL) was added to a mixture of RBM7-148 (added from a stock solution in 2.5 mM in DMSO, final concentration: 125 µM) and putative inhibitors in buffer B (final volume of 100 µL). The reaction was stopped following the same methodology described for the StS1PL fluorogenic assay. Buffer solution B correspond to a 100 mM HEPES buffer, pH 7.4, containing 0.1 mM EDTA, 0.05 % Triton X-100, 0.01 % Pluronic F127 (Biotium), and 100 µM pyridoxal 5'-phosphate.

Fluorogenic assay of hS1PL enzyme for irreversibility

In a 96-well plate, 0.5 µL of hS1PL enzyme in each well (80 µg/µL, from stock solutions in buffer B) were preincubated with 0.5 µL of (2*S*,3*S*)-**24** at 500 µM in DMSO at 37 ºC for 30 min (final volume 1 µL). Next, the experiment was diluted with buffer B containing the substrate RBM7-148 (final concentration: 125 µM) until a final volume of 100 µL. The final concentration of the enzyme was 0.8 µg/µL (as in the fluorogenic activity assay) and the final concentration of the putative irreversible inhibitor was 5 µM.

Subsequently, the mixture was incubated for different set times: 5, 10, 30, 60, 120 and 180 min at 37 ºC and the enzymatic reaction was stopped as usual. The amount of umbelliferone formed was determined on SpectraMax M5 (Molecular Devices) microplate reader (λex/em = 355/460 nm), using a calibration curve.

4.3.3 Lipidomic analyses

Lipidomic analysis

Into 6-wells plates with 1 ml of medium, cells were seeded at 250.000 cells/ml (1 ml/well) and allowed to grow for 24h. Medium was replaced with fresh medium (1ml/well) and the specific treatments were added. All compounds were dissolved in MeOH or DMSO and control experiments were performed with the correspondent solvent. Plates were incubated 24 hours more. After that time, cells were collected with 400 µl trypsin-EDTA and 600 µl F-12 HAM.

Cell concentration was determined by Trypan Blue staining.

To proceed with the sphingolipid extraction, samples were centrifuged 3 min at 10000 rpm, washed with 200 µl of cold PBS 1% and resuspended in 100 µl of purified water. 500 µl of MeOH, 250 µl of chloroform and internal standards were added. The solution was sonicated and incubated at 48ºC bath for 12h. After that time the samples were allowed to cool to room temperature and 75 µl of 1M KOH in MeOH was added. The samples were sonicated 2h at 37ºC, after that 75 µl of acetic acid were added and the solvent was evaporated under nitrogen stream. Once dry, the samples were resuspended in 500 µl of MeOH and evaporated again under nitrogen stream. Finally, the samples were resuspended in 150 µl of MeOH and prepared for the mass analyses.

Sphingolipids extracts, enriched with internal standards [N- dodecanoylsphingosine, N-dodecanoylglucosylsphingosine, N-dodecanoyl sphingosyl phosphorylcholine , C17-sphinganine (0.2 nmol each), and C17-sphinganine-1-phosphate, (0.1 nmol)] were prepared as described[117] and analyzed by ultraperformance LC (UPLC)-TOFMS or HPLC-MS/MS.

The liquid chromatography-mass spectrometer consisted of a Waters Aquity UPLC system connected to a Waters LCT Premier orthogonal accelerated time of flight mass spectrometer (Waters, Millford, MA), operated in positive electrospray ionisation mode. Full scan spectra from 50 to 1500 Da were acquired and individual spectra were summed to produce data points each 0.2 s. Mass accuracy and reproducibility were maintained by using an independent reference spray by the LockSpray interference. The analytical column was a 100 mm x 2.1mm i.d., 1.7 mm C8 Acquity UPLC BEH (Waters). The two mobile phases were phase A: methanol/water/formic acid (74/25/1 v/v/v); phase B: methanol/formic acid (99/1 v/v), both also contained 5mM ammonium formate. A linear gradient was programmed— 0.0 min: 80% B; 3 min: 90% B; 6 min: 90% B; 15 min: 99% B; 18 min: 99% B; 20 min: 80% B. The flow rate was 0.3 ml min-1.The column was held at 30°C. Quantification was carried out using the extracted ion chromatogram of each compound, using 50 mDa. windows. The linear dynamic range was determined by injecting standard mixtures. Positive identification of compounds was based on the accurate mass measurement with an error <5 ppm and its LC retention time, compared to that of a standard (±2%).

Alternatively, analysis of the extracts was performed by LC/MS/MS with a system consisting of a Waters Alliance 2690 LC pump equipped with an autosampler and connected to a Quattro LC triple-quadrupole mass spectrometer from Micromass (Manchester, UK). Separation was achieved ona Purospher STAR-RP-18 column (125 × 2 mm, 5 μm) (Merck, Darmstadt). The two mobile phases were phase A and phase B as described above. A gradient was programmed: 0.0 min, 50% B; 2 min, 50% B; 7 min, 100% B; 17 min, 100% B; 19 min, 50% B; and 26 min, 50% B. The flow rate was 0.3 ml min−1. MS/MS detection was performed with an electrospray interface operating in the positive ion mode acquiring the following selected reaction monitoring transitions: C17 d-*erythro*-sphinganine-1-phosphate, 368–252, collision energy 18 eV; and S1P, 380–264 Da, collision energy 16 eV.

5. REFERENCES

(1) Thudichum, J. L. W. *A Treatise on the Chemical Constitution of the Brain.*; London : Bailliere, Tindall and Cox: London, **1884**.

(2) Olsen, I.; Jantzen, E. Sphingolipids in Bacteria and Fungi. *Anaerobe* **2001**, *7* (2), 103–112.

(3) Hannun, Y. A.; Obeid, L. M. Principles of Bioactive Lipid Signalling : Lessons from Sphingolipids. *Nat. Rev. Mol. Cell Biol.* **2008**, *9* (February), 139–150.

(4) Maceyka, M.; Spiegel, S. Sphingolipid Metabolites in Inflammatory Disease. *Nature* **2014**, *510*, 58–67.

(5) Spiegel, S.; Milstien, S. The Outs and the Ins of Sphingosine-1-Phosphate in Immunity. *Nat. Rev. Immunol.* **2011**, *11* (6), 403–415.

(6) Kolter, T.; Sandhoff, K. Sphingolipid Metabolism Diseases. *Biochim. Biophys. Acta - Biomembr.* **2006**, *1758* (12), 2057–2079.

(7) Gangoiti, P.; Camacho, L.; Arana, L.; Ouro, A.; Granado, M. H.; Brizuela, L.; Casas, J.; Fabriás, G.; Abad, J. L.; Delgado, A.; Gómez-Muñoz, A. Control of Metabolism and Signaling of Simple Bioactive Sphingolipids: Implications in Disease. *Prog. Lipid Res.* **2010**, *49* (4), 316–334.

(8) Bandhuvula, P.; Saba, J. D. Sphingosine-1-Phosphate Lyase in Immunity and Cancer: Silencing the Siren. *Trends Mol. Med.* **2007**, *13* (5), 210–217.

(9) Hanada, K. Co-Evolution of Sphingomyelin and the Ceramide Transport Protein CERT. *Biochim. Biophys. Acta - Mol. Cell Biol. Lipids* **2014**, *1841* (5), 704–719.

(10) Bourquin, F. E. Questioning the Sphinx: Structural and Functional Studies of Sphingosine-1-Phosphate Lyase, Doctoral Thesis. Universität Zürich, **2010**.

(11) Hla, T. Physiological and Pathological Actions of Sphingosine 1-Phosphate. *Semin. Cell Dev. Biol.* **2004**, *15* (5), 513–520.

(12) Olson, D. K.; Fröhlich, F.; Farese, R. V.; Walther, T. C. Taming the Sphinx: Mechanisms of Cellular Sphingolipid Homeostasis. *Biochim. Biophys. Acta - Mol. Cell Biol. Lipids* **2016**, *1861* (8), 784–792.

(13) Hannun, Y. A.; Obeid, L. M. Many Ceramides. *J. Biol. Chem.* **2011**, *286* (32), 27855–27862.

(14) Riboni, L.; Campanella, R.; Bassi, R.; Villani, R.; Gaini, S. M.; Martinelli-Boneschi, F.; Viani, P.; Tettamanti, G. Ceramide Levels Are Inversely Associated with Malignant

Progression of Human Glial Tumors. *Glia* **2002**, *39* (2), 105–113.

(15) Levade, T.; Malagarie-Cazenave, S.; Gouazé, V.; Ségui, B.; Tardy, C.; Betito, S.; Andrieu-Abadie, N.; Cuvillier, O. Ceramide in Apoptosis: A Revisited Role. *Neurochem. Res.* **2002**, *27* (7–8), 601–607.

(16) Song, M. S.; Posse De Chaves, E. I. Inhibition of Rat Sympathetic Neuron Apoptosis by Ceramide. Role of p75NTR in Ceramide Generation. *Neuropharmacology* **2003**, *45* (8), 1130–1150.

(17) Plummer, G.; Perreault, K. R.; Holmes, C. F. B.; Posse De Chaves, E. I. Activation of Serine/threonine Protein Phosphatase-1 Is Required for Ceramide-Induced Survival of Sympathetic Neurons. *Biochem. J.* **2005**, *385*, 685–693.

(18) Gómez-Muñoz, A. Ceramide 1-Phosphate/ceramide, a Switch between Life and Death. *Biochim. Biophys. Acta - Biomembr.* **2006**, *1758* (12), 2049–2056.

(19) Spiegel, S.; English, D.; Milstien, S. Sphingosine 1-Phosphate Signaling: Providing Cells with a Sense of Direction. *Trends Cell Biol.* **2002**, *12* (5), 236–242.

(20) Spiegel, S.; Milstien, S. Sphingosine-1-Phosphate: An Enigmatic Signalling Lipid. *Nat. Rev. Mol. Cell Biol.* **2003**, *4* (5), 397–407.

(21) Ikeda, M.; Kihara, A.; Igarashi, Y. Sphingosine-1-Phosphate Lyase SPL Is an Endoplasmic Reticulum-Resident, Integral Membrane Protein with the Pyridoxal 5’-phosphate Binding Domain Exposed to the Cytosol. *Biochem. Biophys. Res. Commun.* **2004**, *325* (1), 338–343.

(22) Watterson, K.; Sankala, H.; Milstien, S.; Spiegel, S. Pleiotropic Actions of Sphingosine-1-Phosphate. *Prog. Lipid Res.* **2003**, *42* (4), 344–357.

(23) Takabe, K.; Spiegel, S. Export of Sphingosine-1-Phosphate and Cancer Progression. *J. Lipid Res.* **2014**, *55* (9), 1839–1846.

(24) Rivera, J.; Proia, R. L.; Olivera, A. The Alliance of Sphingosine-1-Phosphate and Its Receptors in Immunity. *Nat. Rev. Immunol.* **2008**, *8* (10), 753–763.

(25) Gräler, M. H.; Goetzl, E. J. The Immunosuppressant FTY720 down-Regulates Sphingosine 1-Phosphate G-Protein-Coupled Receptors. *FASEB J.* **2004**, *18* (3), 551–553.

(26) Wymann, M. P.; Schneiter, R. Lipid Signalling in Disease. *Nat. Rev. Mol. Cell Biol.* **2008**, *9* (2), 162–176.

(27) Brinkmann, V.; Billich, A.; Baumruker, T.; Heining, P.; Schmouder, R.; Francis, G.; Aradhye, S.; Burtin, P. Fingolimod (FTY720): Discovery and Development of an Oral Drug to Treat Multiple Sclerosis. *Nat Rev Drug Discov* **2010**, *9* (11), 883–897.

(28) Maceyka, M.; Sankala, H.; Hait, N. C.; Le Stunff, H.; Liu, H.; Toman, R.; Collier, C.; Zhang, M.; Satin, L. S.; Merrill, A. H.; Milstien, S.; Spiegel, S. SphK1 and SphK2, Sphingosine Kinase Isoenzymes with Opposing Functions in Sphingolipid Metabolism. *J. Biol. Chem.* **2005**, *280* (44), 37118–37129.

(29) Veldhovens, P. P. Van; Mannaerts, G. P. Subcellular Localization and Membrane Topology of Sphingosine- 1- Phosphate Lyase in Rat Liver*. *J. Biol. Chem.* **1991**, *266* (19), 12502–12507.

(30) Bourquin, F.; Riezman, H.; Capitani, G.; Gru, M. G. Structure and Function of Sphingosine-1-Phosphate Lyase , a Key Enzyme of Sphingolipid Metabolism. *Structure* **2010**, *18*, 1054–1065.

(31) Saba, J. D.; Hla, T. Point-Counterpoint of Sphingosine 1-Phosphate Metabolism. *Circ. Res.* **2004**, *94* (6), 724–734.

(32) Reiss, U.; Oskouian, B.; Zhou, J.; Gupta, V.; Sooriyakumaran, P.; Kelly, S.; Wang, E.; Merrill, A. H.; Saba, J. D. Sphingosine-Phosphate Lyase Enhances Stress-Induced Ceramide Generation and Apoptosis. *J. Biol. Chem.* **2004**, *279* (2), 1281–1290.

(33) Mukhopadhyay, D.; Howell, K. S.; Riezman, H.; Capitani, G. Identifying Key Residues of Sphinganine-1-Phosphate Lyase for Function in Vivo and in Vitro. *J. Biol. Chem.* **2008**, *283* (29), 20159–20169.

(34) Weiler, S.; Braendlin, N.; Beerli, C.; Bergsdorf, C.; Schubart, A.; Srinivas, H.; Oberhauser, B.; Billich, A. Orally Active 7- Substituted (4-Benzylphthalazin-1-Yl)-2- Methylpiperazin-1-Yl]nicotinonitriles as Active-Site Inhibitors of Sphingosine 1- Phosphate Lyase for the Treatment of Multiple Sclerosis. *J. Med. Chem.* **2014**, *57* (12), 5074–5084.

(35) Bagdanoff, J. T.; Donoviel, M. S.; Nouraldeen, A.; Tarver, J.; Fu, Q.; Carlsen, M.; Jessop, T. C.; Zhang, H.; Hazelwood, J.; Nguyen, H.; Baugh, S. D. P.; Gardyan, M.; Terranova, K. M.; Barbosa, J.; Yan, J.; Bednarz, M.; Layek, S.; Courtney, L. F.; Taylor, J.; Digeorge-Foushee, A. M.; Gopinathan, S.; Bruce, D.; Smith, T.; Moran, L.; O'Neill, E.; Kramer, J.; Lai, Z.; Kimball, S. D.; Liu, Q.; Sun, W.; Yu, S.; Swaffield, J.; Wilson, A.; Main, A.; Carson, K. G.; Oravecz, T.; Augeri, D. J. Inhibition of Sphingosine-1-Phosphate Lyase for the Treatment of Autoimmune Disorders. *J. Med. Chem.* **2009**, *52* (13), 3941–3953.

(36) Bot, M.; Van Veldhoven, P. P.; de Jager, S. C. A.; Johnson, J.; Nijstad, N.; Van Santbrink, P. J.; Westra, M. M.; Van Der Hoeven, G.; Gijbels, M. J.; Müller-Tidow, C.; Varga, G.; Tietge, U. J. F.; Kuiper, J.; Van Berkel, T. J. C.; Nofer, J. R.; Bot, I.; Biessen, E. A. L. Hematopoietic Sphingosine 1-Phosphate Lyase Deficiency Decreases Atherosclerotic Lesion Development in LDL-Receptor Deficient Mice. *PLoS One* **2013**, *8* (5), 1–13.

(37) Stoffel, W.; Grol, M. Chemistry and Biochemistry of 1-Desoxysphinganine-1-Phosphonate (Dihydrosphingosine-1-Phosphonate). *Chem. Phys. Lipids* **1974**, *13*, 372–388.

(38) Boumendjel, A.; Miller, P. F. Synthesis of an Inhibitor of Sphingosine-1-Phosphate Lyase. *Tetrahedron Lett.* **1994**, *35* (6), 819–822.

(39) Bandhuvula, P.; Tam, Y. Y.; Oskouian, B.; Saba, J. D. The Immune Modulator FTY720 Inhibits Sphingosine-1-Phosphate Lyase Activity. *J. Biol. Chem.* **2005**, *280* (40), 33697–33700.

(40) Bassi, R.; Anelli, V.; Giussani, P.; Tettamanti, G.; Viani, P.; Riboni, L. Sphingosine-1-Phosphate Is Released by Cerebellar Astrocytes in Response to bFGF and Induces Astrocyte Proliferation through Gi-Protein-Coupled Receptors. *Glia* **2006**, *53* (6), 621–630.

(41) Schwab, S. R.; Pereira, J. P.; Matloubian, M.; Xu, Y.; Huang, Y.; Cyster, J. G. Lymphocyte Sequestration Through S1P Lyase Inhibition and Disruption of S1P Gradients. *Science (80-.).* **2005**, *309* (5741), 1735–1739.

(42) Billich, A.; Beerli, C.; Bergmann, R.; Bruns, C.; Loetscher, E. Cellular Assay for the Characterization of Sphingosine-1-Phosphate Lyase Inhibitors. *Anal. Biochem.* **2013**, *434* (2), 247–253.

(43) Loetscher, E.; Schneider, K.; Beerli, C.; Billich, A. Assay to Measure the Secretion of Sphingosine-1-Phosphate from Cells Induced by S1P Lyase Inhibitors. *Biochem. Biophys. Res. Commun.* **2013**, *433* (3), 345–348.

(44) Ohtoyo, M.; Tamura, M.; Machinaga, N.; Muro, F.; Hashimoto, R. Sphingosine 1-Phosphate Lyase Inhibition by 2-Acetyl-4-(Tetrahydroxybutyl)imidazole (THI) under Conditions of Vitamin B6 Deficiency. *Mol. Cell. Biochem.* **2015**, *400*, 125–133.

(45) Gugasyan, R.; Coward, A.; O'Connor, L.; Shortman, K.; Scollay, R. Emigration of Mature T Cells from the Thymus Is Inhibited by the Imidazole-Based Compound 2-Acetyl-4-Tetrahydroxybutylimidazole. *Immunology* **1998**, *93* (3), 398–404.

(46) Ohtoyo, M.; Machinaga, N.; Inoue, R.; Hagihara, K.; Yuita, H.; Tamura, M.; Hashimoto, R.; Chiba, J.; Muro, F.; Watanabe, J.; Kobayashi, Y.; Abe, K.; Kita, Y.; Nagasaki, M.; Shimozato, T. Component of Caramel Food Coloring, THI, Causes Lymphopenia Indirectly via a Key Metabolic Intermediate. *Cell Chem. Biol.* **2016**, *23* (5), 555–560.

(47) Bagdanoff, J. T.; Donoviel, M. S.; Nouraldeen, A.; Carlsen, M.; Jessop, T. C.; Tarver, J.; Aleem, S.; Dong, L.; Zhang, H.; Boteju, L.; Hazelwood, J.; Yan, J.; Bednarz, M.; Layek, S.; Owusu, I. B.; Gopinathan, S.; Moran, L.; Lai, Z.; Kramer, J.; Kimball, S. D.; Yalamanchili, P.; Heydorn, W. E.; Frazier, K. S.; Brooks, B.; Brown, P.; Wilson, A.; Sonnenburg, W. K.; Main, A.; Carson, K. G.; Oravecz, T.; Augeri, D. J. Inhibition of Sphingosine 1-Phosphate Lyase for the Treatment of Rheumatoid Arthritis: Discovery of (E)-1-(4-((1 R,2 S,3 R)-1,2,3,4-Tetrahydroxybutyl)-1 H -Imidazol-2-Yl)ethanone Oxime (LX2931) and (1 R,2 S,3 R)-1-(2-(Isoxazol-3-Yl)-1 H -Imidazol-4-Yl)but. *J. Med. Chem.* **2010**, *53*, 8650–8662.

(48) Bigaud, M.; Guerini, D.; Billich, A.; Bassilana, F.; Brinkmann, V. Second Generation S1P Pathway Modulators: Research Strategies and Clinical Developments. *Biochim. Biophys. Acta - Mol. Cell Biol. Lipids* **2014**, *1841* (5), 745–758.

(49) Weiler, S.; Braendlin, N.; Beerli, C.; Bergsdorf, C.; Schubart, A.; Srinivas, H.; Oberhauser, B.; Billich, A. Orally Active 7-Substituted (4-Benzylphthalazin-1-Yl)-2-Methylpiperazin-1-Yl]nicotinonitriles as Active-Site Inhibitors of Sphingosine 1-Phosphate Lyase for the Treatment of Multiple Sclerosis. *J. Med. Chem.* **2014**, *57*, 5074–5084.

(50) Cosconati, S.; Novellino, E. The First Sphingosine 1-Phosphate Lyase Inhibitors against Multiple Sclerosis: A Successful Drug Discovery Tale. *J. Med. Chem.* **2014**, *57*, 5072–5073.

(51) Dinges, J.; Harris, C. M.; Wallace, G. A.; Argiriadi, M. A.; Queeney, K. L.; Perron, D. C.; Dominguez, E.; Kebede, T.; Desino, K. E.; Patel, H.; Vasudevan, A. Hit-to-Lead Evaluation of a Novel Class of Sphingosine 1-Phosphate Lyase Inhibitors. *Bioorg. Med. Chem. Lett.* **2016**, *26* (9), 2297–2302.

(52) Argiriadi, M. A.; Banach, D.; Radziejewska, E.; Marchie, S.; DiMauro, J.; Dinges, J.; Dominguez, E.; Hutchins, C.; Judge, R. A.; Queeney, K.; Wallace, G.; Harris, C. M. Creation of a S1P Lyase Bacterial Surrogate for Structure-Based Drug Design. *Bioorg. Med. Chem. Lett.* **2016**, *26* (9), 2293–2296.

(53) Deniz, U.; Ozkirimli, E.; Ulgen, K. O. A Systematic Methodology for Large Scale Compound Screening: A Case Study on the Discovery of Novel S1PL Inhibitors. *J. Mol.*

Graph. Model. **2016**, *63*, 110–124.

(54) Schumann, J.; Grevot, a.; Ledieu, D.; Wolf, a.; Schubart, a.; Piaia, a.; Sutter, E.; Cote, S.; Beerli, C.; Pognan, F.; Billich, a.; Moulin, P.; Walker, U. J. Reduced Activity of Sphingosine-1-Phosphate Lyase Induces Podocyte-Related Glomerular Proteinuria, Skin Irritation, and Platelet Activation. *Toxicol. Pathol.* **2015**, *43* (5), 694–703.

(55) Copeland, R. A. Evaluation of Enzyme Inhibitors in Drug Discovery: A Guide for Medicinal Chemists and Pharmacologists. In *Evaluation of Enzyme Inhibitors in Drug Discovery: A Guide for Medicinal Chemists and Pharmacologists: Second Edition*; Wiley-Interscience, Ed.; John Wiley & Sons, **2005**; pp 214–248.

(56) Storici, P.; De Biase, D.; Bossa, F.; Bruno, S.; Mozzarelli, A.; Peneff, C.; Silverman, R. B.; Schirmer, T. Structures of Gamma-Aminobutyric Acid (GABA) Aminotransferase, a Pyridoxal 5’-Phosphate, and [2Fe-2S] Cluster-Containing Enzyme, Complexed with Gamma-Ethynyl-GABA and with the Antiepilepsy Drug Vigabatrin. *J. Biol. Chem.* **2004**, *279* (1), 363–373.

(57) Lee, H.; Le, H. V.; Wu, R.; Doud, E.; Sanishvili, R.; Kellie, J. F.; Compton, P. D.; Pachaiyappan, B.; Liu, D.; Kelleher, N. L.; Silverman, R. B. Mechanism of Inactivation of GABA Aminotransferase by (E)- and (Z)-(1S,3S)-3-Amino-4-Fluoromethylenyl-1-Cyclopentanoic Acid. *ACS Chem. Biol.* **2015**, *10* (9), 2087–2098.

(58) Pan, Y.; Gerasimov, M. R.; Kvist, T.; Wellendorph, P.; Madsen, K. K.; Pera, E.; Lee, H.; Schousboe, A.; Chebib, M.; Bra, H.; Craft, C. M.; Brodie, J. D.; Schiffer, W. K.; Dewey, S. L.; Miller, S. R.; Silverman, R. B. (1S,3S)-3-Amino-4-Difluoromethylenyl-1-Cyclopentanoic Acid (CPP-115), a Potent γ-Aminobutyric Acid Aminotransferase Inactivator for the Treatment of Cocaine Addiction. *J. Med. Chem.* **2012**, *55* (1), 357–366.

(59) Singh, J.; Petter, R. C.; Baillie, T. a; Whitty, A. The Resurgence of Covalent Drugs. *Nat. Rev. Drug Discov.* **2011**, *10* (4), 307–317.

(60) Fukuda, T.; Sugiyama, K.; Arima, S.; Harigaya, Y. Total Synthesis of Salinosporamide A. *Org. Lett.* **2008**, *10* (19), 1–10.

(61) Ooi, H.; Ishibashi, N.; Iwabuchi, Y.; Ishihara, J.; Hatakeyama, S. A Concise Route to (+)-Lactacystin. *J. Org. Chem.* **2004**, *69* (11), 7765–7768.

(62) Goebel, M. T.; Marvel, C. S. The Oxidation of Grignard Reagents. *J. Am. Chem. Soc.* **1933**, *1693* (7), 1693–1696.

(63) Masamune, B. S.; Ali, S. A.; Snitman, D. L.; Garvey, D. S. Highly Stereoselective Aldol Condensation Using an Enantioselective Chiral Enolate. *Angew. Chem. Int. Ed. Engl.* **1980**, *19* (7), 557–558.

(64) Ho, Tse-lok; Olah, G. A. Silane/iodine-Based Cleavage of Esters and Ethers under Neutral Conditions*. *Proc. Natl. Acad. Sci.* **1978**, *75* (1), 4–6.

(65) Grijalvo, S.; Llebaria, A.; Delgado, A. Straightforward Access to Simplified Sphingosine-1-Phosphate Analogues. *Synth. Commun.* **2007**, *37* (16), 2737–2751.

(66) Pradere, U.; Garnier-amblard, E. C.; Coats, S. J.; Amblard, F.; Schinazi, R. F.; Llc, R. F. S. P.; States, U. Synthesis of Nucleoside Phosphate and Phosphonate Prodrugs. *Chem. Rev.* **2014**, *114*, 9154–9218.

(67) Seco, M.; Quin, E.; Riguera, R. A Practical Guide for the Assignment of the Absolute Configuration of Alcohols , Amines and Carboxylic Acids by NMR. *Tetrahedron: Asymmetry* **2001**, *12* (53), 2915–2925.

(68) Zheng, X.; Gandour, R. D.; Edgar, K. J. Probing the Mechanism of TBAF-Catalyzed Deacylation of Cellulose Esters. *Biomacromolecules* **2013**, *14*, 1388–1394.

(69) K., Takashi, H.; Kato, N.; Iwashima, M. . I. Determination of Absolute Configurations of Tertiary Alcohols by NMR Spectroscopy. *Chem. Lett.* **1999**, *28*, 1181–1182.

(70) Louzao, I.; Garcı, R.; Seco, M.; Quin, E.; Riguera, R. Absolute Configuration of Ketone Cyanohydrins by 1 H NMR : The Special Case of Polar Substituted Tertiary Alcohols. *Org. Lett.* **2009**, *11* (1), 53–56.

(71) Kobayashi, M. The Fucofuranoside Method for Determining the Absolute Configuration of the Tertiary Alcohols Substituted with Methyl and Two Methylene Groups. *Tetrahedron* **1998**, *54*, 10987–10998.

(72) Ariza, X.; Cornellà, J.; Font-bardia, M.; Garcia, J.; Ortiz, J.; Sµnchez, C.; Solans, X. Stereocontrolled Synthesis of Highly Functionalized Quaternary Carbon Centers : A Route to a -Substituted Serines **. *Angew. Chem. Int. Ed.* **2009**, *48* (23), 4202–4205.

(73) Dess, D. B.; Martin, J. C. A Useful 12-1-5 Triacetoxyperiodinane (the Dess-Martin Periodinane) for the Selective Oxidation of Primary or Secondary Alcohols and a Variety of Related 12-1-5 Species ’". *J. Am. Chem. Soc.* **1991**, *113* (19), 7277–7287.

(74) Su, J. T.; Goddard, W. A. Enhancing 2-Iodoxybenzoic Acid Reactivity by Exploiting a Hypervalent Twist. *J. Am. Chem. Soc.* **2005**, *127* (41), 14146–14147.

(75) Wang, S. S.; Tam, J. P.; Wang, B. S. H.; Merrifield, R. B. Enhancement of Pep Tide Coupling Reactions by 4-Dimethylaminopyridine. *Int. J. Pept. Protein Res.* **1981**, *18*, 459–467.

(76) Litvinenko, L. M.; Kirichenko, A. I. Ref DMAP. *Dokl. Chem. Engl. Transl.* **1967**, 763.

(77) Steglich, W.; Höfle, G. N,N-Dimethyl-4-Pyridinamine, a Very Effective Acylation Catalyst. *Angew. Chem. Int. Ed. Engl.* **1969**, *8* (12), 981.

(78) Ishihara, K.; Kubota, M.; Kurihara, H.; Yamamoto, H. Scandium Trifluoromethanesulfonate as an Extremely Active Lewis Acid Catalyst in Acylation of Alcohols with Acid Anhydrides and Mixed Anhydrides. *J. Org. Chem.* **1996**, *61* (14), 4560–4567.

(79) El-Faham, A.; Albericio, F. Peptide Coupling Reagents, More than a Letter Soup. *Chem. Rev.* **2011**, *111* (11), 6557–6602.

(80) Hu, D. X.; Grice, P.; Ley, S. V. Rotamers or Diastereomers? An Overlooked NMR Solution. *J. Org. Chem.* **2012**, *77*, 5198–5202.

(81) Flack, H.D.; Bernardinelli, G. The Use of X-Ray Crystallography to Determine Absolute Configuration. *Chirality* **2008**, *20*, 681–690.

(82) Albright, A. L.; White, J. M. Determination of Absolute Confi Guration Using Single Crystal X-Ray Diffraction. In *Metabolomics Tools for Natural Product Discovery*; 2013; Vol. 1055, pp 149–162.

(83) van der Sluis, P.; Hezemans, A. M. F.; Kroon, J. Crystallization of Low-Molecular-Weight Organic Compounds for X-Ray Crystallography. *J. Appl. Crystallogr.* **1989**, *22* (4), 340–344.

(84) Murakami, T.; Furusawa, K. Efficient Stereodivergent Synthesis of Erythro - and Threo - Sphingosines : Unprecedented Reversal of the Stereochemistry in the Addition. **2002**, *58*, 9257–9263.

(85) Blot, V.; Jacquemard, U.; Reissig, H. U.; Kleuser, B. Practical Syntheses of Sphingosine-1-Phosphate and Analogues. *Synthesis (Stuttg).* **2009**, *5*, 759–766.

(86) Triola, G.; Fabriàs, G.; Casas, J.; Llebaria, A. Synthesis of Cyclopropene Analogues of Ceramide and Their Effect on Dihydroceramide Desaturase. *J. Org. Chem.* **2003**, *68* (26), 9924–9932.

(87) Horino, Y.; Kimura, M.; Tanaka, S.; Okajima, T. Preparation, Structure, and Unique

Thermal [2+2],[4+2], and [3+2] Cycloaddition Reactions of 4-Vinylideneoxazolidin-2-One. *Chem. Eur. J.* **2003**, *9* (11), 2416–2438.

(88) In Our Hands, the N Benzoyl Group Is Still Bulky Enough to Allow High Stereoselectivities in the Hydroboration Step and Is Much Easier to Remove That the N Tosyl Group (Unpublished Results).

(89) Seco, M.; Quin, E.; Riguera, R. The Assignment of Absolute Configuration by NMR. *Chem. Rev.* **2004**, *104* (1), 17–117.

(90) Latypov, S. K.; Seco, J. M.; Quiñoá, E.; Riguera, R. Are Both the (R) - and the (S)-MPA Esters Really Needed for the Assignment of the Absolute Configuration of Secondary Alcohols by NMR? The Use of a Single Derivative. *J. Am. Chem. Soc.* **1998**, *120* (5), 877–882.

(91) Gemal, A. L.; Luche, J. L. Lanthanoids in Organic Synthesis. 6. Reduction of .alpha.-Enones by Sodium Borohydride in the Presence of Lanthanoid Chlorides: Synthetic and Mechanistic Aspects. *J. Am. Chem. Soc.* **1981**, *103*, 5454–5459.

(92) Pazos, Y.; Leiro, V.; Seco, M.; Qui, E.; Riguera, R. Boc – Phenylglycine : A Chiral Solvating Agent for the Assignment of the Absolute Configuration of Amino Alcohols and Their Ethers by NMR. *Tetrahedron: Asymmetry* **2004**, *15*, 1825–1829.

(93) He, Y.; Wang, B.; Dukor, R. K.; Nafie, L. A. Determination of Absolute Configuration of Chiral Molecules Using Vibrational Optical Activity: A Review. *Appl. Spectrosc.* **2011**, *65* (7), 699–723.

(94) Barron, L. D.; Buckingham, A. D. Vibrational Optical Activity. *Chem. Phys. Lett.* **2010**, *492* (4–6), 199–213.

(95) Reina, E.; Camacho, L.; Casas, J.; Van Veldhoven, P. P.; Fabrias, G. Determination of Sphingosine-1-Phosphate Lyase Activity by Gas Chromatography Coupled to Electron Impact Mass Spectrometry. *Chem. Phys. Lipids* **2012**, *165* (2), 225–231.

(96) Nieves, I.; Sanllehí, P.; Abad, J.-L. L.; Fabriàs, G.; Casas, J.; Delgado, A. Chemical Probes of Sphingolipid Metabolizing Enzymes. In *Bioactive Sphingolipids in Cancer Biology and Therapy*; Hannun, Y., Luberto, C., Obeid, L., Mao, C., Eds.; Springer International Publishing: Cham, 2015; pp 437–469.

(97) Bedia, C.; Camacho, L.; Casas, J.; Abad, J. L.; Delgado, A.; Van Veldhoven, P. R.; Fabrias, G. Synthesis of a Fluorogenic Analogue of Sphingosine-1-Phosphate and Its Use to

Determine Sphingosine-1-Phosphate Lyase Activity. *ChemBioChem* **2009**, *10* (5), 820–822.

(98) Bourquin, F.; Riezman, H.; Capitani, G.; Grutter, M. G. Structure and Function of Sphingosine-1-Phosphate Lyase, a Key Enzyme of Sphingolipid Metabolism. *Structure* **2010**, *18* (8), 1054–1065.

(99) Sanllehí, P.; Abad, J. L.; Casas, J.; Bujons, J.; Delgado, A. Bacterial versus Human Sphingosine-1-Phosphate Lyase (S1PL) in the Design of Potential S1PL Inhibitors. *Bioorganic Med. Chem.* **2016**, *24* (18), 4381–4389.

(100) Nieves, I.; Rayo, P.; Delgado, A. Straightforward Access to Spisulosine and 4,5-Dehydrospisulosine Stereoisomers: Probes for Pro Fi Ling Ceramide Synthase Activities in Intact Cells. *J. Org. Chem.* **2013**, *78* (12), 5858–5866.

(101) Canals, D.; Mormeneo, D.; Fabriàs, G.; Llebaria, A.; Casas, J.; Delgado, A. Synthesis and Biological Properties of Pachastrissamine (Jaspine B) and Diastereoisomeric Jaspines. *Bioorganic Med. Chem.* **2009**, *17* (1), 235–241.

(102) Cingolani, F.; Futerman, A. H.; Casas, J. Ceramide Synthases in Biomedical Research. *Chem. Phys. Lipids* **2016**, *197*, 25–32.

(103) Coant, N.; Sakamoto, W.; Mao, C.; Hannun, Y. A. Ceramidases, Roles in Sphingolipid Metabolism and in Health and Disease. *Adv. Biol. Regul.* **2016**.

(104) Gardner, N. M.; Riley, R. T.; Showker, J. L.; Voss, K. A.; Sachs, A. J.; Maddox, J. R.; Gelineau-van Waes, J. B. Elevated Nuclear Sphingoid Base-1-Phosphates and Decreased Histone Deacetylase Activity after Fumonisin B1 Treatment in Mouse Embryonic Fibroblasts. *Toxicol. Appl. Pharmacol.* **2016**, *298*, 56–65.

(105) Castegnaro, M.; Garren, L.; Galendo, D.; Gelderblom, W. C. A.; Chelule, P.; Dutton, M. F.; Wild, C. P. Analytical Method for the Determination of Sphinganine and Sphingosine in Serum as a Potential Biomarker for Fumonisin Exposure. *J. Chromatogr. B Biomed. Appl.* **1998**, *720* (1–2), 15–24.

(106) Schrödinger Release 2016-1, Schrödinger, LLC. Schrödinger Release 2016-1, Schrödinger, LLC: New York, NY, 2016.

(107) Schrödinger Release 2016-1: Maestro, Schrödinger. Schrödinger Release 2016-1: Maestro, Schrödinger, LLC: New York, NY, 2016.

(108) Madhavi Sastry, G.; Adzhigirey, M.; Day, T.; Annabhimoju, R.; Sherman, W. Protein and

Ligand Preparation: Parameters, Protocols, and Influence on Virtual Screening Enrichments. *J. Comput. Aided. Mol. Des.* **2013**, *27* (3), 221–234.

(109) Olsson, M. H. M.; SØndergaard, C. R.; Rostkowski, M.; Jensen, J. H. PROPKA3: Consistent Treatment of Internal and Surface Residues in Empirical P K a Predictions. *J. Chem. Theory Comput.* **2011**, *7* (2), 525–537.

(110) Schrödinger Release 2016-1: Macromodel, Schrödinger. Schrödinger Release 2016-1: Macromodel, Schrödinger, LLC: New York, NY, **2016**.

(111) Harder, E.; Damm, W.; Maple, J.; Wu, C.; Reboul, M.; Xiang, J. Y.; Wang, L.; Lupyan, D.; Dahlgren, M. K.; Knight, J. L.; Kaus, J. W.; Cerutti, D. S.; Krilov, G.; Jorgensen, W. L.; Abel, R.; Friesner, R. A. OPLS3: A Force Field Providing Broad Coverage of Drug-like Small Molecules and Proteins. *J. Chem. Theory Comput.* **2016**, *12* (1), 281–296.

(112) Schrödinger Release 2016-1: Maestro-Desmond Interoperability Tools. Schrödinger Release 2016-1: Maestro-Desmond Interoperability Tools, D. E. Shaw Research: New York, NY, **2016**.

(113) Schrödinger Release 2016-1: Desmond Molecular Dynamics System. Schrödinger Release 2016-1: Desmond Molecular Dynamics System, D. E. Shaw Research: New York, NY, **2016**.

(114) Shivakumar, D.; Williams, J.; Wu, Y.; Damm, W.; Shelley, J.; Sherman, W. Prediction of Absolute Solvation Free Energies Using Molecular Dynamics Free Energy Perturbation and the Opls Force Field. *J. Chem. Theory Comput.* **2010**, *6* (5), 1509–1519.

(115) Guo, Z.; Mohanty, U.; Noehre, J.; Sawyer, T. K.; Sherman, W.; Krilov, G. Probing the Alpha-Helical Structural Stability of Stapled p53 Peptides: Molecular Dynamics Simulations and Analysis: Research Article. *Chem. Biol. Drug Des.* **2010**, *75* (4), 348–359.

(116) Bowers, K.; Chow, E.; Xu, H.; Dror, R.; Eastwood, M.; Gregersen, B.; Klepeis, J.; Kolossvary, I.; Moraes, M.; Sacerdoti, F.; Salmon, J.; Shan, Y.; Shaw, D. Scalable Algorithms for Molecular Dynamics Simulations on Commodity Clusters. In *ACM/IEEE SC 2006 Conference (SC'06)*; Tampa, Florida. **2006**.

(117) Merrill, A. H.; Sullards, M. C.; Allegood, J. C.; Kelly, S.; Wang, E. Sphingolipidomics: High-Throughput, Structure-Specific, and Quantitative Analysis of Sphingolipids by Liquid Chromatography Tandem Mass Spectrometry. *Methods* **2005**, *36*, 207–224.

6. SUMMARY IN SPANISH

Los esfingolípidos (SLs) son componentes estructurales universales de las membranas celulares eucariotas y en los últimos 30 años han demostrado tener no sólo un papel estructural, si no estar también involucradas en procesos de señalización, así como en una amplia gama de respuestas celulares. Por lo tanto, el desarrollo de compuestos capaces de dirigirse específicamente a las enzimas del metabolismo de los SLs representa un área de investigación atractiva para el tratamiento de múltiples trastornos.

La ruta metabólica de los SLs tiene un solo punto de salida, mediado por la esfingosina 1-fosfato liasa (S1PL), enzima dependiente de piridoxal 5'-fosfato (PLP), que degrada de manera irreversible la esfingosina 1-fosfato (S1P) en 2-hexadecenal y fosfoetanolamina (PE). Es una de las proteínas responsables de la regulación de los niveles intracelulares de S1P y contribuye a lo que se denomina "reóstato esfingolipídico", un sistema que regula el destino celular mediante el ratio de S1P, que se considera una molécula proliferativa, y los esfingolípidos apoptogénicos Sphingosina (So) y Ceramida (Cer).

En este contexto, la inhibición de la S1PL se ha relacionado con trastornos autoinmunes, enfermedades inflamatorias o con la desregulación celular en varios tipos de cáncer, por lo que se considera una diana prometedora para el desarrollo de nuevos fármacos.

En 1994, Boumendjel y Miller describen el inhibidor **2VS1P** como mezcla racémica, con una IC_{50} de 2.4 µM en preparaciones microsomales de hígado de rata como fuente de enzima. No se describía ningún mecanismo reacción para el inhibidor, de modo que sugerimos un mecanismo irreversible (Figura 6.1), similar a lo que encontramos en otros enzimas dependientes de PLP que son inhibidos por análogos al sustrato pero con la presencia de una insaturación en α del grupo amino. Un ejemplo típico lo encontramos en la Vigabatrina, inhibidor de la GABA amino transferasa (GABA-AT), aprobado como fármaco antiepiléptico. Así que, como objetivo principal de esta tesis, se planteó la síntesis de los 4 estereoisomeros de un análogo de **2VS1P** de cadena truncada, **24** (Figura 6.1) y ensayar biológicamente su potencia y su mecanismo de acción con enzima purificado (humano, hS1PL o de *Symbiobacterium thermophilum*, StS1PL).

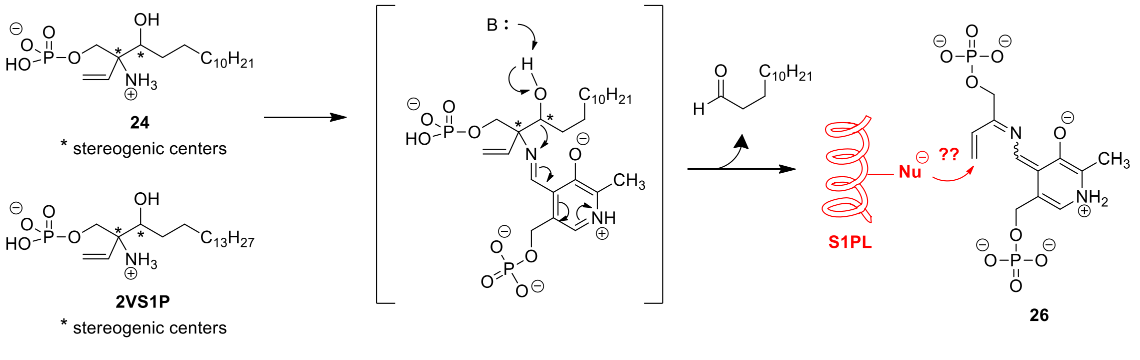

Figura 6.1. Mecanismo de inhibición postulado para 24. Para 2VS1P se correspondería el mismo mecanismo pero el aldehído escindido correspondería a un C16 en vez de a un C13.

Con este fin, se diseñó una síntesis para llegar al fosfato **24** a través del intermedio proquiral ya descrito **15** (Esquema 6.1).

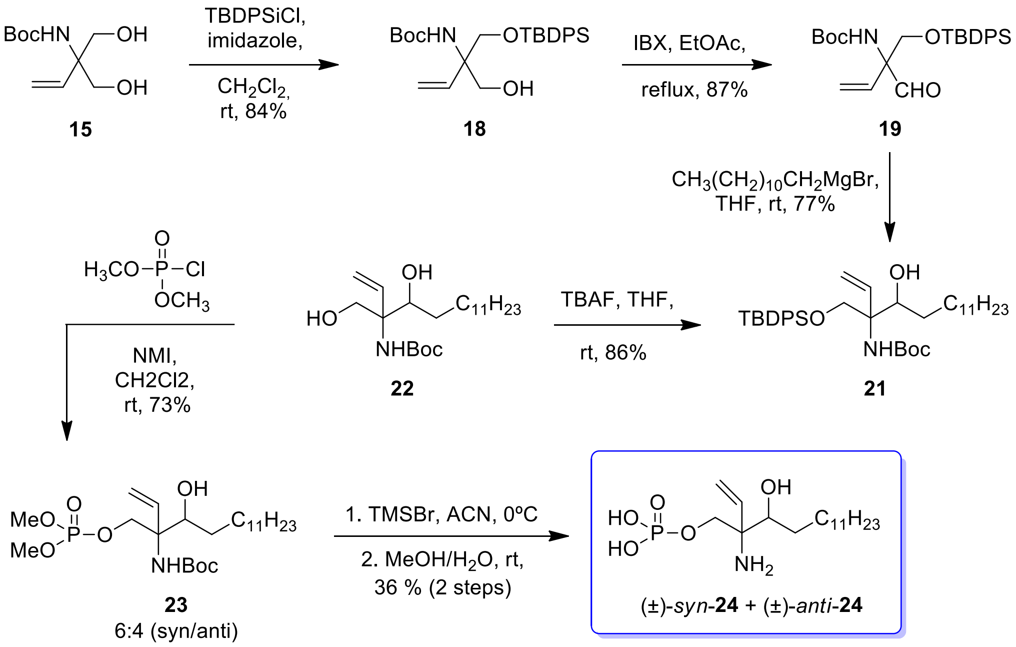
BocHN
OH
OH
15
TBDPSiCl,
imidazole,
CH2Cl2,
rt, 84%
BocHN
OTBDPS
OH
18
IBX, EtOAc,
reflux, 87%
BocHN
OTBDPS
CHO
19
CH3(CH2)10CH2MgBr,
THF, rt, 77%
TBDPSO
OH
C11H23
NHBoc
21
TBAF, THF,
rt, 86%
HO
OH
C11H23
NHBoc
22
H3CO–P(O)–Cl
OCH3
NMI,
CH2Cl2,
rt, 73%
MeO
MeO
P–O
OH
C11H23
NHBoc
23
6:4 (syn/anti)
1. TMSBr, ACN, 0ºC
2. MeOH/H2O, rt,
36 % (2 steps)
HO
HO
P–O
OH
C11H23
NH2
(±)-syn-24 + (±)-anti-24

Esquema 6.1. Síntesis de (±)-*syn*-**24** y (±)-*anti*-**24** a partir del precursor descrito **15**.

Gracias a la diferencia de Rf de los diastereomeros de **23**, podemos separar *syn*/*anti* por columna cromatográfica flash y obtener como producto final las dos mezclas racémicas (±)-*syn*-**24** y (±)-*anti*-**24**.

La resolución enantiomérica se intentó llevar a cabo mediante la derivatización de **23** con el agente de derivatización quiral ácido 2-metoxifenilacético (MPA) dando lugar a **32**, y aunque se lograron resolver los enantiómeros, no se encontraron las condiciones para hidrolizar el MPA frente al fosfato, si no que se obtenía la estructura cíclica **33** en su lugar.

El mismo tipo de derivatización se intentó en **21**, dando lugar a **25**. Por TLC se consiguió la separación de los 4 enantiómeros, pero por cromatografía flash se lograron obtener solamente las cabezas y las colas de columna puras, el resto eran mezclas y los rendimientos de recuperación, muy bajos. Aun así, la obtención de los 4 enantiomeros resueltos era posible con el uso de los dos (*R* o *S*)-MPA por separado.

Tanto las estructuras mencionadas anteriormente, como la metodología de resolución de enantiomeros, se resumen en la Figura 6.2.

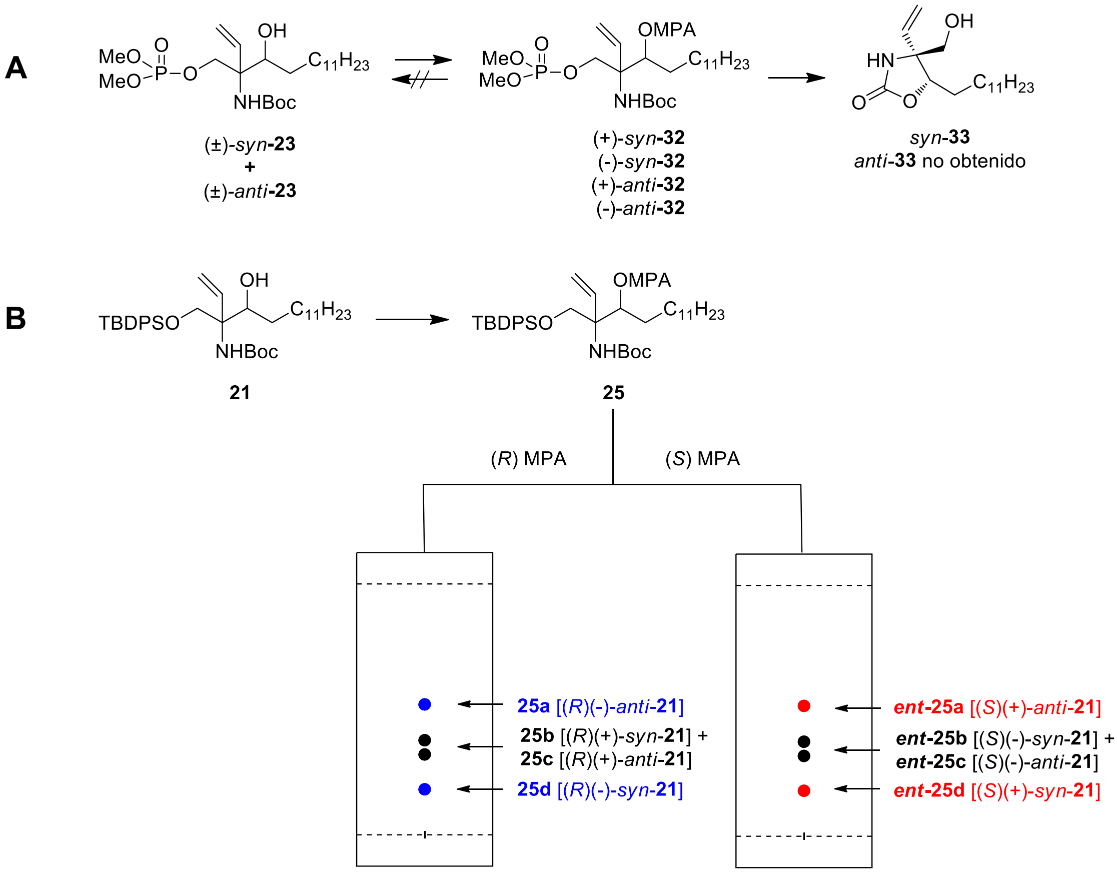
A
MeO
MeO
P
O
NHBoc
OH
C11H23
(±)-syn-23
+
(±)-anti-23
OMPA
(+)-syn-32
(-)-syn-32
(+)-anti-32
(-)-anti-32
HN
OH
syn-33
anti-33 no obtenido
B
TBDPSO
21
25
(R) MPA
(S) MPA
25a [(R)(-)-anti-21]
25b [(R)(+)-syn-21] +
25c [(R)(+)-anti-21]
25d [(R)(-)-syn-21]
ent-25a [(S)(+)-anti-21]
ent-25b [(S)(-)-syn-21] +
ent-25c [(S)(-)-anti-21]
ent-25d [(S)(+)-syn-21]

Figura 6.2. A: Resolución de los 4 enantiómeros de **23** a través de la derivatización con MPA. Durante su hidrólisis obtenemos la estructura cíclica 33. **B:** Resolución de los 4 enantiómeros de **21** a través de la doble derivatización con (*R*)-MPA o (*S*)-MPA.

Usando la metodología de Riguera *et al.*, se pudo determinar la configuración de C3, carbono unido al alcohol secundario, y la de C2, que corresponde a un carbono cuaternario, se determinó utilizando la técnica de NOE sobre el intermedio cíclico **33**, obtenido por la ruta A de la Figura 6.2.

Finalmente se optó por una tercera vía sintética a partir del alcohol vinílico cíclico **44**, obtenido a partir de **18** (Esquema 6.1) por la que se obtenía el alcohol **45**, siendo separables en este punto las mezclas *syn*/*anti* por columna cromatográfica.

La resolución de enantiómeros y la determinación de la configuración absoluta de C3 se llevó a cabo mediante los desplazamientos de señales en los espectros de RMN de **46** y en C2 por NOEs de las estructuras **51**. La síntesis hasta el producto final **24** se realizó a través de **22** como se indica en el Esquema 6.1, dónde se comparó la configuración absoluta con la que habíamos calculado en la ruta sintética previamente utilizada. Todo este proceso se resume en el Esquema 6.2, a continuación.

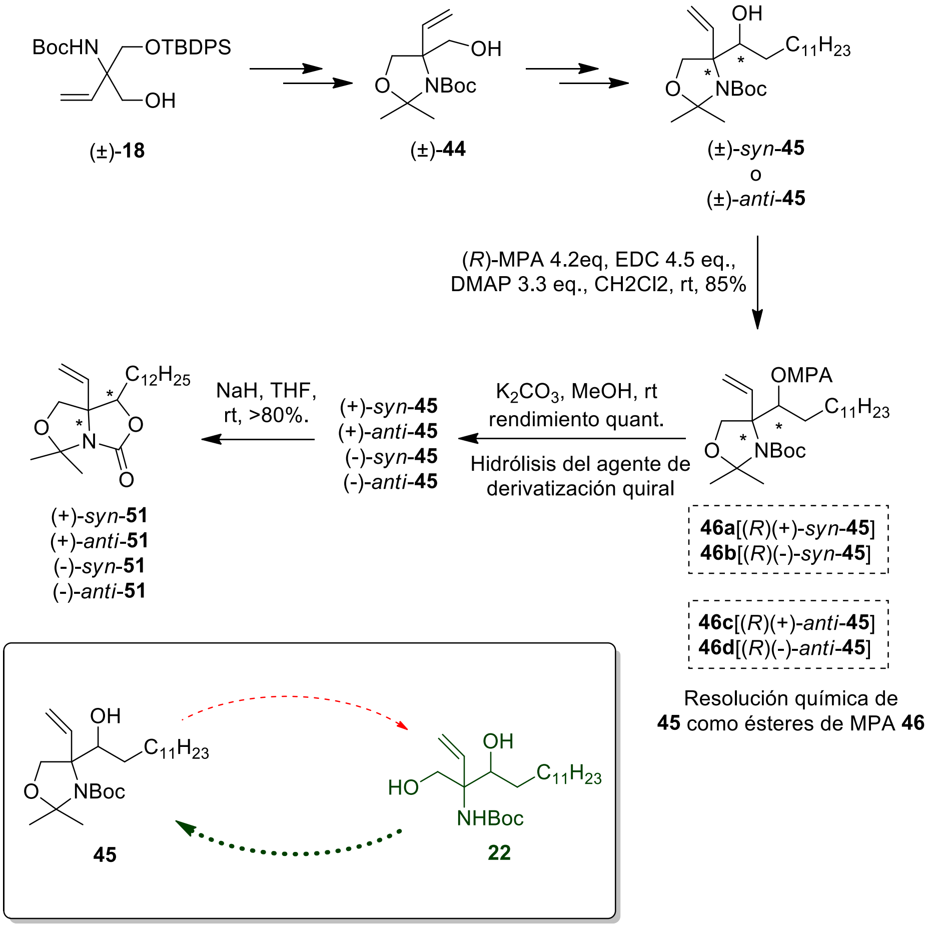
BocHN
OTBDPS
OH
(±)-18
OH
O
NBoc
(±)-44
OH
C11H23
O
NBoc
(±)-syn-45
o
(±)-anti-45
(R)-MPA 4.2eq, EDC 4.5 eq.,
DMAP 3.3 eq., CH2Cl2, rt, 85%
OMPA
C11H23
O
NBoc
46a[(R)(+)-syn-45]
46b[(R)(-)-syn-45]
46c[(R)(+)-anti-45]
46d[(R)(-)-anti-45]
Resolución química de
45 como ésteres de MPA 46
K2CO3, MeOH, rt
rendimiento quant.
Hidrólisis del agente de
derivatización quiral
(+)-syn-45
(+)-anti-45
(-)-syn-45
(-)-anti-45
NaH, THF,
rt, >80%.
C12H25
O
N
O
O
(+)-syn-51
(+)-anti-51
(-)-syn-51
(-)-anti-51
OH
C11H23
O
NBoc
45
HO
OH
C11H23
NHBoc
22

Esquema 6.2. Síntesis y resolución enantiomérica de **45** y **51**. Se comparan los resultados con el producto **22** obtenido por rutas anteriores.

En este caso se mejoran notablemente los rendimientos de resolución enantiomérica, aunque desafortunadamente, para derivatizar **45** con MPA, fue necesario utilizar un exceso de DMAP en la reacción de acoplamiento que terminó racemizando parte de la muestra. Tal y como demuestran los resultados obtenidos por HPLC quiral y VCD, se obtiene (-)-*syn*-**45** enantioméricamente puro, (+)-*syn*-**45** enriquecido con un 94% ee y (±)-*anti*-**45** como mezcla racémica.

A través de este intermedio y con la colaboración del grupo del Dr. Jordi Garcia (Universitdad de Barcelona, Departamento de Química Orgánica e Inorgánica) se llegaron a los productos finales detallados en la Figura 6.3, con los que se llevaran a cabo estudios de inhibición de S1PL, viabilidad celular y esfingolipidómicas.

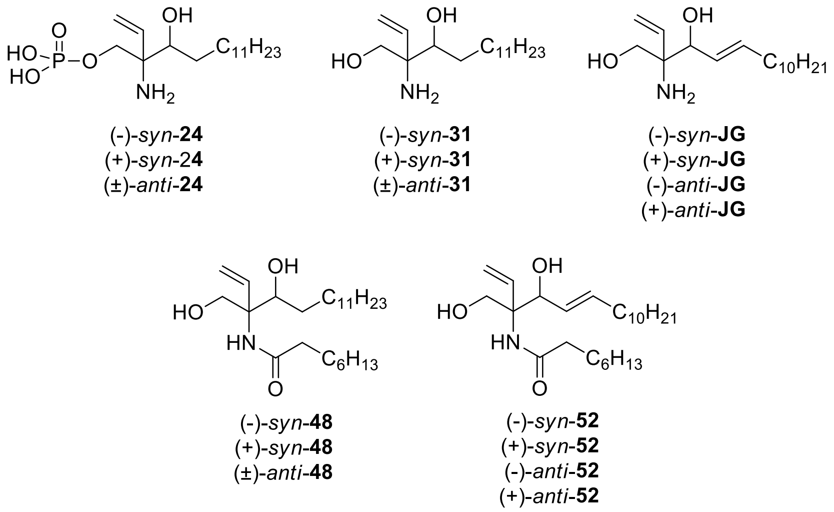

(-)-*syn*-**24**
(+)-*syn*-**24**
(±)-*anti*-**24**

(-)-*syn*-**31**
(+)-*syn*-**31**
(±)-*anti*-**31**

(-)-*syn*-**JG**
(+)-*syn*-**JG**
(-)-*anti*-**JG**
(+)-*anti*-**JG**

(-)-*syn*-**48**
(+)-*syn*-**48**
(±)-*anti*-**48**

(-)-*syn*-**52**
(+)-*syn*-**52**
(-)-*anti*-**52**
(+)-*anti*-**52**

Figura 6.3. Compuestos finales para ensayos biológicos.

Se calculó la IC_{50} = 12.2 µM de **24** *in vitro* en enzima purificado como mezcla racémica en *Symbiobacterium termophilum* S1PL (StS1PL) y se encontró en la S1PL humana (hS1PL) que el eutómero correspondía al (2*S*,3*S*)-**24** y presentaba una IC_{50} de 33.4 µM. Estudios de ESI-MS y ensayos de dilución muestran un comportamiento típico de inhibidor irreversible o de unión fuerte.

Los análogos de So **JG** y su saturado **31** muestran una moderada actividad inhibitoria frente a hS1PL, especialmente en el estereoisómero de configuración natural (2*S*,3*R*), lo que sugiere que no es necesario el fosfato para encontrar actividad inhibidora de S1PL, aunque este le confiere más potencia.

Las LD_{50} de los diferentes isómeros de las moléculas de la Figura 6.3, fueron calculadas en la línea celular A549 y, lamentablemente, sus valores son muy cercanos a su IC_{50}.

Los experimentos de lipidómica, también realizados en células A549 y respecto al metabolismo de estos compuestos, sugieren que (2*S*,3*R*)-**JG** y (±)-*anti*-**31** son sustratos de la Ceramida Sintasa 2 (CerS2), que produce largas cadenas de Cers, pero que no lo son de la CerS5 o la CerS6. Es la primera vez que se encuentra un sustrato selectivo para una CerS. Además, las vinilCer **48** y **52** son hidrolizadas por ceramidasas (CDases) y sólo la configuración natural de los aminodioles libres vuelve a ser acilada, en concordancia con los resultados anteriores.

Respecto a los efectos en el esfingolipidoma natural, todos los diastereomeros de los análogos de vinilceramidas **48** y **52** parecen inhibir la síntesis *de novo*, siendo la serina palmitoiltransferasa (SPT) una potencial diana, ya que se observa tras su administración en las células un descenso de los niveles globales de Cers, esfingomielinas (SMs) y glucosilceramidas (GlcCer).

Estudios computacionales y de dinámica molecular sugieren que el fosfato del cofactor del enzima PLP puede actuar como base, capturando el protón del C3(OH) en la primera etapa de la reacción retroaldólica, excepto para el isómero (2*R*,3*R*)-**24**, en la cual, la base más probable es el mismo fosfato en C1 de su base esfingoide el que extraiga el protón. En cuanto a los nucleófilos probables para ser candidatos a reaccionar con el vinilo después de la escisión de la cadena alifática del enzima y que podrían ser los responsables del comportamiento irreversible de estas moléculas se describen la lisina L353 para los intermedios provinentes de las aldiminas C2(*S*) y las lisinas L353 y L359 para los provinentes de C2(*R*), siendo posible en los dos casos esta reacción.

7. SUPPORTING INFORMATION (CD)

Supplementary data related to the present doctoral thesis can be found in the attached CD. The following material is included:

- PDF file of the Doctoral Thesis
- NMR spectral data from section 4.1.5